N° d'ordre : 42572

ÉCOLE DOCTORALE N° 072 : SCIENCES POUR L'INGÉNIEUR

THÈSE

pour obtenir le grade de

Docteur

délivré par

L'Université Lille 1: Sciences et Technologies

Spécialité Doctorale: Génie Électrique

présentée et soutenue publiquement par

Haibo ZHANG

le 22 decembre 2017

Analysis and Performance Enhancement of a Series Parallel Offshore Wind Farm Topology Integrated into a HVDC Grid

Directeur de thèse : **Christophe SAUDEMONT**
Co-encadrants de thèse : **François GRUSON, Diana M. FLOREZ R.**

Membres du jury:

M. Abdelkrim BENCHAIB	SuperGrid Institute	Rapporteur
M. Fabrice LOCMENT	Université de Technologie de Compiègne	Rapporteur
M. Jun LIANG	Cardiff University	Examinateur
M. Florent MOREL	École Centrale de Lyon	Examinateur
Mme. Betty SEMAIL	Université Lille 1	Examinatrice
M. François GRUSON	ENSAM Lille	Co-encadrant
Mme. Diana M. FLOREZ R.	HEI Lille	Co-encadrante
M. Christophe SAUDEMONT	HEI Lille	Directeur

Laboratoire d'Électrotechnique et d'Électrique de Puissance de Lille
Université Lille 1: Sciences et Technologies, 59650,Villeneuve d'Ascq, France

献给我的父母和姐姐们
Dedicated to my parents and sisters

Acknowledgements

This PhD work, done in the last three years in L2EP, is not only a result of my own dedication and perseverance, but also a credit to the kind and helpful people that I have worked with. I would like to express my gratitude to everyone who has supported me in the last three years.

My appreciation starts with the valuable comments from the jury of my defense: M. Abdelkrim benchaib, M. Fabrice Locment, M. Florent Morel. I was very honored to invite the director of my laboratory L2EP, Mme. Betty Semail, to become the chairman of the jury. My special gratitude to Professor Jun Liang, who traveled to Lille from UK to participate my PhD defense. He had offered me to work with him for one month in the University of Cardiff. He is precise, efficient, trustful, and enlightened me in many technical problems.

I would like to express my sincere gratitude to my PhD director, M. Christophe Saudemont, for accepting me as his first PhD student. He gave me a lot of freedom to understand this project, and put my ideas into practice. I also appreciate the contribution of my co-supervisor Mme. Diana M. Florez R. in my thesis.

I am extremely grateful to M. François Gruson. He is always inspiring, and gave me very helpful advises during the last three years. Without him, this work would be much less attractive.

With his recommendation, I had the opportunity to work in ENSAM, where I got to know other helpful researchers in my field. These memories are still fresh in my mind: M. Xavier Guillaud who taught me basic knowledges on power conversion in François's office at the beginning of my PhD, M. Moez Belhaoune who helped me to revise my presentation slides in the last afternoon before my first year PhD defense, M. Frédéric Colas who helped a lot on the experimental tests, and many other great colleagues in ENSAM.

Most of my unforgettable memories happened in the Room RR120 in the Maison de la Recherche of HEI. Many thanks to my friends and colleagues who had accompanied me over there: My best French teacher Jonathan, Iranian genius Siyamak, problem solver Fabien, Anouar, Faycal, Mouloud, Lounes, Amine, Géraldine, Sid-Ali and "his daughter" Loubna, gaucho Adrien, indispensable LiveTree engineers Gregoire and Benoit, Laura (Ah! Il n'y pas de chauffage!), Volahasina (Attention, Doritos Roulette), le grand chercheur Libanais Jad, Serbian talent Vojislav, and finally the great Chinese: Xing, Xingyu, Tuo.

Last but not least, I would like to give my infinite gratefulness to my parents and my sisters. They are the strongest support for me that give me confidence in overcoming any difficulties in my life.

Abstract

The massive exploitation of far offshore wind energy relies heavily on the High Voltage Direct Current (HVDC) transmission system, in which dedicated offshore substations for converting power from AC into DC are necessary. However, the bulky offshore platform is costly and its installation is complicated.

In this frame, this thesis aims to contribute to the study of a pure DC offshore wind farm topology which exports its energy to onshore without using an offshore centralized power conversion substation. The examined wind farm topology is called Series Parallel Wind Farm (SPWF), which comprises several clusters of wind turbines connected in series, so that the output converters of the wind turbines step up the voltage to a higher level for direct power transmission. However, this distinctive feature of series connection evinces the unfeasibility of independent operation of the connected units. The output voltages of wind turbines depend not only on their own power production, but also on the power production of the entire cluster. As a consequence, unbalanced power production of wind turbines due to uneven wind speed distributed in the wind farm, leads to output voltage variation of wind turbines. Furthermore, the elimination of offshore substation merges the wind farm collection system and the HVDC transmission system, leaving a part of the system variables uncontrolled.

The work carried out in this thesis begins with the identification of the basic elements to constitute the SPWF. Afterwards, the operation of the series connected wind turbines is explained and its overvoltage characteristic is described and emphasized. An overvoltage limitation control strategy is thus developed, which requires an active participation of the onshore converter in limiting the wind turbines output voltages. Hence, the onshore Multilevel Modular Converter (MMC) as well as the HVDC cables models are examined. The control strategy is applied to both Point-to-Point (P2P) HVDC transmission system and Multi-Terminal DC (MTDC) systems. The results validate the feasibility of the proposed strategy and demonstrate its advantage of no power curtailment requirement to limit the wind turbines output voltage.

Key word: Series Parallel Wind Farm (SPWF), Multilevel Modular Converter (MMC), HVDC transmission, Multi-Terminal DC (MTDC), Overvoltage limitation.

Résumé

L'énergie éolienne est très abondante lorsque l'on se situe à des distances éloignées des côtes maritimes. Toutefois, l'exploitation de la puissance électrique que l'on peut en tirer, peut nécessiter de recourir à des systèmes de transport de l'électricité en Courant Continu Haute Tension (HVDC). Ces systèmes nécessitent généralement la présence d'une sous-station située en mer (offshore), dédiée à l'adaptation de tension entre le réseau de distribution en mer (souvent AC) et le réseau de transport. Cette plateforme est volumineuse, son coût élevé et son installation compliquée.

Cette thèse s'intéresse à une topologie de ferme éolienne offshore DC qui transporte son énergie vers l'onshore sans utiliser de sous-station offshore. Ce type de ferme éolienne est appelé Ferme Eolienne Série Parallèle (SPWF). Il est composé de plusieurs grappes d'éoliennes interconnectées en série, de sorte que cette interconnexion engendre directement un niveau de tension adapté à la tension du réseau HVDC. Cependant, la connexion en série implique un couplage en courant de ces éoliennes et par conséquence la tension de chacune d'entre elle n'est plus constante. Un déséquilibre de production d'énergie causé, par exemple, par une distribution disparate de la vitesse de vent dans la grappe d'éoliennes, conduit à des variations des tensions en sortie des éoliennes. Ces variations de tension peuvent, dans certains cas, engendrer des surtensions aux bornes d'une éolienne dans la grappe et éventuellement l'endommager. Une action sur la puissance produite par les éoliennes permet d'éviter ces surtensions mais elle réduit la production de la ferme. Une stratégie permettant de limiter les éventuelles surtensions en sortie des éoliennes, tout en maintenant la production d'énergie, est proposée et développée dans ce mémoire. Cette stratégie est d'abord validée dans un contexte de connexion point à point, en considérant une transmission HVDC basée sur des câbles DC et un Convertisseur Modulaire Multiniveaux (MMC) permettant de la connecter au réseau onshore. Dans un second temps, la ferme SPWF est intégrée dans des systèmes DC multi-terminaux (MTDC). Les résultats de simulation démontrent la faisabilité et la viabilité de la stratégie et montrent qu'aucune réduction de puissance n'est alors nécessaire pour limiter les tensions en sortie des éoliennes.

Mots clés: Ferme Eolienne Série Parallèle (SPWF), Convertisseur Modulaire Multiniveaux (MMC), Courant Continu Haute Tension (HVDC), DC Multi-Terminaux (MTDC), Limitation de surtension.

Contents

List of Figures

List of Tables

List of Acronyms

AAM	Arm Average Model. 90, 93
AVM	Average Value Model. 93
B2B	Back-to-Back. 27, 28, 38, 39, 44
BCA	Balancing Capacitor Algorithm. 92, 93, 98
CAPEX	Capital Expenditure. 5
DFIG	Doubly Fed Induction Generator. 25, 27
EMF	Electromotive Force. 63
EWEA	European Wind Energy Association. 3
HAWT	Horizontal Axis Wind Turbine. 16
HFT	High Frequency Transformer. 82
FFTS	Fractional Frequency Transmission System. 37
HVAC	High Voltage Alternating Current. 3
HVDC	High Voltage Direct Current. 3, 111
LFAC	Low Frequency Alternating Current. 37
MMC	Multilevel Modular Converter. 7, 89, 111
MTDC	Multi-Terminal HVDC. 7, 133, 136
LCC	Line Commutated Converter. 36, 89, 133
MPPT	Maximum Power Point Tracking. 23, 63, 112, 124
MVAC	Medium Voltage Alternating Current. 30
P2P	Point-to-Point. 3, 39, 47
PMSG	Permanent Magnet Synchronous Generator. 25, 58
PWM	Pulse Width Modulation. 36
SCIG	Squirrel Cage Induction Generator. 25, 26
SM	Sub Module. 90, 92
SPWF	Series Parallel Wind Farm. 133, 134, 136, 151, 157, 159
SPWM	Sinusoid Pulse Width Modulation. 68
STATCOM	STATic synchronous COMpensator. 34
SVC	Static Var Compensator. 34
SVD	Singular Value Decomposition. 146
SWF	Series Wind Farm. 57, 58, 67, 81–83, 89, 90, 116, 119, 123, 133, 151, 158

TSO Transmission System Operator. 5, 45
ULM Universal Line Model. 105, 127
VAWT Vertical Axis Wind Turbine. 16
VSC Voltage Source Converter. 36, 89, 133
XPLE Cross-Linked Polyethylene. 105

List of Symbols

i_{sq}	Generator stator q-axis current. 65, 66
i_{ul_j}	MMC arm currents, u upper arm, l lower arm, $j \in \{a, b, c\}$. 94
J_{eq}	Moment of shaft inertia. 63
λ_0	Flux linkage of the rotor permanent magnets. 66
λ_{opt}	Optimal tip-speed ratio. 21, 23, 63, 64
λ	Tip-speed ratio. XI, 19–21, 62
L_s	Generator inductance. 66
L_{SR}	HVDC smoothing reactor. 58, 73, 74
L_{arm}	MMC arm inductor. 93, 101
L_g	Grid phase inductor. 94, 101
L_{sd}	Generator stator d-axis inductance. 65, 66
L_{sq}	Generator stator q-axis inductance. 65, 66
l_c	Cable length. 34, 38
m	Number of series connected units in one cluster. 57, 59, 61, 73
n_p	Pole pairs. 26, 66
$\hat{p}_{WF}$	Wind farm power production adjusted according to overvoltage limitation strategy. 120, 122, 123
$\hat{p}_{cable}$	Cable power losses adjusted according to overvoltage limitation strategy. 120
$\hat{p}_{out}$	Output power of a wind turbine adjusted according to overvoltage limitation strategy. 121, 122
$\hat{p}_{received}$	Received power at onshore side adjusted according to overvoltage limitation strategy. 120
$\hat{\mathbf{p}}_{\mathbf{out}}$	Output power array/matrix of wind turbines adjusted according to overvoltage limitation strategy. 121–123
$\mathbf{p}_{\mathbf{out}}$	Output power array/matrix of wind turbines. 59, 113, 114, 119, 120, 123
ρ	Air density. 20, 21, 62, 64
$P_{WF,nom}$	Nominal power production of a wind farm. 73
$P_{c,max}$	Maximum admissible active power in the cable. 34
P_{em}	Electromagnetic power. 64, 65
P_{nom}	Nominal power production of an electrical system. 72, 73
$P_{out,nom}$	Nominal output power of a wind turbine. 59, 123
P_{tot}	Available power in the wind. 20
$P_{w,nom}$	Wind turbine mechanical nominal power. 23
P_w	Mechanical power that extracted from the wind. 20, 21, 23, 62, 65
p_{AC}	AC side instantaneous power. 96
p_{DC}	DC side instantaneous power. 96
$p_{WF,ave}$	Average power production of a wind farm. 61
p_{WF}	Power production of a wind farm. 59, 111–114, 119, 123
p_{out}	Output power of a wind turbine. 59, 111–113, 120, 121
R_s	Generator resistance. 65, 66

R_{arm}	MMC arm resistor. 93, 101
R_g	Grid phase resistor. 94, 101
r	Wind turbine blade rotor radius. 19–21, 23, 62, 64
S_b	Wind turbine swept area of blades. 20
S_{MVA}	Apparent power. 30
T_{em}	Electromagnetic torque. 63–66
T_w	Torque of the blade induced by wind. 21, 62, 63
$\hat{u}_{HVDC,gctl}$	HVDC voltage level adjusted according to the global control strategy. 120, 124
$\hat{u}_{HVDC,opt}$	Optimal HVDC voltage level. 120, 125
$\hat{u}_{HVDC}$	HVDC voltage adjusted according to overvoltage limitation strategy. 119–122
$\hat{\mathbf{u}}_{\mathbf{out}}$	Output voltage array/matrix of wind turbines adjusted according to overvoltage limitation strategy. 113, 119
$\mathbf{u}_{\mathbf{out}}$	Output voltage array/matrix of wind turbines. 59, 113
$U_{DC,nom}$	Nominal DC voltage of an electrical system. 72, 73
$U_{HVDC,nom}$	Nominal HVDC link voltage. 73, 74, 120, 123, 124
U_{L-L}	Root Mean Square (RMS) value of a phase to phase voltage. 30, 34, 38
U_{L-N}	Root Mean Square (RMS) value of a phase to neutral voltage. 34
U_{limit}	Overvoltage limitation of a wind turbine. 61, 112, 113, 119, 121–123
$U_{out,nom}$	Nominal output voltage of a wind turbine. 59, 61, 112, 114, 115, 119, 123
u_{CL}	Voltage of a cluster. 57, 58
u_{C_i}	Sub module capacitor voltage. 90
$u_{Ctot_{ulj}}$	MMC arm equivalent capacitors, u upper arm, l lower arm, $j \in \{a, b, c\}$. 94
u_{HVDC}	HVDC link voltage. 57–59, 135
u_{SM_i}	Sub module output voltage. 90
u_{diff_j}	MMC differential voltage, $j \in \{a, b, c\}$. 94
u_{out}	Output voltage of a wind turbine. 59, 111, 113, 135
u_{sd}	Generator d-axis stator output voltage. 65, 66
u_{sq}	Generator q-axis stator output voltage. 65, 66
u_{ul_j}	MMC arm voltages, u upper arm, l lower arm, $j \in \{a, b, c\}$. 94
u_{v_j}	MMC coupling voltage derived by mathmatical change of variables, $j \in \{a, b, c\}$. 94
$v_{w,cut-in}$	Cut-in wind speed. 22, 23
$v_{w,cut-out}$	Cut-out wind speed. 22
$v_{w,nom}$	Nominal wind speed. 22, 23
v_w	Wind speed. 19–21, 23, 62, 63
v_{g_j}	Grid phase to ground voltages, $j \in \{a, b, c\}$. 94
Ω_m	Mechanical rotational speed of the wind turbine rotor. 19, 21, 23, 26, 62–66
$\Omega_{m,nom}$	Nominal mechanical rotational speed of the wind turbine blades. 23, 65
$\Omega_{m,opt}$	Optimal rotational speed of the wind turbine blades. 21, 23

ω_e Electrical rotational speed of the wind turbine rotor. 26, 65, 66

W_j^{Σ} MMC arm stored energy, $j \in \{a, b, c\}$. 96, 99

General introduction

Contents

Background of the thesis

The exploitation of renewable energy resources for electricity production has been a matter of great interest over the last decades in the target of reducing fossil fuel consumption and greenhouse gas emissions. In 2009, the Renewable Energy Directive set a policy to reach a 20% of renewables in total energy consumption of the European Union (EU) for the 2013-2020 period [Rene 09]. Under the encouragement of national policies, the share of renewable energy has already increased to 17% by the end of 2015 and is expected to rise further to 21% in 2020 and 24% in 2030. [Revi 16]. Within this EU framework, deployment of wind energy resources is crucial to comply with the objective of a system with higher shares of renewable energy in the transition towards a more competitive, secure and sustainable energy system. In Europe, wind energy accounts for the largest proportion of renewable energy installation rate. The total installed capacity of wind power reached 153.7 GW by the end of 2016, 141.1 GW onshore and 12.6 GW offshore, accounting for 17% of Europe's total installed power generation capacity. This figure could rise to 323 GW by 2030, 253 GW onshore and 70 GW offshore, producing 24% of the EU's power demand in 2030, according to [Wind 15].

From these scenarios, the attention shifts towards offshore wind project developments. Offshore wind energy is a major driver of investment decisions in Europe. In 2016, €27.5 billion, including €18.2 billion offshore were invested in wind energy projects [Wind 17]. The United Kingdom (UK) has the largest amount of offshore wind capacity in Europe, particularly in the North Sea where there are more abundant wind power resources, representing 40.8% of all installations. The WindEurope (formerly the European Wind Energy Association (EWEA)) published in 2009 a 20 Year Offshore Network Development Master Plan [EWEA 09], in which operating and future offshore projects are reported, as can be seen in Figure 1.

To be able to exploit more abundant wind energy far from shore, the transmission system must be flexible and reliable. There are two types of transmission technologies for connecting offshore wind power to onshore utility grids. Most of the large offshore wind farms currently in operation are rather close to shore and are grid-connected via High Voltage Alternating Current (HVAC) cables. Although very few projects of wind farms are located far from shore, High Voltage Direct Current (HVDC) transmission is the best option in the long run due to the lower transmission losses.

The deployment of offshore wind energy requires a dedicated and flexible offshore electricity system. The vision of a meshed HVDC system has gain increased attention since it provides a redundant, reliable and secure energy supply with lower generation costs compared to a Point-to-Point (P2P) connection of offshore wind farms to shore. Moreover, the integration of other renewable energy and the interconnections between countries with different AC power grids become possible.

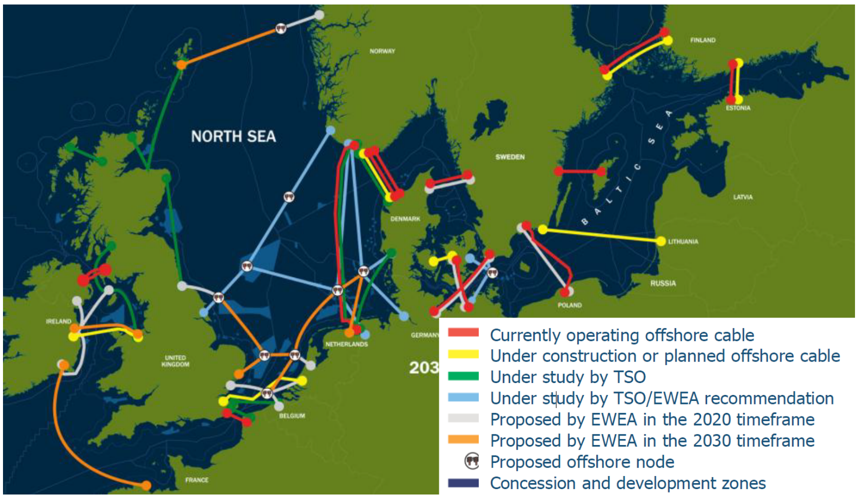

Figure 1 – WindEurope's 20 Year Offshore Network Development Master Plan.

Motivations

Offshore wind speed is potentially stronger and more constant than on land because of the absence of topographic influence, which lead to a much higher power production. The wind resource map for Europe shown in Figure 2 illustrates this characteristic and reveals the greatest wind energy potential along north-eastern coasts and the North Sea in this area.

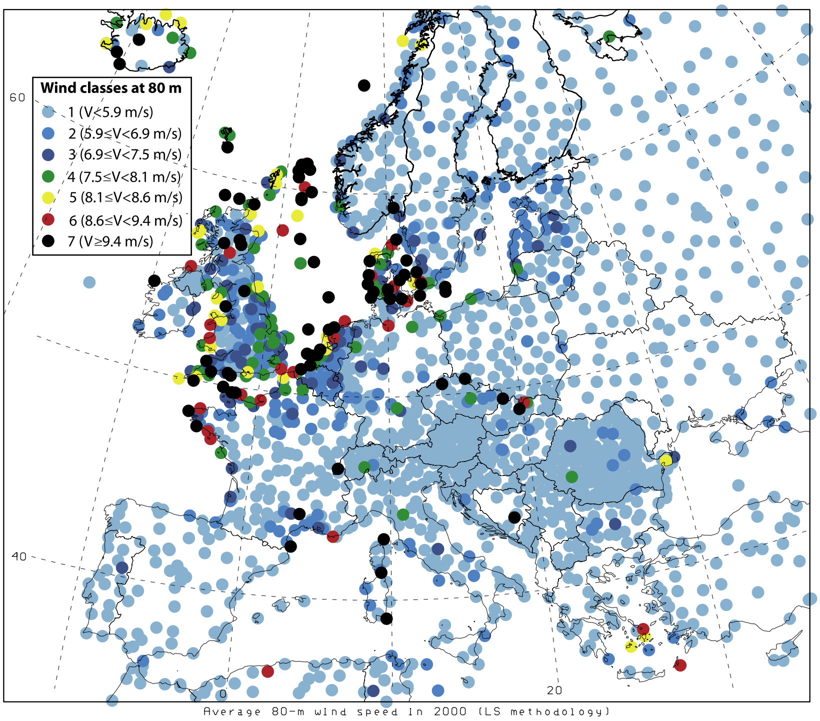

Figure 2 – European map of wind speed extrapolated to 80 m in height and averaged over all days of the year 2000 at surface and sounding stations [Arch 05].

The wind power generation system for onshore and offshore wind turbines is similar. However, since offshore wind farms are exposed to a tough environment, the overall Capital Expenditure (CAPEX) breakdown of offshore wind farms changes significantly. In an onshore wind farm, the wind turbines account for 70% of the total cost, while in an offshore wind farm, costs of turbines, balance of plant and installation and commissioning are relatively evenly distributed [Rene 10]. Consequently, it is worth taking into consideration each component of the offshore wind farm in order to reduce the overall project expenditure.

The tender prices for offshore wind farms have decreased significantly in recent years [Krie 16b]. Taking the tender prices of Danish wind farms as an example, in 2010 DONG Energy was the only bidder to develop Anholt offshore wind farm rated at 400 MW, with tariff of 1051 øre/MWh (141.3 €/MWh). In 2015 Vattenfall AB won the tender among 4 bidders to build Horns Rev III at 770 øre/MWh (103.1 €/MWh). Most notably, only one year later in 2016, Vattenfall AB won the project of Danish Kriegers Flak, a 600 MW wind farm in the Baltic Sea among 7 bidders. The price decreased by about half to 372 øre/MWh (49.9 €/MWh). As a conclusion, offshore wind becomes profitable without government subsidies. However, the price for offshore station remains very high. The Kriegers Flak offshore wind farm, shown in Figure 3, is planned to exchange 400 MW power between Danish and German Transmission System Operators (TSOs). Since East Denmark grid is synchronised with the Nordic power system, and the Germany electrical grid is part of the continental synchronous zone, a frequency transformation is necessary.

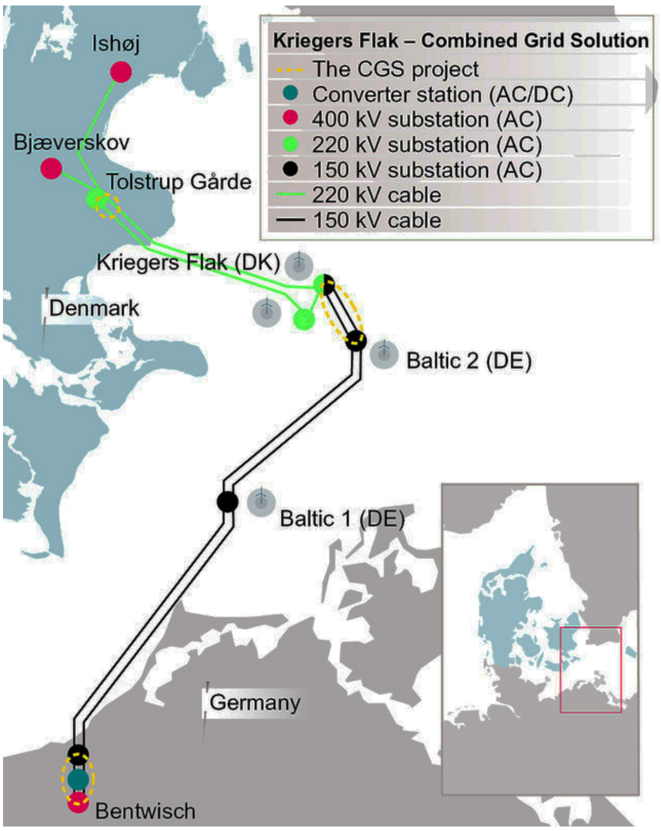

Figure 3 – Kriegers Flak, a 400 MW offshore interconnection between two TSOs Energinet.dk from Denmark and 50Hertz from Germany [Krie 16a].

The first considered option was to place one HVDC offshore converter, however this solution was abandoned due to the under-estimation of the cost of the offshore converter substation. Hence, the adopted solution consists of two voltage source converters that convert electricity from AC to DC and then from DC to AC. The two converters back-to-back will be placed in the German coast, avoiding roughly 50% premium for an offshore platform. The final arrangement of this project is shown in Figure 3.

The construction of the centralized power converter is expensive and difficult. The cost model in [Lund 06] indicates that only the supporting platform for a 300 MW converter costs at least €25 million. As reported in [Rene 10], the offshore substation takes up 7% of the total wind farm investment. This rate will further increase as the ratings of wind turbines increase and thus lowering the cost of turbines foundations.

Objectives and thesis outline

Conventional offshore wind turbines generate AC output voltage. The collection system and transmission system require a substation to transform medium AC voltage into either HVAC or HVDC. The penetration of power electronics has promoted the study of the integration of DC technology into the wind farm collection systems. This thesis investigates a DC offshore wind farm with clusters of series connected wind turbines. The work presented in this thesis attempts to answer the following questions: "How to control DC series connected wind turbines? and how to integrate the pure DC wind farm without an offshore platform into the electrical grid?". This work develops and discusses different control strategies used to avoid large variation of wind turbine output voltages due to unbalanced power production.

This research can be organized into three levels of work as shown in Figure 4, consisting of the design, operation and grid integration of the examined offshore wind farm. In the design level, the key components of a DC offshore wind turbine are both identified and sized. In the operation level, the operation of a series connection of wind turbines is developed. Both works from these two levels contribute to the study of the integration of the series parallel offshore wind farm into the electrical grid. The thesis is thus organized as follows:

Chapter 1 gives an introduction of DC offshore wind farm technologies. It describes the main technologies used to form an offshore wind farm including the arrangement of elements in a collection system and the methods for transmitting power from offshore to onshore. Several offshore wind farm topologies are introduced and compared.

Chapter 2 presents the basics of forming a wind farm with series connected DC wind turbines. The principle of the series offshore wind farm and its main advantages and drawbacks are introduced. Based on the wind farm characteristics, the DC wind turbine generation and conversion systems are developed. Afterwards, the operation of a series connection and the local limitation controllers used to protect the wind turbines against operation beyond their

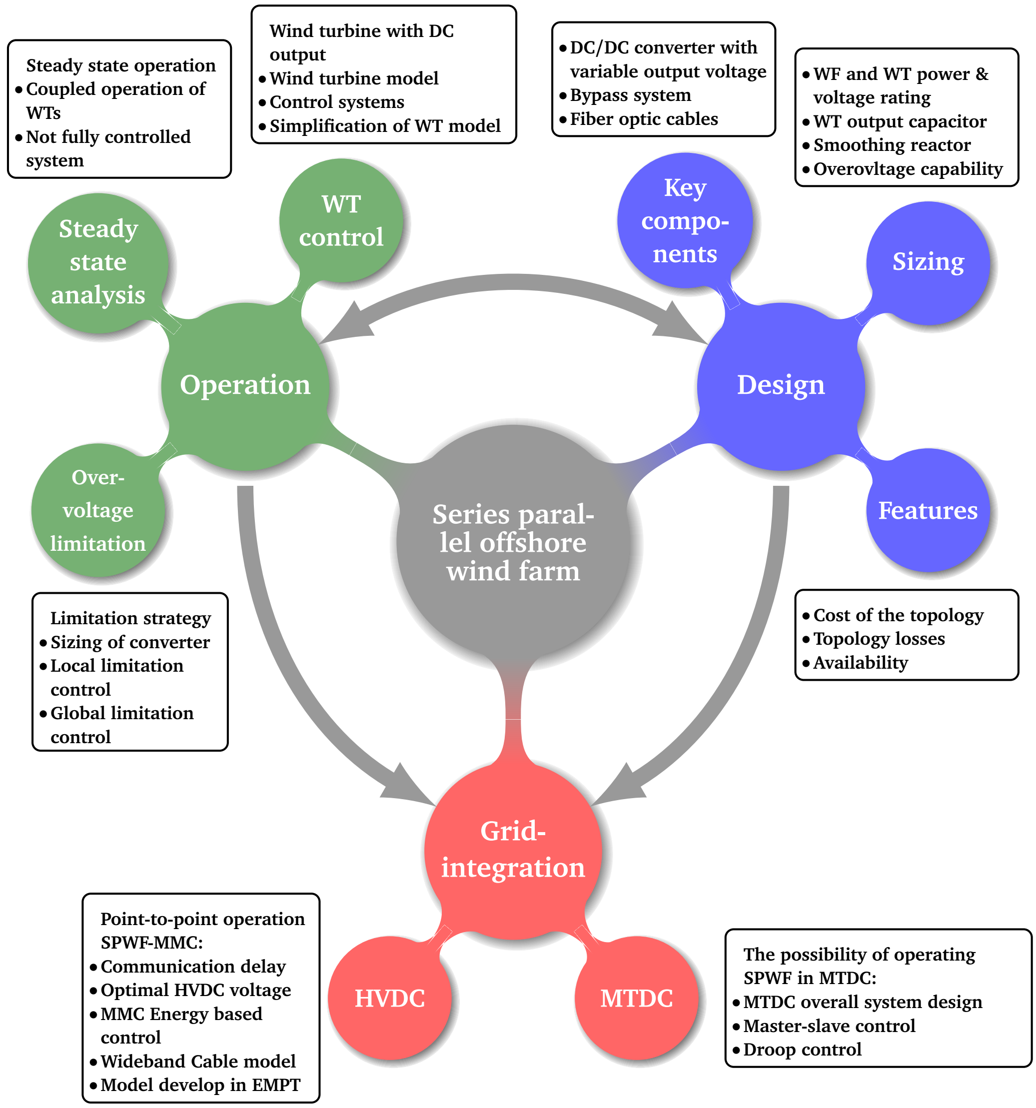

Figure 4 – Thesis outline divided into three levels of study.

overvoltage capabilities are described.

Chapter 3 provides a framework for understanding the operation of the DC series offshore wind farm in a point-to-point system. The model of the Multilevel Modular Converter (MMC) and energy based control are developed. The HVDC cable models are as well discussed in this chapter as the lack of offshore substation couples the wind farm collection and the transmission system. The principle of a global control strategy relying on communication is introduced.

Chapter 4 deals with the operation of the offshore wind farm in Multi-Terminal HVDC (MTDC) grids. The control methods of MTDC grids are first introduced and therefore applied to a series parallel offshore wind farm integrated into a hybrid MTDC system.

Chapter 5 bring the thesis to a close stating the overall conclusions and key findings of the research work carried, as well as directions for further research work.

List of publications

This work has resulted in the following publications:

1. H. Zhang, F. Gruson, D. Flórez and C. Saudemont. "Intergrating a Series Parallel Offshore Wind Farm into a Multi-Terminal DC Grid and Coordinated Control Scheme". In: ELECTRIMACS. 2017.

2. H. Zhang, F. Gruson, D. Flórez and C. Saudemont. "Analysis of the Influence of Different Cable Modelling for DC series Offshore Wind Farm". In: Power Electronics and Applications (EPE'16 ECCE Europe), 2016 18th European Conference on. IEEE, 2016. p. 1-9.

3. H. Zhang, F. Gruson, D. Flórez and C. Saudemont. "Control Strategies of a DC Based Offshore Wind Farm with Series Connected Collection Grid". In: Energy Conference (ENERGYCON), 2016 IEEE International (pp. 1-6). IEEE.

4. H. Zhang, F. Gruson, D. Flórez and C. Saudemont. "Improved Overvoltage Limitation Control Approach of a DC Series Offshore Wind Farm Based on MMC". In: Electrotechnical Conference (MELECON), 2016 18th Mediterranean (pp. 1-6). IEEE. (**Best student paper award first prize**)

5. H. Zhang, F. Gruson, D. Flórez and C. Saudemont. "Design and Control of a DC Series Offshore Wind Farm Based on HVDC-MMC". In: Symposium de Genie Electrique. 2016.

References

[Arch 05] C. L. Archer and M. Z. Jacobson. “Evaluation of global wind power”. *Journal of Geophysical Research: Atmospheres*, Vol. 110, No. D12, 2005. XI, 4

[EWEA 09] EWEA. “Oceans of Opportunity”. Tech. Rep., 2009. 3

[Krie 16a] “Kriegers Flak - Combined Grid Solution”. 2016. Available online at https://en.energinet.dk/, accessed on 14/10/2017. XI, 5

[Krie 16b] “Kriegers Flak - the largest offshore wind farm in the Baltic Sea”. 2016. Available online at http://efkm.dk/media/7878/factsheet-kriegers-flak.pdf, accessed on 14/04/2017. 5

[Lund 06] S. Lundberg. *Wind Farm Configuration and Energy Efficiency Studies-Series DC versus AC Layouts*. PhD thesis, Chalmers University of Technology, 2006. 6

[Rene 09] “Renewable energy directive (2009/28/EC)”. 2009. Available online at https://ec.europa.eu/energy/en/topics/renewable-energy/renewable-energy-directive, accessed on 14/02/2017. 3

[Rene 10] Renewables Advisory Board. “Offshore wind sector: value breakdown”. Tech. Rep., 2010. 5, 6

[Revi 16] “Revised renewable energy directive (2009/28/EC)”. 2016. Available online at https://ec.europa.eu/energy/en/topics/renewable-energy/renewable-energy-directive, accessed on 14/02/2017. 3

[Wind 15] WindEurope. “Wind energy scenarios for 2030”. Tech. Rep., 2015. Available online at https://www.ewea.org/, accessed on 24/09/2017. 3

[Wind 17] WindEurope. “Wind in power 2016 European statistics”. Tech. Rep., 2017. Available online at https://windeurope.org/about-wind/statistics/, accessed on 14/04/2017. 3

Chapter 1

State of the Art of Offshore Wind Power Systems

目不能两视而明，耳不能两听而聪。
The person attempting to travel two roads at once will get nowhere.

«劝学» 荀子
Encouraging Learning, Hsun Tzu

Contents

1.1 Introduction

Offshore wind technology has many advantages over its onshore counterpart [Bilg 11]: The issues of visual impact and noise can be nearly eliminated by installing the wind turbines far away from shore, which in return enables the use of bigger wind turbines. The average wind energy is usually more abundant and more constant because of the absence of topographic influence at offshore, which is suitable for larger offshore wind farm projects with significantly higher production per unit installed.

Although the mechanical and electrical principles of onshore and offshore wind turbines to capture and then convert wind energy into electrical energy have no difference, the offshore wind farm is more expensive and more complex to install and to maintain. In an offshore wind farm, the wind turbines account for only 40% of total cost, against up to 70% in onshore wind farms. The offshore wind farm is not only more demanding in the reliability of wind turbine blades, generators, foundations and power cables but also in efficient techniques for power collection, power transmission and power integration into the AC grid.

This chapter introduces the basics of offshore wind farms including the wind turbine structures, wind power generation, collection and transmission systems as shown in Figure 1.1. Offshore wind turbines exhibit other characteristics, apart from having larger blades and higher power rating generators, these turbines have very different foundation technologies than the onshore wind turbines. Most existing offshore wind turbines are located in shallow water, so that fixed-bottom monopile foundation is enough for supporting the wind turbines at sea [Bret 09]. However, more and more technologies emerge, as the wind turbines moving further away from shore to the deep sea [Bret 09][Wind 17b][Burt 11].

The conversion components comprise wind turbine blades, shafts, gearboxes and generators. These are all mounted on the turbine foundations, and are essential for capturing and converting the kinetic energy from the wind into electrical power.

Subsequently, it is then necessary to gather all the electrical power generated by each

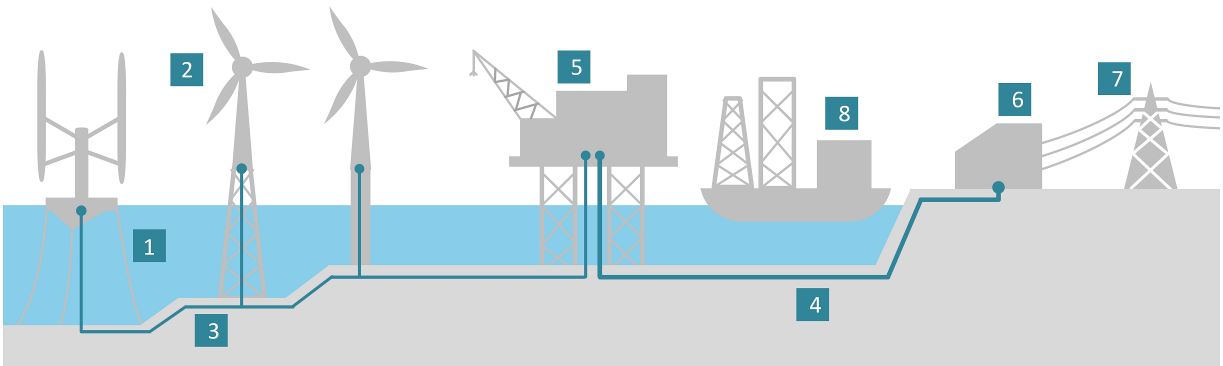

Figure 1.1 – General arrangement of an offshore wind farm: 1: Wind turbines, 2: Foundations, 3: Collection cables, 4: Transmission cables, 5: Offshore substation, 6: Onshore station, 7: Onshore grid, 8: Installation and maintenance.

wind turbine and transmit it into the onshore grid. In a conventional offshore wind farm, the process is as follows: the generated power from all the wind turbines is collected at an offshore substation, where it is transformed or converted and then transmitted towards onshore AC power grid by submarine cables.

The organization of this chapter is as follows: Structures and mechanical characteristics of offshore wind turbines are first described, then the power conversion principles are introduced. Afterwards the collection and transmission systems are explained which allows the analysis of suitable topologies for large offshore wind farms.

1.2 Offshore wind turbine technology

Since the first offshore wind turbine was installed in Sweden in 1990 [Burt 11], the power rating of offshore wind turbines has been growing constantly. The average power rating of turbines installed in 2016 was 4.8 MW, 15.4% larger than 2015 [Wind 17a]. Furthermore, the average water depth and distance to shore of offshore wind farms have also been increasing. Therefore, many different designs and improvements related to offshore wind turbines have emerged. This section gives an introduction of current development of offshore wind turbine technology.

1.2.1 Wind turbine foundation

As offshore wind turbines are structures placed in adverse conditions, the foundation design is extremely challenging. Different types of foundation are proposed and used in practice. These can be classified into two categories: Fixed-bottom and floating foundations.

Floating foundations, are typically used in deep water (>50 m) applications due to technical barriers of fixed-bottom foundations [Zoun 15]. Nevertheless, the fixed-bottom foundations are dominant in the shallow water. In the same way as onshore foundations, the main function of offshore fixed-bottom foundations is to support the weight of wind turbines on the sea. However, the offshore ones need to be designed to have more endurance to withstand stronger wind, and, more importantly, the sea current.

1.2.1.1 Fixed-bottom foundation technology

A variety of fixed-bottom foundations are available in the market. Figure 1.2 shows four basic types of fixed-bottom foundations: monopile, tripod, jacket and gravity-based structure.

1. *Monopile*: Monopile foundation is the currently most widespread type in shallow water (<20 m) attributable to its simplicity and low cost. However, the market share is likely to slightly decrease by virtue of more and more wind farm projects located in deep

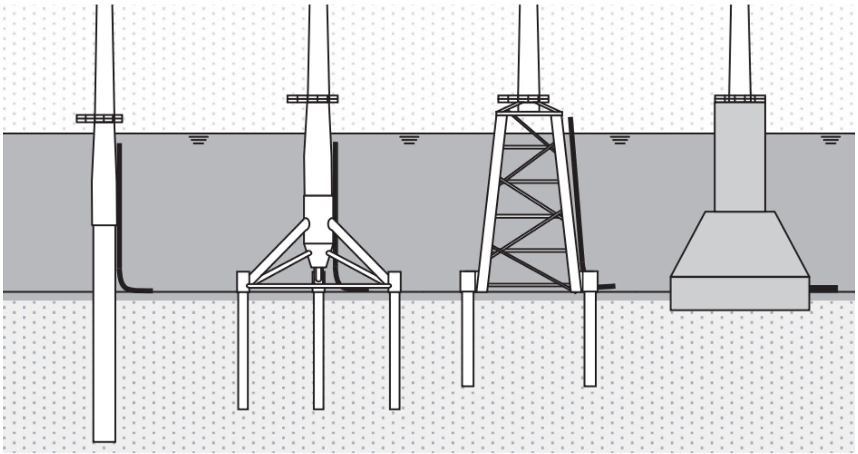

Figure 1.2 – Fixed-bottom foundations: monopile, tripod, jacket, gravity-based [Van 06].

sea. This structure is made of a single cylindrical steel tube. One end of the tube penetrates into the seabed according to actual environmental conditions. The wind turbine foundations planned to be used in the offshore wind farms near Saint Nazaire and Calvados are of this type. The adopted monopiles have a diameter of 7 m and penetrate 20 m into the seabed [Fren 17].

2. *Tripod*: Tripod foundation consists of a central cylindrical steel pile connected to three cylindrical steel tubes, through which the structure penetrates into the seabed. The production and installation of the tripod is complex and therefore it is relatively expensive [Van 06]. It is designed to be used in deep water but has not been used for many projects to date.

3. *Jacket*: Jacket foundation uses relatively complex steel structures and provides robust support in deep water. It is used in water depth around 50 m. The deepest application of jacket foundations for offshore wind turbines to date has been 45 m at the Beatrice Demonstration Project [Seid 07]. Jacket foundation is also adopted in offshore substation due to its robustness. The wind turbine foundations used in the sea out of Le Tréport, Saint Brieuc and Iles d'Yeu et de Noirmoutier are of this type, owing to the heavy 8 MW wind turbines used in these wind farms [Fren 17].

4. *Gravity-based*: The gravity type support structure is based on concrete material at the bottom of the monopile to provide reinforced stability to the structure. The structure requires a flat seabed. It is used in water depth around 20 m to 30 m. The wind turbine foundations used in the sea near Fécamp are of this type [Fren 17].

1.2.1.2 Floating foundation

For placing wind turbines in even deeper water (>50 m), aforementioned solutions becomes uneconomical because of the use of large amount of materials. Floating structures are considered as a better solution. The floating foundation comprises a main floater and mooring lines which are fixed to the floater at one end and attached to the seabed at the other end. There are many other designs of the floaters in the market and some representatives are listed as follows:

1. The *Hywind* Spar-Buoys concept has a floating part similar to a monopile structure shown in Figure 1.3. A demo wind turbine has been in operation since 2009 in Norway [Niel 06].
2. The *Blue H* Concept is based on the tension leg platform. A first prototype is placed off the coast of Italy in 2008 [Hube 08].
3. The *WindFloat* Concept is developed by EDP and EDPR in Portugal. The floating foundation is semi-submersible and is stabilized by the use of "water entrapment plates" on the bottom of its three pillars. A demo project of 2 MW has been connected to the grid by the end of 2011 [Rodd 10].
4. Ideol developed a French floating wind turbine demo project called *Floatgen* with a 2 MW wind turbine, constructed by Bouygues TP in 2017 [Berh 16], shown in Figure 1.4. This demo wind turbine is the first offshore wind turbine installed in France. Another demo project, *EolMed*, with 4 floating wind turbines rated at 6.2 MW is planned near the coast of Gruissan, France.

Other examples of floating projects related to constructional design of wind turbines are described in the next subsection.

1.2.2 Constructional design: horizontal vs vertical axis

Figure 1.5 shows the main components of a three-blade Horizontal Axis Wind Turbine (HAWT) compared to a ϕ-type Vertical Axis Wind Turbine (VAWT). It can be seen that the VAWT offers a symmetrical design with fewer components. However, current wind turbine market is dominated by HAWTs since its power conversion efficiency is superior to VAWTs, which has been proven by decades of research and development [Burt 11].

Figure 1.3 – *Hywind* 2.3 MW prototype deployed off the coast of Norway.

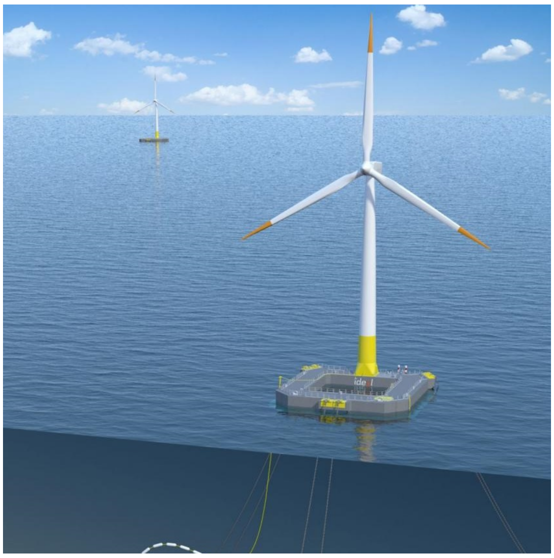

Figure 1.4 – *Floatgen* floating project developed by IDEOL France.

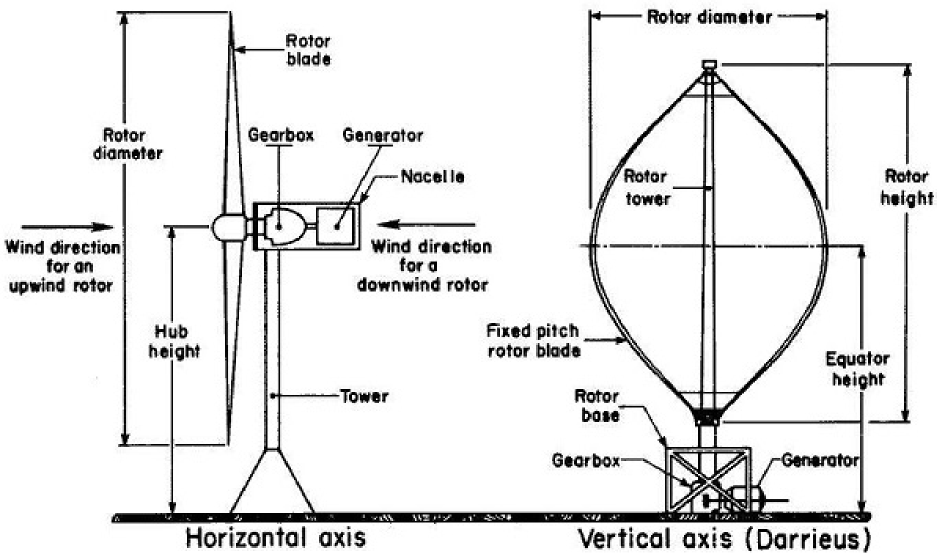

Figure 1.5 – Main components of a HAWT and a ϕ-type VAWT [Hau 13].

The majority of the HAWTs possess three blades. Similar to many design considerations, the choice of the number of blades is a compromise between performance and cost. The optimal power coefficient of a three-blade wind turbine is 3% more than a two-blade wind turbine, while four-blade only offers 1% more than a three-blade. Moreover, a wind turbine having three blades is more dynamically stable. A two-blade solution offers a balanced mechanical design while it causes the so-called wobbling phenomenon [Hau 13], since, when the rotor is yawed to face the wind direction (to capture the maximum energy from the wind), two blades at the horizontal position vibrate leading to mechanical stress on the turbine shaft. The largest world's commercial two-blade offshore wind turbine is the Mingyang SCD 6MW which has been deployed because it has less attack area to the wind so as to deal with the typhoon conditions that frequently occur in the East China Sea [Ming 15].

The deployment of HAWTs in the offshore wind turbine market is largely because it is based on proven and mature technologies for onshore wind turbines. However, the need for exploiting offshore wind energy in the deep sea has encouraged the use of floating foundations, described in previous section 1.2.1).

Although the three-blade HAWTs are still used in many projects using floating foundations like the Hywind [Niel 06], Windfloat [Rodd 10], there are some works that have raised doubts on using HAWTs as the optimal design for floating applications [Suth 12][Borg 14]. Instead, they suggest that VAWTs, (of which many types has been developed based on the patent of the French engineer Georges Darrieus in 1922), become a promising replacement due to:

1. Fewer components: HAWTs must have a yaw control system which orients its blades to the wind direction before the blades can rotate. In contrast, the yaw system can be eliminated in a VAWT as its blades can be hit by the wind from any direction. Fewer components lead to cost reduction and a more reliable system.

2. Machinery position: The generation system and the blades of HAWTs are mounted on the top of the turbine tower which can be around 100 m above the sea level. This requires complex installation process and specific lifting cranes [Borg 14]. In contrast, VAWTs usually have its generation system at the bottom [Vita 11]. This also protects workers from climbing tall and dangerous turbine towers.

3. No gravitational fatigue: HAWTs have a limiting factor due to gravitational fatigue since the heavy blades create a bending moment [Borg 14], which does not exist in VAWTs.

4. Upscaling: Above benefits naturally lead to the fact that it is possible to have accommodation for larger electric generator above 10 MW in the VAWTs.

5. Tilt: The floating foundation for HAWTs has a low tolerance to the tilts and the strong heeling moment generated by the wind. While the vertical axis design has a relative low gravity center the heeling moment can be reduced at least 40% [Nenu 17], thus reducing the floater cost.

In Europe, there have been several projects on floating VAWTs such as the NOVA project with V-type VAWT shown in Figure 1.6a, the DeepWind project with ϕ-type VAWT shown in Figure 1.6b, the INFLOW project with H-type VAWT shown in Figure 1.6c and the SeaTwirl-developed helical-type VAWT shown in Figure 1.6d.

1.2.3 Aerodynamic basics of conversion of kinetic wind energy into mechanical energy

No matter the wind turbine has a horizontal axis or a vertical axis, it serves to convert the kinetic energy of the wind into useful mechanical energy and thereafter into electrical power.

Both horizontal axis and vertical axis wind turbines follow the same process: the turbine blades capture a part of the kinetic energy of the wind and start to rotate around their axis. The blades are connected (directly or through a gearbox) to a main shaft which spins a generator rotor. Finally the useful mechanical energy is converted into electricity by taking advantage of the properties of electromagnetism [Acke 05][Cour 08].

Although they harness the wind kinetic energy in different ways, there is no difference between HAWTs and VAWTs with respect to the energy conversion. Since the VAWTs are not widely used in the industry, their mathematical models are not studied comprehensively as the HAWTs in the literature.

In this thesis the three-blade HAWT is used. Nevertheless, the introduction of the HAWT's aerodynamic basics in this subsection also helps to understand how the VAWT works.

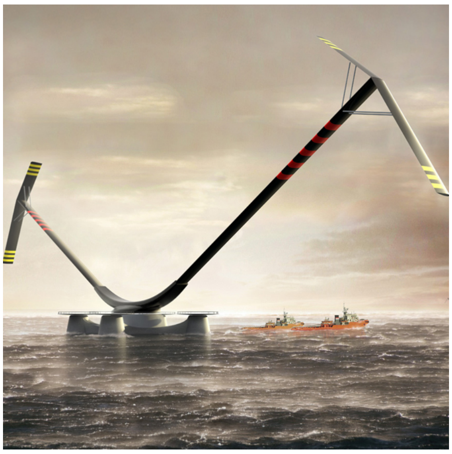

(a) NOVA project [NOVA 10]

(b) DeepWind project [Deep 14]

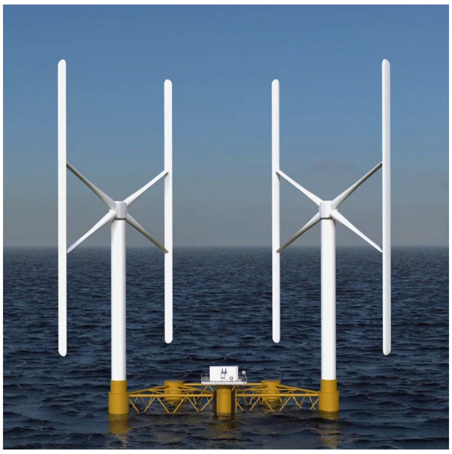

(c) INFLOW project [INFL 17]

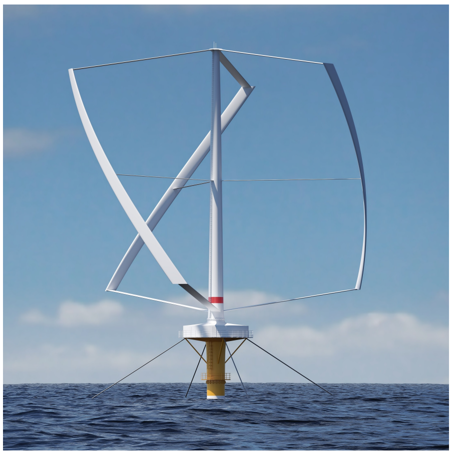

(d) SeaTwirl project [SeaT 17]

Figure 1.6 – Offshore floating projects with VAWTs.

1.2.3.1 Tip-speed ratio

The tip-speed ratio λ is defined as the ratio between the tangential speed of the HAWT blade tip and the wind speed v_w.

$$\lambda = \frac{\text{Tip speed of wind turbine blade}}{\text{Wind speed}} = \frac{\Omega_m r}{v_w} \tag{1.1}$$

where

r = the radius of the swept area of the blades (m)
Ω_m = rotational speed of the rotor (rad/s)
v_w = wind speed (m/s)

The tip-speed ratio is an important concept in wind turbine operation. If the wind turbine rotor rotates too slowly, most wind energy would pass through the wind turbine blades. If the wind turbine rotor rotates too fast, the blades would appear like a wall to the wind. In order to have the maximum efficiency, the wind turbine rotor has to spin at a specific speed to match the coming wind speed.

1.2.3.2 Power coefficient

The total kinetic power P_{tot} of the wind passing through a blade swept area $S_b = \pi r^2$ with a speed v_w is

$$P_{tot} = \frac{1}{2}\rho\pi r^2 {v_w}^3 \tag{1.2}$$

However, a wind turbine cannot extract all available wind power to convert it into mechanical power. The theoretical maximum proportion of power that a wind turbine can extract from the wind is given by the Betz's limit, at $16/27 \approx 59.3\%$ [Lecl 04]. A practical three-blade wind turbine can achieve about 80% of the Betz's limit, whose aerodynamic efficiency is around 48%. The ratio between extracted power P_w and total power P_{tot} in the wind is called power coefficient C_p and is defined as:

$$C_p = \frac{P_w}{P_{tot}} \tag{1.3}$$

From equations 1.2 and 1.3, the extracted power by the wind turbine can be deduced:

$$P_w = \frac{1}{2} C_p \rho\pi r^2 {v_w}^3 \tag{1.4}$$

It has been mentioned that the tip-speed ratio λ affects the power efficiency. Another factor that impacts the power efficiency is the pitch angle β of the blade. The pitch angle refers to the angle of attack of the blades to the wind which can directly adjust the torque exerted by the wind on the turbine blades. Figure 1.7 shows the coefficient curves of an experimental wind turbine as a function of λ and β [Hau 06]. It can be found that the bigger the pitch angle the lower the portion of power that can be extracted from the wind.

In practical, pitch angle is kept at a small value for maximum power production from the

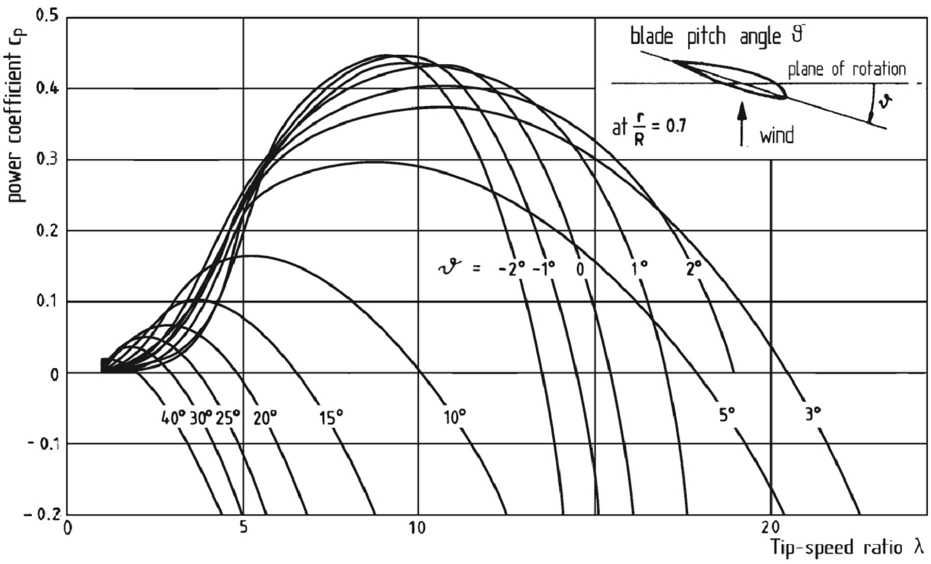

Figure 1.7 – Characteristic of C_p as a function of λ and β [Hau 06].

cut-in wind speed to the rated wind speed. Under very strong wind conditions, pitch angle increases which prevents the blade from being damaged.

When the pitch is kept constant, power coefficient C_p is reduced as a function of the tip-speed ratio. As can be seen in Figure 1.7, each curve has its maximum power coefficient $C_{p,max}$.

The wind turbine rotor has to spin at a specific rotational speed $\Omega_{m,opt}$ to match the facing wind speed in order to achieve the optimal tip-speed ratio λ_{opt}, where wind turbines obtain the maximum efficiency.

1.2.3.3 Torque coefficient

Notice that it is the torque exerted by the wind on the blades, which produces their rotation. At very low wind speed conditions, the torque is insufficient to turn the blades due to friction. The tip-speed ratio, therefore, equals to zero, leading to zero power production, according to Equation 1.4. However there is a non-zero torque applied to the blade. Hence, it is necessary to define the torque coefficient T_w for the purpose of describing the operation of the wind turbine from a mechanical point of view:

$$T_w = \frac{P_w}{\Omega_m} = \frac{1}{2} C_t \rho \pi r^3 {v_w}^2 \tag{1.5}$$

With the torque coefficient C_t determined as:

$$C_t \lambda = C_p \tag{1.6}$$

The corresponding torque curve of Figure 1.7 is shown in Figure 1.8.

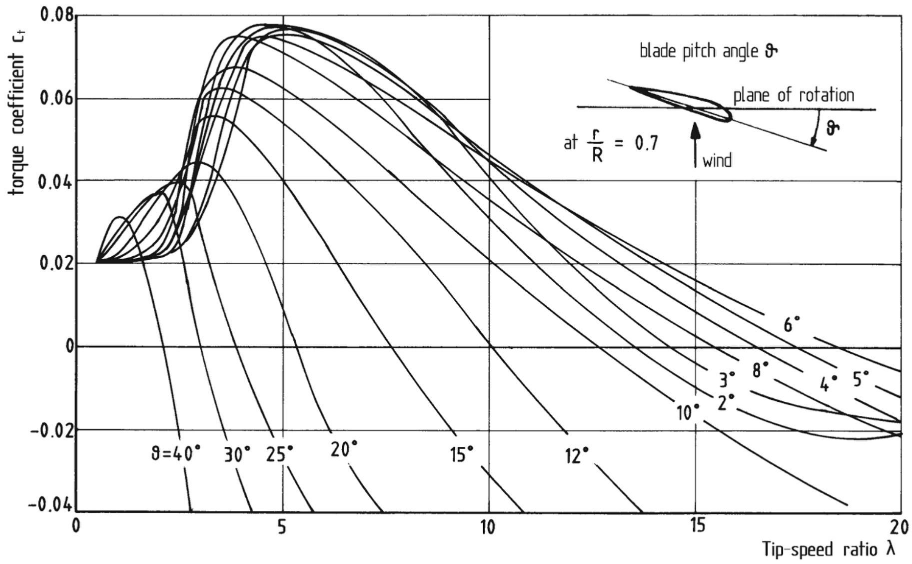

Figure 1.8 – Characteristic of C_t as a function of λ and β [Hau 06].

1.2.3.4 Ideal power curve

Figure 1.9a shows an ideal power curve of a wind turbine which relates the generated power to the wind speed. Real wind turbines with different characteristics may show discrepancies from this curve. The power curve in Figure 1.9a is split into four distinct operating regions according to the cut-in wind speed $v_{w,cut-in}$, nominal wind speed $v_{w,nom}$ and cut-out wind speed $v_{w,cut-out}$.

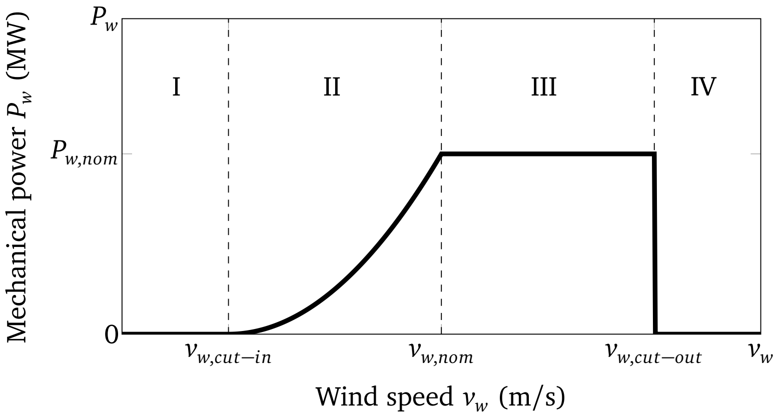

(a) Turbine mechanical power associated to the wind speed.

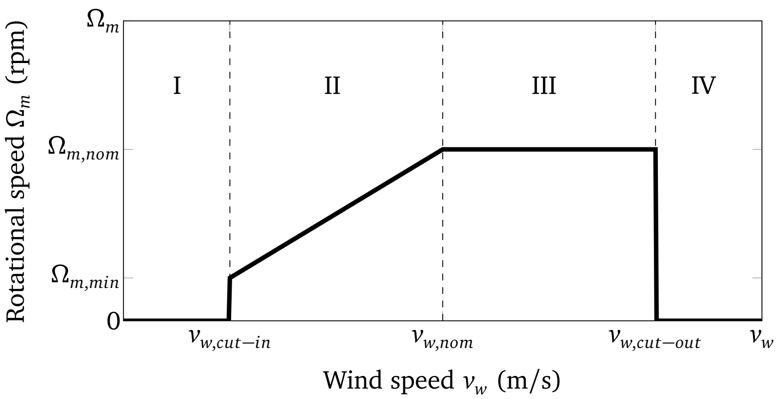

(b) Turbine mechanical speed variation with the wind speed.

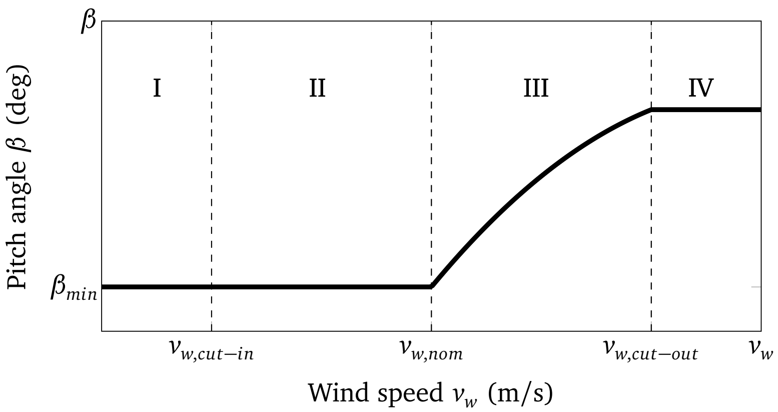

(c) Pitch angle variation with the wind speed.

Figure 1.9 – Performance curves of an ideal wind turbine.

When wind speeds fall below the cut-in speed, in region I, there is insufficient torque on the blades, so the wind turbine is blocked by the mechanical brake. The wind turbine is kept in parking mode.

In region II, the wind turbine aims at extracting as much power as possible. As presented in Figure 1.9b, the wind turbine runs at optimal rotational speed $\Omega_{m,opt}$, which is linear to the wind speed, in order to keep the tip-speed ratio at its optimal value λ_{opt}. The slope of the curve in the range between $v_{w,cut-in}$ and $v_{w,nom}$ equals to

$$\frac{\Omega_{m,opt}}{v_w} = \frac{\lambda_{opt}}{r} \tag{1.7}$$

In this region, the pitch angle of the wind turbine blades is kept at an optimal attack angle for a given wind as seen in Figure 1.9c.

When the wind speed increases to $v_{w,nom}$, the wind turbine power reaches its power rating $P_{w,nom}$ as well as the nominal rotational speed $\Omega_{m,nom}$. In order to avoid the damage of the mechanical part of the wind turbine, the rotational speed is kept at $\Omega_{m,nom}$. However, even with a constant rotational speed, the generated power could still increase as the wind speed rises. Therefore, the wind turbine relies on the pitch control to achieve constant power production regime of region III, as depicted in Figure 1.9a. The variation of the pitch angle in the corresponding operation regions is illustrated in Figure 1.9c.

As the wind speed further increases, it will reach a cut-out speed beyond which mechanical components of wind turbines can be damaged. As a result, the braking system operates to shut down and keep it in region IV.

1.2.3.5 Maximum power point tracking

The power production of an ideal wind turbine associated to the rotor rotational speed is shown as black curves in Figure 1.10. It can be seen that for a specific wind speed, the power P_w has a maximum point. The trajectory linking these points forms a red solid line, as shown in the figure, is called the Maximum Power Point Tracking (MPPT) curve which only depends on the rotational speed Ω_m:

$$P_w \propto {\Omega_m}^3 \tag{1.8}$$

By controlling the wind turbine generator to rotate at given speeds, the operating points of a wind turbine can always stay on the trajectory, therefore achieving MPPT [El A 04].

The above aerodynamic basics help to understand the operation of wind turbines. However, in practice, not all wind turbines have been designed to have all aforementioned functions. For instance, in early 1990s most wind turbines were designed to operate at a fixed rotational speed because of its simplicity and low fabrication and maintenance costs. In consequence, it was not possible to realize MPPT with such a wind turbine. Indeed, apart from

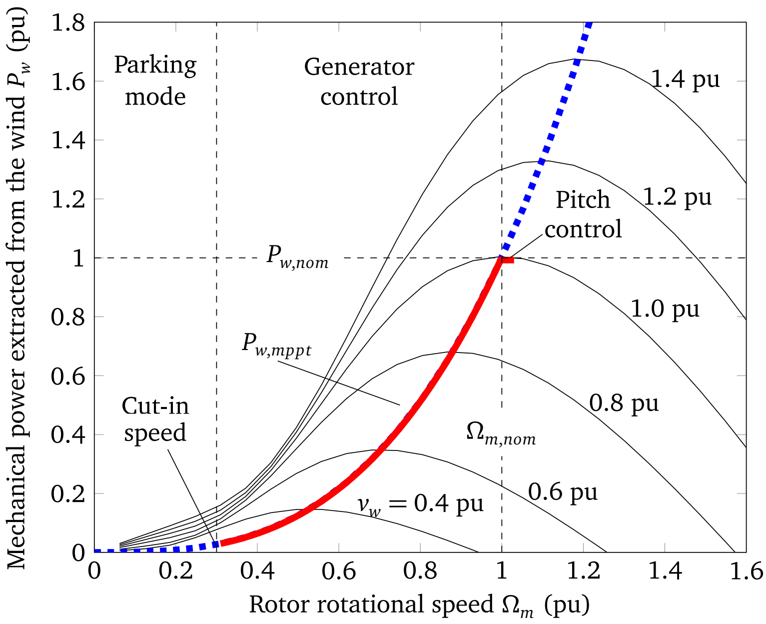

Figure 1.10 – Turbine mechanical power curves under different wind speeds.

the aerodynamics, a wind turbine design takes into consideration cost, efficiency and many other technical and mechanical constraints [Acke 05].

1.2.4 Large commercial wind turbines

Currently, a variety of wind turbines of power rated from several kilowatts to several megawatts are available. However, for offshore applications, wind turbines are designed to have megawatt-ratings. There are many ways to classify the wind turbines. One criterion concerns the methods for limiting power taken from the wind when its available power in the wind becomes higher than the wind speed the wind turbine is designed for. This criterion leads to the following classification: *stall-controlled*, *active stall-controlled* and *pitch-controlled* wind turbines [Chen 09].

A *stall-controlled* wind turbine has fixed pitch angle blades and is aerodynamically designed to have different power efficiency regarding the wind speed. When the wind speed is relatively low, the wind turbine operates at high efficiency. When the wind speed is higher than the wind speed the wind turbine is designed for, the blades create turbulence on the sides that are not facing the wind, in order to stop the lifting force on the blades, as seen in Figure 1.11. In this way the rotational speed is limited and the power efficiency is reduced. This is a passive aerodynamic method which leads to simple, low cost and robust control of the wind turbine, but with relatively poor controllability of the power capture.

A more advanced control method refers to *active stall-controlled*. Active stall-controlled blades are aerodynamically similar to its passive counterpart except that, when the wind speed surpasses the designed speed for the wind turbine, the pitchable blade increases its attack angle to the wind in order to make the blade goes into a deeper stall. Therefore,

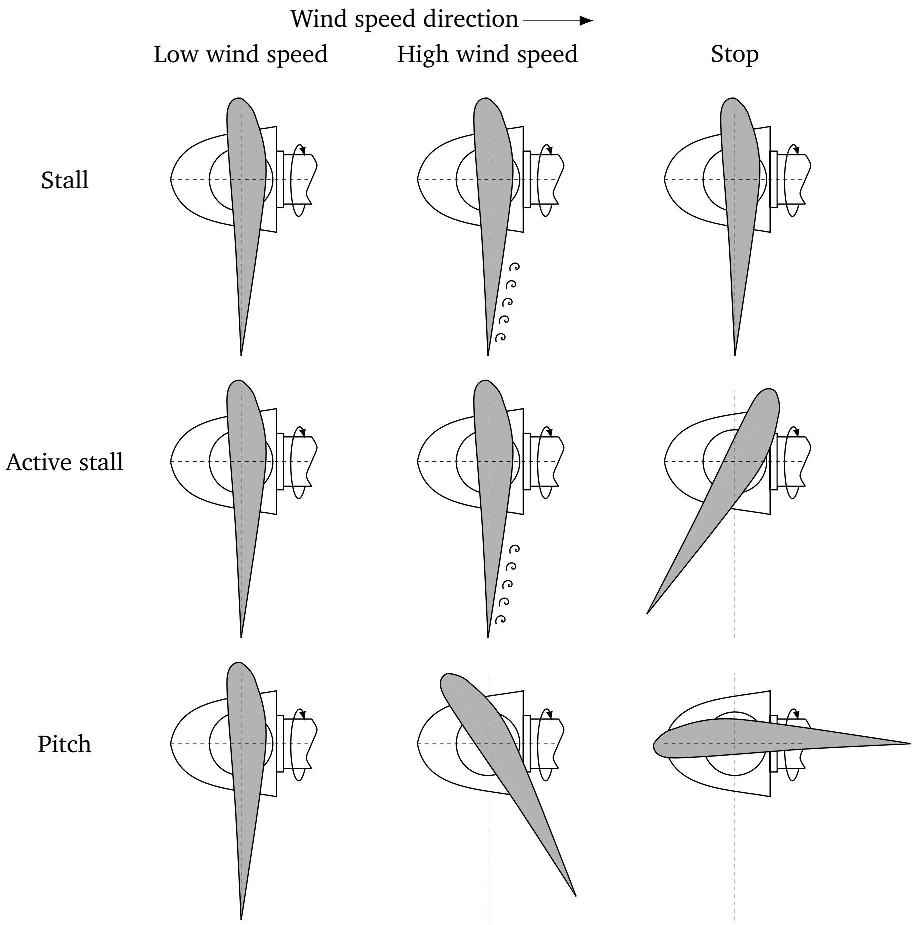

Figure 1.11 – Wind turbine with stall control, active stall control, pitch control: view from blade tip to nacelle hub.

the power efficiency is significantly reduced [Acke 05]. Notice that the angular sensitivity is high, so that a small increase of the attack angle can cause a deep stall. The advantage of active stall over passive stall is a more accurate control of the wind turbine power generation.

A *pitch-controlled* wind turbine has an active control system that can continuously vary its pitch angle. At low wind speed, the pitch angle is kept constant at an optimal value to make the wind turbine extract maximum power from the wind. When the wind speed becomes higher, the pitch angle increases gradually (the attack angle decreases) to limit the power extracted from the wind. A clear difference between pitch control and active stall control system is that the pitch angles are in opposite directions, as shown in Figure 1.11.

The lift on the blades is gradually reduced by using pitch control. Angular sensitivity is relatively low compared to active stall [Acke 05]. Other criterion is related to the generator rotational speed variability, leading to the classification in two types: *fixed-speed* and *variable-speed* wind turbines that in turn, can be categorized according to the generator type, or even the size of power converters. This subsection discusses the most common wind turbine types in current market. Regarding to the generators, three types of technologies are available for both onshore and offshore wind turbines: Squirrel Cage Induction Generator (SCIG), Doubly Fed Induction Generator (DFIG) and Permanent Magnet Synchronous Generator (PMSG).

1.2.4.1 Squirrel Cage Induction Generator (SCIG) based fixed-speed wind turbine

The early wind turbines operated mostly at fixed speed. The fixed speed refers to the mechanical rotational speed of the wind turbine generator rotor Ω_m. Figure 1.12 shows the structure of a fixed-speed wind turbine equipped with a Squirrel Cage Induction Generator (SCIG) which is also known as "Danish concept".

The generator rotor is coupled to the blade shaft via a gearbox. The generator stator is connected directlyto the grid and as a result, the rotation speed of the rotor is held constant regardless of the wind speed. However, the slip of the generator allows slight variation of rotation speed between 1-2% [Sloo 03]. For a generator with 2 pole pairs, its mechanical rotation speed should be slightly greater than the synchronous speed of 1500 rpm (f_g is 50 Hz) to operate at generator mode.

As an induction machine, the SCIG is not self-excited. Therefore, it is necessary to connect a capacitor bank across the stator terminals to supply reactive power to the machine [Chen 09]. It can also serve as a reactive power compensation to the grid, in order to achieve a power factor close to one [Chen 09].

The rotor of this kind of wind turbine should be locked until the wind speed is high enough to accelerate the rotor to a required fixed speed. In the wind market, there are wind turbines of this kind using all three power limit control methods in high wind condition [Hans 07].

The major advantage of the fixed-speed wind turbines are their simplicity. However, they cannot change their rotational speed to operate at maximum efficiency. An improvement of the fixed-speed wind turbine is the two rotational speed operation to increase the power production. To do that, the SCIG has changeable number of pole pairs [Sloo 03]. At low wind speed, all pole pairs are inserted while at high wind speed, parts of the pole pairs are removed. As the electrical rotor speed ω_e remains constant at the grid frequency and $\omega_e = n_p\Omega_m$, the mechanical rotor speed increases due to the reduction of the number of pole pairs n_p.

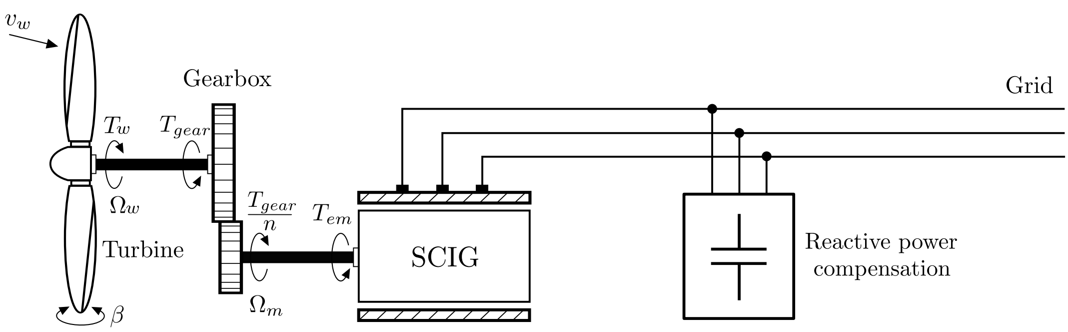

Figure 1.12 – SCIG-based fixed-speed wind turbine connected directly to the grid.

1.2.4.2 Doubly Fed Induction Generator (DFIG) based wind turbine with partial-scale power converter

Ideally, it is expected to continuously adjust the rotational speed in response to the wind speed variation in order to keep the wind turbine operation at a maximum efficiency. For this reason, some variable-speed wind turbines are developed, even that they are more costly and complex.

The first alternative is the Doubly Fed Induction Generator (DFIG) based variable-speed wind turbine. The asynchronous generator has wound rotor windings connected to a partial-scale power converter shown in Figure 1.13. The stator of the DFIG is connected directly to the grid while the wounded rotor of the generator is connected to the grid via slip rings and a Back-to-Back (B2B) power converter. Since it is difficult for wound rotor to have very high pole pairs, it is necessary to insert a gearbox between the rotor shaft and the turbine blade shaft to ensure high rotational speed of the rotor. One of the roles of the power converter is to provide excitation current for the rotor windings, and generally this converter is scaled at about 30% of the nominal power of the wind turbine [Mull 02].

As the generator stator is connected directly to the grid of constant 50 Hz frequency, the internal magnetic field induced by the rotor should be kept at a constant frequency. However, the rotor speed of a variable-speed wind turbine is supposed to change with wind speed. The role of the B2B converter is to provide this slip frequency to the rotor terminals by absorbing power from the grid or injecting power to the grid. When the rotor runs at sub-synchronous mode (below synchronous rotational speed), the grid power is fed to the rotor through the converter. On the contrary, when the rotor runs at over-synchronous mode (above synchronous rotational speed), the converter feeds power back into the grid. From the view of the stationary stator, the combined internal magnetic field is thus kept constant. The power converter should be able to operate bi-directionally. In this way, the rotor speed is able to vary in the range of ±30% around the nominal speed [Mull 02][Chen 09].

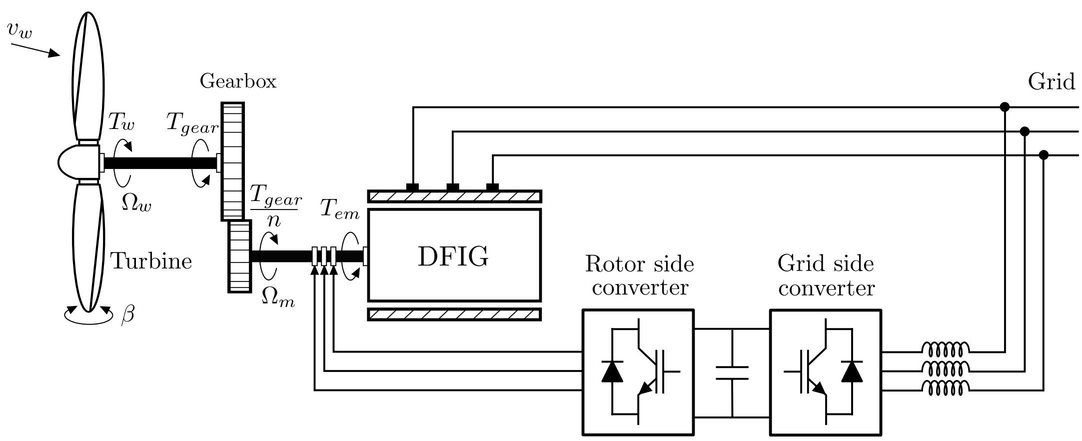

Figure 1.13 – DFIG-based variable-speed wind turbine.

1.2.4.3 Permanent Magnet Synchronous Generator (PMSG) based wind turbine with full-scale power converter

Another alternative for wind turbine generators is the use of synchronous machines. There are two kinds of excitation, either by permanent magnets or by wound field. As the wound field synchronous generator uses current to excite the rotor windings, slip rings and brushes are required to be mounted on the generator shaft. Therefore, recently the high performance of self excited PMSG based wind turbine with full-scaled power converter, shown in Figure 1.14, becomes dominant for high power rating applications.

Compared to wound rotor, another advantage of the permanent magnet rotor is its higher pole pairs [DDer 13]. The direct-drive multi-pole design of PMSGs avoids the use of gearbox and slip ring which enables a more compact and robust system, highly suitable for offshore applications. Recent falling price of the permanent magnets increases the use of PMSG for high power rating wind turbines [Mada 13]. Therefore, the PMSG is a clear trend for further high power wind turbines.

A PMSG with a high number of pole-pairs with no gearbox has been adopted by Siemens (SWT-6.0-120), GE Energy (4.1-113), Alstom (Haliade 150 sold to GE Energy in 2015) [Mada 13]. The stator of the PMSG is wounded like the DFIG. However, it is connected to the grid via a full-scale B2B voltage source converter which decouples the generator and the grid. Because of the full-scale design, the wind turbine is able to operate at optimal efficiency in larger wind speed range than the DFIG solution (because of its converter, sized around 30% of its nominal power). Furthermore, the converter allows the control of active and reactive powers independently at the turbine side.

The power converter used for the PMSG is therefore more expensive than for the DFIG. However, the cost is compensated by the elimination of the gearbox [DDer 13]. Moreover, the efficiency of the PMSG is higher than other types of generators as the excitation is provided without any energy supply [Mich 08], [Acke 05].

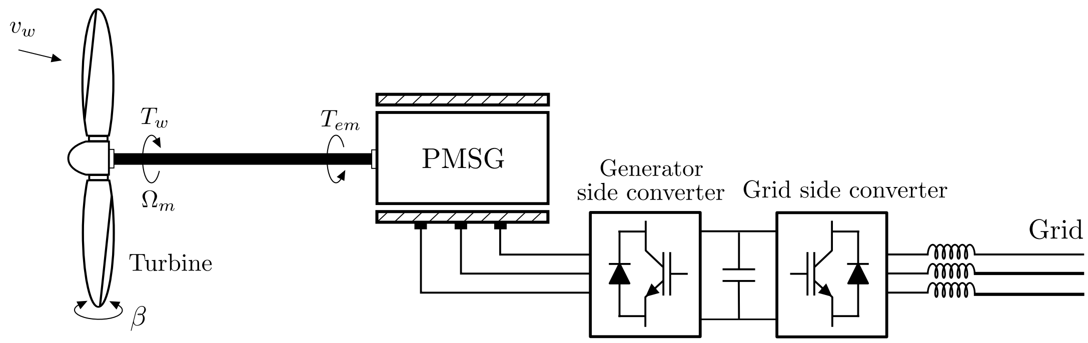

Figure 1.14 – Variable-speed wind turbine using a PMSG and a full-scale power converter.

1.2.4.4 Wind turbine with DC output

In the recent years, several configurations of wind turbines with DC outputs heve been proposed in the literature [Lund 06][Meye 07a][Max 09][Monj 12]. Aiming to connect the wind turbines directly into a pure DC wind farm. Most proposed configurations follow the scheme shown in Figure 1.15. It uses a PMSG followed by an active or passive rectifier, and a DC/DC transformer to step up the voltage level as well as to provide galvanic isolation. The active rectifier shown in the figure is based on full bridge VSC-based IGBTs, which provides full control capability of the active and reactive powers generated by the PMSG. This operates in the same ways as in the conventional PMSG-based wind turbine with AC output.

Conventional wind turbines which normally have AC transformers at their outputs to step up voltage level before being connected to the grid, are different from the DC wind turbines output voltages that are stepped up by high power DC/DC transformers. There are proposals using simple buck or boost converters [Veil 14], but the most adopted is the configuration with a DC/AC inverter and an AC/DC rectifier interfaced through a transformer in order to provide insulation to the wind turbine.

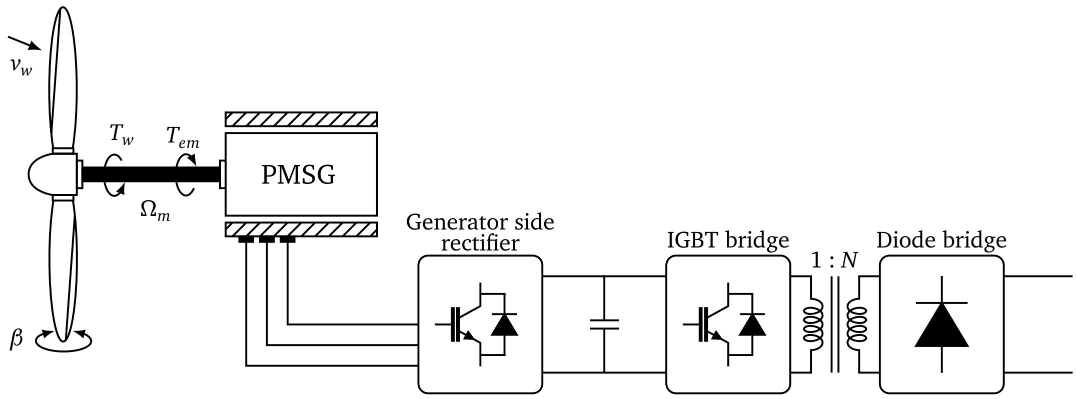

Figure 1.15 – General structure of a wind turbine for series connection

1.3 Offshore power collection system

The power generated by the wind turbines has to be transmitted to onshore grid in order to be used. Connecting each of the wind turbines directly to the grid is not only low efficient but also expensive. Instead, wind power is generally collected at offshore and brought it to a central collection point. Hence, the collected power is transmitted to onshore together using only one link. The interconnection of individual wind turbines and the gathering of the total generated power in a collecting point for transmission is called power collection system. Several proposals of collection systems, both in AC and DC, are reviewed in this section.

1.3.1 MVAC collection system

There is a variety of Medium Voltage Alternating Current (MVAC) collection system topologies available in the literature. Here we introduce two topologies that can be found in both literature and in existing projects. The most practical and straightforward is the *radial type* collection configuration. In the radial collection system, several wind turbines are connected in parallel to a feeder cable in a string configuration.

The feeder cable carries all the generated power in this string to the hub where they are gathered and transformed. The number of wind turbines in each feeder is not necessarily the same but should respect the maximum power rating of the cable. Since the current is higher at the hub end than at the end of the feeder, the feeder can use cables with different conductor cross-sections. Radial collection system is simple to control, needs low investment on submarine cables and switch gears, while its reliability is relatively low since faults at hub end will cause full feeder power generation loss [Bahi 12].

The radial collection system is used in the on-going wind farm project "Banc de Guérande", with 80 wind turbines of 6 MW power, off the coast of Saint Nazaire, France since 2015 [Banc 15] as shown in Figure 1.16. The voltage level of the MVAC collection system is typically 33 kV [Mada 13], so as the voltage level used in the "Banc de Guérande" project. The number of strings in this project is 14 and in each string there are 5 or 6 wind turbines. As a result, the power rating of the feeder at hub end is 30 MVA or 36 MVA. The nominal current in the feeder cable I_{feeder} is calculated as:

$$I_{feeder} = \frac{\frac{S_{MVA}}{3}}{\frac{U_{L-L}}{\sqrt{3}}} = \frac{30\ (36)\ MVA}{\sqrt{3} \times 33\ kV} = 525\ (630)\ A$$

The *ring type* collection grid configuration is a high reliable solution. Its improved security comes from an extra cable connecting the furthermost wind turbine to the hub. In case of break down of the feeder at any point of the string, the ring feeder is physically separated into two radial feeders and thus the lost of the entire feeder power generation is avoided. However, in the ring type layout, feeder cables need to have the same conductor cross-sections to withstand the full feeder power rating. Figure 1.17 is an example of double-sided ring collection system which is used in Amrumband West offshore wind farm[Fact 11].

1.3.2 MVDC collection system

The development of HVDC technology in long distance energy transmission has intensified the research on the design of MVDC collection systems. The idea is to use DC in the whole wind farm generation system (wind turbine with DC output, DC collection system and DC transmission system), which shows advantages regarding low cable losses, more compact components, higher reliability and lower cost of maintenance [Meye 07b].

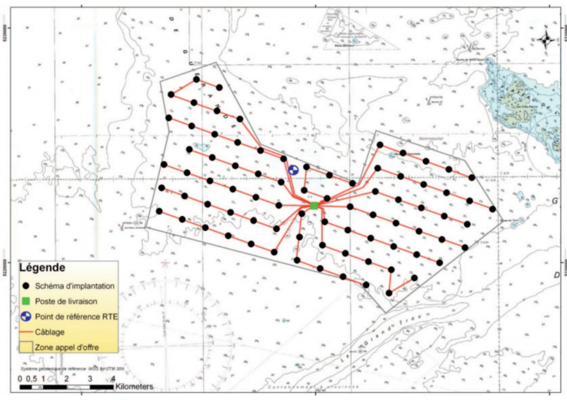

Figure 1.16 – Offshore wind farm "Banc de Guèrande" near Saint Nazaire, France.

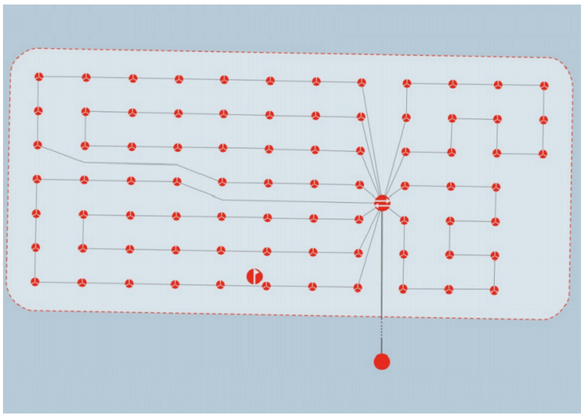

Figure 1.17 – Offshore wind farm "Amrumbank West" at the German North Sea.

However, an offshore wind farm using pure DC is still a topic of research and not yet adopted in the industry.

Theoretically, all the layouts for MVAC collection systems can be used for DC collection systems. For example, [Shao 10] presents the layouts of DC collection systems which are identical to the AC collection system layouts shown by [Bahi 12], except that the voltage step up component in the DC collection grid involves DC/DC converters, rather than AC power transformers.

Although actual projects are not available, there are some specific considerations for DC collection systems [Mada 13]:

1. Number of DC/DC transformation steps (see Figure 1.18a and 1.18c);
2. Possible series connection of wind turbines with DC outputs (see Figure 1.18d).

Collection systems, in Figure 1.18a and 1.18b use one step-up stage. The drawback of using one step-up stage is the low voltage level either in the collection system or in the transmission system. Figure 1.18a uses wind turbine DC/DC converters to increase the voltage level directly to the transmission level. With today's available medium voltage rectifier (AC: 3.3 kV to 4 kV AC or DC: 5 kV to 6 kV [Lise 11]), this configuration would lead to very high transformation ratio. Configuration shown in Figure 1.18b has the same issue of high transformation ratio in the centralized converter. In additional, the medium voltage (5 kV to 6 kV) in the collection system would cause high power losses in the cables.

To avoid too high transformation ratio and too low system voltage, there are two possible solutions. One straightforward solution, in Figure 1.18c, is to have two step-up stages similar to the conventional AC collection grid. Its advantages are the usability of medium voltage power converters in the wind turbines, reasonable transformation ratio in the centralized converter. Its disadvantages are more power electronic components, leading to higher losses and increased cost. Another solution is to use only one step-up stage, but connecting the dispersed converters in series, as in Figure 1.18d. This topology is first studied in [Lund 06].

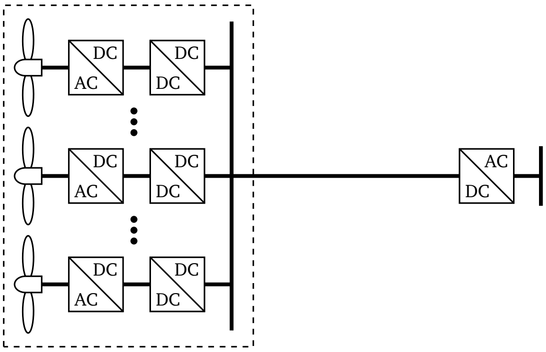

(a) One step-up stage with dispersed converters in parallel.

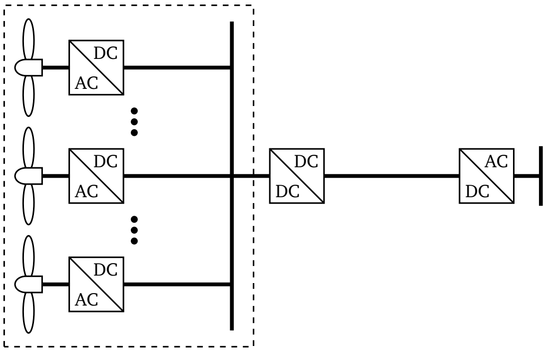

(b) One step-up stage with one centralized converter.

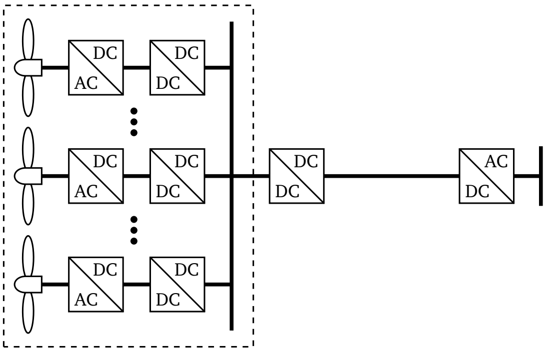

(c) Two step-up stages with dispersed converters in parallel and one centralized converter.

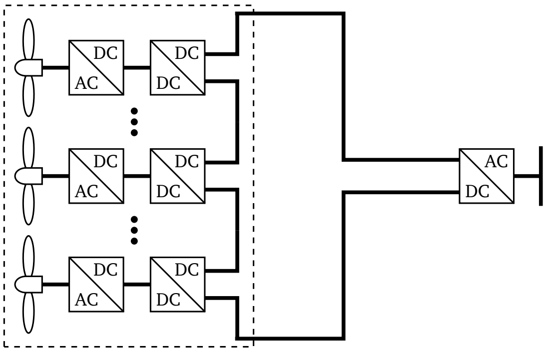

(d) One step-up stage with dispersed converters in series.

Figure 1.18 – Configuration of DC collection grid.

Whereas topology in Figure 1.18a requires the wind turbines output voltages to be increased to high voltage at several hundred kilovolts, the series connection allows voltage step-up in the wind turbines to medium voltage around 30 kV. Although megawatt-rating medium frequency DC/DC converters are not yet commercially available, it is much more achievable than the first solution. The disadvantage is the constraint of wind turbines sharing the same current, leading to a variable output voltage. As a result, the DC/DC converter in this configuration must have the capability of varying its output voltage.

1.4 Power transmission system

In order to transfer power from offshore collection point to onshore grid, both HVAC and HVDC transmission can be used. Some papers also mention small wind farms using lower AC voltage level for transmission[Lund 06], however it is not considered here since that transmission at this voltage level leads high losses, which is not practical for distant offshore applications. Some other alternative technologies are also introduced below.

1.4.1 HVAC transmission

HVAC transmission system possesses one offshore and one onshore station interlinked by three-phase submarine cables. Both stations include power transformers to step up and step down the voltage to different levels. The general configuration of HVAC transmission of offshore wind farm is shown in Figure 1.19.

One critical problem of HVAC transmission is its power transmission capability. This is particularly true for underground or submarine transmission. The reactive power generated by the cable shunt capacitance is significant. It is reported in [Burg 08] that the overhead line has a capacitance from 9 to 14 nF/km, while underground cable capacitance ranges from 200 to 300 nF/km. Typical charging current in the case of 380 kV underground cables is significantly high at about 15 A/km.

The capacitance of submarine cables is higher due to close laying and high dielectric constant of the insulation of cables. A cross section of a 3-core belted type AC cable is shown in Figure 1.20. It can be seen that the shunt capacitors are present between cable phases as well as between cables and sheath. By performing Δ−Y transformation, the cable shunt capacitor C_c is a combination of core-to-sheath capacitor C_{cs} and core-to-core capacitor C_{cc}:

$$C_c = C_{cs} + 3C_{cc} \tag{1.9}$$

For submarine high voltage applications, the cables are generally single cored and separately laid, and hence have their own insulation and sheath. The capacitor between core-to-core is thus much smaller than the core-to-sheath capacitor.

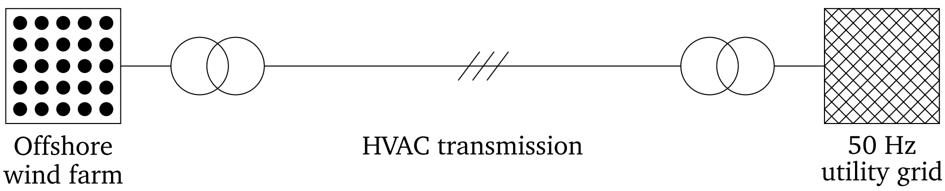

Figure 1.19 – HVAC transmission for offshore wind farm.

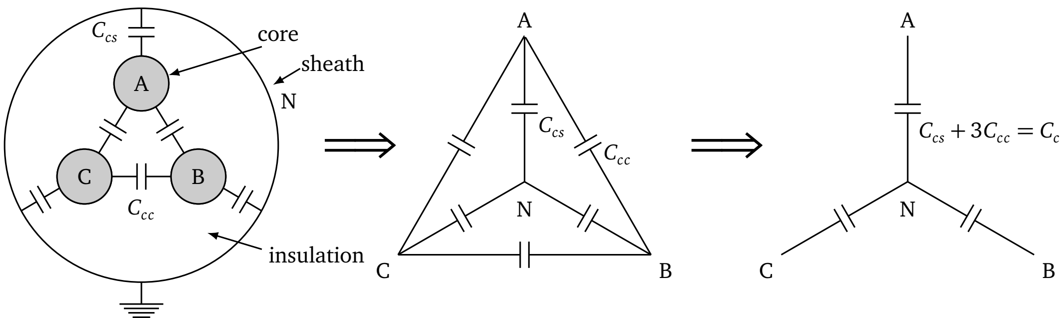

Figure 1.20 – Distribution of shunt capacitors in a 3-core belted type AC cable.

The HVAC cables with single core separate laying are shown in Figure 1.21.

The potential difference equals the AC phase to ground voltage U_{L-N} as the metallic sheath needs to be grounded. Hence the charging current I_{charge}:

$$I_{charge} = \frac{U_{L-N}}{X_c} = \frac{1}{X_c}\frac{U_{L-L}}{\sqrt{3}} = 2\pi f_g c_c l_c \frac{U_{L-L}}{\sqrt{3}} \tag{1.10}$$

$$P_{c,max} = 3\frac{U_{L-L}}{\sqrt{3}}\sqrt{I_{nom}^2 - I_{charge}^2} = \sqrt{3}U_{L-L}\sqrt{I_{nom}^2 - I_{charge}^2} \tag{1.11}$$

where

U_{L-N} = phase to ground voltage (V)
U_{L-L} = phase to phase voltage (V)
f_g = grid frequency (Hz)
c_c = shunt capacitance per kilometer (μF/km)
l_c = cable length (km)
$P_{c,max}$ = maximum transmissible active power (W)

According to equations (1.10) and (1.11) and the cable parameters listed in Table 1.1, the maximum transmissible active power in a cable of 100 km and 220 kV is 295 MW out of 402 MVA cable power capacity. This indicates that HVAC cables must be sized above the nominal active power they are supposed to carry. The charging current becomes considerable large as the cable length increases and there will be no transmission capacity available for the active power [Negr 06], [Monj 12] and [Acke 05]. The cable distance limitations of HVAC cables under two voltage levels are reported in Figure 1.22. It is expected that with the increase of voltage level and of transmissible power, the transmission distance is reduced.

Hence, for longer transmission distance, additional reactive compensation equipments such as shunt capacitor banks, Static Var Compensator (SVC) or STATic synchronous COMpensator (STATCOM) are required to improve the active power transmission capacity [Chen 09]. For underground cable, the compensation units are installed section by section between the

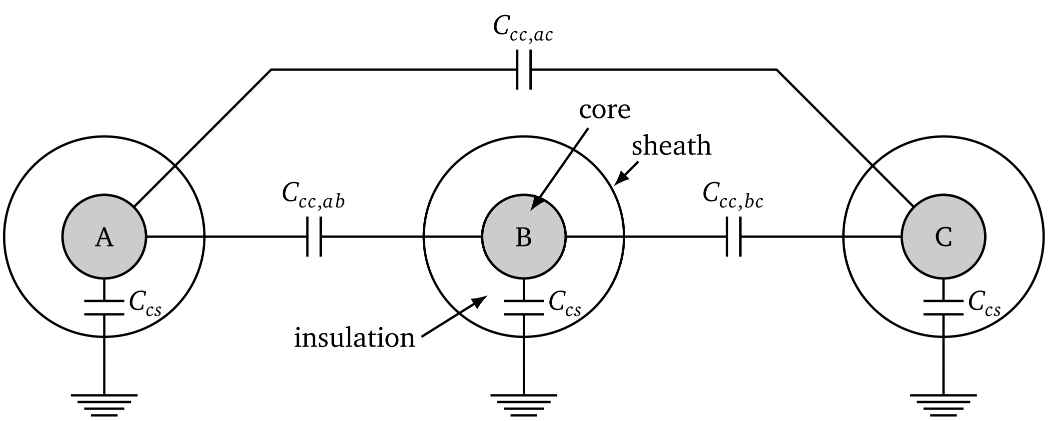

Figure 1.21 – Distribution of shunt capacitors in three-phase single core HVAC cables.

	220 kV	400 kV
Cable section (mm^2)	1000	1200
Nominal current (A)	1055	1323
Resistance (mΩ)	0.048	0.046
Inductance (mH/km)	0.37	0.39
Capacitance (μF/km)	0.18	0.18

Table 1.1 – HVAC cable parameters rated at 220 kV and 400 kV [Negr 06].

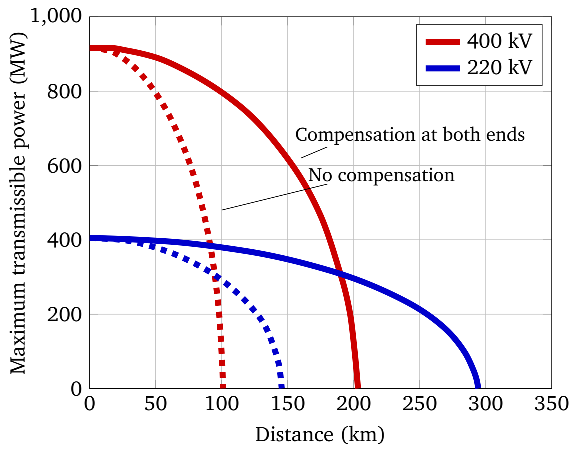

Figure 1.22 – Transmission capabilities of HVAC with variation of the cable length.

two terminals of the cables; while for offshore submarine cable, the installation of compensation devices between terminals is not possible. They are only placed either onshore or offshore, or in both [Monj 12].

Nevertheless, HVAC is a proven technology and is still the most suitable solution for the connection of offshore wind farms located at relatively short distance from land. However, with the emergence of offshore wind farms located more than 100 km, HVAC is not technically feasible at 50 Hz or 60 Hz frequency.

1.4.2 HVDC transmission

HVDC becomes more efficient than HVAC in long distance submarine transmission. HVDC transmission is free from reactive power and uses less cables than HVAC. Whereas HVDC transmission requires higher initial installation cost on its AC/DC and DC/AC converter station, the investment cost for HVDC transmission lines or cables is lower. The power losses due to HVDC converters are relatively high but they do not vary with distance [Rude 00]. On the contrary, the power losses increase significantly with the increase of length of HVAC cables. This results in the well-known break-even distance: at approximately 50 km using underground cable or 400 km using overhead lines [Siem 11][Bres 07][Acke 05], HVDC is cheaper in total.

Costs versus the break-even distance of HVDC transmission is plotted in Figure 1.23. This figure shows a cost comparison of HVAC and HVDC transmission taking into account:

1. Costs of AC transformer stations and DC converter stations
2. Costs of HVAC lines and HVDC cables
3. Power losses in capitalized values of AC transmission and DC transmission.

Currently, wind park projects using HVDC offshore transmission are constructed about

100 km away from the German coast in the North Sea. Those HVDC offshore projects are listed in Table 1.2 and are also shown in Figure 1.24 as green dots. It can be noticed that the distance of these projects from shore are all around or outside of the HVAC transmissible limit. At such distance, HVDC becomes the only feasible solution to collect the remote wind energy.

The general HVDC transmission configuration is plotted in Figure 1.25. The wind power is first sent into an AC collection system and converted into DC power at an offshore AC/DC substation. At the other end, an onshore converter station receives the DC power and converts it into the AC grid.

Depending on the commutation technologies, HVDC converters are divided into two main categories: Line Commutated Converter (LCC) and Voltage Source Converter (VSC). The economic and technical comparisons of LCC and VSC are given in many works [Erli 13], [Reed 13]. The VSC technology is particularly favourable for offshore wind farm applications since its capability of bidirectional power flow almost instantaneously by changing the current direction, black start ability after grid failure, independently control of active and reactive powers, considerably smaller footprint, etc. The disadvantages of classical VSC are higher losses resulted from the high switching frequency of self-commutated devices by using of the Pulse Width Modulation (PWM). Loss rate is about 3% and 2% in conventional two-level and three-level VSC [Du 07],[Bres 07],[Bahr 08] and [Mada 13]. This is the main

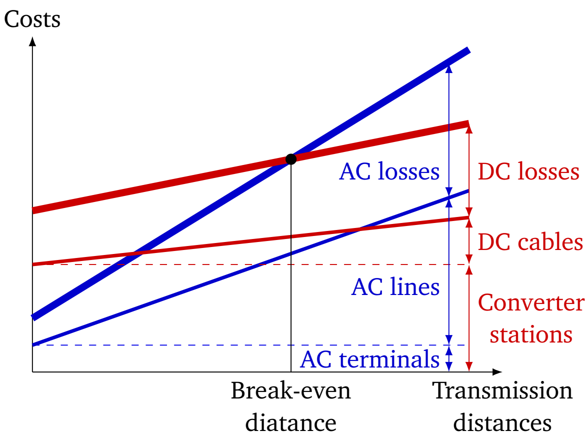

Figure 1.23 – Cost of HVAC versus HVDC transmision.

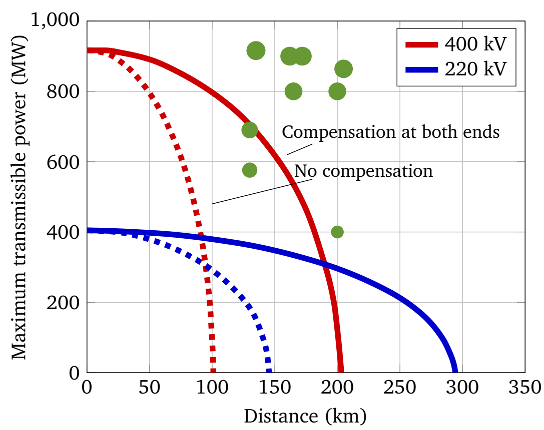

Figure 1.24 – Transmission limitation of HVAC and HVDC offshore wind farms (green dots).

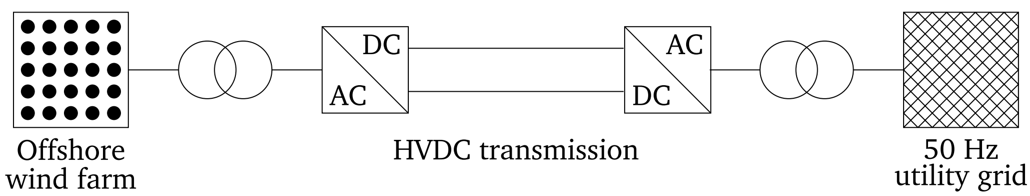

Figure 1.25 – HVDC transmission for offshore wind farm.

reason that has prevented it from being used in very high power rating transmission in the last two decades.

The MMC has recently proved itself to be a superior option of voltage source converter for HVDC transmission since it offers considerable electrical and operational advantages [Sami 16], [Huss 12] and [Li 11]. The losses of MMC conversion station can be as low as 1% loss rate per station [Huss 12] and [Rohn 10]. The low power losses enables MMC to handle higher power rating as shown in the Table 1.2. Only one 2-level VSC is used in the BorWin1 project which is rated at 400 MW. MMC stations are also more compact. It does not need harmonic filter on the AC side as it ensures nearly perfect sinusoidal AC voltage waveform.

1.4.3 Other transmission methods

HVAC and HVDC are the two transmission methods that can be found in industrial applications. The HVAC transmission is relatively cheap and simple in short distance offshore applications while it is not feasible for long distance power transmission. Although HVDC is thus dominating in projects of long transmission distance as discussed before, it still has technical challenges to be solved, such as cheaper HVDC breakers (the hybrid HVDC circuit breaker developed by ABB costs 20-30% of the cost of full VSC AC/DC converter [Jovc 11]), high power high voltage DC/DC converters and DC grid fault clearing strategies [Van 10].

In the interest of seeking alternative transmission solutions, some studies have contributed to improvements on either HVAC or HVDC transmission, described below.

1.4.3.1 LFAC transmission

LFAC stands for Low Frequency Alternating Current (LFAC), also named as Fractional Frequency Transmission System (FFTS), uses lower frequency than the utility frequency for

Table 1.2 – List of offshore wind farms using HVDC technology [Pier 17].

Project	Status (to date 2017)	Power (MW)	Cable length (km) Submarine	Cable length (km) Underground	Voltage (kV)	Converter
BorWin1	In commission	400	125×2	75×2	±150	ABB 2-level
BorWin2	In commission	800	125×2	75×2	±300	Siemens MMC
BorWin3	In construction	900	130×2	30×2	±320	Siemens MMC
DolWin1	In commission	800	75×2	90×2	±320	ABB CTLC
DolWin2	In commission	916	45×2	90×2	±320	ABB CTLC
DolWin3	In construction	900	79×2	83×2	±320	Alstom MMC
HelWin1	In commission	576	85×2	45×2	±250	Siemens MMC
HelWin2	In commission	690	85×2	45×2	±320	Siemens MMC
SylWin1	In commission	864	160×2	45×2	±320	Siemens MMC

power transmission in order to introduce less charging current in the cables. The low frequency idea has been already used in other applications. For example, railway electrification systems in Germany and Switzerland use 50/3 Hz [Fisc 12] and those in USA use 25 Hz [Acke 05].

If 16.7 Hz AC is adopted for offshore wind farm transmission, the low frequency can be applied in both collection and transmission systems as shown in Figure 1.26. At onshore side, an AC-AC converter should be used to transform the low frequency into the frequency of the onshore power grid.

AC/AC converter proposals in the literature for LFAC Systems are categorized into converters with DC link and without DC link. A classical AC/AC converter without DC link is the cycloconverter using a Back-to-Back (B2B) connection of two thyristor bridges. This converter has practical use in today's large applications but it is bulky and of bad performance. A summary of other AC/AC converters based on full-controlled power switched are listed in the following [Anto 17]:

- Direct or indirect Matrix converters;
- Two-level VSC based B2B AC/AC converter;
- MMC-based B2B AC/AC converter;
- MMC-based direct AC/AC converter.

The main advantages of a low AC frequency approach lie in three areas:

1. For the transmission system: At a low frequency, the amount of charging current and subsequent reactive power would be significantly lower. Therefore, the system is accessible to longer distance compared to HVAC at normal grid frequency. To explain the impact of the frequency on the cable charging current, Equation 1.10 is rewritten here:

$$I_{charge} = 2\pi f_g c_c l_c \frac{U_{L-L}}{\sqrt{3}} \tag{1.12}$$

As the frequency is 1/3 of the normal frequency, it leads to only 1/3 charging current.

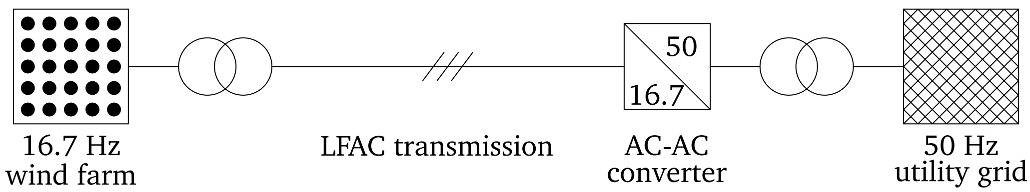

Figure 1.26 – LFAC transmission for offshore wind farm.

2. Same as the HVAC transmission, the LFAC has zero-crossing of the current so that commercial AC circuit breaker can be used in the LFAC applications.

3. For the collection system: The mechanical design of the wind turbine can be simplified. The wind turbine rotational speed is slow due to aerodynamic reason. For this fact, direct drive PMSG is usually designed to be multipoles and DFIG is equipped with a high ratio gearbox in order to operate at 50 Hz. The low frequency allows direct-driven PMSG to have less pole pairs and DFIG to have lower ratio gearbox.

Nevertheless, the feasibility of LFAC is still being discussed. The main concern is related to the sizes of the transformers and the AC/AC converter.

1. Although the wind turbine design can be simplified, the difficulty of re-design the power transformer is increased. This transformer takes a larger size and weight which may offset the benefit of simplified mechanical design of the wind turbine.

2. The sizing problem also arises to the offshore substation. For the same power rating, lower frequency requires a larger size transformer, and therefore transformers will be more expensive [Liu 15]. This is not practical for offshore station since the installation of the transformer requires a very large supporting platform. Table 1.3 shows a comparison of a 200 MVA transformer at 50 Hz and 16.7 Hz [Rudd 16]. The size, weight and cost of a 16.7 Hz transformer are almost the triple of those of a 50 Hz transformer.

3. The switching of direct AC/AC converter is complex and its use for high power is not fully mastered. The VSC-based and MMC-based B2B AC/AC converters are bulky and not suitable for offshore applications, while the potential candidate MMC direct AC/AC converter is still far from industrial applications.

Table 1.3 – Comparison of a 200 MVA transformer at 50 Hz and 16.7 Hz.

Frequency (Hz)	Size (m^3)	Weight (t)	Cost (M€)
16.7	157	374	15
50	53	125	5

1.4.3.2 Diode-based HVDC transmission

Recently, a Point-to-Point (P2P) HVDC link structure based on the diode rectifier, shown in Figure 1.27, has been proposed to connect PMSG-based offshore wind farm to onshore grid [Blas 11] [Blas 10]. This system has several advantages such as cost savings in equipment, high reliability and efficiency. However, the diode rectifier induces large current harmonics, so that a big filter bank is required [Nguy 14].

Due to the uncontrollability of the offshore diode bridge, there are restrictions to control the offshore AC collection grid voltage. One solution is to use the wind turbine generator side rectifier to control the DC link voltage of the wind turbine, whereas the output converter accomplishes the AC collection grid regulation. But this indicates that MPPT control of wind turbines cannot be achieved.

An improvement of above topology is the hybrid topology proposed in [Nguy 14], which comprises a series connection of a 12-pulse diode rectifier with a VSC at offshore side as shown in Figure 1.28. This topology improves the controllability of the system compared to the previous non-controlled diode bridges, by using the offshore VSC to control the AC collection grid voltage at constant magnitude and frequency. It also functions as an active filter to absorb current harmonics. Each offshore converter bridge shares one third of the nominal power rating of the wind farm. For a 500 MW wind farm, a VSC rated at 167 MW is thus used and the rest is distributed on the 12-pulse diode rectifier.

This topology has the same footprint requirement as the full-scale rating VSC, while the cost of power semiconductor devices and gate drivers is reduced to 53.47% [Nguy 14]. The diode based HVDC link is further investigated by Siemens to participate in MTDC grids, as shown in Figure 1.29. The wind power is first collected in the substations with small footprint at offshore. It is claimed to potentially reduce 80% topside volume, 20% transmission losses and save as much as 30% overall cost, compared to conventional VSC transmission technology with a centralized offshore substation [Siem 15].

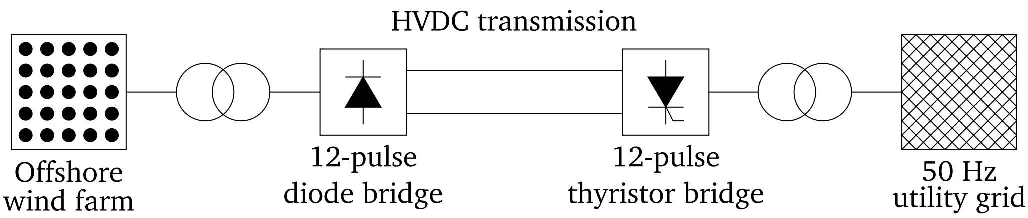

Figure 1.27 – Point-to-Point HVDC link based on diode rectifier.

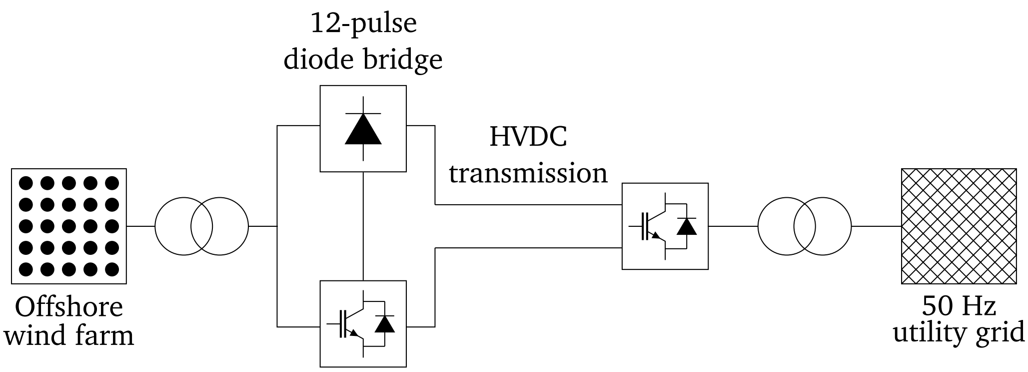

Figure 1.28 – Improved Point-to-Point HVDC link based on a hybrid offshore converter which comprises a diode rectifier and a VSC.

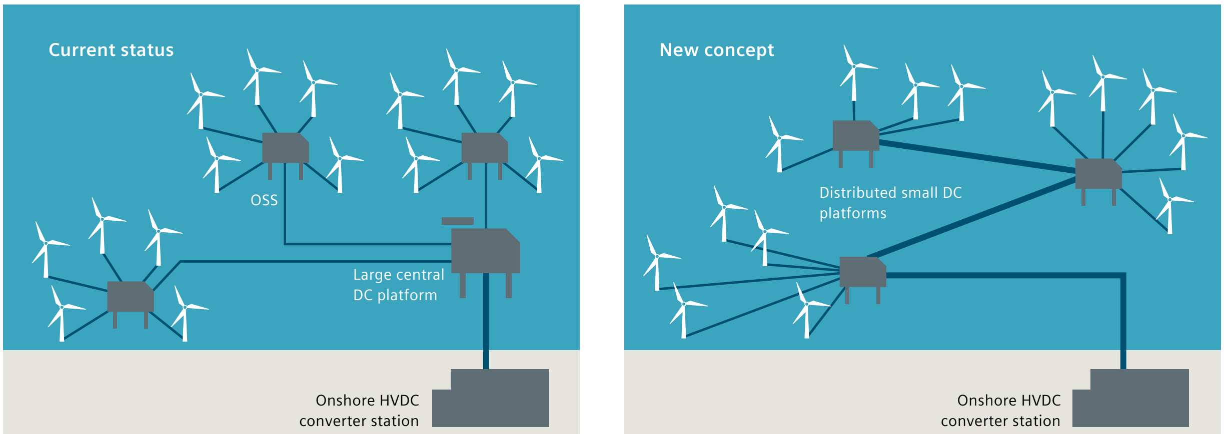

Figure 1.29 – DC grid topology based on diode rectifier transmission proposed by Siemens [Flye 15].

1.5 Topologies of large wind farms

This section introduces and compares suitable solutions for large offshore wind farms. Theoretically, the offshore wind farm can adopt the architecture of either combination of aforementioned collection and transmission systems, but not all of those combinations are economically or technically reasonable. For example, if the transmission system is in AC, there is no point of using a DC collection, which causes unnecessary power conversion. Furthermore, the LFAC and diode-based HVDC transmission are not considered in this section due to their disadvantages explained in Subsection 1.4.3 and lack of sufficient studies in the literature.

The most practical and interesting solutions for large offshore wind farms are: pure AC collection and transmission system (Figure 1.30a), pure DC collection and transmission system (Figure 1.30c), hybrid system (Figure 1.30b) and pure DC with series converters solution (Figure 1.30d).

1.5.1 Solution 1: MVAC-HVAC

The first topology represents the most common offshore wind generation electrical system so far. Such offshore wind farms use AC in both collection and transmission system, as shown in Figure 1.30a. The transformer inside the wind turbine first increases the produced AC voltage (typically 690 V for low power rating wind turbines and 3.3 kV for high power rating wind turbines [Lise 11]) to MVAC (typically with voltage range of 20-30 kV) and then the power is gathered at the hub, where a substation transformer converts the MVAC voltage to HVAC for transmission. As mentioned in Subsection 1.4.1 this solution, because of the use of HVAC transmission, is not a suitable choice for wind farms located more than 50-100 km from shore. Within these distances, reactive power compensation equipments are still necessary to improve the power quality [Chen 09].

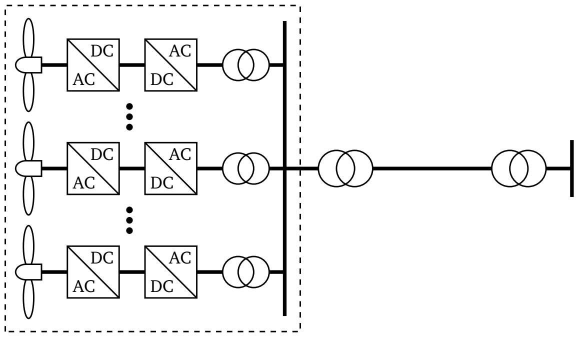

(a) Solution 1: MVAC-HVAC.

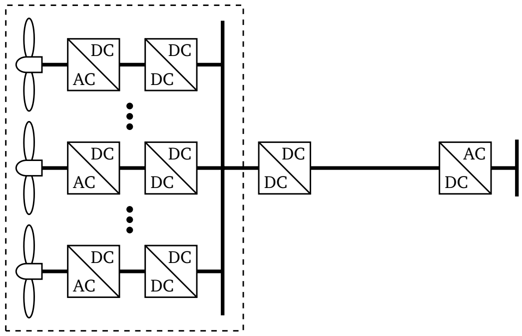

(b) Solution 2: MVDC-HVDC.

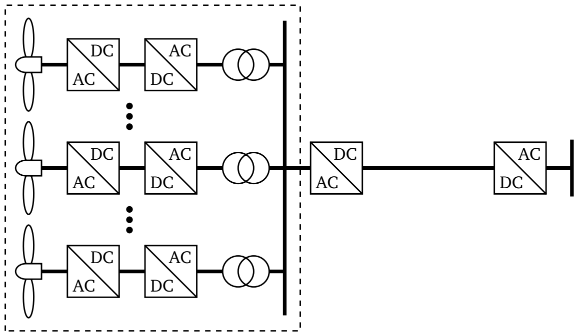

(c) Solution 3: MVAC-HVDC.

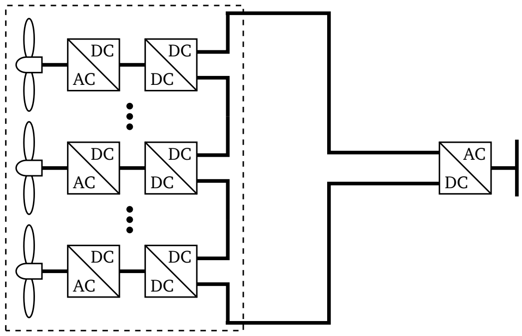

(d) Solution 4: Series Parallel-HVDC.

Figure 1.30 – Wind farm topologies for long distance transmission.

1.5.2 Solution 2: MVDC-HVDC

The overall arrangement of the solution MVDC/HVDC is very similar the MVAC/HVAC topology, except that the AC cables are replaced by DC cables, and the traditional transformers are replaced by DC/DC converters. Figure 1.30b shows a MVDC/HVDC topology using a DC/DC converter inside each wind turbine and also a DC/DC converter between the collection system DC bus and transmission system HVDC link.

In this topology, each wind turbine can be individually controlled by its own DC/DC converter. The DC voltage level in the collection system is controlled by the offshore substation. The transmission voltage is thus controlled by the onshore converter. This topology is a reasonable DC solution since the voltage levels between different stages are not very large, as explained previously in Subsection 1.3.2.

1.5.3 Solution 3: MVAC-HVDC

Figure 1.30c shows the MVAC-HVDC topology which is another type of wind farm that can be found in commission and in planning. The collection system is in AC which enables the use of existing wind turbine technologies. The DC transmission is used in order to cope with the problem related to the production of high reactive power by AC cables in long distance transmission.

All the offshore projects summarized in Table 1.2 [Pier 17] propose to install an offshore converter substation to transfer AC voltage produced by the wind turbines to DC, and transmit the power through submarine cables to the onshore side. On the other end, an onshore converter transforms the power from DC to AC and injects it into the AC grid. The AC voltage in the collection system is controlled by the offshore rectifier station and the transmission voltage is controlled by the onshore inverter station.

1.5.4 Solution 4: Series Parallel-HVDC

As the offshore converter substation demands a large initial investment on the offshore platform and maintenance during service, a possible solution is the series or series parallel topology proposed in [Lund 06] (Figure 1.30d). This topology does not require an offshore centralized substation. As mentioned in Subsection 1.3.2, this wind farm connects the output converters of wind turbines to reach the HVDC transmission voltage level without using a centralized conversion step. The parallel connection of several clusters increases the overall wind farm power.

1.5.5 Comparison of solutions

Wind farms with above 4 architectures are compared in [Monj 12] regarding cables length and weight, wind farm overall losses and energy availability. All 4 offshore wind farms are supposed to be located at 100 km offshore, comprising 40 wind turbines of 5MW rated power capacity. These 40 wind turbines are placed in a 7 km × 4 km offshore site. The distance between each unit is 0.9 km. The series parallel architecture used in this comparison has 2 clusters with 20 wind turbines in each cluster. Selection of different number of clusters has very few influence on the cable costs and losses, but does has influence on the wind farm power availability.

1.5.5.1 Cables cost

The cables used in the comparison are selected from technical aspects [ABB 06] according to their required ratings. The result in Table 1.4 shows that HVDC transmission needs lower amount of copper than HVAC transmission, which is reasonable since HVDC uses less number of cables.

Solution 4 Series Parallel-HVDC has advantages regarding cable copper weight thanks to its unique collection system. Moreover, if only the cables used in the collection system are considered, the solution 4 needs 61 tons of cables, only one third of that used in traditional MVAC collection systems as solutions 1 and 2.

Table 1.4 – Cable conductor weight of 4 topologies

	Transmission			Collection			Total
Solution	Type	Voltage (kV)	Weight (t)	Type	Voltage (kV)	Weight	Weight
1	HVAC	184	803	MVAC	33	166	969
2	HVDC	±150	535	MVDC	±25	116	651
3	HVDC	±150	535	MVAC	33	166	701
4	HVDC	±150	535	SP	-	61	596

1.5.5.2 Centralized converters and platforms

The construction of the centralized power converter is expensive and difficult. For example, it is reported in [IREN 16] that the HVDC platform deployed by the DolWin 2, designed to connect three wind farms, has a mass about 20,000 tonnes. The cost model in [Lund 06] indicates that only the platform for a 300 MW converter costs at least €25 million. The Kriegers Flak offshore wind farm is the first European wind farms that interconnects two asynchronous utility grids. The original plan of this project was to place one HVDC converter offshore. However, this plan was abandoned due to under-estimation of the offshore converter substation cost. Instead, the project placed two converters B2B in the German coast.

The number of offshore platforms of the four wind farm topologies are listed in Table 1.5. Solutions 1-3 require both offshore and onshore stations while solution 4 takes the advantage of eliminating the offshore platform.

1.5.5.3 System Losses

The power losses are present in all electrical components in the wind farm. The comparison considers main power losses in the cables, transformers and converters. This consideration is justified, because the main differences among these 4 topologies are lie in these components. Other miscellaneous losses are similar and thus can be neglected due to their existences in every topology.

In Figure 1.31, the transformer losses are included in the converter losses. HVDC transmission has less cable losses than HVAC transmission, as expected. Thanks to the elimination of one offshore centralized converter, solution 4 Series Parallel-HVDC leads to the lowest converter losses and presents the lowest total losses among these four topologies.

Table 1.5 – Number of converter stations of four topologies.

Solution	1	2	3	4
Number of offshore substations	1	1	1	0

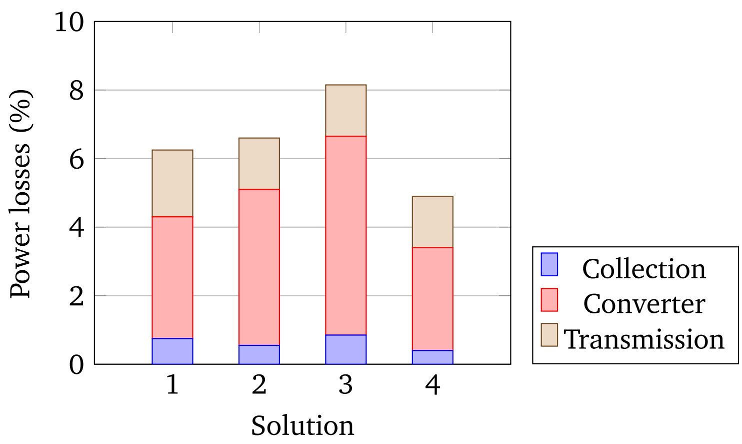

Figure 1.31 – Power losses of 4 wind farm topologies.

1.5.5.4 Energy availability

The energy availability is one important indicator to follow the performance of a wind farm. There are two approaches to define the wind farm availability, based on time and energy. Availability based on time is an easy and straightforward calculation method, while it is unable to take into account the energy produced by wind farms due to the variation of the wind speed. Especially for solution 4 which has a totally different structure, time based availability cannot reflect correctly the amount of energy production in this type of wind farm. In this comparison, the energy based availability is used:

$$\text{Energy availability} = \frac{\text{Energy transmitted}}{\text{Theoretical energy produced}}$$

Energy based availability is more valid to evaluate how much energy is transmitted to the Transmission System Operator (TSO) and makes possible to evaluate the wind turbine performance, whereas it requires more complex calculation. As can be seen from Table 1.6, the availability of wind farms adopting DC collection system is lower than that of AC collection systems. Furthermore, solution 4 exhibits the lowest availability since its series connection. However, the availability of solution 4 highly depends on the control strategy applied. The control strategy used in [Monj 12] supposes that wind turbines have no overvoltage capabilities. On the contrary, the strategy used in [Lund 06] supposes that wind turbine have, to some extent, overvoltage capabilities.

An illustrative example of the differences of power production by these two proposals

Table 1.6 – Availability of four topologies [Monj 12].

Solution	1	2	3	4
Availability	95%	94%	95%	82%

is shown in Figure 1.32. The wind turbine output power and voltage are 1 pu, and the HVDC voltage is 4 pu. In the former method, the loss of one wind turbine in cluster 1 leads to the reduction of the HVDC voltage to 3 pu and results in 1 pu extra power reduction in the cluster 2 as shown in Figure 1.32b. This is not necessary if the wind turbines have overvoltage capability in some extent, as proposed in [Lund 06]. In this case, the faulted unit only affects the units in its own cluster. As shown in Figure 1.32c, output voltages of units in the first cluster increase to 1.33 pu while those in the second cluster remain unchanged. As a result, the energy availability can be improved by using to a certain extent over-sized power converters in the wind turbines.

1.5.5.5 Consideration on the reliability of Series Parallel-HVDC solution

Reliability is a key factor for offshore wind farm performance. Although it is not possible to provide an accurate index for the Series Parallel-HVDC (solution 4) since no such wind farm has been applied yet, there are some estimations based on the experience data of the main components acquired from existing offshore wind farms. It is shown that the majority of failures of offshore wind farms happen on the local wind turbines units, submarine cables, offshore platform converters and circuit breakers. Only evaluating the reliability based on the main components by using basic techniques for series and parallel systems defined in [Alla 13], the authors of [Bahi 12] found that the reliability of DC series wind farm is fairly high due to shorter cumulative cable length and reduction of one offshore substation. Besides, it is reported that there were continuous accidents of the BorWin1 HVDC platform from the beginning of its service [Dirt 11], making the assumption that no offshore substation increase wind farm reliability in a more convincing way.

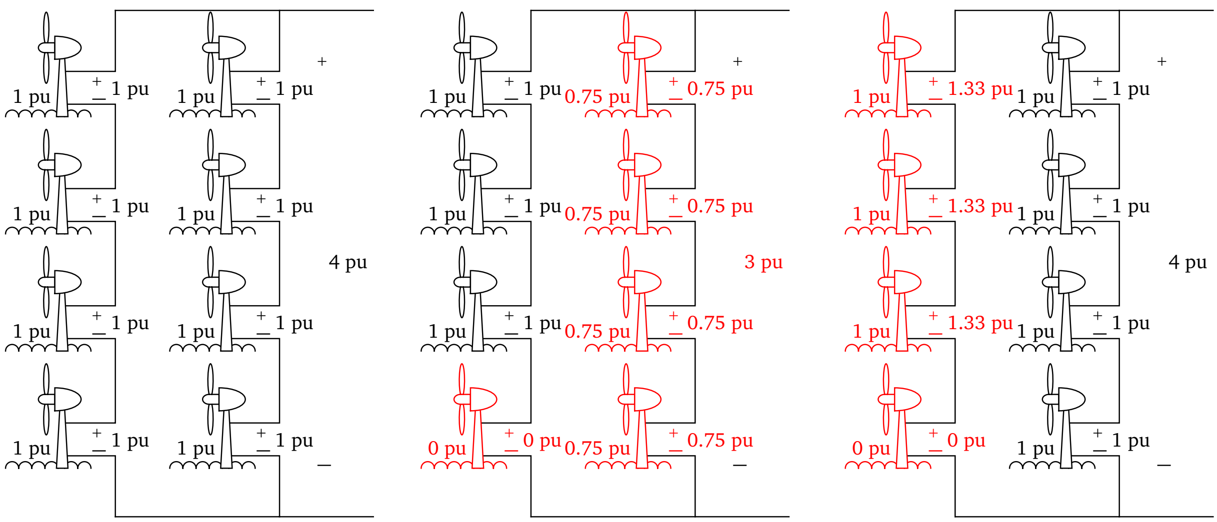

(a) Normal operation of 8 units in 2 clusters.

(b) Fault handling method in [Monj 12].

(c) Fault handling method in [Lund 06].

Figure 1.32 – Power production of a series-parallel offshore wind farm with different control strategies after one wind turbine is bypassed.

1.6 Conclusion

This chapter gives the state of art of offshore wind power systems. The most important elements for constructing an offshore wind farm are introduced. The chapter aims to overview current development of offshore wind farms and to find the potential cost reduction based on present-today technologies.

Currently it is generally accepted that the break-even distance between HVDC and HVAC for offshore wind farms is around 80 km. Most commissioned offshore wind farms so far are located near the sea coast, therefore P2P HVAC transmission links are the most common transmission method. VSC-HVDC P2P links are mostly constructed for long-distant wind farms. The MMC converters is now dominating the HVDC transmission. LFAC and diode based HVDC are proposed in the literature as candidates for long distance transmission, while no clear evidence has been found for its usage in offshore market. Hence, they are not further considered in this thesis.

After reviewing the collection and transmission systems, four offshore wind farm topologies are selected for comparison in [Monj 12]. A summary of these four potential topologies is presented in this chapter. Finally the series parallel topology is selected as the focus of this thesis because the following reasons:

1. The elimination of offshore centralized converter avoid the initial investment on the offshore platform;
2. An higher efficiency due to less conversion stages;
3. Less cables used in the collection system;
4. All above reasons lead to higher system reliability;
5. Less expenditure on the system maintenance.

The drawback of this Series Parallel-HVDC architecture is mainly related to the low availability resulting from its series connection. In Part 1.5.5.5, it is mentioned that over-sizing the wind turbine output converters can contribute to increase the availability of this architecture. It is further studied in the following chapters.

References

[ABB 06] ABB. *HVDC Light - Cables Submarine and land power cables*. 2006. 43

[Acke 05] T. Ackermann. *Wind power in power systems*. John Wiley & Sons, 2005. 18, 24, 25, 28, 34, 35, 38

[Alla 13] R. N. Allan *et al.* *Reliability evaluation of power systems*. Springer Science & Business Media, 2013. 46

[Anto 17] D. Antony. *Contrôle et Modélisation du Convertisseur Multi-Modulaire AC-AC pour les Liaisons Offshore à Haute Tension et Basse Fréquence*. PhD thesis, Univerté Grenoble Alpes, 2017. 38

[Bahi 12] H. J. Bahirat, B. A. Mork, *et al.* "Comparison of wind farm topologies for offshore applications". In: *Power and Energy Society General Meeting*, pp. 1–8, IEEE, 2012. 30, 31, 46

[Bahr 08] M. Bahrman. "HVDC transmission overview". In: *Transmission and Distribution Conference and Exposition, 2008. T&D. IEEE/PES*, pp. 1–7, IEEE, 2008. 36

[Banc 15] "Banc de Guérande, Projet de Parc Eolien au Large de Saint Nazaire". 2015. Available online at http://parc-eolien-en-mer-de-saint-nazaire.fr, accessed on 13/03/2017. 30

[Berh 16] C. Berhault, I. Le Crom, G. Le Bihan, and J.-M. Rousset. "SEM-REV, de 2007 à 2016, du projet au site opérationnel: retour d'expérience". In: *XIVèmes Journées Nationales Génie Côtier – Génie Civil*, pp. 467–476, 2016. 16

[Bilg 11] M. Bilgili, A. Yasar, and E. Simsek. "Offshore wind power development in Europe and its comparison with onshore counterpart". *Renewable and Sustainable Energy Reviews*, Vol. 15, No. 2, pp. 905–915, 2011. 13

[Blas 10] R. Blasco-Gimenez, S. Ano-Villalba, J. Rodriguez-D'Derlée, F. Morant, and S. Bernal-Perez. "Distributed voltage and frequency control of offshore wind farms connected with a diode-based HVdc link". *IEEE Transactions on Power Electronics*, Vol. 25, No. 12, pp. 3095–3105, 2010. 39

[Blas 11] R. Blasco-Gimenez, S. Ano-Villalba, J. Rodriguez-D'Derlée, S. Bernal-Perez, and F. Morant. "Diode-based HVdc link for the connection of large offshore wind farms". *IEEE Transactions on Energy Conversion*, Vol. 26, No. 2, pp. 615–626, 2011. 39

[Borg 14] M. Borg, A. Shires, and M. Collu. "Offshore floating vertical axis wind turbines, dynamics modelling state of the art. Part I: aerodynamics". *Renewable and Sustainable Energy Reviews*, Vol. 39, pp. 1214–1225, 2014. 17, 18

[Bres 07] P. Bresesti, W. L. Kling, R. L. Hendriks, and R. Vailati. "HVDC connection of offshore wind farms to the transmission system". *IEEE Transactions on energy conversion*, Vol. 22, No. 1, pp. 37–43, 2007. 35, 36

[Bret 09] S.-P. Breton and G. Moe. "Status, plans and technologies for offshore wind turbines in Europe and North America". *Renewable Energy*, Vol. 34, No. 3, pp. 646–654, 2009. 13

[Burg 08] K. Burges, J. Bömer, C. Nabe, G. Papaefthymiou, M. Maher, C. Mills, and J. Hunt. *Study on the comparative merits of overhead electricity transmission lines versus underground cables*. 2008. 33

[Burt 11] T. Burton, N. Jenkins, D. Sharpe, and E. Bossanyi. *Wind energy handbook*. John Wiley & Sons, 2011. 13, 14, 16

[Chen 09] Z. Chen, J. M. Guerrero, and F. Blaabjerg. "A review of the state of the art of power electronics for wind turbines". *IEEE Transactions on power electronics*, Vol. 24, No. 8, pp. 1859–1875, 2009. 24, 26, 27, 34, 41

[Cour 08] V. Courtecuisse. *Supervision d'une centrale multisources à base d'éoliennes et de stockage d'énergie connectée au réseau électrique*. PhD thesis, Arts et Métiers ParisTech, 2008. 18

[DDer 13] J. J. R. D'Derlée. *Control strategies for offshore wind farms based on PMSG wind turbines and HVdc connection with uncontrolled rectifier*. PhD thesis, Universitat politècnica de valència, 2013. 28

[Deep 14] "DeepWind Project". 2014. Available online at http://www.deepwind.eu/, accessed on 30/07/2017. 19

[Dirt 11] "Dirty electricity probe at Borwin1". 2011. Available online at http://renews.biz/68145/dirty-electricity-probe-at-borwin1/, accessed on 19/04/2017. 46

[Du 07] C. Du. *VSC-HVDC for Industrial Power Systems*. PhD thesis, Chalmers University of Technology, 2007. 36

[El A 04] S. El Aimani. *Modélisation des différentes technologies d'éoliennes intégrées dans un réseau de moyenne tension*. PhD thesis, Ecole Centrale de Lille, 2004. 23

[Erli 13] I. Erlich, F. Shewarega, C. Feltes, F. W. Koch, and J. Fortmann. "Offshore wind power generation technologies". *Proceedings of the IEEE*, Vol. 101, No. 4, pp. 891–905, 2013. 36

[Fact 11] "Factsheet Offshore Windpark Amrumbank West". 2011. Available online at http://www.eon.com, accessed on 13/03/2017. 30

[Fisc 12] W. Fischer, R. Braun, and I. Erlich. "Low frequency high voltage offshore grid for transmission of renewable power". In: *Innovative Smart Grid Technologies (ISGT Europe), 2012 3rd IEEE PES International Conference and Exhibition on*, pp. 1–6, IEEE, 2012. 38

[Flye 15] "Flyer: New DC Grid Access Solution". 2015. Available online at https://www.energy.siemens.com/nl/pool/hq/power-transmission/grid-access-solutions/dc-solutions/DC-Flyer.pdf, accessed on 17/10/2017. XII, 41

[Fren 17] "French offshore wind farm projects". 2017. Available online at http://www.4coffshore.com/, accessed on 13/03/2017. 15

[Hans 07] A. D. Hansen and L. H. Hansen. "Wind turbine concept market penetration over 10 years (1995–2004)". *Wind energy*, Vol. 10, No. 1, pp. 81–97, 2007. 26

[Hau 06] E. Hau and H. Von Renouard. *The wind resource*. Springer, 2006. XI, 20, 21

[Hau 13] E. Hau. *Wind turbines: fundamentals, technologies, application, economics*. Springer Science & Business Media, 2013. XI, 17

[Hube 08] F. Huber. "The first floating wind turbines". In: *Proceedings of 2nd International Conference on Ocean Energy (ICOE 2008), Brest, France*, 2008. 16

[Huss 12] V. Hussennether, J. Rittiger, A. Barth, D. Worthington, G. Dell'Anna, M. Rapetti, B. Hhnerbein, and M. Siebert. "Projects BorWin2 and HelWin1–large scale multilevel voltage-sourced converter technology for bundling of offshore wind-power". *Proc. Cigre Session, Paris, France*, pp. B4–306, 2012. 37

[INFL 17] "INFLOW Project". 2017. Available online at https://www.inflow-fp7.eu/, accessed on 30/07/2017. 19

[IREN 16] IRENA. "Innovation outlook: offshore wind". Tech. Rep., 2016. 44

[Jovc 11] D. Jovcic, D. Van Hertem, K. Linden, J.-P. Taisne, and W. Grieshaber. "Feasibility of DC transmission networks". In: *Innovative Smart Grid Technologies (ISGT Europe), 2011 2nd IEEE PES International Conference and Exhibition on*, pp. 1–8, IEEE, 2011. 37

[Lecl 04] L. Leclercq. *Apport du stockage inertiel associé à des éoliennes dans un réseau électrique en vue d'assurer des services systèmes*. PhD thesis, Université Lille 1, 2004. 20

[Li 11] W. Li, L.-A. Gregoire, and J. Bélanger. "Control and performance of a modular multilevel converter system". In: *CIGRÉ Canada, Conference on Power Systems, Halifax*, 2011. 37

[Lise 11] M. Liserre, R. Cardenas, M. Molinas, and J. Rodriguez. "Overview of multi-MW wind turbines and wind parks". *IEEE Transactions on Industrial Electronics*, Vol. 58, No. 4, pp. 1081–1095, 2011. 31, 41

[Liu 15] S. Liu, X. Wang, L. Ning, B. Wang, M. Lu, and C. Shao. "Integrating offshore wind power via fractional frequency transmission system". *IEEE Transactions on Power Delivery*, 2015. 39

[Lund 06] S. Lundberg. *Wind Farm Configuration and Energy Efficiency Studies-Series DC versus AC Layouts*. PhD thesis, Chalmers University of Technology, 2006. 29, 31, 32, 43, 44, 45, 46

[Mada 13] A. Madariaga, J. Martín, I. Zamora, I. M. De Alegria, and S. Ceballos. "Technological trends in electric topologies for offshore wind power plants". *Renewable and Sustainable Energy Reviews*, Vol. 24, pp. 32–44, 2013. 28, 30, 31, 36

[Max 09] L. Max. *Design and control of a DC collection grid for a wind farm*. Chalmers University of Technology, 2009. 29

[Meye 07a] C. Meyer. *Key Components for Future Offshore DC Grids*. *Aachener Beiträge des ISEA*, Shaker, 2007. 29

[Meye 07b] C. Meyer, M. Hoing, A. Peterson, and R. W. De Doncker. "Control and design of DC grids for offshore wind farms". *IEEE Transactions on Industry applications*, Vol. 43, No. 6, pp. 1475–1482, 2007. 30

[Mich 08] G. Michalke. *Variable speed wind turbines-modelling, control, and impact on power systems*. PhD thesis, Technische Universität, 2008. 28

[Ming 15] "Mingyang SCD 6MW technical report". 2015. Available online at http://www.mywind.com.cn/program/products.aspx?MenuID=02030201&ID=33, accessed on 14/08/2017, in Chinese. 17

[Monj 12] P. Monjean. *Optimisation de l'architecture et des flux énergétiques de centrales à énergies renouvelables offshore et onshore équipées de liaisons en continu*. PhD thesis, Arts et Métiers ParisTech, 2012. 29, 34, 35, 43, 45, 46, 47

[Mull 02] S. Muller, M. Deicke, and R. W. De Doncker. "Doubly fed induction generator systems for wind turbines". *IEEE Industry applications magazine*, Vol. 8, No. 3, pp. 26–33, 2002. 27

[Negr 06] N. B. Negra, J. Todorovic, and T. Ackermann. "Loss evaluation of HVAC and HVDC transmission solutions for large offshore wind farms". *Electric power systems research*, Vol. 76, No. 11, pp. 916–927, 2006. 34, 35

[Nenu 17] "Nénuphar offshore wind turbines". 2017. Available online at http://www.nenuphar-wind.com, accessed on 30/07/2017. 18

[Nguy 14] T. H. Nguyen, D.-C. Lee, and C.-K. Kim. "A series-connected topology of a diode rectifier and a voltage-source converter for an HVDC transmission system". *IEEE Transactions on Power Electronics*, Vol. 29, No. 4, pp. 1579–1584, 2014. 39, 40

[Niel 06] F. G. Nielsen, T. D. Hanson, B. Skaare, *et al.* "Integrated dynamic analysis of floating offshore wind turbines". In: *Proceedings of 25th International Conference on Offshore Mechanics and Arctic Engineering, Hamburg, Germany, OMAE2006-92291*, 2006. 16, 17

[NOVA 10] "NOVA Project". 2010. Available online at https://www.cranfield.ac.uk/case-studies/research-case-studies/nova-novel-offshore-vertical-axis-turbine, accessed on 30/07/2017. 19

[Pier 17] E. Pierri, O. Binder, N. G. Hemdan, and M. Kurrat. "Challenges and opportunities for a European HVDC grid". *Renewable and Sustainable Energy Reviews*, Vol. 70, pp. 427–456, 2017. 37, 43

[Reed 13] G. F. Reed, H. A. Al Hassan, M. J. Korytowski, P. T. Lewis, and B. M. Grainger. "Comparison of HVAC and HVDC solutions for offshore wind farms with a procedure for system economic evaluation". In: *Energytech, 2013 IEEE*, pp. 1–7, IEEE, 2013. 36

[Rodd 10] D. Roddier, C. Cermelli, A. Aubault, and A. Weinstein. "WindFloat: A floating foundation for offshore wind turbines". *Journal of renewable and sustainable energy*, Vol. 2, No. 3, p. 033104, 2010. 16, 17

[Rohn 10] S. Rohner, S. Bernet, M. Hiller, and R. Sommer. "Modulation, losses, and semiconductor requirements of modular multilevel converters". *IEEE transactions on Industrial Electronics*, Vol. 57, No. 8, pp. 2633–2642, 2010. 37

[Rudd 16] J. Ruddy, R. Meere, and T. O'Donnell. "Low Frequency AC transmission for offshore wind power: A review". *Renewable and Sustainable Energy Reviews*, Vol. 56, pp. 75–86, 2016. 39

[Rude 00] R. Rudervall, J. Charpentier, and R. Sharma. "High voltage direct current (HVDC) transmission systems technology review paper". *Energy week*, Vol. 2000, p. 2, 2000. 35

[Sami 16] S. Samimi, F. Gruson, P. Delarue, F. Colas, M. M. Belhaouane, and X. Guillaud. "MMC Stored Energy Participation to the DC Bus Voltage Control in an HVDC Link". *IEEE Transactions on Power Delivery*, Vol. 31, No. 4, pp. 1710–1718, 2016. 37

[SeaT 17] "SeaTwirl Project". 2017. Available online at http://seatwirl.com/, accessed on 30/07/2017. 19

[Seid 07] M. Seidel. "Jacket substructures for the REpower 5M wind turbine". In: *Conference Proceedings European Offshore Wind*, 2007. 15

[Shao 10] S. J. Shao and V. G. Agelidis. "Review of DC system technologies for large scale integration of wind energy systems with electricity grids". *Energies*, Vol. 3, No. 6, pp. 1303–1319, 2010. 31

[Siem 11] Siemens. "High voltage direct current transmission proven technology for power exchange". Tech. Rep., 2011. 35

[Siem 15] "Siemens presents new DC grid connection for offshore wind farms". 2015. Available online at https://www.siemens.com/press/pool/de/events/2015/energymanagement/2015-10-dc-grid/presentation-dc-grid-e.pdf, accessed on 30/07/2017. 40

[Sloo 03] J. G. Slootweg. *Wind power: Modelling and impact on power system dynamics*. PhD thesis, Delft University of Technology, 2003. 26

[Suth 12] H. J. Sutherland, D. E. Berg, and T. D. Ashwill. "A retrospective of VAWT technology". *Sandia Report No. SAND2012-0304*, 2012. 17

[Van 06] J. Van Der Tempel. *Design of support structures for offshore wind turbines*. 2006. XI, 15

[Van 10] D. Van Hertem and M. Ghandhari. "Multi-terminal VSC HVDC for the European supergrid: Obstacles". *Renewable and sustainable energy reviews*, Vol. 14, No. 9, pp. 3156–3163, 2010. 37

[Veil 14] E. Veilleux and P. W. Lehn. "Interconnection of direct-drive wind turbines using a series-connected DC grid". *IEEE Transactions on Sustainable Energy*, Vol. 5, No. 1, pp. 139–147, 2014. 29

[Vita 11] L. Vita. *Offshore floating vertical axis wind turbines with rotating platform*. PhD thesis, Technical University of Denmark, 2011. 18

[Wind 17a] WindEurope. "The European offshore wind industry". Tech. Rep., 2017. 14

[Wind 17b] WindEurope. "Floating Offshore Wind Vision Statement". Tech. Rep., 2017. 13

[Zoun 15] E. Zountouridou, G. Kiokes, S. Chakalis, P. Georgilakis, and N. Hatziargyriou. "Offshore floating wind parks in the deep waters of Mediterranean Sea". *Renewable and Sustainable Energy Reviews*, Vol. 51, pp. 433–448, 2015. 14

Chapter 2

Series DC wind farm basics

The only true wisdom is in knowing you know nothing.

Socrates

Contents

2.1 Introduction

In Chapter 1, some offshore wind farm topologies are described, from which the DC series parallel offshore wind farm architecture is selected to be studied in this thesis. The main advantage of this topology is the low cost and the low switching losses thanks to the elimination of the offshore centralized converter and platform [Lund 06][Monj 12].

This chapter introduces the general characteristics of the series connection of the aforementioned topology. Due to wind turbulence, which may be close to 30% for adjacent turbines [Bart 07], power differences in the series connection would cause certain wind turbines to attain much higher output voltage stress than other units. This varying output voltage of wind turbines is one of the drawbacks of series connection. Based on the description of this characteristic the parameters of the electrical components of the wind farm are dimensioned and fault protection solutions are proposed. Due to the variable output voltage characteristic, the DC/DC converter used in the wind turbines should be able to have a variable input/output voltage ratio. In addition, some components are not commercially available, for example the insulation technology at high potential, while they are necessary for this particular architecture. It is assumed in this chapter that the transformer of the DC/DC converter is capable of providing galvanic insulation in this topology.

Afterwards, the wind turbine model and control are described. Then, a simplified wind turbine model is presented. As the focus of this chapter is on the behaviour of several wind turbines connected in series, the onshore converter and HVDC cables are considered as an ideal voltage source. This assumption is made because the design and operating principles of the wind turbines in the collection system are not affected by the dynamics of the transmission system. Additionally, the investigation of this topology begins with only one cluster. The wind farm with wind turbines connected in one series cluster is named as Series Wind Farm (SWF).

2.2 Series connection of wind turbines

This section introduces the steady state operation of a series connection of wind turbines with DC outputs. It serves to describe the coupled operation characteristics of the SWF. The selection of the wind turbine generator, converter, and fault protection system are based on these characteristics.

2.2.1 System Overview

Figur.1e 2.1 shows a series connection of wind turbines with DC output voltages. The cluster has m units, WT_1, WT_2, ... , WT_m, and the sum of the output voltages equals the cluster voltage u_{CL}. The onshore converter controls the HVDC transmission voltage u_{HVDC}. Since

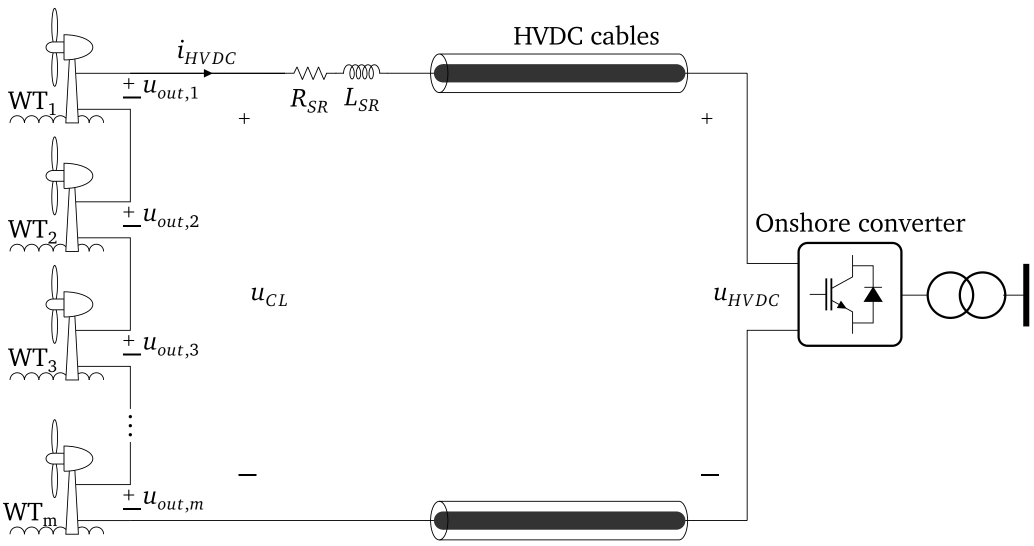

Figure 2.1 – Series connected wind turbines with DC output voltages.

the cluster is directly connected to the transmission system, u_{CL} equals u_{HVDC} if the voltage drops in the cables and in the smoothing reactor are negligible. The series connected wind turbines share a common cluster current i_{HVDC}. The smoothing reactor L_{SR} will be described later in this chapter and the HVDC cables and the onshore converter will be introduced in the next chapter.

The collection system includes dispersed converters in order to step up the voltage. These converters are the DC/DC converters at the outputs of the wind turbines. Figure 2.2 shows the general structure of the wind turbine for series connection. As wind farms are located far away from the shore, the maintenance is time consuming and expensive. Wind turbines with lower operation and maintenance costs are favourable. For the purpose of reducing operation and maintenance costs, the direct-drive Permanent Magnet Synchronous Generator (PMSG) based turbine is adopted in the SWF. Step-up of the voltage from the lower generator side to the higher cluster collection side is realized by a DC/DC converter.

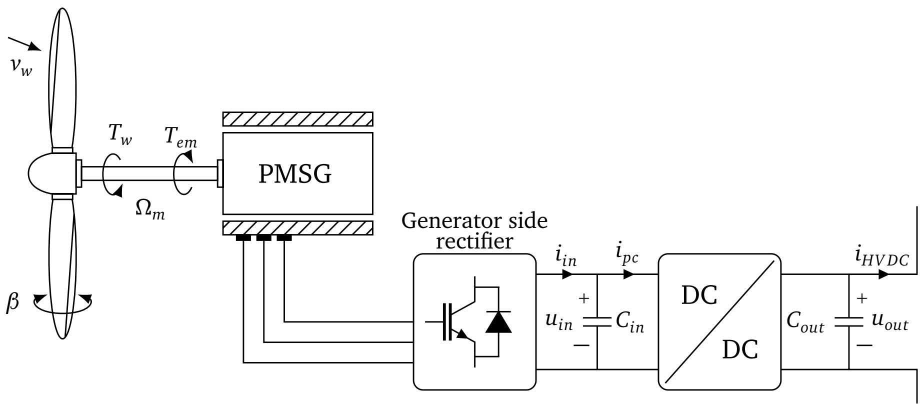

Figure 2.2 – General structure of a wind turbine for series connection.

2.2.2 Steady state operation of series connection

The output power and voltage of the wind turbine $\mathrm{WT_x}$ in Figure 2.1 are denoted as $p_{out,x}$ and $u_{out,x}$, $x \in (1,2,...,m)$, respectively. The sum of the power is the wind farm power production p_{WF} and the sum of the voltage is the HVDC voltage u_{HVDC}, assuming that the voltage drops in the cables and in the smoothing reactor are negligible.

$$u_{HVDC} = \sum_{x=1}^{m} u_{out,x} \tag{2.1}$$

The current of the wind farm is then the division of the wind farm power p_{WF} by the voltage u_{HVDC}. It is identical to the output current of each wind turbine:

$$i_{HVDC} = \frac{p_{WF}}{u_{HVDC}} = \frac{p_{out,x}}{u_{out,x}} \tag{2.2}$$

Assuming that the power electronics devices in wind turbines are ideal and have infinite voltage and current capabilities, the operation of wind turbines follows the Kirchhoff Circuit Laws. Output voltage of the x^{th} wind turbine is defined as:

$$u_{out,x} = u_{HVDC}\frac{p_{out,x}}{p_{WF}} \tag{2.3}$$

Equation (2.3) gives the theoretical output voltage of a wind turbine in a DC series offshore. It implies that the output voltage does not only depend on its own power $p_{out,x}$, but also on the instant power production of the entire wind farm p_{WF}. As the wind may vary quite differently across the whole wind farm, turbines are not likely to operate in the same wind condition, output power and then the voltage will definitely change continuously.

To illustrate the steady state operation, a series cluster of 5 wind turbines of nominal power $P_{out,nom}$ and voltage $U_{out,nom}$ of 1 pu, is considered. We take

$$P_{out,nom} = 1$$

$$U_{out,nom} = 1$$

then, the HVDC voltage is 5 pu. The power production and corresponding steady state output voltages of wind turbines are:

$$\mathbf{p_{out}} = \begin{pmatrix} 1 \\ 0.9 \\ 0.8 \\ 0.7 \\ 0.6 \end{pmatrix} \qquad \mathbf{u_{out}} = u_{HVDC}\frac{p_{out,x}}{p_{WF}} = \frac{5}{4}\begin{pmatrix} 1.0 \\ 0.9 \\ 0.8 \\ 0.7 \\ 0.6 \end{pmatrix} = \begin{pmatrix} 1.25 \\ 1.125 \\ 1 \\ 0.875 \\ 0.75 \end{pmatrix}$$

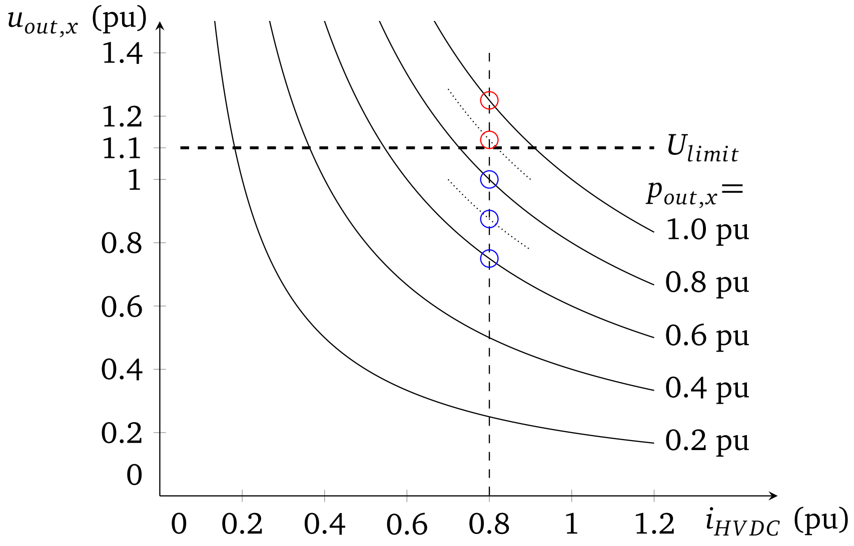

Figure 2.3 – Illustration of the operating points of the 5 wind turbines. Blue circles: in the overvoltage capability; Red circles: beyond the overvoltage capability.

The operating points of units are illustrated in Figure 2.3. It is shown that wind turbines have the same current while their output voltages are quite different. WT_1 has nominal power production while its output voltage is 1.25 pu, 25% higher than nominal voltage. As a result, the turbines are required to have in some extent overvoltage capabilities. If the overvoltage capabilities of wind turbines are at 1.1 pu as shown in Figure 2.3, two units WT_1 and WT_2 would operate out of the capability ranges.

2.2.3 Definition of overvoltage

For a typical variable speed wind turbine, output power is sensitive to the variation of wind speed between the interval of the cut-in and the rated wind speed. However, at the stage of the wind farm planning, in order to reduce the wake effect in wind farm performance, the distance between two neighbouring wind turbines is set up to 500 to 800 m [Acke 05]. The placement causes uneven wind speed across the wind farm, and thus disparity of wind power extraction among wind turbines.

This is not an issue in a traditional wind farm where wind turbines are connected in parallel to a centralized converter and therefore being able to operate independently. While this does become a problem for series parallel wind farm where units are connected in series. Units capturing different wind power share the same current in one cluster, which results in uneven allocation of output voltage across them. Wind speed changes with time and location resulting in continuous imbalance of power production among units in the same cluster. Therefore, DC series wind turbines require wide voltage variation capability.

As mentioned above, when a particular wind turbine output power is higher than the average power production of its cluster, this unit output voltage increases. If the HVDC voltage is regulated to be m times the wind turbine nominal voltage $U_{out,nom}$, this unit's output voltage will rise above its nominal value. In this situation, this particular unit is in overvoltage regime.

To describe the variation of the wind turbine output voltage more precisely, the Figure 2.4 is used. Initially, the output voltage of the wind turbine x WT_x is constant, the currents on both sides of the output capacitor $i_{out,x}$ and i_{HVDC} remain unchanged. An imbalance occurs if the power generation of WT_x is either lower or higher than the average power generation in the cluster, so:

- When the power generation of a wind unit is lower than the average power generation $p_{WF,ave}$ in the cluster, this imbalance is reflected directly by the current inside the wind turbine and that in the cluster. As shown in Figure 2.4a, a higher current from the generator side charges the output capacitor, which consequently increases the voltage across the wind turbine output.
- When the unit power production is lower than the average level $p_{WF,ave}$ in the cluster, the stored electrostatic energy is discharged to compensate the current gap, leading to a reduction of the output voltage, as shown in Figure 2.4b.

In both cases, the steady state is again achieved when the values of the two currents become equivalent.

As a result, the high voltage sides of the wind turbine DC/DC converters must be over-rated in order to enable wind turbines to support this additional voltage. The maximum voltage level that a wind turbine converter can support is its *overvoltage capability* U_{limit}, defined as:

$$U_{limit} = (1+\alpha)U_{out,nom} \tag{2.4}$$

where α is the *overvoltage ratio*.

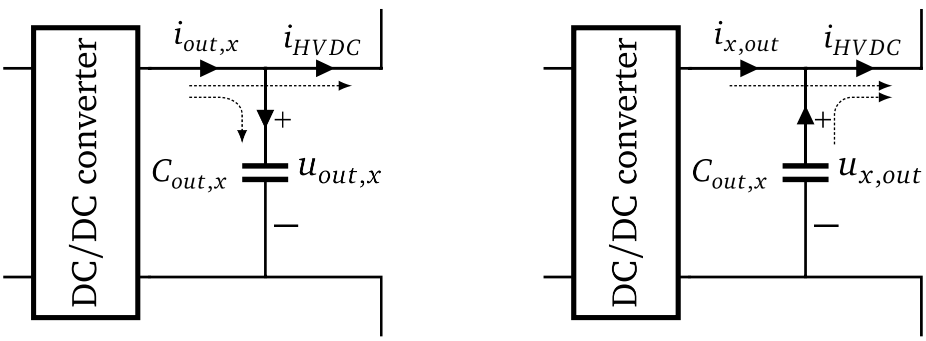

(a) $p_{out,x} < p_{WF,ave}$ (b) $p_{out,x} > p_{WF,ave}$

Figure 2.4 – Power production imbalance between the wind turbine and the average value of the cluster.

2.3 Wind turbine generation and conversion systems

This section describes the model and control of the DC series wind turbine, including the mechanical part of the wind turbine, the permanent magnet synchronous generator and the DC/DC converter. Several DC/DC converters structures are found in the literature for DC offshore wind farm applications. But for DC series offshore wind farms, converters with variable output voltage capability are required. The overall control of the DC series wind turbine is presented and then, a simplified wind turbine model is proposed for simulation purposes.

2.3.1 Power generation in the wind turbine

The wind turbine power generation is simplified into three stages in this subsection: the blades, the shaft and the generator. Mathematical models of the mechanical and electrical parts of the generation system are described.

2.3.1.1 Mechanical part

The mechanical part includes the torque that the wind imposes on the blades to rotate the shaft. The aerodynamic basics of the conversion of wind energy to mechanical energy are explained in Section 1.2.3. The relationship between the wind speed and the power captured by the wind turbine is rewritten here:

$$P_w = \frac{1}{2} C_p \rho \pi r^2 {v_w}^3 \tag{2.5}$$

Correspondingly, the torque that the blade imposes to the shaft is:

$$T_w = \frac{P_w}{\Omega_m} = \frac{1}{2} C_t \rho \pi r^3 {v_w}^2 \tag{2.6}$$

The power coefficient C_p is a turbine-specific non-linear function of the tip speed ratio λ and the pitch angle β of the blade. In order to establish the mathematical model, an approximation of the power coefficient C_p, according to [Heie 14], is:

$$C_p = 0.4(\frac{116}{\lambda_i} - 0.4\beta - 5)\exp^{-\frac{21}{\lambda_i}} + 0.02\lambda \tag{2.7}$$

$$\lambda_i = \frac{1}{\frac{1}{\lambda + 0.08\beta} - \frac{0.035}{\beta^3 + 1}} \tag{2.8}$$

The wind applies a torque T_w on the wind turbine shaft which links the wind turbine blades and the generator rotor. The shaft is normally modelled as a two-mass model [Chen 07] [Mich 10]. In this study a one-lumped mass model, as in reference [Yin 07], is used for the sake of simplicity. The rotational speed of the blades is equal to the rotational speed of the generator rotor since no gearbox is used. The rotation of the rotor with permanent magnets mounted induces an Electromotive Force (EMF) and a current in the stator windings, which create the electromagnetic torque T_{em}. The direction of this torque is opposite to the rotating direction of the rotor:

$$\frac{d\Omega_m}{dt} = \frac{1}{J_{eq}}(T_w - T_{em} - B_m\Omega_m) \tag{2.9}$$

where J_{eq} is the moment of inertia of the shaft and B_m is the coefficient of viscous friction which is set to zero in this study. Equations (2.5) to (2.9) establish the torque model of the wind turbine shown in Figure 2.5. The mechanical system has three inputs:

1. The wind speed v_w: which is not controllable;
2. The pitch angle β: which has a profound influence on the system efficiency. With a pitch system, the pitch angle can be controlled and thus the torque induced by the power extracted from the wind T_w can also be controlled;
3. The electromagnetic torque T_{em}: which can be controlled if an active power rectifier is available.

As a result, there are one uncontrollable variable and two controllable variables. The purpose of the control system of the wind turbine mechanical system is to extract the optimal power and assure the operation of the wind turbine within established rotational speed limits and generator electrical power limits. These two aims are accomplished by adjusting the two controllable variables: the electromagnetic torque T_{em} and the pitch angle β.

At low wind speed, the Maximum Power Point Tracking (MPPT) is applied by matching the rotational speed Ω_m to get optimal tip-speed ratio λ_{opt}, with the pitch angle set at its

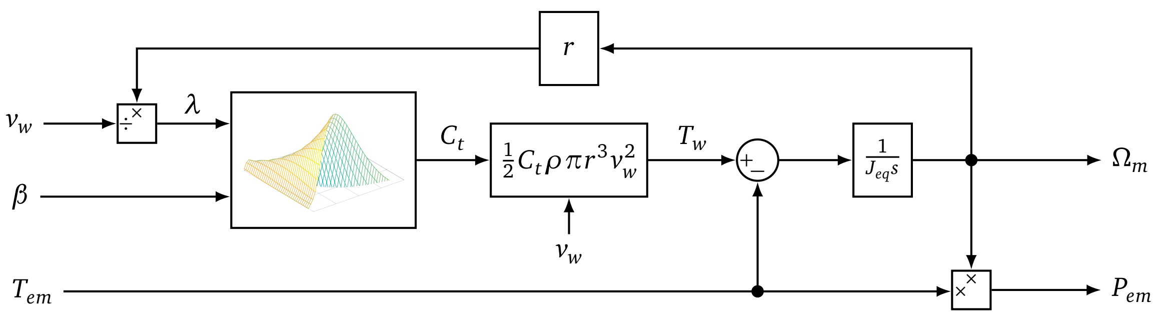

Figure 2.5 – Torque model of the wind turbine.

initial optimal value, β_{ini}. As the wind speed increases, the power generated by the wind turbine also increases. Once the wind turbine reaches its nominal power, the pitch angle increases to reduce the aerodynamic power.

In this study, it is assumed that the nominal power is reached at nominal rotational speed, which may not apply for real industrial wind turbines. To prevent mechanical damages to the blades, some wind turbines rotate at constant speed before reaching the nominal power production. As the wind speed increases, the tip-speed ratio decreases and the power efficiency decreases. However, the power production keeps increasing since it is proportional to the cube of wind speed. This characteristics can be found in many high power rating wind turbines [El A 04][Lecl 04].

The overall control system of the wind turbine mechanical system is shown in Figure 2.6. The MPPT provides the electromagnetic torque reference $T_{em,ref}$ based on the operational points for maximum efficiency. An analytical expression for the maximum power is based on the rotational speed, the maximum C_p coefficient $C_{p,max}$ and the optimal tip-speed ratio λ_{opt}:

$$P_{em,ref} = \frac{\frac{1}{2}\rho\pi r^5 C_{p,max}{\Omega_m}^3}{{\lambda_{opt}}^3} \tag{2.10}$$

When the rotational speed reaches its nominal value, the wind turbine produces the nominal power. If the wind speed keeps increasing, the power production is then limited by a saturation at nominal power. However, the rotational speed Ω_m will keep increasing.

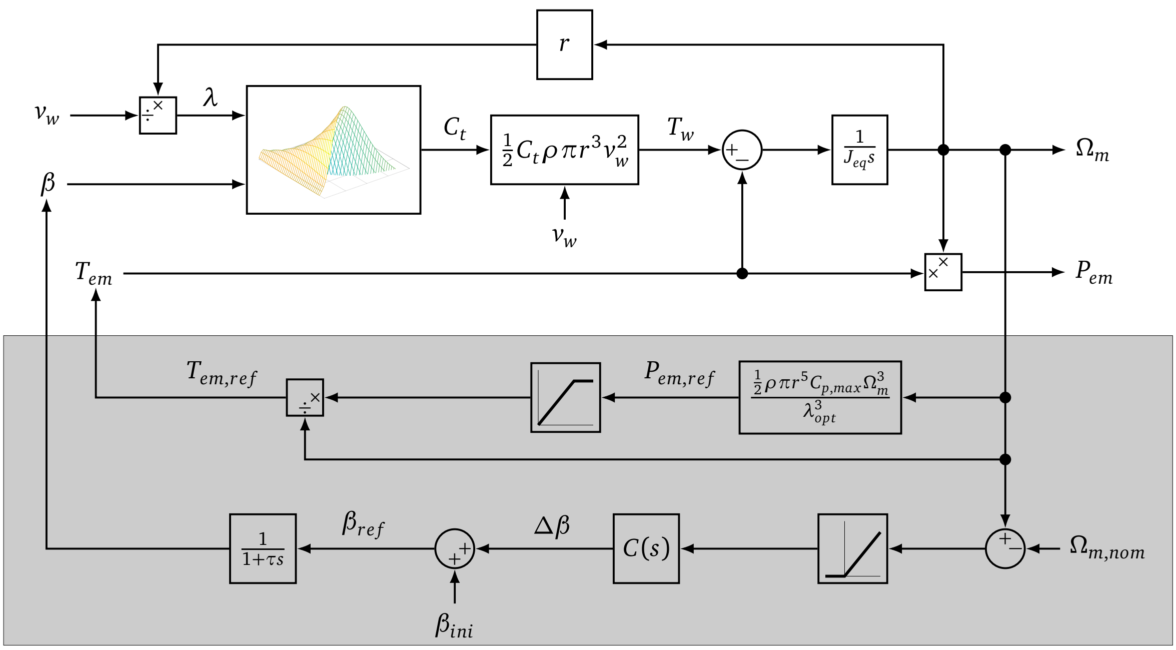

Figure 2.6 – Control system of the wind turbine mechanical part.

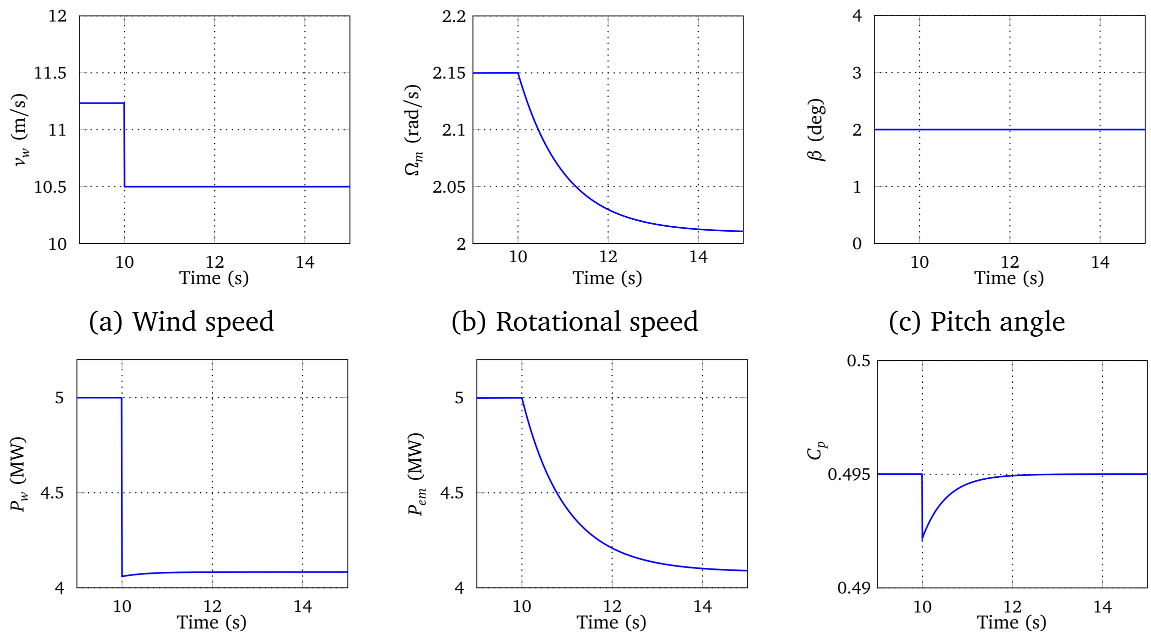

(a) Wind speed (b) Rotational speed (c) Pitch angle

(d) Captured wind power (e) Electromagnetic power (f) Power efficient

Figure 2.7 – Simulation results of a 5 MW wind turbine.

In order not to avoid the damage of the wind turbine, the difference between the rotational speed Ω_m and the nominal rotational speed $\Omega_{m,nom}$ is regulated to zero by increasing the pitch angle and decreasing the aerodynamic power efficiency.

A 5 MW wind turbine is simulated. The wind turbine rotational speed and the power variation due to a drop of wind speed from a nominal value 11.25 m/s to 10.5 m/s is shown in Figure 2.7. At the moment when the wind speed steps down, the power coefficient C_p and the captured wind power P_w decrease immediately. According to Equation (2.9), the difference of the captured power P_w and the electromagnetic power P_{em} slows down the rotational speed. The new rotational speed gives a new electromagnetic power reference $P_{em,ref}$ to the system according to the MPPT equation (2.10). Finally these two powers are balanced. The rotational speed decreases to 2.01 rad/s to match the reduced wind speed, and the power coefficient comes back to the maximum value.

2.3.1.2 Permanent magnet synchronous generator

The rotation of the wind turbine shaft induces an emf and a current in the stator windings of the PMSG, which also causes the electromagnetic torque T_{em}.

A PMSG is usually modelled directly in dq synchronous reference frame [Yin 07]:

$$u_{sd} - e_{sd} = L_{sd}\frac{di_{sd}}{dt} + R_s i_{sd} - \omega_e i_{sq} \tag{2.11}$$

$$u_{sq} - e_{sq} = L_{sq}\frac{di_{sq}}{dt} + R_s i_{sq} + \omega_e i_{sd} \tag{2.12}$$

$$T_{em} = 1.5n_p((L_{sd} - L_{sq})i_{sd}i_{sq} + i_{sq}\lambda_0) \tag{2.13}$$

where

n_p = the pole pairs of the rotor;
ω_e = the electrical rotational speed as $\omega_e = n_p\Omega_m$;
u_{sd} = the d-axis generator stator output voltage;
u_{sq} = the q-axis generator stator output voltage;
e_{sd} = the d-axis electric potential, equals 0;
e_{sq} = the q-axis electric potential, equals $\omega_e\lambda_0$;
λ_0 = the flux linkage of the rotor permanent magnets;
L_{sd} = the d-axis generator stator inductance;
L_{sq} = the q-axis generator stator inductance;
R_s = the generator stator resistance.

By assuming that the machine has surface mounted magnets, the inductances in dq frame are equal, $L_{sd}=L_{sq}=L_s$. The torque equation 2.13 can be then simplified to:

$$T_{em} = 1.5n_p i_{sq}\lambda_0 = k_t i_{sq} \tag{2.14}$$

The equivalent circuit in dq is shown in Figure 2.8a and 2.8b.

The generator side rectifier is controlled to extract the maximum power from the wind. Based on the wind turbine model described before, the control system is also in dq synchronous frame. The reference of the d component of the current i_{sd} is set to 0. The q component i_{sq} is then linear with respect to the torque reference given by the MPPT strategy according to Equation (2.14).

The outputs of the current controllers are then used to provide a trade-off voltage reference for u_{sd} and u_{sq}. The control diagram of the generator side rectifier is shown in Figure 2.9.

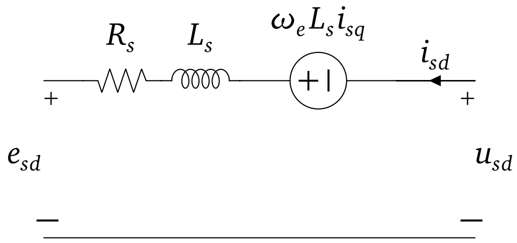

(a) d-axis equivalent circuit.

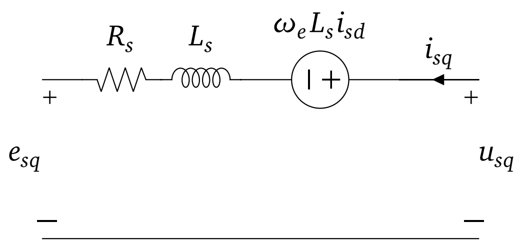

(b) q-axis equivalent circuit.

Figure 2.8 – PMSG equivalent circuit in the dq synchronous frame.

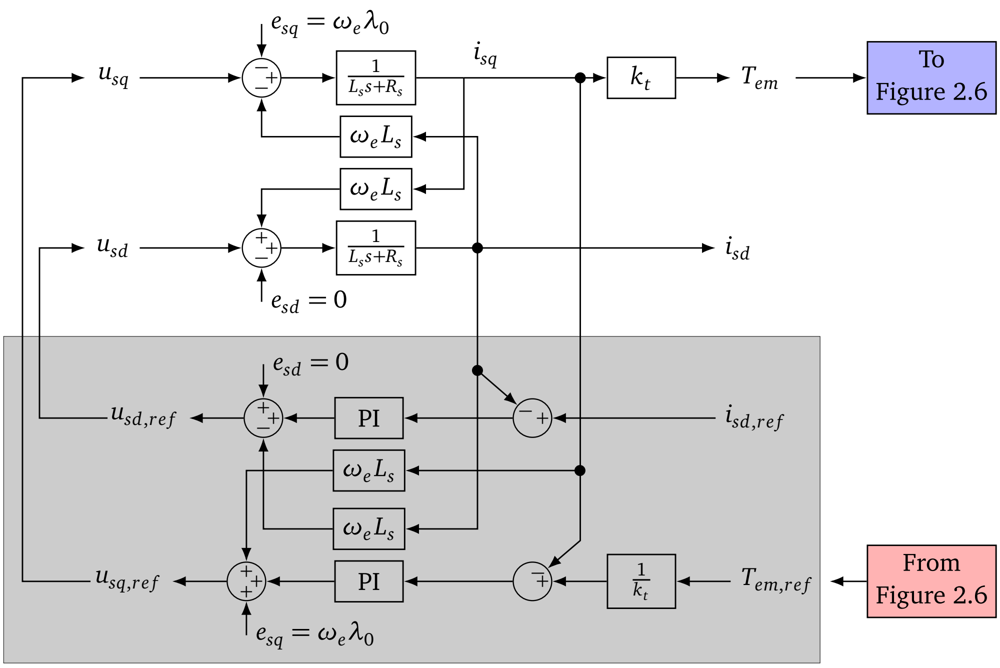

Figure 2.9 – PMSG mathematical model in the dq synchronous reference frame.

2.3.2 High power DC/DC converter

The DC/DC converter is used to step up the voltage from the generator side to the output side of the wind turbine. The most adopted DC/DC converters in the literature are: full bridge converter (FBC) [Eric 07], single active bridge (SAB) [De D 91], dual active bridge converter (DAB) [Kher 92], [Zhao 14] and series resonant converter (SRC) [Stei 88].

As assumed later in Subsection 2.3.5, the insulation of the wind turbine is provided by a transformer in the DC/DC converter. Some DC/DC converters for high power application but without transformers, as reported in the literature [Fils 14], [Jovc 09], are not considered in this thesis.

The transformer in the DC/DC converter operates at medium frequency (up to a few kilo-Hertz) in order to reduce the weight and volume of the converter. The study in [Bahm 16] states that there is no necessity to operate the transformer at high frequency since the volume would not be reduced furthermore due to the isolation constraints.

The advantages and disadvantages of these four converters, based on the comparison work in [Meye 07], [Max 09], [Monj 12], are listed in Table 2.1.

The choice of DC/DC transformer may differ according to the arrangement of the collection grid (presented in Section 1.3). It has been mentioned previously that it is necessary for a DC/DC converter to have variable output voltage capability in order to operate in the series connection. As a result, the full bridge and dual active bridge converter types are applicable to the SWF. In this section, the full bridge converter is used because of its low cost and simplicity of control.

Table 2.1 – Advantages and disadvantages of four types of DC/DC converters.

	Advantages	Disadvantages
Full Bridge Converter	• Fixed commutation frequency (phase shift control) • Variable transformation ratio	• Inductor on the high-voltage side • Hard switch - commutation loss • Uni-directional power flow
Single Active Bridge	• Few passive components • Fixed commutation frequency (phase shift control)	• Fixed transformation ratio • Hard switch - commutation loss • Uni-directional power flow
Dual Active Bridge	• Bi-directional power flow, can provide auxiliary power to the wind turbine • Variable transformation ratio	• Limited soft switch boundaries - commutation loss • More expensive
Resonant Converter	• Soft switch • No filter inductance at output	• Fixed transformation ratio • Lack of controllability due to variable switching frequency

2.3.2.1 Full bridge converter

The full bridge converter is a DC/DC converter suitable for high power applications. The circuit arrangement is shown in Figure 2.10.

The input bridge composed of 4 IGBTs on primary side creates a high frequency square wave to the transformer side. It is not necessary to use Sinusoid Pulse Width Modulation (SPWM) to create a sinusoid waveform, as the output is not connected to loads or grids. This square wave is rectified by the diodes on the secondary side and filtered by an inductor. Since low voltage side is directly connected to the DC link capacitor, the full bridge converter is required to include an inductor on the high voltage side which is one of the drawbacks of this type of converter.

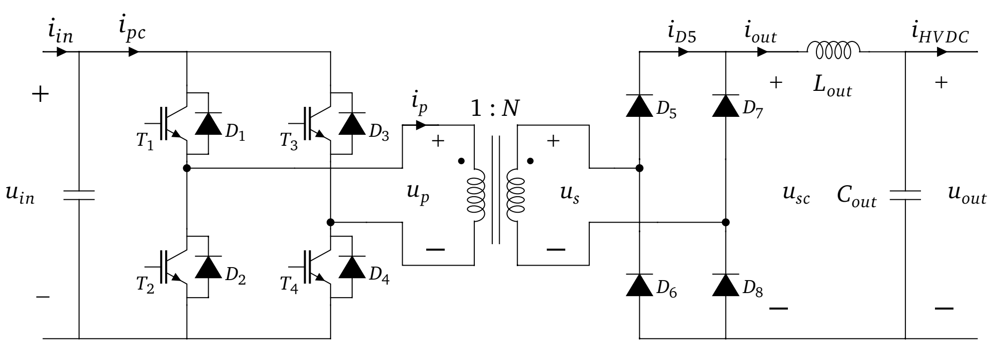

Figure 2.10 – DC/DC full bridge converter.

2.3.2.2 Control methods

The *duty cycle* control and *phase-shift* methods, used to control the full bridge converter are presented hereinafter.

1. The easier way to control the full bridge converter is to use *duty cycle control*. The operation diagram is shown in Figure 2.11. Switches T_1 and T_2, T_3 and T_4 are turned on and off complementary. The amplitude of the duty cycle enables to adjust the time of on-state of switches T_1 and T_3. When T_1 and T_4 are in the on-state, the DC link charges the transformer. Diodes D_5 and D_8 are forward biased and conduct current i_{out} to the output capacitor C_{out}. u_s is proportional to the input voltage u_{in} with a coefficient of transformer ratio N, times the duty cycle D, $u_s = NDu_{in}$. During the second interval, T_1 and T_3 are in the on-state, the primary side of the transformer is in short circuit through D_1 and T_3, and the voltage on the secondary side u_s is thus 0.

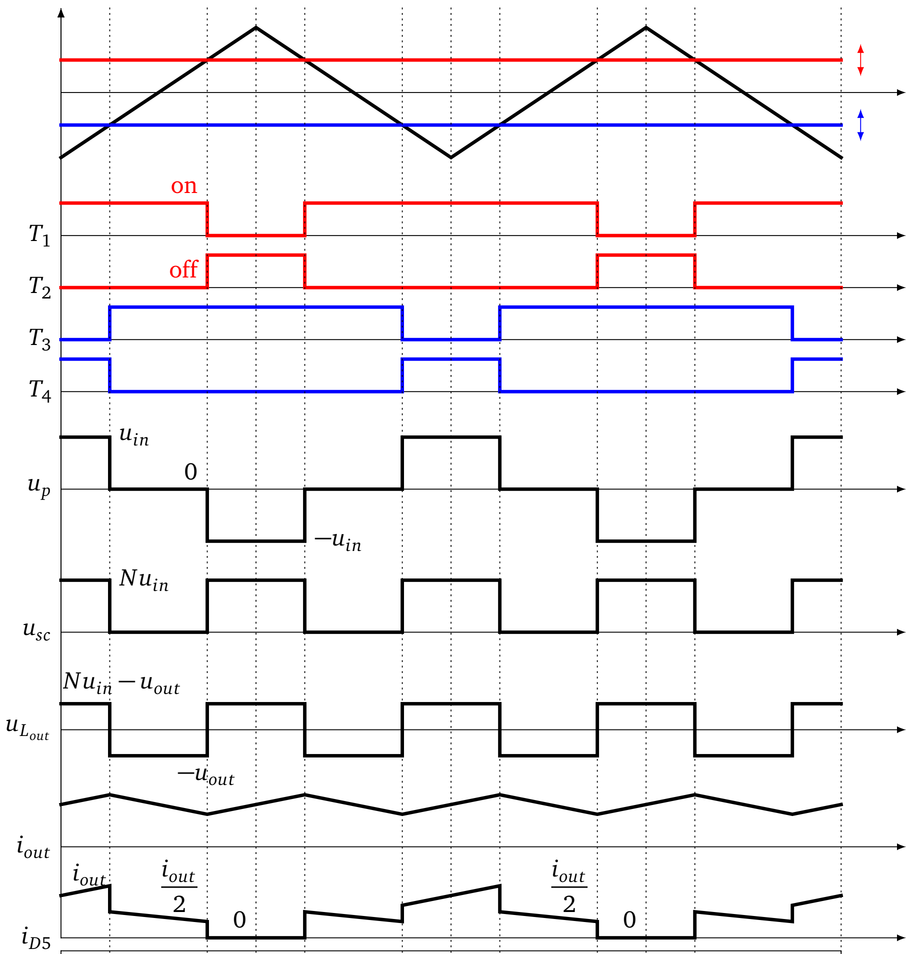

1	2	3	4	5	6	1	2	3	4	Mode no
T_1 T_4	T_1 D_3	D_2 D_3	T_2 T_3	D_1 T_3	T_2 D_4	T_1 T_4	T_1 D_3	D_2 D_3	T_2 T_3	primary bridge
D_5 D_8	D_5D_8 D_6D_7	D_6 D_7	D_6 D_7	D_5D_8 D_6D_7	D_5 D_8	D_5 D_8	D_5D_8 D_6D_7	D_6 D_7	D_6 D_7	secondary bridge

Figure 2.11 – DC/DC full bridge converter with duty cycle control.

However, the current of the inductor cannot be interrupted. Each leg of the rectifier is in charge of half of the total current i_{out}, as shown in the waveform of i_{D5}. In the next interval, T_2 and T_3 are switched on, which gives a negative voltage across the primary side of the transformer. u_s also becomes negative and forward biased diodes D_6 and D_7. Intervals 5 is similar to interval 2 where each diode in the secondary bridge conducts half of the current. In the continuous current mode, the duty cycle reference is calculated as:

$$D = \frac{1}{N}\frac{u_{out}}{u_{in}} \tag{2.15}$$

2. Alternatively the full bridge converter can be controlled by *phase-shift control*. The two switching legs are then controlled individually. Every arm is turned on half of the period. The output voltage is adjusted by shifting the second leg switch-on angle δ, and thus regulating the intervals where both T_1 and T_3 are in the on-state. The operation diagram is plotted in Figure 2.12.

   The intervals are similar to the previous PWM control. If the phase shift $\delta = 0$, which implies that the two legs are in phase, u_p is 0 and the output voltage is also 0. If $\delta = 180$ degrees, the duty cycle is equal to 1.

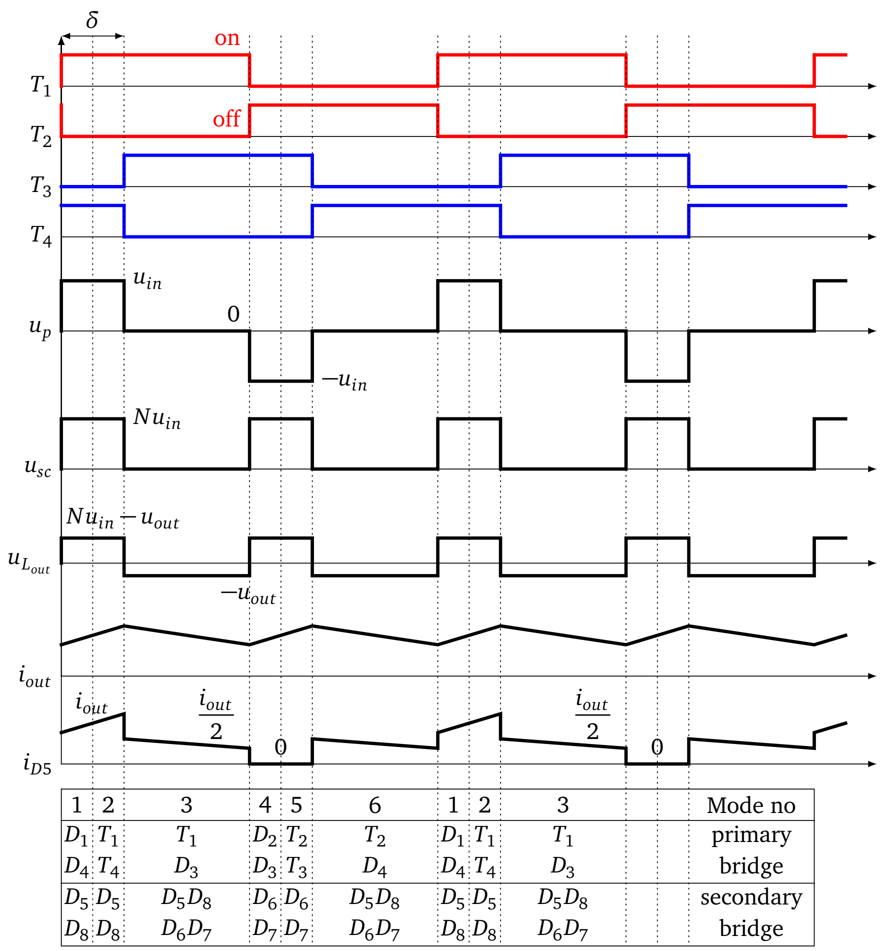

Figure 2.12 – DC/DC full bridge converter with phase shift control.

Then the phase shift angle can be calculated as:

$$\delta = \frac{180}{N}\frac{u_{out}}{u_{in}} \tag{2.16}$$

A dual-loop PI output voltage controller is designed as shown in Figure 2.13. The inner loop is the current loop with a time constant of 3.5 ms. The outer voltage loop time constant is chosen to be 10 times longer than the inner loop. There are two scenarios for this DC/DC converter used in the series connected wind turbine. In the first scenario all the series wind turbine have the same power variation therefore the same input current variation. In Figure 2.14, a step of 0.2 pu is illustrated, from 1.0 pu to 0.8 pu at $t = 0.5s$. The step change of the current i_{in} produces some fluctuations in the input voltage which is, however, regulated to its nominal value in 30 ms. Since the input and output voltage do not change before and after the power step, the duty cycle D stays constant.

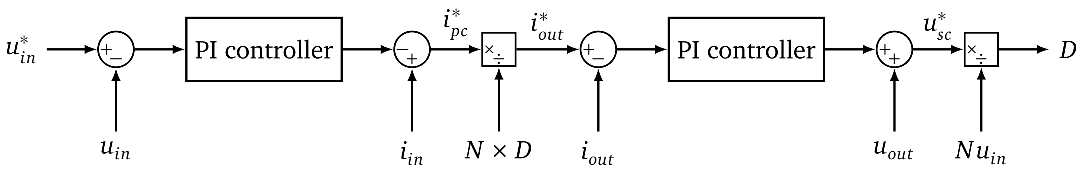

Figure 2.13 – Full bridge DC/DC converter input voltage dual loop control blocks.

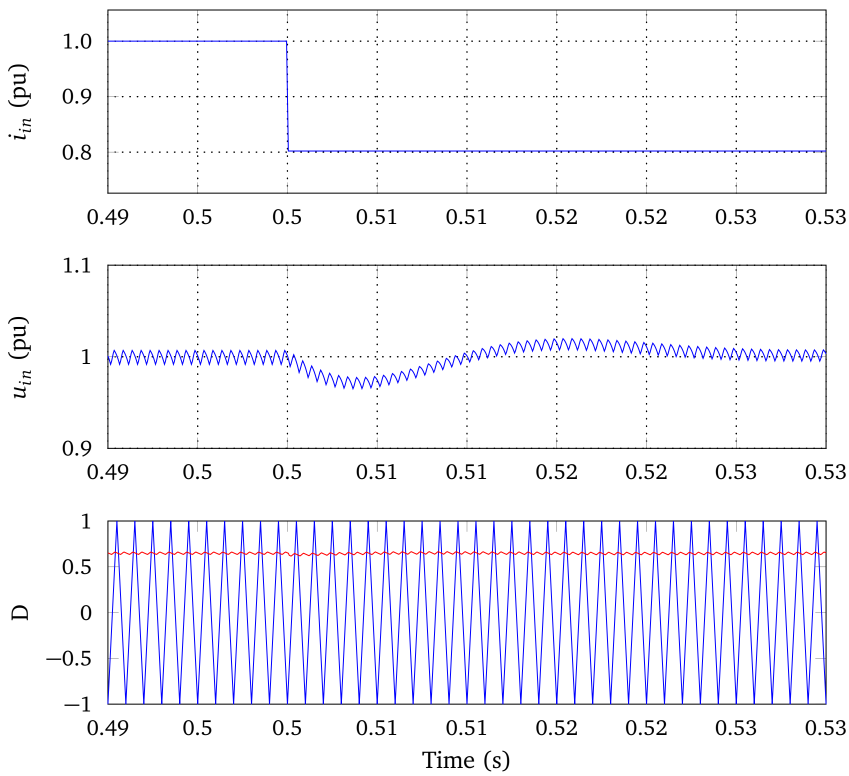

Figure 2.14 – Behaviour of the full bridge converter response to an input power variation.

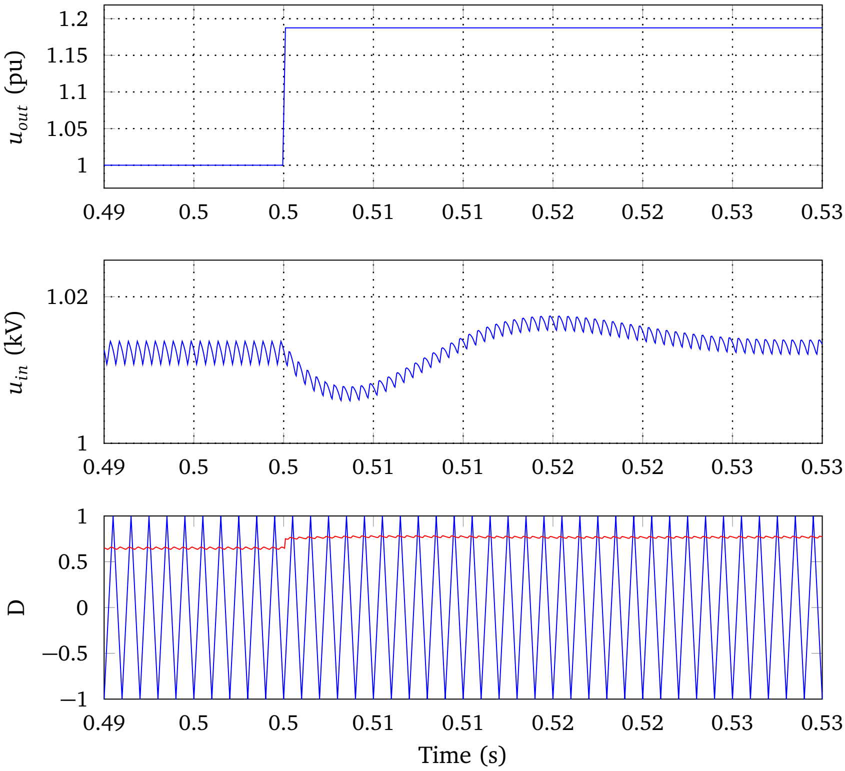

Figure 2.15 – Behaviour of the Full bridge converter response to an output voltage variation.

In the second scenario the input power stays constant while the output voltage increases due to power variation in the other wind turbines. For example, Figure 2.3 illustrates a wind turbine with nominal power production while its output voltage increases beyond overvoltage limit. In such case, as can be seen in Figure 2.15, the duty cycle D increases because the ratio between the output and input voltage u_{out}/u_{in} increases.

2.3.3 Output capacitor of the DC/DC converter

In AC power system, the kinetic inertia of power generators characterizes the system dynamics and is responsible for ensuring that the AC system does not collapse due to a system fault [Zhu 13][Kund 94]. The rotating mass of power generators will absorb or release kinetic energy with an inertia so that the speed of rotation does not change very fast and thus, the frequency of AC system does not vary substantially. The same behaviour applies to DC link capacitance in the DC power system, where the stored electrostatic energy charges or discharges to counteract the DC link voltage variation during power mismatches. As a consequence, similarly to the AC system, DC power system dynamics are characterized by the capacitance of the DC link. The electrostatic constant of capacitor [Kund 94] is defined as follows,

$$H_c = \frac{\frac{1}{2} C_{DC} {U_{DC,nom}}^2}{P_{nom}} \tag{2.17}$$

where

C_{DC} = the capacitance of a DC link;
$U_{DC,nom}$ = the nominal voltage across a DC link;
P_{nom} = the nominal power of a DC link station.

The sizing of output capacitor takes into account the system dynamics and the economic aspect. The larger the output capacitor, the slower the variation of the output voltage. However, the cost for larger capacitor will also increase. So the capacitance size is a trade-off between the voltage requirements and the capacitor cost. A typical selection of H_c electrostatic constant for HVDC VSC is 30 to 40 ms (kJ/MVA) suggested in [Jaco 10]. The capacitor of each full bridge converter C_{out} can be viewed as a fraction of the HVDC capacitance. As a result, the cumulative capacitance of m wind turbines is chosen to be between 30 to 40 ms, based on the same value used in a typical VSC. However, a more considered selection could be done in a future study. The output capacitor of each converter is calculated as:

$$C_{out} = \frac{2mH_cP_{WF,nom}}{{U_{HVDC,nom}}^2} \tag{2.18}$$

For a cluster with 20 wind turbines of 5 MW rating power and a nominal HVDC voltage of 640 kV, the wind turbine output capacitor is then designed to be 293 µF for an electrostatic constant of 30 ms.

2.3.4 DC smoothing reactor

As both ends of the system, (the wind turbine output and the onshore voltage source) are capacitive, a reactor L_{SR} should be added to the system. This reactor is sized to a value big enough to limit the gradient of current boost during critical faults such as short circuit on the HVDC cables, as shown in Figure 2.16.

When the device detects the current in the HVDC cables increases to a pre-set safety level, the protection system will be triggered to shut the whole system off. The size of the reactor is designed to prevent the current from increasing to this level before the protection system is activated. This process is illustrated in Figure 2.17.

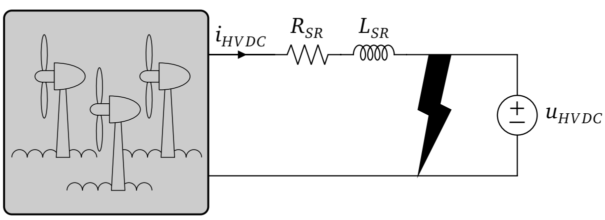

Figure 2.16 – Cable short circuit of a series connection.

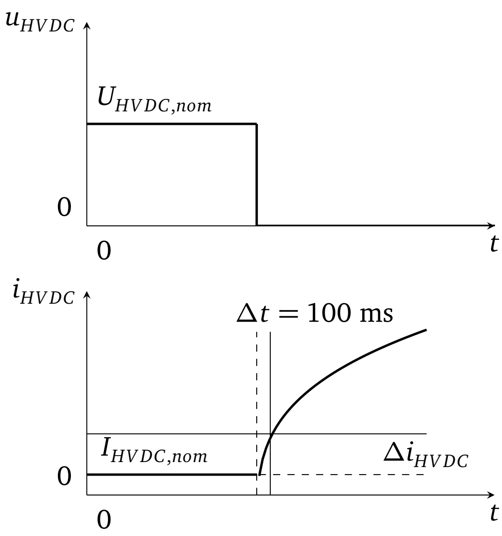

Figure 2.17 – Illustration of HVDC current rise after a short circuit of a pair of cables.

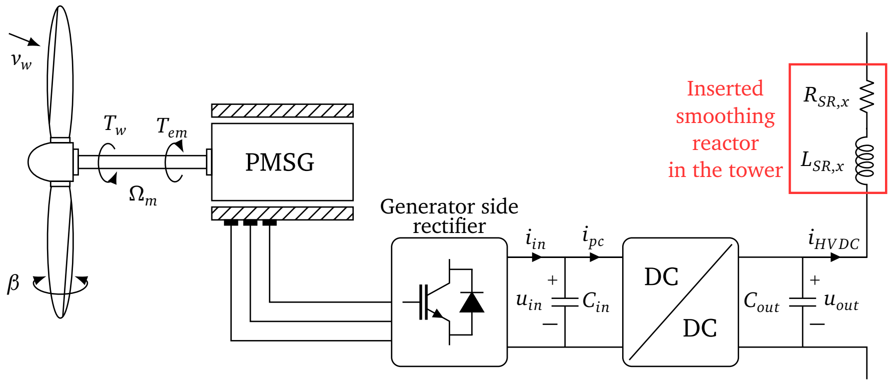

Figure 2.18 – Smoothing reactors are separately placed into the wind turbine tower.

$$L_{SR} = \frac{U_{HVDC,nom}}{\frac{\Delta i_{HVDC}}{\Delta t}} \tag{2.19}$$

The $\Delta i_{HVDC}/\Delta t$ value used in a ±320 kV MMC project is 6.4 MA/s, so the reactor used should be 100 mH. The big reactor is split evenly to as many parts as the number of wind turbines and thus each part of the reactor $L_{SR,x}$ is small enough to fit directly inside the wind turbine tower shown in Figure 2.18.

2.3.5 Insulation technology

Since there is no an offshore converter, the collection and transmission parts of this wind farm are coupled. In addition, the wind turbines are coupled because of the series connection. The insulation of the wind turbines becomes a critical issue for this topology, especially for the first and last units which have as high potential as half of the HVDC voltage $\frac{1}{2}u_{HVDC}$.

Unfortunately such a high insulation technology is not yet commercially available. Although several works propose the use of the DC/DC transformer for insulation purpose, it remains an open challenge for the industry [Mada 13]. In this thesis, it is assumed that this problem will be solved in the future. For now, it is assumed that the DC/DC transformer is able to ensure the insulation capability.

2.3.6 Wind turbine unit fault and protection system

A bypass protection system against faults is mandatory in the DC series collection grid. To prevent the failure of a single unit from triggering a cascading failure in the cluster, a DC breaker immediately cuts off the wind turbine if any inside fault is detected. In the same time, the output should have a short circuit path for current to flow through. There are two bypass solutions proposed.

The first solution is to add two DC breakers at the output of the DC/DC converter, and a connector across the output capacitor. This solution directly cuts off the entire wind turbine from the cluster. Two medium power rated DC breakers disconnect the wind turbine electrical parts from the series connection, and another switch closes to provide a path for the cluster current. The scheme is shown in Figure 2.19a.

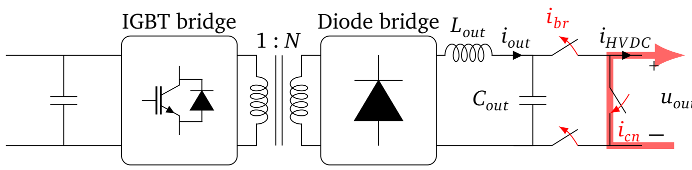

(a) Diagram of bypass solution 1.

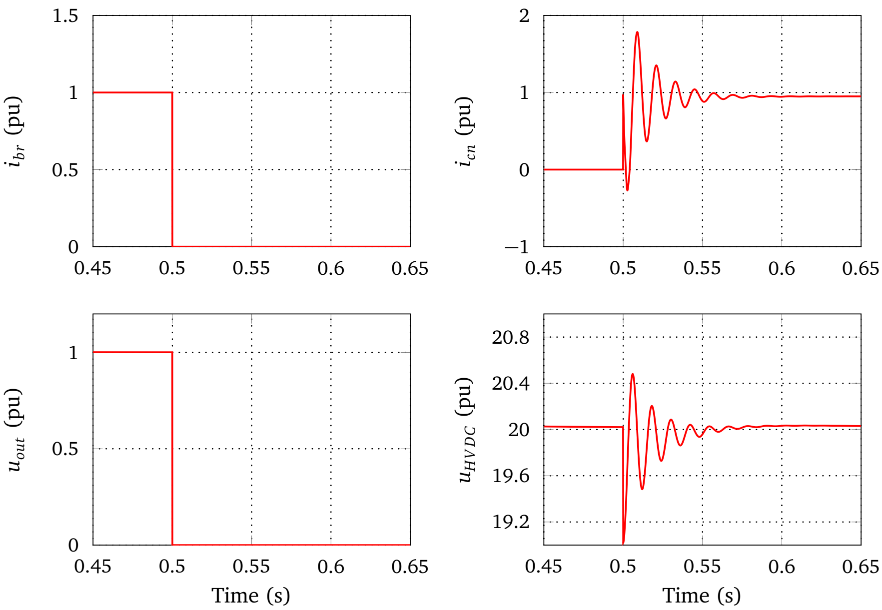

(b) Behaviour of the wind turbine by using bypass solution 1.

Figure 2.19 – Wind turbine bypass solution 1: DC breakers at output of the wind turbine.

Figure 2.19b shows the response of voltage and current due to the trigger of the protection system of one wind turbine in a wind farm with 20 units. The input current and output voltage step directly to 0 after the wind turbine is cut off from the cluster. The current in the connector i_{cn} increases from 0 to the HVDC current. However, the HVDC voltage stays constant since it is controlled by the onshore converter.

The second solution proposes to block the IGBT bridge, turn the wind turbine into idle mode. The diode bridge serves as the path for HVDC current as shown in Figure 2.20a. In this case, the output capacitor C_{out} is short-circuited, so that it dissipates its energy gradually to 0. Therefore, the variation of the HVDC voltage in this solution is not significant compared to the direct bypass scheme of the above solution.

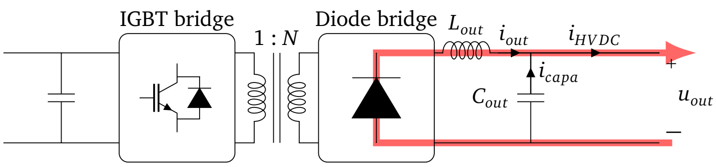

(a) Diagram of bypass solution 1.

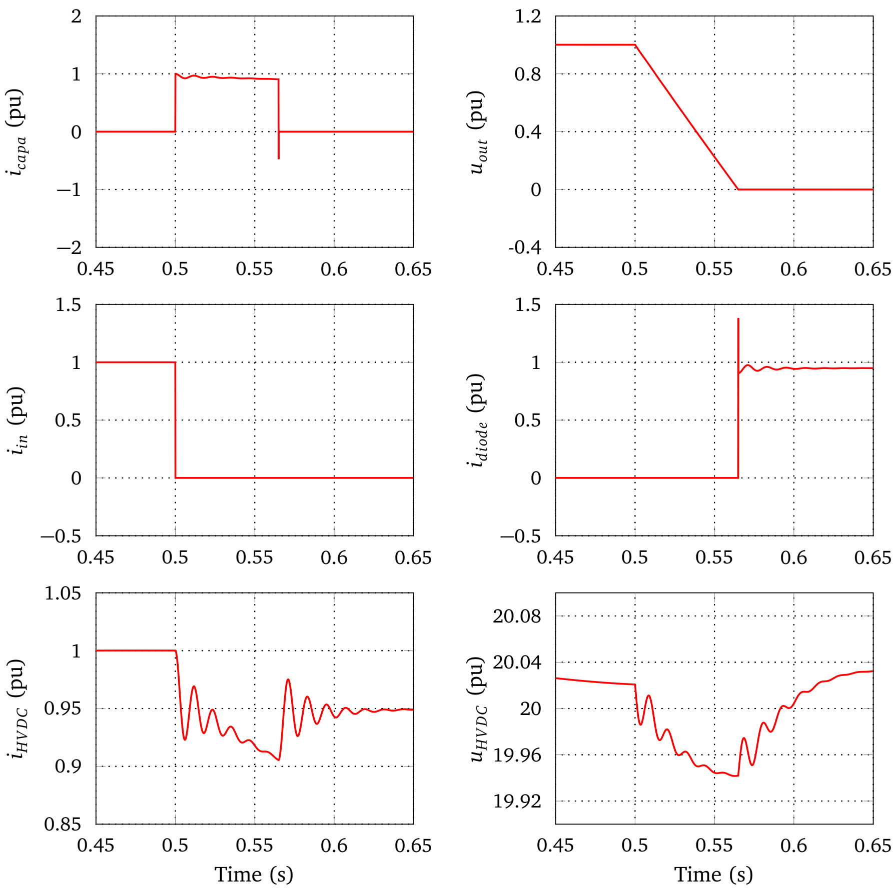

(b) Behaviour of the wind turbine by using bypass solution 2.

Figure 2.20 – Wind turbine bypass solution 2: Diode bridge taken as a current path.

2.3.7 Summary of the control system of the series connected wind turbine

The combination of the maximum power control of wind turbine generator side rectifier and the full bridge converter, used to control the wind turbine in normal operation in the series connection is presented in Figure 2.21.

In normal operation, these two controllers are allocated with different functions. The control of generator side rectifier is designed to realize MPPT, which produces the current references to the current control loop. The outputs of the control loop are the voltage references in the dq reference frame for the rectifier. The conversion from dq to abc frame requires the measurement of the electrical rotational speed of the generator.

Finally the switching of the rectifier can be obtained by comparing the voltage reference to the DC side voltage u_{in}. This DC link voltage u_{in} is kept constant by the DC/DC converter. The function of this large DC link capacitor C_{in} is to decouple the wind turbine generator part and the DC/DC converter part. The DC/DC converter takes the role of stepping up the DC voltage from the low level at the generator side to the output high voltage. Note that the control of the DC/DC converter is different from general applications, where the output voltage is to be controlled. In normal operation of the series wind turbine, the DC/DC converter does not control its output voltage. Instead, the output voltage is imposed by the cluster voltage with a proportional relationship to relative share of the wind turbine power production in the cluster power.

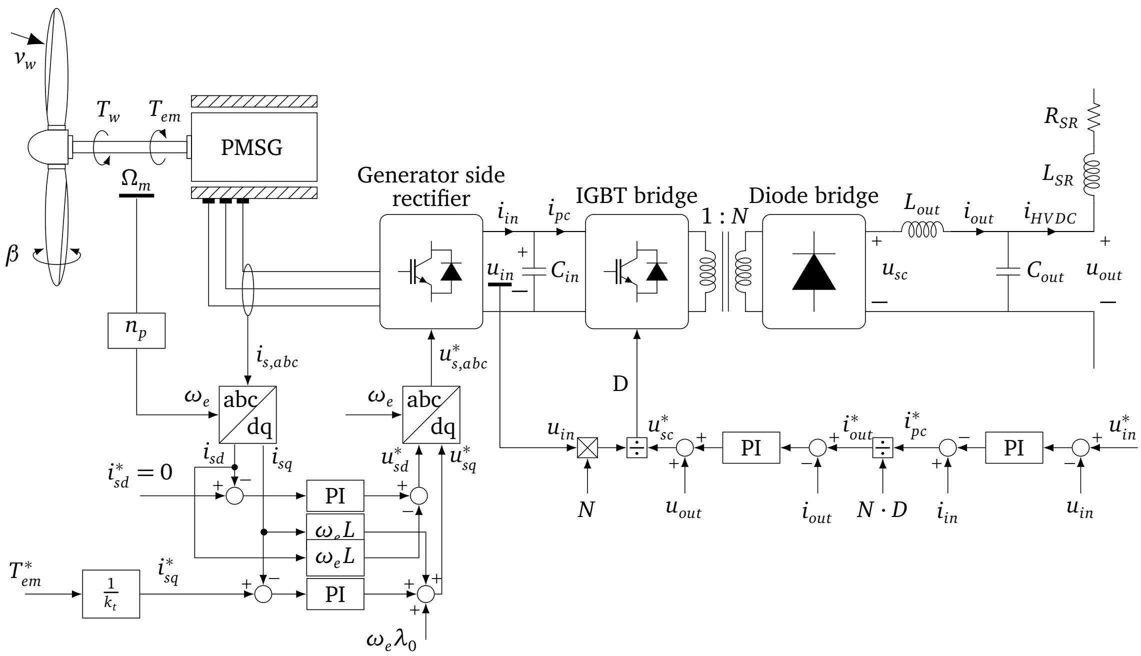

Figure 2.21 – Control diagram of the entire system of an offshore wind turbine to be connected in series.

2.3.8 Wind turbine model simplification

In order to study the operating principles and characteristics of a SWF with a number of series connected DC wind turbines, a simplified wind turbine model is necessary. Similar to the assumptions made to develop the simplified model of parallel connected DC wind turbines in [Robi 10], it is assumed here that the series connected wind turbine control system operates such that:

1. The DC link voltage is maintained constant by the DC/DC converter, and thus the generator and rectifier are decoupled from the DC/DC converter;
2. The generator side rectifier controls the wind turbine to achieve the MPPT.

Due to the inertia of the wind turbine shaft and blades, the electromagnetic power can be regarded as the wind power passing through a first-order filter with a time constant T_s [Cour 08], [Wang 12]. The dynamics of the rectifier and the DC/DC converter can be ignored because the mechanical dynamics of large wind turbine are usually around several seconds [Hans 08].

It is possible to further simplify this model by using an average model of the DC/DC full bridge converter, as shown in Figure 2.22. The input captured wind power, P_w, is non-linear, and depends on the wind speed, power coefficient, as discussed in Subsection 2.3.1.1. In normal operation, the DC link voltage is controlled to be constant, and thus the variation of the electromagnetic power is reflected by a variation of the controlled current source.

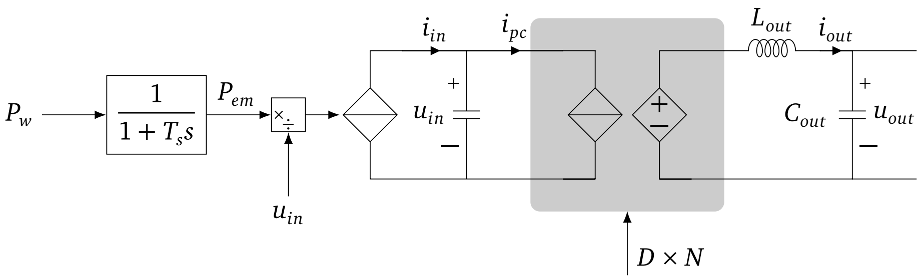

Figure 2.22 – Simplified wind turbine model for simulation study.

2.4 Operation of a series connection

In this study, 5 MW wind turbines are used because it is currently the most used power rating in offshore wind energy markets. In each wind turbine, an individual full scale rectifier is used to fully control the active and reactive powers of the generator.

The output voltage of generators is set to 3.3 kV. The reason for this value instead the more typical 690 V is to avoid too high currents inside the wind generator [Mada 13].

The nominal output voltage of the wind turbine is 32 kV. In this way, a cluster with 20 series wind turbines can establish a transmission HVDC voltage level of ±320 kV. The parameters of the DC/DC full bridge converter is shown in Table 2.2. A connection of 20 wind turbines is considered for an illustrative simulation. Figure 2.23 illustrates the variation of the wind speed, the output power and voltage, the duty cycle of the DC/DC converter of each wind turbine as well as the HVDC current variation.

Table 2.2 – Parameter of DC/DC converter in the series connected wind turbine

Nominal output power	$P_{out,nom}$	5	MW
DC link voltage	$U_{in,nom}$	3.3	kV
Nominal output voltage	$U_{out,nom}$	32	kV
Transformer ratio	N	15	
DC link capacitor	C_{in}	10	mH
Output capacitor	C_{out}	293	µH
Output inductor	L_{out}	100	mH

The output power variation of these 20 wind turbines is plotted in Figure 2.23b. These curves show a reduction of the wind speed blowing from the last wind turbine WT_{20} to the first wind turbine WT_1. For the sake of convenience, every four wind turbines are supposed to have the same power variation. 1 pu corresponds the nominal values of a single wind turbine, power generation or output voltage.

In Figure 2.23c the output voltages of these wind turbines evolving with their power are shown. It can be noticed that the output voltages of $WT_{1\text{-}4}$ increase gradually to around 1.2 pu until 25 s, while their power remains constant at 1 pu. Due to this increase of the voltage, the duty cycles of the DC/DC converters of $WT_{1\text{-}20}$ also increase since the ratios between the increasing output voltage and constant DC link voltage become larger. Finally, after 25 s, the wind speed is equal for all these 20 wind turbines, the output voltages reach 1 pu. However, it should be noticed that their power productions were reduced to 0.8 pu.

From 5 s to 25 s, there are clearly over-voltages of certain wind turbines due to imbalanced power productions. It has been defined in 2.2.3 that in the series connection, a certain extend of overvoltage is necessary to keep a safe operation of the wind turbines. To accomplish this, the DC/DC converter should be over-sized. The transformer ratio should also be set above its nominal value. As shown in the Table 2.2 the transformer ratio is designed to be 15, while the ratio between nominal output voltage and DC link voltage is $32/3.3 \approx 9.7$. The diode bridge at the high voltage side of the transformer should also be able to operate at a certain overvoltage level.

However, because the wind variation is unpredictable, this certain overvoltage level is difficult to be assessed. Furthermore, the oversizing of the DC/DC transformer increases its volume, which is not practical for offshore applications. Subsequently, overvoltage limitation control should be developed.

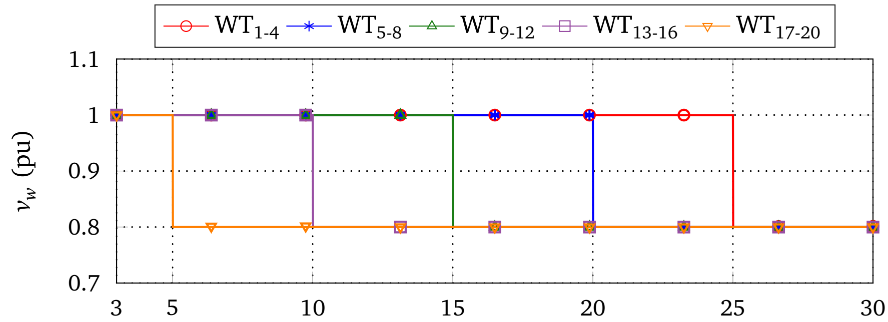

(a) Wind speed variation of each wind turbine.

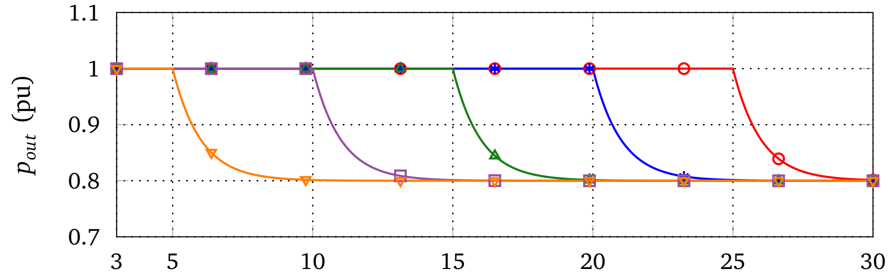

(b) Output power of each wind turbine.

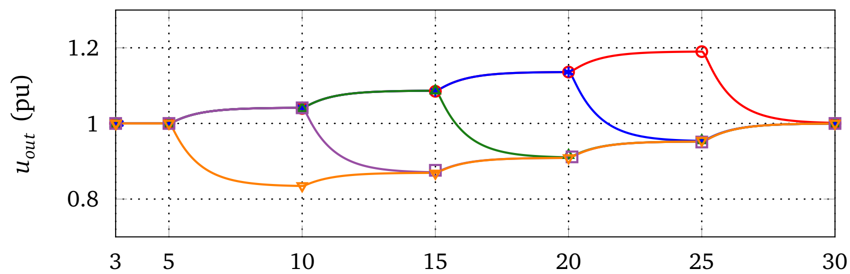

(c) Output voltage of each wind turbine.

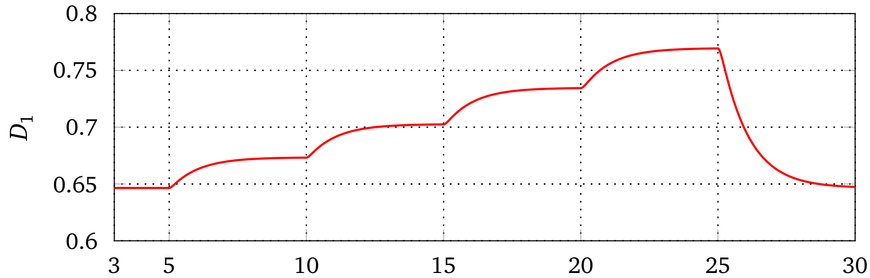

(d) Duty cycle of the DC/DC converter of WT_1.

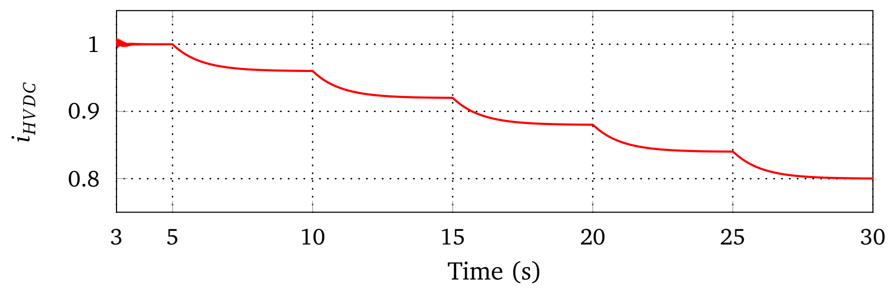

(e) HVDC current variation.

Figure 2.23 – Behaviour of the series connection of twenty wind turbines with infinite over-voltage capabilities.

2.5 Overvoltage limitation methods

The normal operation of a SWF comprising 20 units is simulated in Section 2.4 and the bypass methods are described in Section 2.3.6. The wind turbines output DC/DC converters are assumed to have infinite overvoltage capabilities in these two sections. Whereas the wind speed across an offshore wind farm may not be dramatically different, it is difficult to assess a sufficient level of overvoltage capability. It has also been considered that the fault occurring on several units in the wind farm would immediately push up the output voltage level across wind turbines, and could deteriorate the wind turbines' ability to overcome imbalanced wind speed. Therefore, it is necessary to develop overvoltage limitation methods to restraint the output voltages of wind turbines within safe limits.

A direct overvoltage limitation method consists in controlling the wind turbine output voltage when overvoltage occurs. The wind turbines can be designed to have certain extent of overvoltage, as long as the output voltage increases to this limit, one of the wind turbine converter is allocated to maintain this voltage at limitation level.

Since there are only two converters in the wind turbine, in normal control, one of the converters is responsible for controlling the DC link voltage and the other one is responsible for power control, which aims at extracting maximum power from the wind. In overvoltage limitation control, one of the converters has to abandon its previous duty and shift to output voltage control. In [Lund 06], the DC/DC converter is assigned to control the output voltage and the generator side rectifier is assigned to control the DC link voltage. Alternatively, in [Shi 13], the generator side rectifier is assigned to control the output voltage and the DC/DC converter controls the DC link voltage in both normal and limitation mode. This method is shown in Figure 2.24. However, no matter which converter is shifted to accomplish the overvoltage limitation, the wind turbine is not able to track maximum power.

As shown in Figure 2.24, when the sensor measures the output voltage reaching the overvoltage limitation, an output voltage controller will be triggered to regulate the wind turbine to operate at the overvoltage limitation level. The output of the voltage limitation controller is taken as a compensation torque to the inner current controller. The value of this torque will always be negative and thus, the torque reference for the inner current loop will decrease.

In both alternatives, the torque imposed by the wind is greater than the reference electromagnetic torque. As a result, the wind turbine will accelerate, but its speed is limited by the rotational speed controller, which increases the pitch angle in order to send wind power into the wind turbine system. Therefore, the wind turbine decelerates and the input power decreases.

In this thesis, this kind of control is named as local control, since it focuses in the individual wind turbine. The advantage of a local control is that the communication between wind turbines is not necessary, which leads to an accurate and reliable control. But its disadvantages are the following:

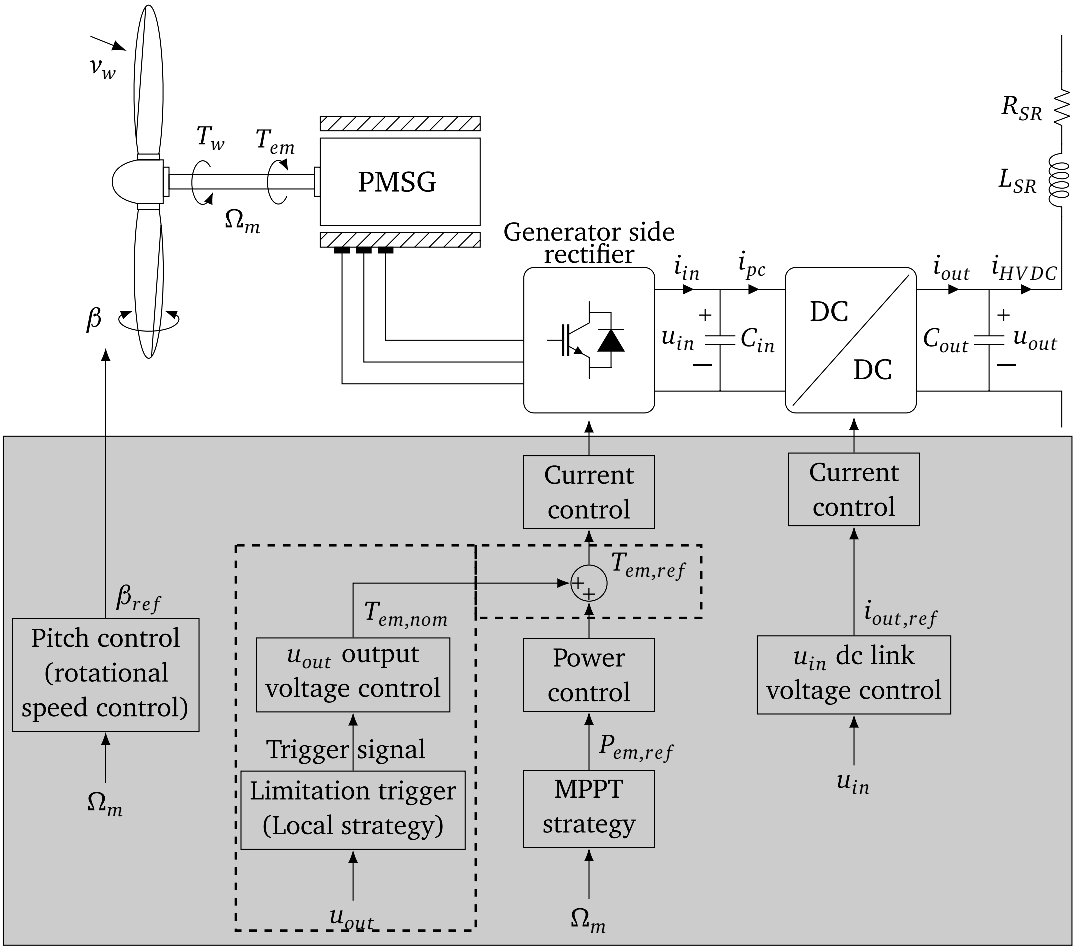

Figure 2.24 – Local control strategy for overvoltage limitation of series connected wind turbines.

1. The most obvious issue is related to power losses. As explained, the wind turbine converters has no the ability to track the maximum power since one converter is allocated for controlling the output voltage. Therefore the decreased power efficiency leads to less power extracted from the wind.

   The amount of power loss is difficult to estimate, but it depends on the converters overvoltage capability. The larger rating converter used, the higher cost of the converter, and the less power loss caused by local control. It is also suggested in [Lund 06] that, 35% over-sizing of each wind turbine output converter is economically acceptable. However, this conclusion is made on fault-free scenarios. Bypassing more than one wind turbines in one cluster, subsequent to various failures, can easily force the sound units to withstand higher voltage, and thus the variation range is substantially limited. Moreover, over-sizing the high voltage side of the DC/DC converter will substantially increase the volume of the High Frequency Transformer (HFT) [Bahm 16]. As a consequence, simply adopting largely over-sized converters is not a reliable and cost-efficient method for a SWF.

2. In addition, local control may cause other wind turbines to operate in overvoltage

mode. Since the decrease of the power of one wind turbine causes the entire wind farm power to decrease, those wind turbines operating in the margin of their overvoltage capabilities may enter into limitation modes, which further decreases the power production of the whole wind farm.

2.6 Conclusion

In this chapter the wind turbine used in the SWF has been designed. The PMSG is used for power conversion and the transformer-insulated full bridge DC/DC converter is used for voltage step-up. Differently from conventional applications of the DC/DC converter which controls the output voltage, in the SWF, the output voltage of the wind turbine is left uncontrolled. In this way the output voltage can vary according to the power production of the wind turbine. The control system of the entire wind turbine operating in normal condition is given.

The operation behaviour of a series connection is described. For the sake of convenience, a simulation using simplified wind turbine models is used to validate the behaviour of this kind of wind farm. It is important to notice that the variation of wind turbine power leads to fluctuation of wind turbine output voltages, and thus the duty cycle of the DC/DC converter. As a result, wind turbine output DC/DC converters should be over-sized in order to operate in overvoltage mode.

Due to wind turbulence, which may be close to 30% for adjacent turbines [Bart 07], power differences in the series connection would cause certain wind turbines to operate at much higher power stress than other units. The local overvoltage limitation control strategy is described in this chapter. The local control is reliable and requires no communication between wind turbines but it also leads to power curtailment.

Since there are only two converters that can be used in the wind turbine, it is necessary to expand the investigation outside the wind turbine, in order to explore other overvoltage limitation methods. Therefore, in the next chapter, the operation of a DC SWF integrated into a HVDC transmission system will be investigated. The influence of the HVDC cables and onshore converters on the SWF is studied.

References

[Acke 05] T. Ackermann. *Wind power in power systems*. John Wiley & Sons, 2005. 60

[Bahm 16] M. A. Bahmani, T. Thiringer, A. Rabiei, and T. Abdulahovic. "Comparative Study of a Multi-MW High-Power Density DC Transformer With an Optimized High-Frequency Magnetics in All-DC Offshore Wind Farm". *IEEE Transactions on power delivery*, Vol. 31, No. 2, pp. 857–866, 2016. 67, 82

[Bart 07] R. J. Barthelmie, S. T. Frandsen, M. Nielsen, S. Pryor, P.-E. Rethore, and H. E. Jørgensen. "Modelling and measurements of power losses and turbulence intensity in wind turbine wakes at Middelgrunden offshore wind farm". *Wind Energy*, Vol. 10, No. 6, pp. 517–528, 2007. 57, 83

[Chen 07] Z. Chen, Y. Hu, and F. Blaabjerg. "Stability improvement of induction generator-based wind turbine systems". *IET Renewable Power Generation*, Vol. 1, No. 1, pp. 81–93, 2007. 63

[Cour 08] V. Courtecuisse. *Supervision d'une centrale multisources à base d'éoliennes et de stockage d'énergie connectée au réseau électrique*. PhD thesis, Arts et Métiers ParisTech, 2008. 78

[De D 91] R. W. De Doncker, D. M. Divan, and M. H. Kheraluwala. "A three-phase soft-switched high-power-density DC/DC converter for high-power applications". *IEEE transactions on industry applications*, Vol. 27, No. 1, pp. 63–73, 1991. 67

[El A 04] S. El Aimani. *Modélisation des différentes technologies d'éoliennes intégrées dans un réseau de moyenne tension*. PhD thesis, Ecole Centrale de Lille, 2004. 64

[Eric 07] R. W. Erickson and D. Maksimovic. *Fundamentals of power electronics*. Springer Science & Business Media, 2007. 67

[Fils 14] K. Filsoof, A. A. Hagar, and P. W. Lehn. "A transformerless modular step-up dc–dc converter for high power applications". *IET Power Electronics*, Vol. 7, No. 8, pp. 2190–2199, 2014. 67

[Hans 08] A. D. Hansen and G. Michalke. "Modelling and control of variable-speed multi-pole permanent magnet synchronous generator wind turbine". *Wind Energy*, Vol. 11, No. 5, pp. 537–554, 2008. 78

[Heie 14] S. Heier. *Grid integration of wind energy: onshore and offshore conversion systems*. John Wiley & Sons, 2014. 62

[Jaco 10] B. Jacobson, P. Karlsson, G. Asplund, L. Harnefors, and T. Jonsson. "VSC-HVDC transmission with cascaded two-level converters". In: *Cigré session*, pp. B4–B110, 2010. 73

[Jovc 09] D. Jovcic. "Step-up DC–DC converter for megawatt size applications". *IET Power Electronics*, Vol. 2, No. 6, pp. 675–685, 2009. 67

[Kher 92] M. Kheraluwala, R. W. Gascoigne, D. M. Divan, and E. D. Baumann. "Performance characterization of a high-power dual active bridge dc-to-dc converter". *IEEE Transactions on industry applications*, Vol. 28, No. 6, pp. 1294–1301, 1992. 67

[Kund 94] P. Kundur, N. J. Balu, and M. G. Lauby. *Power system stability and control*. Vol. 7, McGraw-hill New York, 1994. 72

[Lecl 04] L. Leclercq. *Apport du stockage inertiel associé à des éoliennes dans un réseau électrique en vue d'assurer des services systèmes*. PhD thesis, Université Lille 1, 2004. 64

[Lund 06] S. Lundberg. *Wind Farm Configuration and Energy Efficiency Studies-Series DC versus AC Layouts*. PhD thesis, Chalmers University of Technology, 2006. 57, 81, 82

[Mada 13] A. Madariaga, J. Martín, I. Zamora, I. M. De Alegria, and S. Ceballos. "Technological trends in electric topologies for offshore wind power plants". *Renewable and Sustainable Energy Reviews*, Vol. 24, pp. 32–44, 2013. 75, 78

[Max 09] L. Max. *Design and control of a DC collection grid for a wind farm*. Chalmers University of Technology, 2009. 67

[Meye 07] C. Meyer. *Key Components for Future Offshore DC Grids*. *Aachener Beiträge des ISEA*, Shaker, 2007. 67

[Mich 10] G. Michalke and A. D. Hansen. "Modelling and control of variable speed wind turbines for power system studies". *Wind Energy*, Vol. 13, No. 4, pp. 307–322, 2010. 63

[Monj 12] P. Monjean. *Optimisation de l'architecture et des flux énergétiques de centrales à énergies renouvelables offshore et onshore équipées de liaisons en continu*. PhD thesis, Arts et Métiers ParisTech, 2012. 57, 67

[Robi 10] J. Robinson, D. Jovcic, and G. Joós. "Analysis and design of an offshore wind farm using a MV DC grid". *IEEE Transactions on Power Delivery*, Vol. 25, No. 4, pp. 2164–2173, 2010. 78

[Shi 13] G. Shi, Z. Wang, M. Zhu, X. Cai, and L. Yao. "Variable speed control of series-connected DC wind turbines based on generalized dynamic model". In: *Renewable Power Generation Conference (RPG 2013), 2nd IET*, pp. 1–6, IET, 2013. 81

[Stei 88] R. L. Steigerwald. "A comparison of half-bridge resonant converter topologies". *IEEE transactions on Power Electronics*, Vol. 3, No. 2, pp. 174–182, 1988. 67

[Wang 12] Y. Wang. *Evaluation de la Performance des Réglages de Fréquence des Eoliennes à l'Echelle du Système Electrique: Application à un Cas Insulaire*. PhD thesis, Ecole Centrale de Lille, 2012. 78

[Yin 07] M. Yin, G. Li, M. Zhou, and C. Zhao. "Modeling of the wind turbine with a permanent magnet synchronous generator for integration". In: *Power Engineering Society General Meeting, 2007. IEEE*, pp. 1–6, IEEE, 2007. 63, 65

[Zhao 14] B. Zhao, Q. Song, W. Liu, and Y. Sun. "Overview of dual-active-bridge isolated bidirectional DC–DC converter for high-frequency-link power-conversion system". *IEEE Transactions on Power Electronics*, Vol. 29, No. 8, pp. 4091–4106, 2014. 67

[Zhu 13] J. Zhu, C. D. Booth, G. P. Adam, A. J. Roscoe, and C. G. Bright. "Inertia emulation control strategy for VSC-HVDC transmission systems". *IEEE Transactions on Power Systems*, Vol. 28, No. 2, pp. 1277–1287, 2013. 72

Chapter 3

Series wind farm in Point-to-Point HVDC transmission

Vous devez passer votre vie à aimer et à penser; c'est la véritable vie des esprits.

Voltaire

Contents

3.1 Introduction

In Chapter 2, it was presented that the wind turbines in series connection may operate in overvoltage mode due to imbalanced power production. Although it is suggested that the wind turbine output DC/DC converter might be designed to a have certain overvoltage capability, it is difficult to determine how much overvoltage capability is suitable.

The issue of overvoltage limitation is crucial to the operation of a Series Wind Farm (SWF). However, there is a paucity of literature focusing on this issue. In references [Lund 06], [Shi 13], a local overvoltage limitation control is proposed, which uses either the output converter or the generator side rectifier in the wind turbine to control the output voltage when it reaches the maximum overvoltage capability. This method is reliable and requires no communication between series connected wind turbines. However, it also causes power curtailment since it proposes the reduction of power production of certain units in order to re-balance the wind turbines output voltages. Moreover, the amount of power losses is unpredictable since there is a number of elements that influence the wind speed across the wind farm. In addition to the oversized rating of the converters, the power curtailment is also affected by the failure rate of wind turbines.

The inconvenience of the aforementioned overvoltage limitation method makes necessary the investigation outside the wind farm. As long as the power is generated in the wind farm, it is transmitted to onshore and integrated into the power grid. Hence, the entire studied system is composed of three parts: the offshore wind farm, the power transmission system and the grid integration. The offshore wind farm with wind turbines in series connection has been studied in Chapter 2, the remaining two issues are investigated in this chapter.

The previous chapter has mentioned two HVDC technologies, the Line Commutated Converter (LCC) and Voltage Source Converter (VSC). This chapter focuses on VSC-based HVDC technology and uses Multilevel Modular Converter (MMC) as onshore converter substation. The difference between the MMC and the conventional 2-level VSC is discussed in this chapter. Some assumptions are made to simplify the MMC model and an energy based arm average model which takes into account the MMC stored energy is given. The equations governing the physical system are analysed and a control system in dq reference frame is developed to ensure an accurate tracking of reference signals. The control system includes DC voltage control or active power control, AC voltage control or reactive power control. Different from conventional 2-level VSC, an extra control loop is required to control the stored energy in the MMC.

In a conventional MVAC-HVDC offshore wind farm, the offshore substation decouples the transmission system and the collection system. In contrast, in SWF, the collection system (a cluster with series connected wind turbines) is directly linked to the HVDC cable and so, the characteristics of the cable cannot be ignored by simply replacing it with a small capacitor or pi section model. Indeed, the series wind farm and the HVDC cable form a resonant circuit so that the damping ability of the cable is critical when a wind turbine is bypassed.

After describing both transmission and integration systems, a global control strategy is therefore proposed in this chapter, which regulates the HVDC transmission voltage in order to reduce the voltage across the wind turbines at the offshore end.

The optimal voltage level needs to be calculated according to the wind farm working conditions. Since the decrease of voltage level results in the increase of current and thus losses in the cables, an optimal HVDC voltage level associated to the corresponding voltage of the maximum power received at the onshore end. In addition, the local control strategy is proposed to be complementary to the global control. Finally, the entire control system of a Series Wind Farm (SWF) is presented and built in EMTP-RV® [Mahs 07].

3.2 Modular Multilevel Converter (MMC)

In this work, the MMC-HVDC technology is used as onshore converter. MMC is firstly introduced in [Marq 01], and has become the most promising VSC topology so far. Its modular design, enabling the stacking of low voltage rating Sub Modules (SMs), overcomes the limitations of conventional 2-level and 3-level VSC in many aspects, such as lower switching losses, higher voltage ratings and lower harmonic distortion [Nami 15].

The MMC exhibits clear differences in comparison to the 2-level and 3-level VSC mainly because the stored energy is distributed in the arms of the MMC. This particular feature of the MMC requires an extra control loop for its internal dynamics. In this section, the MMC Arm Average Model (AAM) is first presented and then an energy based control system is described. A N+1 voltage level MMC topology is shown in Figure 3.1.

Each arm of this converter is composed of N SMs in series and an inductance. A detailed circuit of the SM with the simplest half bridge topology is given in the figure. There are other topologies proposed in the literature, like full bridge topology which comprises 4 IGBTs, and therefore increasing the losses in the converter but being able to block HVDC current when a short circuit occurs [Nami 15].

The total voltage of the SMs and inductances in the upper and lower arms equals the HVDC voltage. Switching ON/OFF the IGBTs in the SM allows a selective connection and disconnection of this fraction of SM capacitor voltage into the AC grid. If T_1 is turned on and therefore T_2 is turned off, the SM voltage u_{SM_i} is equal to the capacitor voltage u_{C_i}. This SM is in the ON state. On the contrary, this SM is in the OFF state when the SM is short circuited and its voltage u_{SM_i} equals 0. By adjusting the number of switched-on SMs in one phase, the desired sinusoidal voltage at the AC terminal is achieved. For this reason, MMC usually adopts a very high number of SMs in order to produce less harmonics on the AC side. An illustration of the voltage waveform of a 8+1 level MMC is shown in Figure 3.2.

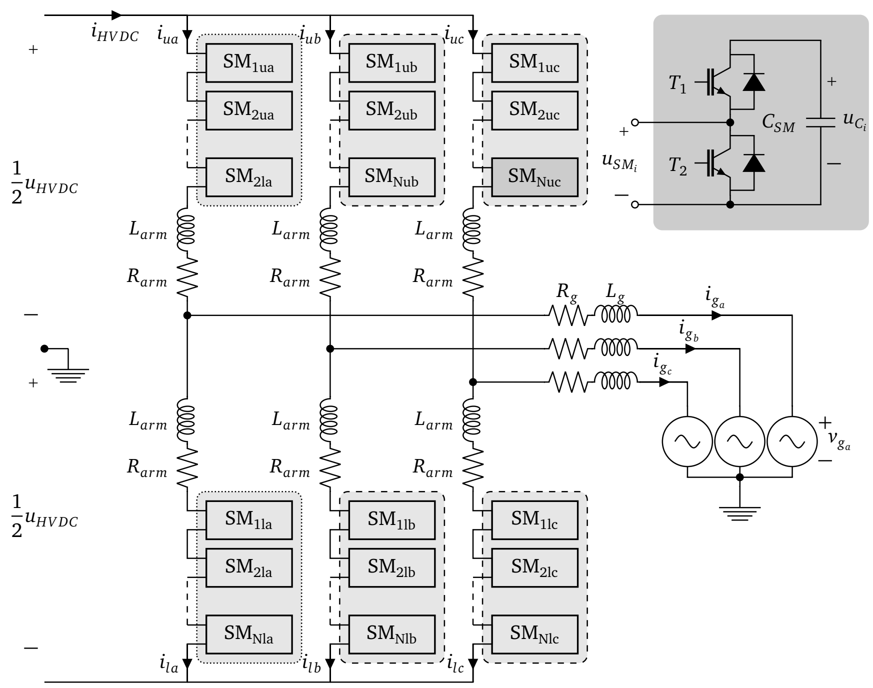

Figure 3.1 – MMC detailed representation with N submodules.

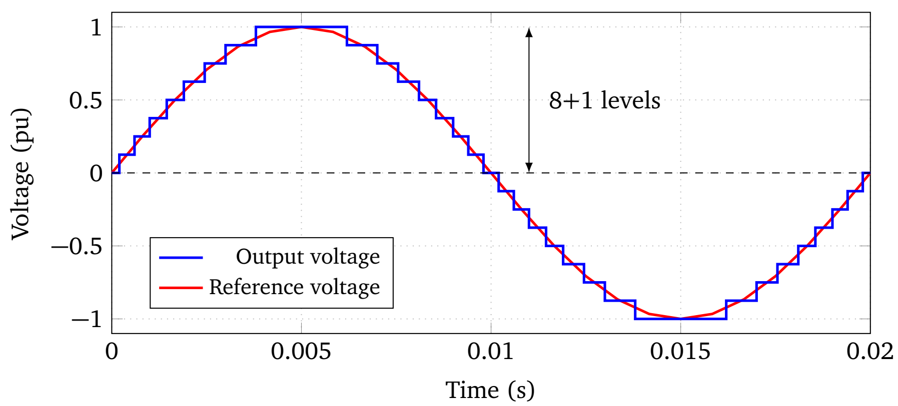

Figure 3.2 – An illustration of the voltage waveform of a MMC with 8 SMs per arm.

This characteristic of the MMC offers many benefits over conventional VSCs, as summarized below [Rohn 10]:

1. Modular design;
2. Simple voltage scaling by a series connection of cells;
3. Distributed location of capacitive energy storages;
4. High resulting switching frequency;
5. Simple realization of redundancy;
6. High front-end flexibility;
7. Filter-less configuration for standard machines or grid converters;

8. Grid connection via standard transformer or transformer-less;
9. Possibility of common DC bus configurations for multi-drive and high-power applications.

However, the high number of semiconductors and gate units is one of the drawbacks of the MMC as it demands a more complicated gating algorithm compared to 2-level or 3-level VSC. The voltage should be distributed evenly in each SM, adding another difficulty to the control system.

3.2.1 Modelling of the MMC

There exist several MMC models in the literature. They are categorized into 4 types by [Saad 15]. Figure 3.3 shows different complexities of these models which are briefly introduced below. The type 3 is modelled in detail since it is the MMC model used in this thesis.

3.2.1.1 The 4 types of MMC models

Type 1 is the most accurate model which contains hundreds of non-linear power switches in one single arm. For example, a 401-level MMC comprises 4800 switches and 4800 diodes. Such a detailed model offers many benefits like the estimation of the switching losses, the simulation different SM topologies and the analysis of the faults inside a converter. However, this type of model requires a high computation effort. Furthermore, Balancing Capacitor Algorithm (BCA) is needed to be implemented, which balances the SM capacitor voltages to maintain them within an acceptable range. Mathematical representation of this model is impossible because of the presence of non-linear power switches.

Type 2 model firstly proposed in [Gnan 11] reduces the SMs of its precedent to ON/OFF resistors. This method allows the derivation of a Norton equivalent circuit for each arm of the MMC, reducing considerably the number of electrical nodes, and hence, the computation effort. BCA needs to be implemented in this model as well.

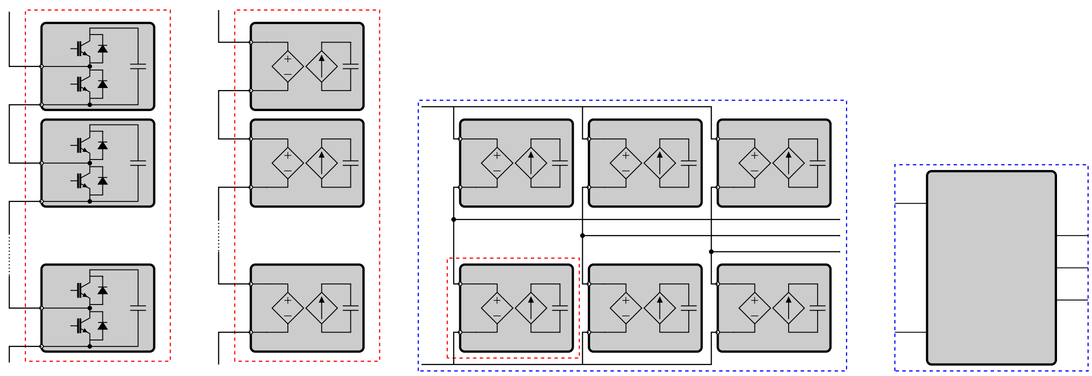

Figure 3.3 – The 4 types of MMC models with decrease in complexity from left to right.

Type 3 model is an Average Value Model (AVM), usually called AAM, assumes that all SM capacitor voltages are balanced by BCA. The SMs are averaged using the concept of conversion function in one arm. Although in this model the information of the switching states is lost, the dynamics and stored energy in each arm are retained [Anto 09]. This model significantly reduces the computation effort compared to the two precedents. Some works further simplify the type 3 MMC model like in [Frey 16], in which the model is reduced to 4 independent state variables assuming that the high level control balances the upper and lower arm voltages in normal operation.

Type 4 model is similar to a classic 2-level VSC converter, with an equivalent capacitor directly connected to the DC terminals. Therefore the energy stored in the MMC cannot be controlled independently. The over-simplification of this model fails to provide an accurate representation of the MMC. As a result, it is discarded as stated in [Akka 16].

3.2.1.2 Arm Average Model of MMC

The AAM of MMC is depicted in Figure 3.4. The AAM model comprises one upper arm and one lower arm for each phase, each being composed of an arm inductor L_{arm}, an arm resistor R_{arm} and an equivalent capacitor C_{tot}.

Since it is assumed that the low level control BCA is well performed, all the SM capacitor voltages are evenly distributed, ($u_{C_1} = u_{C_2} \dots = u_{C_N}$), and the equivalent MMC arm capacitance C_{tot} equals the sum of all SM capacitors C_{SM}/N [Sami 16a].

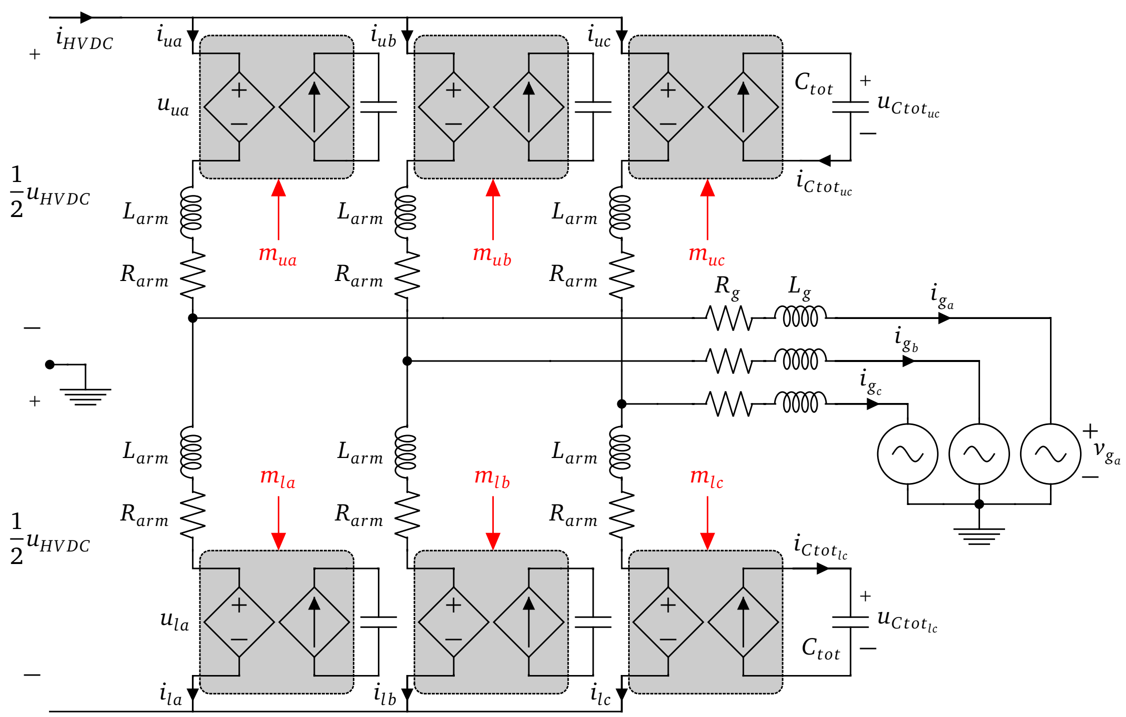

Figure 3.4 – Arm average model of MMC.

By defining the duty cycle $m = n/N$ with n the number of active cells in the arm, new variables are deduced to describe the arm voltages u_{ul_j} and arm capacitor currents $i_{Ctot_{ulj}}$:

$$u_{ul_j} = m_{ul_j} u_{Ctot_{ulj}} \qquad i_{Ctot_{ulj}} = m_{ul_j} i_{ul_j} \tag{3.1}$$

where the subscripts u and l represent the upper arm and the lower arm, and j refers to three phases a, b, c.

The equivalent capacitor owns the physical characteristic as the current–voltage relation (in Figure 3.5):

$$i_{Ctot_{ulj}} = C_{tot} \frac{du_{Ctot_{ulj}}}{dt} \tag{3.2}$$

Following the Kirchhoff's law, the equations describing the MMC system are:

$$\frac{u_{HVDC}}{2} = u_{u_j} + L_{arm} \frac{di_{u_j}}{dt} + R_{arm} i_{u_j} + L_g \frac{di_{g_j}}{dt} + R_g i_{g_j} + v_{g_j} \tag{3.3}$$

$$\frac{u_{HVDC}}{2} = u_{l_j} + L_{arm} \frac{di_{l_j}}{dt} + R_{arm} i_{l_j} - L_g \frac{di_{g_j}}{dt} - R_g i_{g_j} - v_{g_j} \tag{3.4}$$

The addition and subtraction of equations (3.3) and (3.4) yield a decoupled system described by the following set of equations [Anto 09]:

$$\frac{u_{HVDC}}{2} - u_{diff_j} = L_{arm} \frac{di_{diff_j}}{dt} + R_{arm} i_{diff_j} \tag{3.5}$$

$$u_{v_j} - v_{g_j} = \left(L_g + \frac{L_{arm}}{2}\right) \frac{di_{g_j}}{dt} + \left(R_g + \frac{R_{arm}}{2}\right) i_{g_j} \tag{3.6}$$

$$= L_{eq} \frac{di_{g_j}}{dt} + R_{eq} i_{g_j} \tag{3.7}$$

where u_{v_j}, i_{diff_j} and u_{diff_j} are new variables oriented to perform the change of variables:

$$u_{diff_j} = \frac{u_{u_j} + u_{l_j}}{2}; \quad i_{diff_j} = \frac{i_{u_j} + i_{l_j}}{2}; \quad u_{v_j} = \frac{u_{l_j} - u_{u_j}}{2}; \quad i_{g_j} = i_{u_j} - i_{l_j} \tag{3.8}$$

In the MMC phases, the differential currents i_{diff_j} are composed of DC components and harmonic components [Tu 11b]. In normal operation, the sum of the three DC components $i_{diff_j^{DC}}$ equals the HVDC current i_{HVDC}, which defines the power transmitted from the DC to the AC side.

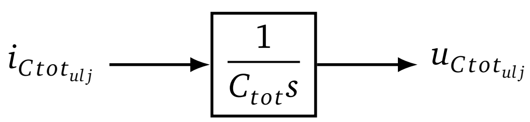

Figure 3.5 – Block diagram of the equivalent capacitor voltage model.

The AC components $i_{diff_j^{AC}}$, also called circulating currents, circulate inside the MMC and do not participate in the power transmission [Sami 16b].

In steady state, the sum of the three phases AC components is null. However, they are related to the arm capacitor voltage fluctuations and allow balancing between the upper and lower arm voltage [Dela 13][Berg 13]. The differential current model is shown in Figure 3.6.

Equation (3.7) can be rewritten in dq reference frame, in which the three phase currents i_{g_j} are transformed to two independent currents i_{g_d} and i_{g_q}:

$$u_{v_d} - v_{g_d} = L_{eq}\frac{di_{g_d}}{dt} + R_{eq}i_{g_d} - \omega_g L_{eq} i_{g_q} \tag{3.9}$$

$$u_{v_q} - v_{g_q} = L_{eq}\frac{di_{g_q}}{dt} + R_{eq}i_{g_q} + \omega_g L_{eq} i_{g_d} \tag{3.10}$$

Figure 3.7 illustrates the grid currents model in both abc and dq reference frame.

Up to this point, the MMC is characterized by 11 independent state variables: six equivalent capacitor voltages defined in Equation (3.2) and five currents, including three arm currents in Equation (3.5) and two phase currents in Equations (3.9) and (3.10). Equations (3.5) and (3.7) decouple the MMC model into two imaginary parts: a DC part and an AC part. They characterize the dynamics of the AC and DC side variables of the MMC, respectively. Furthermore, Equation (3.5) states a unique feature of MMC that, the DC currents in MMC arms are fully controllable, contrary to the non-controllability of the DC currents in traditional VSCs.

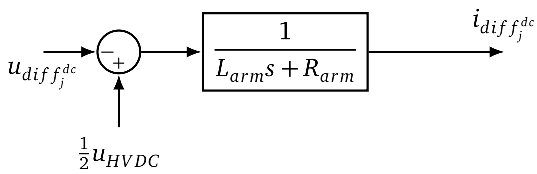

Figure 3.6 – Block diagram of the differential current model.

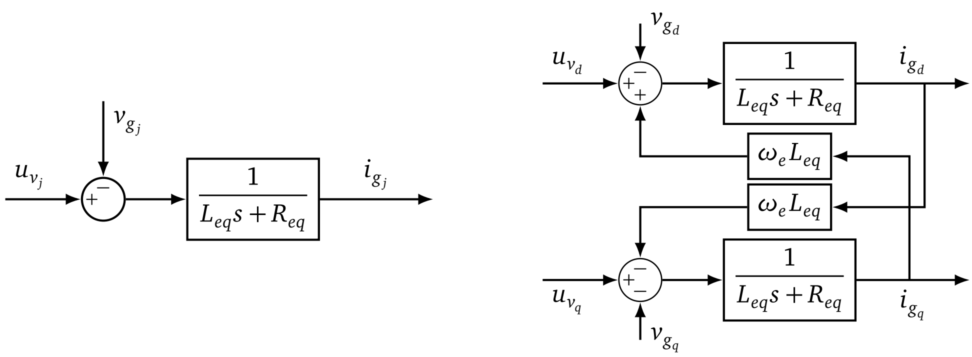

(a) In abc reference frame. (b) In dq reference frame.

Figure 3.7 – Block diagram of the grid current model.

The entire model of MMC in abc reference frame is shown in Figure 3.8.

It is necessary to consider the main difference between MMC and conventional VSC from the point of view of the power arrangement between DC and AC sides. The big capacitor attached to the DC side of the traditional 2-level or 3-level VSC acts like an energy exchange relay. At steady state, the energy is sent from offshore to the capacitor and the same amount of energy is dissipated from the capacitor to the converter. The VSC is an interface which exchanges power but stores no energy inside the converter. At steady state, neglecting the power losses in the converter, the instantaneous active power on the AC side is equal to the instantaneous power at DC side of the VSC (the PLL is designed to align the d-axis voltage):

$$p_{AC} = \frac{3}{2} v_{g_d} i_{g_d} = p_{DC}$$
$$p_{DC} - p_{AC} = 0$$

However, the MMC can be perceived as a reservoir. It has the same functions to exchange power between DC and AC side, and in addition, it stores part of the energy in the arms capacitors. The MMC allocates the power into three parts: DC part, AC part and inside the converter, as shown in Figure 3.9.

The amount of energy stored in the converter is related to the capacitor voltages in the arms. The stored energy per phase W_j^{Σ} can be expressed as:

$$\frac{dW_j^{\Sigma}}{dt} = \frac{1}{2} C_{tot} \Big(\frac{du^2_{Ctot_{uj}}}{dt} + \frac{du^2_{Ctot_{lj}}}{dt} \Big) \tag{3.11}$$

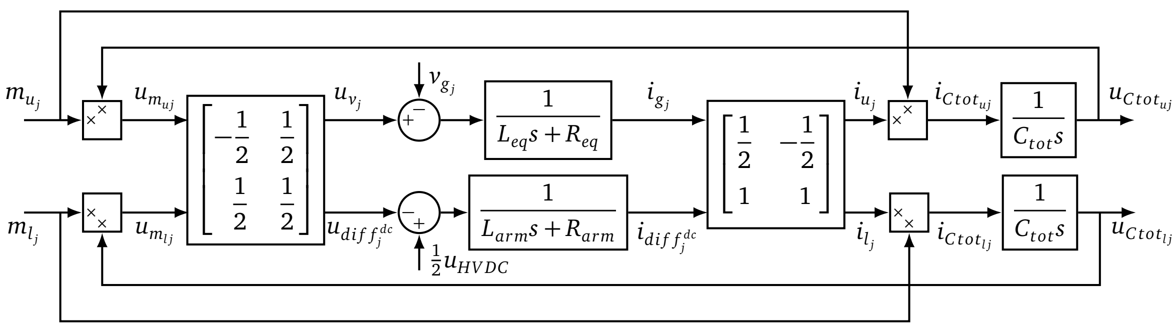

Figure 3.8 – Block diagram of the MMC model in abc frame.

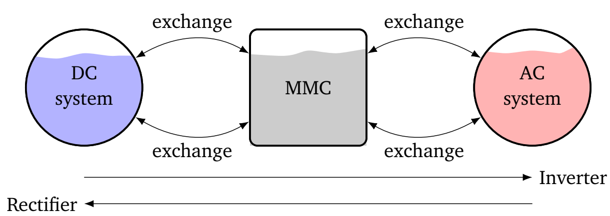

Figure 3.9 – The distribution of energy in the MMC conversion system.

Defining:

$$\frac{u^2_{Ctot_{uj}} + u^2_{Ctot_{lj}}}{2} = \overline{u^2_{Ctot_j}} \tag{3.12}$$

then yields:

$$\frac{dW_j^{\Sigma}}{dt} = C_{tot}\frac{d\overline{u^2_{Ctot_j}}}{dt} \tag{3.13}$$

The amount of stored energy is the difference between the instantaneous power at DC side and AC side:

$$p_{DC_j} - p_{AC_j} = \frac{dW_j^{\Sigma}}{dt} = C_{tot}\frac{d\overline{u^2_{Ctot_j}}}{dt} \tag{3.14}$$

The block diagram of the MMC energy model per-phase is shown in Figure 3.10. All these three parts of energy can be controlled by reversing the model, which is discussed in the next subsection.

3.2.2 Control of MMC

The control system of the MMC can be categorized into two levels, as depicted in Figure 3.11, the high level control (or global control) and the low level control (or SM control). Low level control is in charge of two targets. The first target is to select and activate the correct combination of SMs to achieve the arm voltages references given by the high level control. This can be achieved with different techniques such as Phase-Disposition PWM (PD-PWM) [Saee 10], Phase-Shift PWM (PS-PWM) [Li 15] or Nearest Level Control (NLC) [Tu 11b].

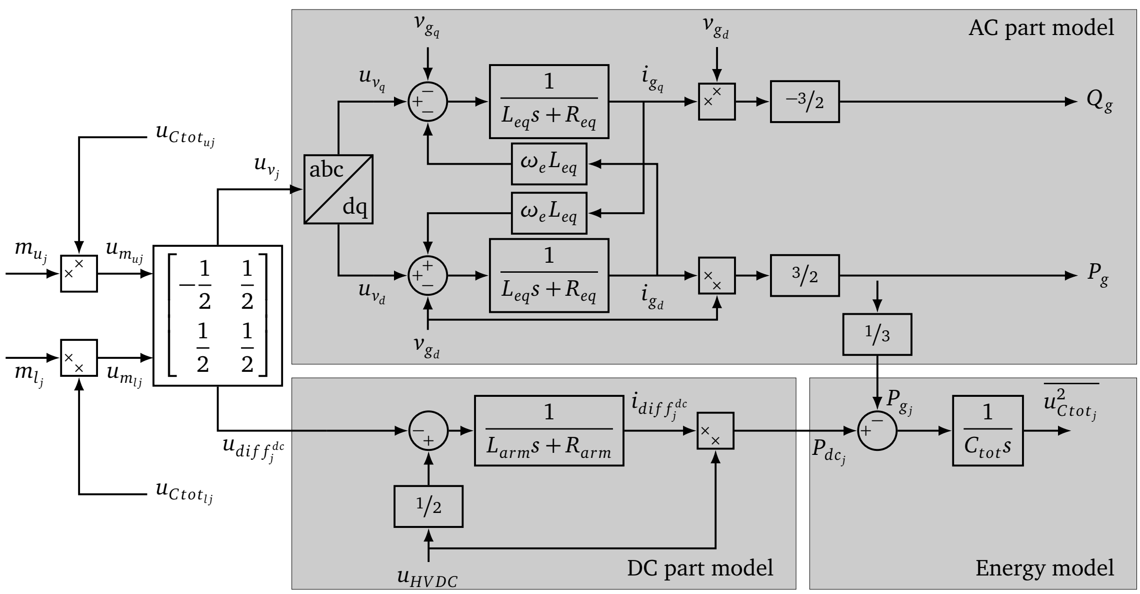

Figure 3.10 – Block diagram of the MMC energy model in dq reference frame.

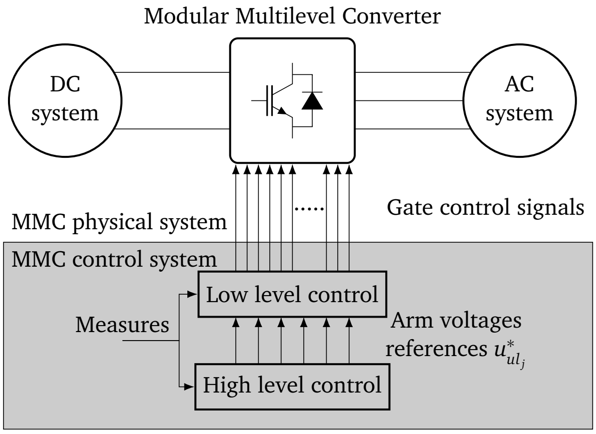

Figure 3.11 – Control hierarchy of a Modular Multilevel Converter.

The second task is to balance the capacitor voltages which is accomplished by the Balancing Capacitor Algorithm (BCA) [Tu 11a]. Since in this thesis, the selected MMC model is the type 3 model, in which the switching status is not presented, the low level control is out of the scope of this work.

High level control is very similar to a 2-level VSC, however the difference resides in its inexplicit capacitor compared to a big explicit DC link capacitor in a 2-level VSC. This level aims at calculating the voltage references for upper and lower arms. This control level is composed of the inner current loops and the outer loops which can be chosen from *active and reactive powers* control, *DC and AC voltages* control and *stored energy* control.

3.2.2.1 Energy control arrangement of the MMC

The energy model of the MMC is expressed in Equation 3.14 and depicted in Figure 3.10. It can be noticed that the energy system has two inputs: the DC power and the AC power. The MMC energy can be controlled by taking either these two powers as a disturbance input.

Figure 3.12 describes the control block diagram by considering the AC power as disturbance.

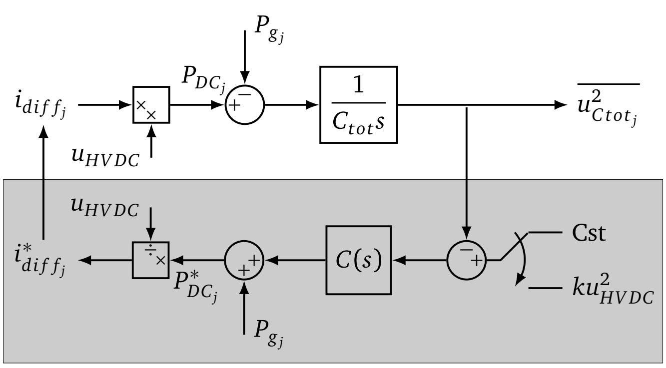

Figure 3.12 – Control diagram of the MMC energy model.

Therefore, the output of the energy controller compensated by the AC power is the reference for the DC power.

The control of the total stored energy in the converter can be achieved by a PI controller. However, selecting different energy references can enable or disable the participation of the internal energy of the converter into the DC bus [Sami 16b]. If the reference is set to a constant value, then the internal energy is decoupled with the DC bus. If the reference is associated to the square of the DC bus voltage $W_j^{\Sigma} = ku_{HVDC}^2$, then the stored energy of the MMC is shared with the DC bus.

3.2.2.2 Control system of the AC part

The dynamics of the imaginary AC part of the MMC are described by Equation (3.7) and the model of the AC part of the MMC in dq frame is shown in Figure 3.7b.

Thanks to the decoupling of d-axis and q-axis currents, the structure of the MMC AC part model is identical to the model of the conventional VSCs. Therefore, two outer voltage loop controllers should be implemented in order to give two references for the inner current control loops.

Referring to the four types of classical controls of the VSC [Raul 14]:

- The d-axis current reference can be either given by an active power controller which regulates the active power exchange between the converter and the AC grid, or by an DC voltage controller which regulates the HVDC voltage;

- The q-axis current reference can be either given by a reactive power controller which regulates the reactive power exchange between the MMC and the AC grid, or by an AC voltage controller which regulates the AC voltage.

The grid current components i_{g_d} and i_{g_q} can be controlled by classical PI controllers in the dq reference frame.

3.2.2.3 Control system of the DC part

The imaginary DC part of the MMC does not exist in the conventional VSC. The dynamics of the DC part are characterized by Equation (3.5) and can be controlled by regulating the differential current $i_{diff_j^{DC}}$ via a PI controller. The reference of this inner control loop is generated by the energy control loop, whose aim is to control the internal energy stored in the MMC, as discussed before.

The overall control loops of the MMC are depicted in Figure 3.13.

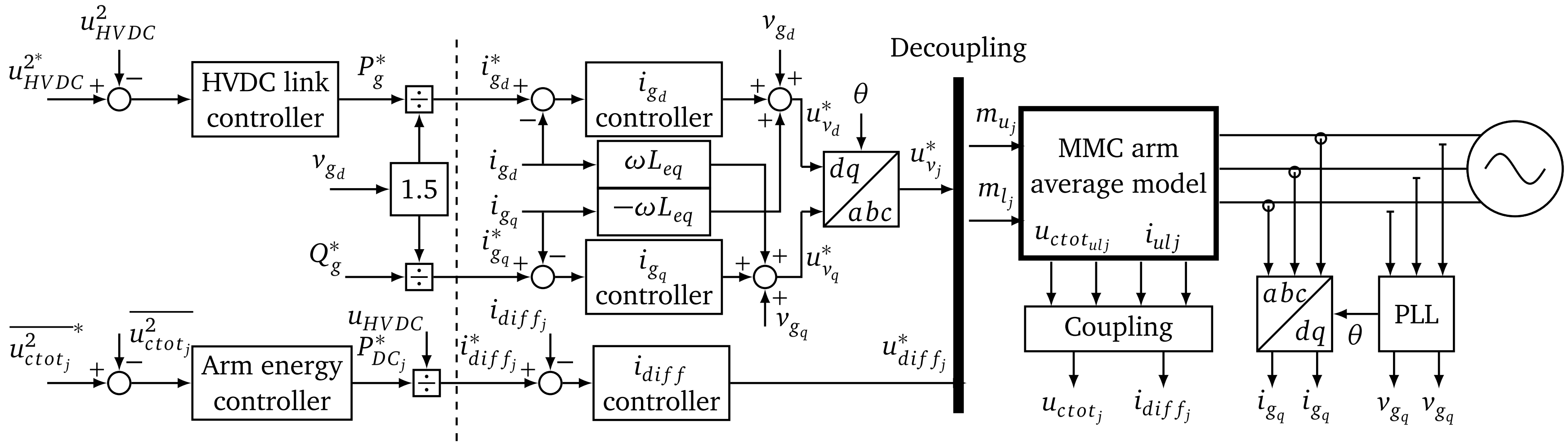

Figure 3.13 – MMC control diagram with its inner and outer loop control.

Table 3.1 – MMC arm average model parameters and control loops response time [Grus 15]

Parameter	Notation	Value
Arm resistor	R_{arm}	1.02 Ω
Arm inductor	L_{arm}	50 mH
Grid resistor	R_g	50 mΩ
Grid inductor	L_g	60 mH
Arm equivalent capacitor	C_{tot}	25 μF
PLL		2 ms
Grid current loop response time		5 ms
Differential current loop response time		10 ms
HVDC voltage loop response time		100 ms
Stored energy loop response time		100 ms

3.2.3 Simulation of MMC

The MMC arm average model and control are implemented in EMTP-RV. The parameters for a 1000 MVA rating MMC and its control loops response time are listed in Table 3.1.

Figure 3.14 shows the behaviour of the MMC response to variations in the AC side active and reactive powers references.

The active power increases from 0 to 300 MW during the interval 0.1 - 0.2 s. Then it is reversed at 0.5 s and finally set to 0 at 1.1 s. The reactive power increases from 0 to 180 MVA with a slope between 0.3 and 0.4 s, and set to 0 at 0.9 s, as seen in Figure 3.14a. The DC side voltage is kept at 640 kV throughout this simulation as depicted in Figure 3.14b.

The HVDC current variation is plotted in Figure 3.14c. This figure shows that, as a voltage source converter, the MMC can reverse its power flow by reversing its current, unlike current source converter which is required to inverse its voltage polarity.

The differential currents of the MMC are depicted in Figure 3.14d. It can be noticed that there is a small oscillation on these currents, but the value of the DC components equals one-third of the HVDC current.

Finally the stored energy (in per unit) per phase is shown in Figure 3.14. With the power variation in the AC side, the stored energy oscillates while the average value remains constant because the reference of energy in the arm is set to be the square of the DC bus voltage. The DC bus voltage is fixed at 640 kV.

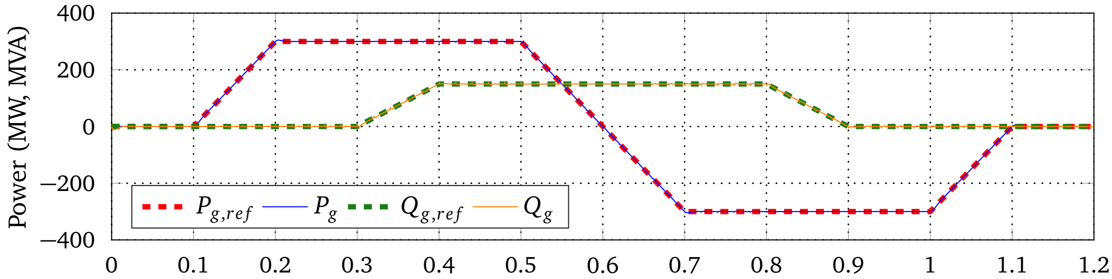

(a) Active and reactive power.

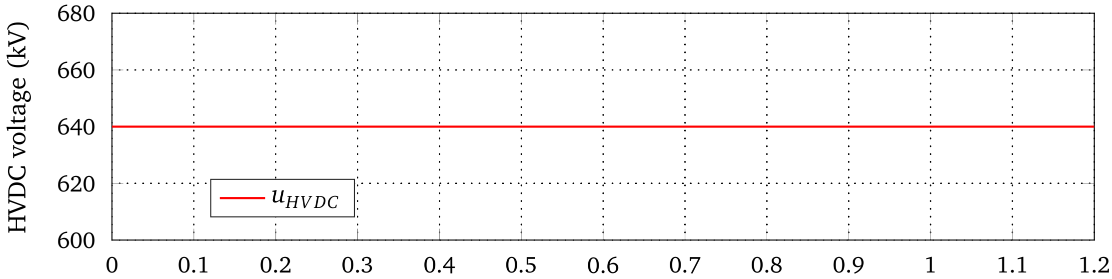

(b) HVDC voltage.

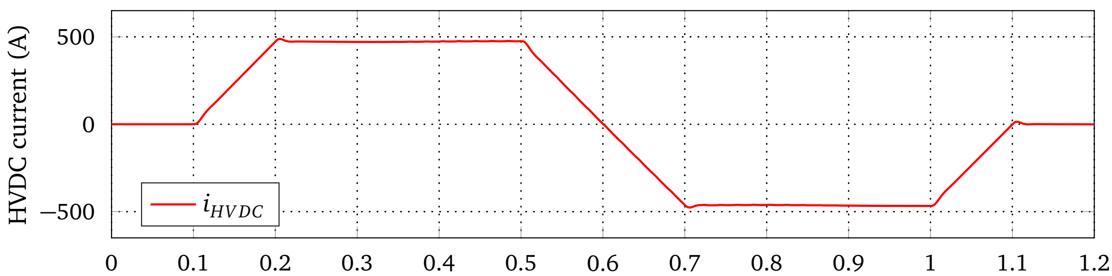

(c) HVDC current.

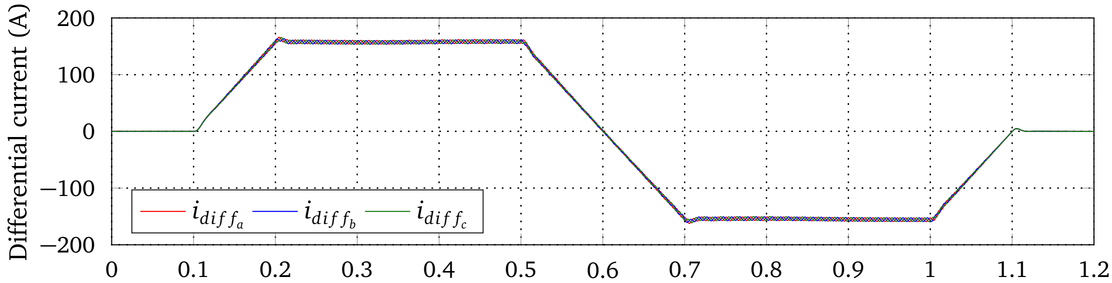

(d) Differential current in the MMC.

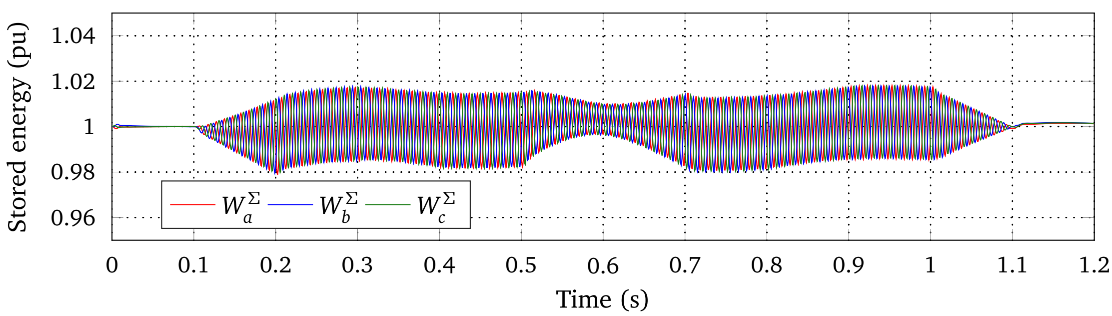

(e) Stored energy in each phase, in per unit.

Figure 3.14 – Simulation results of a MMC with variation on the AC side.

The MMC responses to the variation in the DC side voltage are shown in Figure 3.15. In this case, active and reactive power references are both set at 0, meaning that there is no power exchange between AC and DC sides, as seen in Figure 3.15a. The HVDC voltage is reduced from 640 kV to 608 kV (0.95 pu) at 0.3 s. Since the MMC stored energy reference is set to the square of the DC bus voltage, the stored energy in each phase decreases to $0.95^2 = 0.9025$ pu as shown in Figure 3.15e. The response time of the energy control is 100 ms. The energy flowing out of the MMC to the DC side, results in a negative HVDC current response at 0.3 s. When the system re-balances around 0.8 s, the current returns to 0, as depicted in Figure 3.15c.

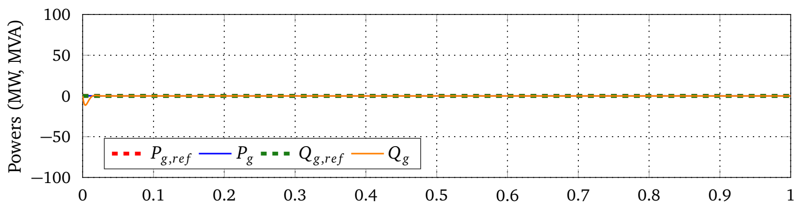

(a) Active and reactive power.

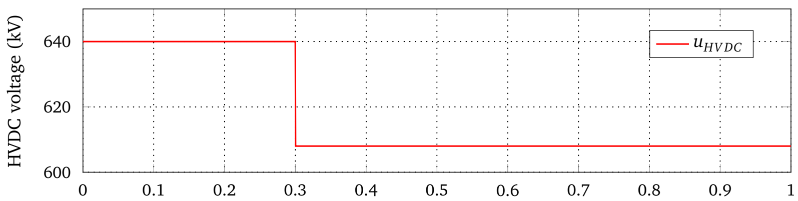

(b) HVDC voltage.

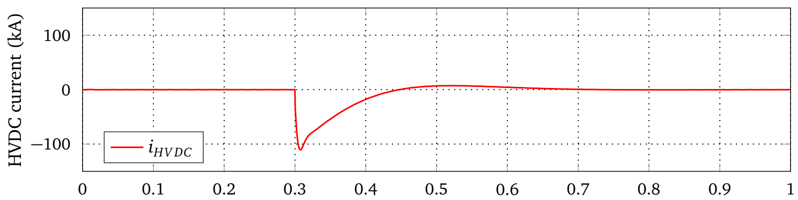

(c) HVDC current.

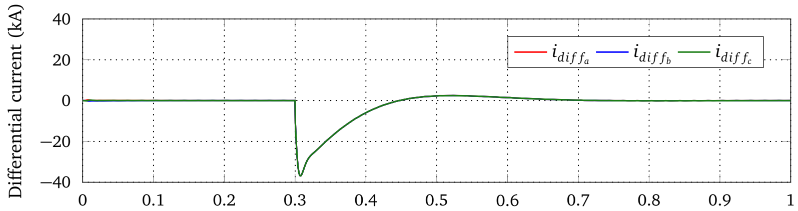

(d) Differential current in the MMC.

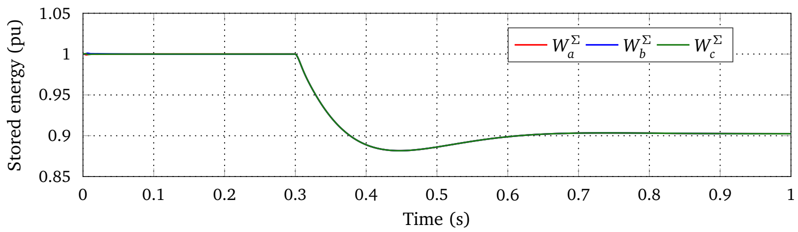

(e) Stored energy in each phase, in per unit.

Figure 3.15 – Simulation results of a MMC with variation on the DC side.

3.3 Cable models

The cable models can be categorized into two groups: distributed parameter models and lumped-parameter models. The distributed parameter models such as the wideband cable model [Morc 99] provide an accurate representation of the complex, frequency-dependent behaviour of power lines and cables. It is usually assumed as a reference for the performances of alternative lumped-parameter models. Despite its accuracy, it cannot be modelled in small signal representation, therefore the analysis of complex power systems is not possible.

In most studies focused on the offshore wind farms or the power converters, the way of interaction of these two systems, the HVDC cable, is usually represented by a lumped-parameter model, such as RC, pi-section or cascade of pi-sections [Wang 12][Chau 11].

In one hand, these models can be effectively converted into state space representation, while in another hand, the frequency-dependent effects of the HVDC cable are neglected [Mart 82].

3.3.1 Resonant circuit SPWF-HVDC

An important fact that results from the studied offshore wind farm with series connected wind turbines is the formation of a resonance circuit. Consequently, an accurate cable model should be adopted to represent the transient characteristic of the HVDC transmission system.

Figure 3.16 shows the resonant system of the studied wind farm. Since the HVDC transmission cable exhibits a capacitive effect, a smoothing reactor as a reactive compensation should be placed between the wind turbines and the MMC.

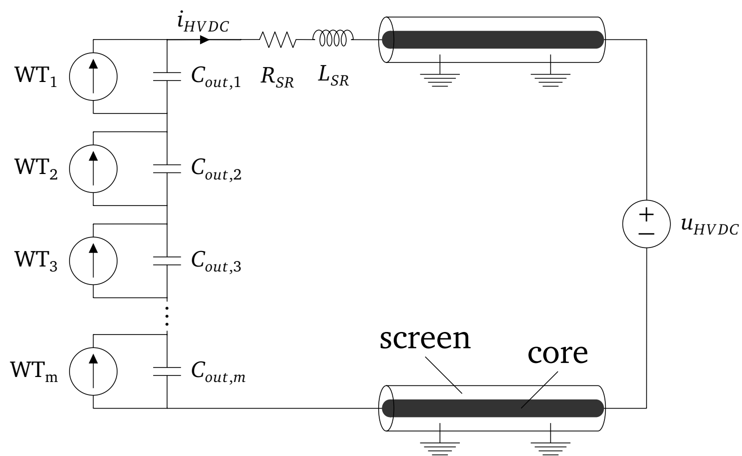

Figure 3.16 – Simplified resonant system of the series wind turbines, the transmission cables and the onshore converter station.

For the sake of clarity, the offshore wind turbines are considered as current sources, and the onshore converter is represented by a voltage source, which is assumed to be perfectly controlled. The uncontrolled elements: the wind turbine output capacitors, DC smoothing reactors and the HVDC cables constitute a RLC resonance circuit.

When a sudden variation of the system variables takes place at either side of the HVDC cable, the circuit oscillates at its resonance frequency. This implies that the cable model should reflect the cable characteristics at both low frequency (DC) and high frequency (resonance frequency). This requirement justifies the use of the Wideband cable model in this thesis.

3.3.2 Wideband model reference in EMTP-RV library

The Wideband cable model is an Universal Line Model (ULM) that can be used for modeling of underground power cables as well as overhead power lines. In the EMTP-RV® library, there is a Wideband cable model design based on a Cross-Linked Polyethylene (XPLE) insulation cable which operates at nominal voltage of ±320 kV with a transmissible power of 1000 MW.

The geometrical and electrical data of this model are shown in Figure 3.17. The used data of the conductors are obtained from [Wach 14]. These data are filled in an EMTP routine which generates the wideband cable model.

3.3.3 HVDC cable models

This section compares four different kinds of cable models: the RC model, representing the DC cable capacitance and resistance (in Figure 3.18), the most common used pi-section model (in Figure 3.19), the Wideband model (in Figure 3.20) with distributed parameters, which is available in the EMTP-RV library, and the coupled pi-section model (in Figure 3.21).

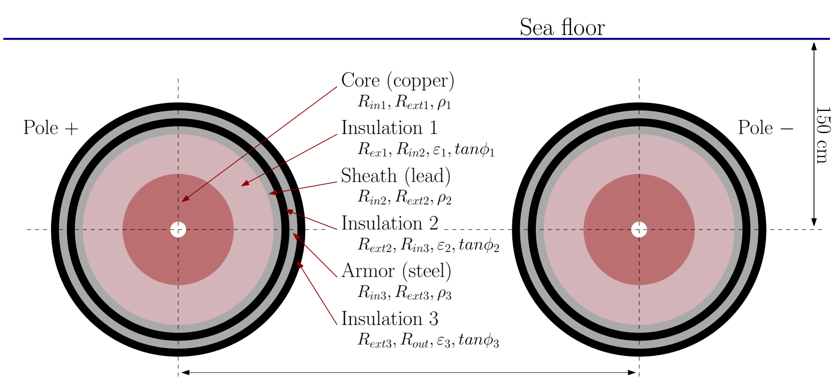

R_{in1}	7.6 mm
R_{ext1}	25.125 mm
ρ_1	$1.664 \cdot 10^{-8}$ Ω.m
ε_1	3.5 F.m^{-1}
$\tan\phi_1$	0.0004
R_{in2}	49.125 mm
R_{ext2}	52.125 mm
ρ_2	$22 \cdot 10^{-8}$ Ω.m
ε_2	2.3 F.m^{-1}
$\tan\phi_2$	0.001
R_{in3}	56.125 mm
R_{ext3}	61.725 mm
ρ_3	$13.8 \cdot 10^{-8}$ Ω.m
ε_1	2.3 F.m^{-1}
$\tan\phi_3$	0.001
R_{out}	66.725 mm
$\rho_{\text{sea floor}}$	0.2 Ω.m

Figure 3.17 – Undersea cable layout and dimensions [Akka 16].

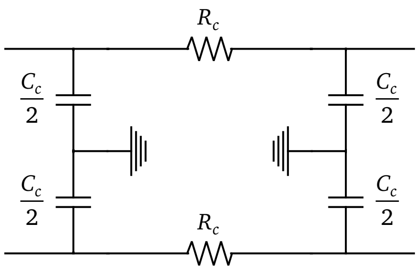

Figure 3.18 – RC model.

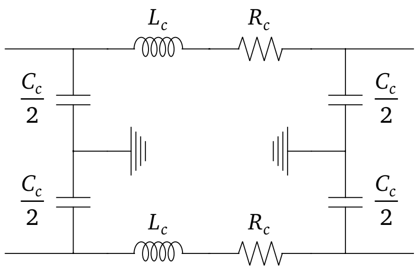

Figure 3.19 – Pi-section model.

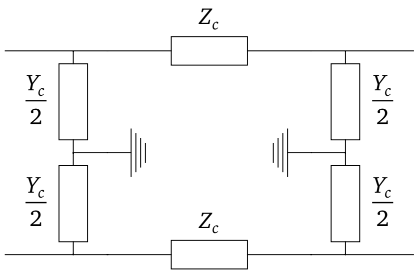

Figure 3.20 – Windeband.

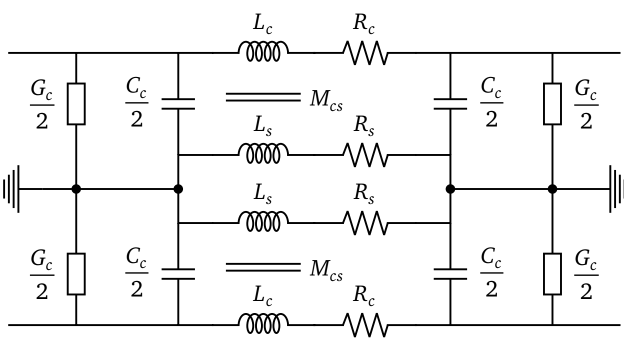

Figure 3.21 – Coupled pi-section model.

This last one proposed in [Raul 14], takes into account the coupling effect of the cable core and screen represented by a mutual inductance M_{cs}. The mutual inductance allows a current to flow through the screen with a significant high resistance, therefore a better damping effect is expected.

In order to fairly compare the impedance of these four models, all the parameters inlcuding the conductor resistance R_c, the conductor inductance L_c, the conductor capacitance

C_c, the screen resistance R_s, the screen inductance L_s and the mutual inductance between the conductor and the screen M_{cs} of the RC model, pi-section model and coupled pi-section model are extracted from the Wideband model matrix at 1 mHz, given by an EMTP-RV routine. At this frequency, the system operation can be seen as an equivalent DC. The EMTP-RV uses a current source with 1 A at the input of the system and calculates the impedance at each frequency. In order to obtain the self-impedances of the cables, the cable pairs are short circuited at one end and the current source injects the current at the other end, as illustrates Figure 3.22. Figure 3.23 shows the frequency scan from 0.01 Hz to 100 kHz of the impedances of four 100 km cables using the mentioned four cable models.

It can be seen that at very low frequency, these four cable models are identical since the parameters of the lumped parameter cables match the Wideband model at 1 mHz, while

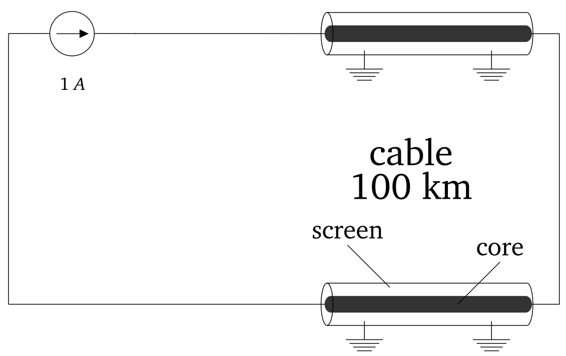

Figure 3.22 – The system for calculating the cables self-impedances.

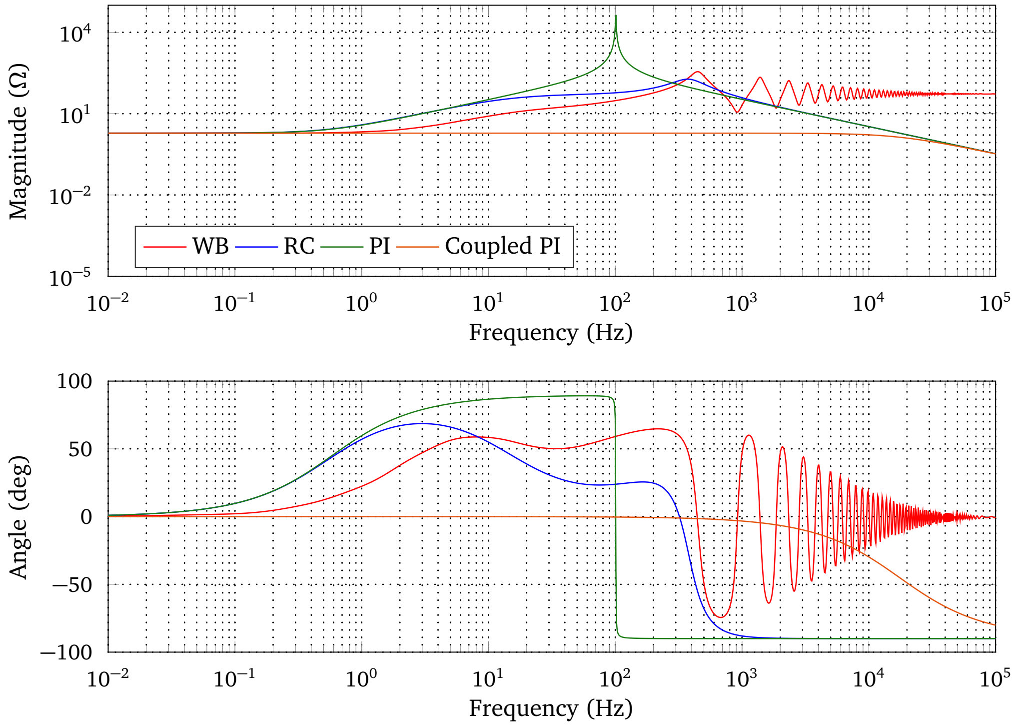

Figure 3.23 – Comparison of the cable impedances of the RC model, classical pi-section model, Coupled pi-section model and the Wideband model.

none of the three lamped cable models can represent the Wideband model at medium and high frequency.

The classical pi-section model has a peak impedance at 100 Hz which is not present in the Wideband and coupled pi-section models. The three lamped models act as low pass filters since their impedances decrease dramatically as the frequency increases above 10 kHz, while the Wideband model converges to a constant magnitude as observed in Figure 3.23.

To have a more precise consideration of the different HVDC cable models in the wind farm impedances, a frequency scan of the system, in Figure 3.24, is carried on in EMTP-RV. The zoom-in from 10 Hz to 250 Hz of the system impedances cen be seen in Figure 3.25. It can be noticed that the classical pi-section model presents a substantial difference when compared to the Wideband model.

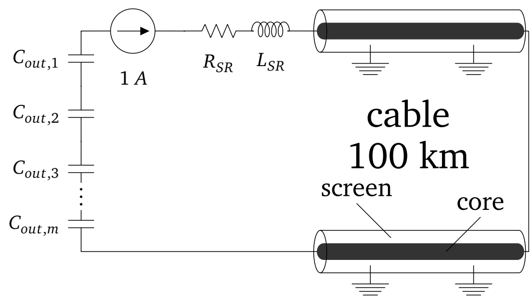

Figure 3.24 – The system for calculating the wind farms impedances.

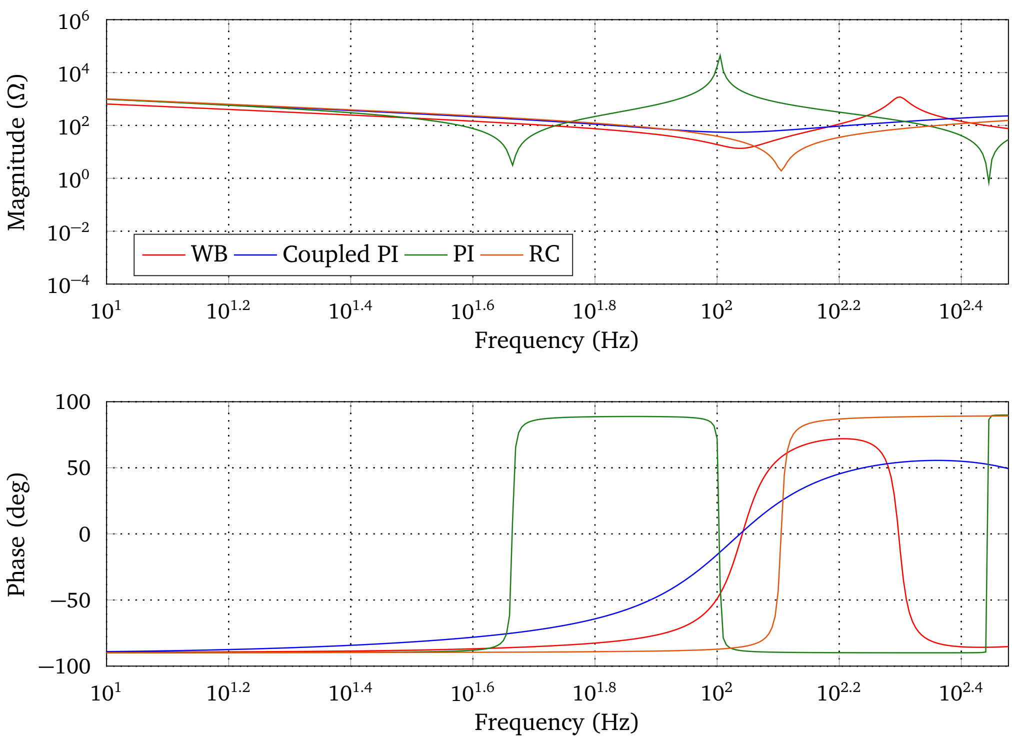

Figure 3.25 – Comparison of the impedances of the wind farms using the RC model, classical pi-section model, Coupled pi-section model and the Wideband model.

When the Wideband model has the lowest magnitude at about 53 Ω, the pi-section model impedance rises to a very high level above 10 kΩ. The sags in the curves indicate their systems resonance frequencies since their impedances decrease to the minimum magnitudes. It is shown that the coupled pi-section model is smooth throughout all this range and its lowest magnitude is higher than the magnitude of the Wideband model. This indicates that the use of the coupled pi-section model in a SWF, may lead to higher damping and less resonance effects than the use of the Wideband model. On the contrary, the RC model has less damping effect compared to Windeband model at its resonance frequency.

The above impedance comparisons demonstrate that lamped parameter cable models can represent the Wideband model at low frequency range, since their parameters are chosen to match the behaviour of the Wideband model at 1 mHz. However, in the SWF, the cable model must be able to represent the cable characteristics not only in DC when the system operates at steady state, but also in higher frequency range when the system inputs have strong variations and the system oscillates at resonance frequency.

Figure 3.26 shows the response of a wind farm with 20 series wind turbines, controlled by onshore MMC response to a reduction in the HVDC voltage of 0.05 pu.

As analysed above, the pi-section has a significant difference from the Wideband model.

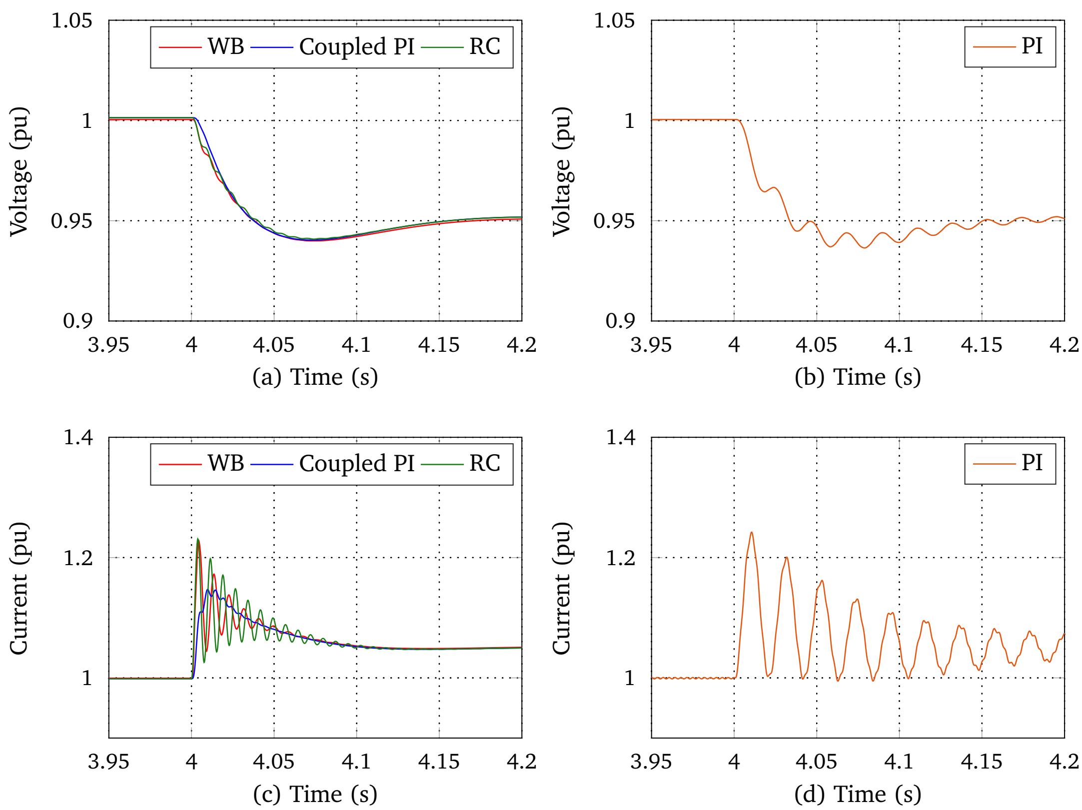

Figure 3.26 – The SWF response to a reduction in the HVDC voltage of 0.05 pu. a) HVDC voltage (Wideband, Coupled pi-section, RC), b) HVDC voltage (PI), c) HVDC current (Wideband, Coupled pi-section, RC), d) HVDC current (PI).

From Figure 3.26c, it can be seen that the HVDC current of the wind farm using the coupled pi-section model has much better damping than the Wideband and RC models. The resonance frequency of the system with RC model is slightly lower than the Wideband model, which matches the previous analysis.

In conclusion, to correctly represent the HVDC cable behaviour, the Wideband model is used in this thesis from now, (unless otherwise stated).

As mentioned, the SWF forms a resonant circuit with the uncontrolled elements: the wind turbine output capacitors, smoothing reactors and the HVDC cables. Therefore, the resonance frequency is also influenced by the selection of the wind turbine output capacitors and the HVDC smoothing reactor.

Figure 3.27 shows the impedances of the SWFs with different wind turbine output capacitors. The resonance frequency increases as the wind turbine output capacitor decreases, with a slight increase of the oscillation frequency. However, when HVDC voltage is reduced to 0.95 pu as shown Figure 3.28, the oscillation with smaller capacitance is damped out in a shorter time which is beneficial.

More importantly, smaller output capacitance contributes to lower current overshoot. The output capacitance is related to the system electrostatic constant H_c as mentioned in Chapter 2. Despite the fact that in some applications, such as in the AC power grid, bigger H_c is preferable since it increases the system inertia. In the SWF, a larger H_c leads to a higher current oscillation amplitude and thus the cables should carry higher overcurrent when the HVDC voltage is stepped down.

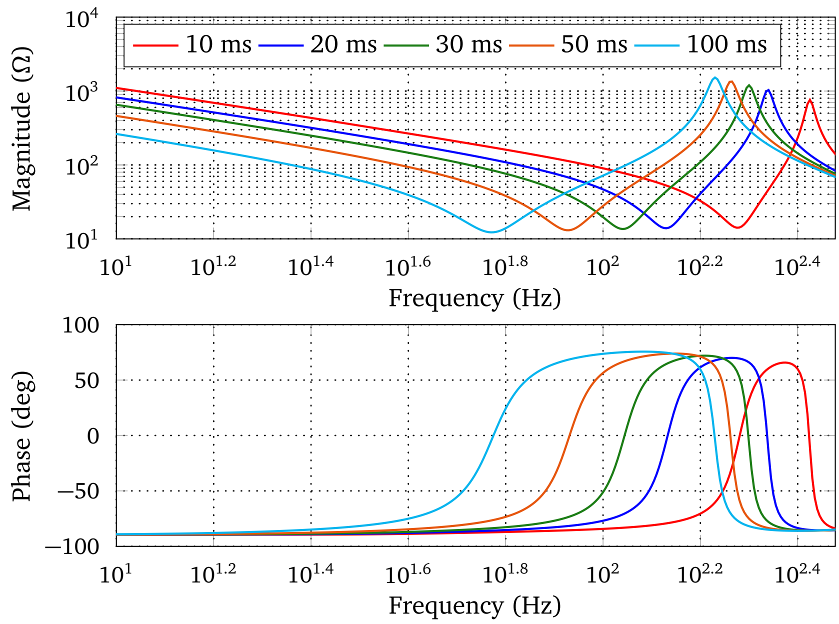

Figure 3.27 – The variation of resonant frequency of the wind farm using Wideband model with different values of H_c.

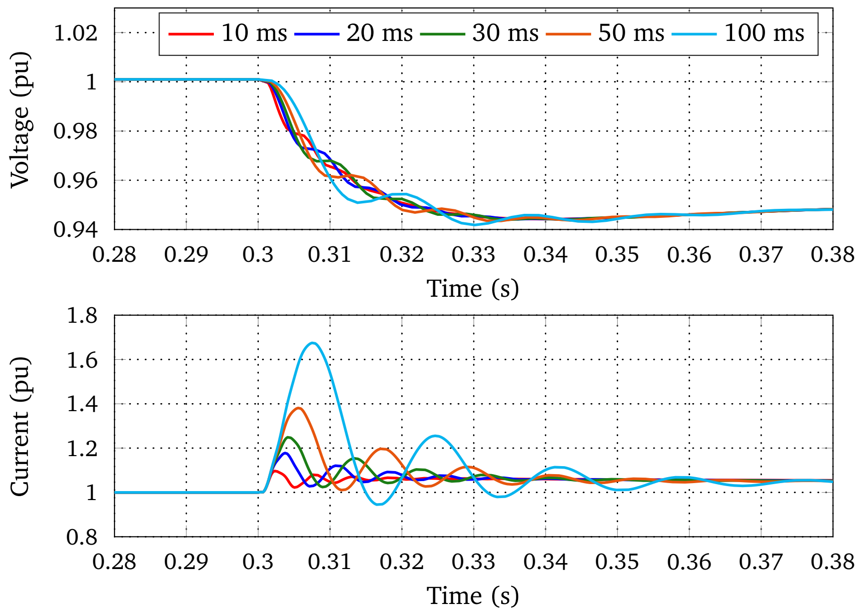

Figure 3.28 – SWF using Wideband model with different H factor response to a reduction in the HVDC voltage to 0.95 pu.

3.4 Global control strategy

The MMC and the HVDC cables presented in the last two sections are required for the achievement of the aim of controlling the HVDC voltage across the series wind farm.

In Chapter 2, a fast local overvoltage control strategy was presented, in which requires no communication between units is needed but undesired power curtailment is expected. This section presents a global control strategy, which ensures the voltage across each wind turbine staying within its overvoltage capability via the HVDC voltage level adjustment. Its principles, as well as its advantages and drawbacks are presented in this section.

3.4.1 Re-examination of the wind turbine output voltage

It has been given in Chapter 2 that the output voltage of a wind turbine in steady state is calculated as:

$$u_{out,x} = u_{HVDC} \frac{p_{out,x}}{p_{WF}}$$

This equation indicates that the x wind turbine $\mathrm{WT_x}$ decreases its output voltage in three conditions:

- The power production $p_{out,x}$ of $\mathrm{WT_x}$ remains unchanged and the whole wind farm power production p_{WF} increases;

- The decrease of the wind turbine WT_x power production $p_{out,x}$, and moreover, because of the power production of WT_x is included in the wind farm power production, the decrease rate of this unit must be greater than the decrease rate of the wind farm:

$$\frac{\Delta p_{out,x}}{p_{out,x}} > \frac{\Delta p_{WF}}{p_{WF}}$$

- The power production of WT_x and the wind farm remain unchanged while the HVDC voltage level decreases.

The power production of the wind farm depends on the wind speed while at the same time it is uncontrollable. If all the wind turbines are initially controlled to operate at Maximum Power Point Tracking (MPPT), increasing power production by means of the control systems is impossible. In addition, the wind turbines that are required to increase power production are not the ones that are at overvoltage. Therefore, even if the wind farm could increase its power production via control systems, the communication between the units would be indispensable.

The second option is adopted in the local overvoltage control described in Section 2.5, in which the wind turbine individual power production is reduced. This control system only operates inside the individual wind turbine unit, so that it is fast and reliable and does not require no communication between the units. This method has the disadvantage of power curtailment. Besides, the decrease of the power production of the unit WT_x will cause the decrease of the whole wind farm power production p_{WF}, which in turn could make operate others wind turbines in overvoltage mode.

The last option implicates the reduction of the HVDC voltage level, which concerns only the control of the onshore converter, while the wind turbines operation remains unchanged. The communication would be indispensable but in the interest of no power curtailment in the wind farm. Therefore, this option is the focus of this section.

3.4.2 Basics of global control strategy

The proposed overvoltage limitation control strategy aims to extract maximum power from the wind while ensuring the operation of each wind turbine within overvoltage capability limits. The control strategy divides the wind farm operation into two operating modes: normal mode and overvoltage limitation mode. In normal mode, the MMC maintains a constant HVDC voltage. The reference of the HVDC voltage u^*_{HVDC} equals the sum of wind turbines nominal output voltages $U_{out,nom}$:

$$u^*_{HVDC} = mU_{out,nom}. \tag{3.15}$$

In normal operation, the wind turbines output voltages vary under their overvoltage capability limit U_{limit}. When the output voltage of any wind turbine reaches its overvoltage limitation level, the onshore converter enters into voltage limitation mode. The HVDC voltage is regulated to a level that can ensure the output voltage of the wind turbine for maximum power production in the wind farm, under the overvoltage limit:

$$u^*_{HVDC} = U_{limit}\frac{p_{WF}}{\max(\mathbf{p_{out}})} \tag{3.16}$$

where

$\mathbf{p_{out}}$ = Output power production array of units $\mathrm{WT_x}$ in the SWF, $x \in (1, 2, ..., m)$;
p_{WF} = Output power production of the SWF.

The control diagram of the global control and corresponding control of the MMC are depicted in Figure 3.29. To illustrate the control strategy, an example of a series wind farm of 5 wind turbines is analysed. Output power and voltage conditions are given in Equation (3.17) and operating points with and whit no global control are illustrated in Figure 3.30.

It is assumed that in nominal operation the power of an individual unit is 1 pu, $u_{out,x}$=$p_{out,x}$=1 pu and the overvoltage limitation level U_{limit} is 1.1 pu. The HVDC link voltage of a DC SWF of 5 wind turbines is therefore 5 pu.

$$\begin{array}{c} \textit{Row} \\ 1 \\ 2 \\ 3 \\ 4 \\ 5 \\ \hline \textit{Sum} \end{array} \quad \mathbf{p_{out}} = \begin{array}{c} \begin{pmatrix} 0.80 \\ 0.70 \\ 0.65 \\ 0.60 \\ 0.55 \end{pmatrix} \\ \hline 3.3 \end{array} \quad \mathbf{u_{out}} = \begin{array}{c} \begin{pmatrix} \boxed{1.21} \\ 1.06 \\ 0.99 \\ 0.91 \\ 0.83 \end{pmatrix} \\ \hline 5 \end{array} \xrightarrow{Eq.(3.16)} \hat{\mathbf{u}}_{\mathbf{out}} = \begin{array}{c} \begin{pmatrix} \boxed{1.10} \\ 0.96 \\ 0.89 \\ 0.83 \\ 0.76 \end{pmatrix} \\ \hline 4.54 \end{array} \tag{3.17}$$

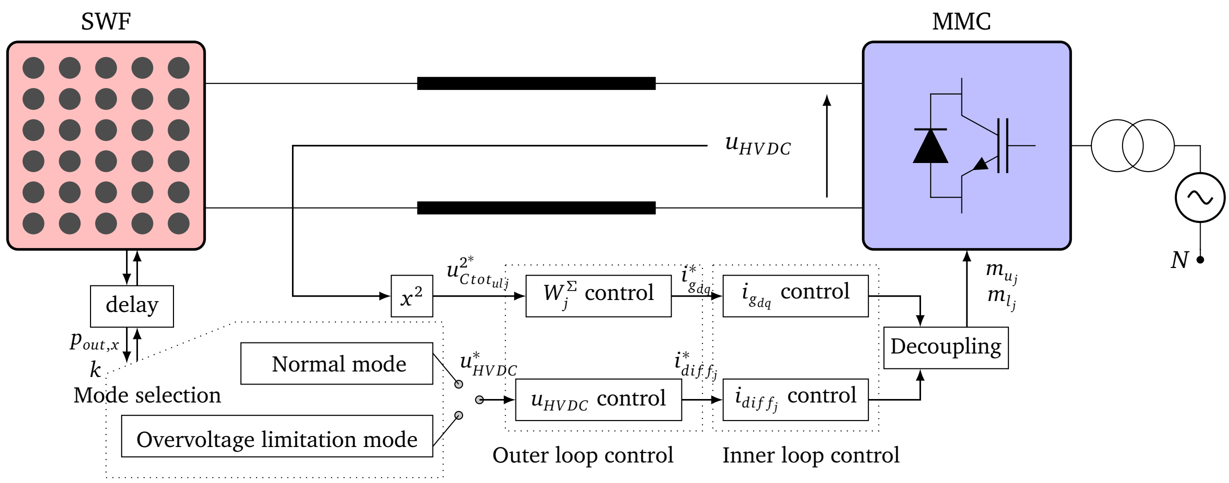

Figure 3.29 – Overall control of the series parallel offshore wind farm.

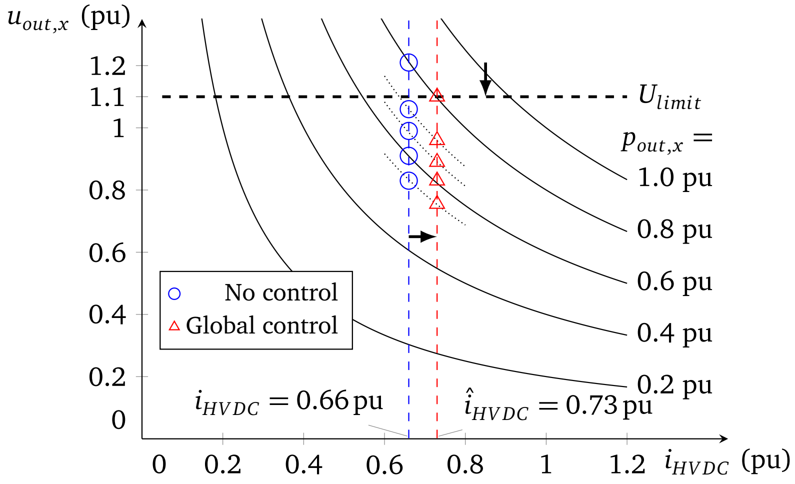

Figure 3.30 – Illustration of the operating points of a wind farm with 5 wind turbines.

If the proposed control strategy is not applied, it can be noticed that the voltage level of the unit WT_1 is forced to 1.21 pu, which exceeds significantly the overvoltage limit (1.1 pu). The global control strategy regulates the HVDC voltage according to (3.16), so the HVDC voltage should be reduced to

$$u^*_{HVDC} = U_{out,nom}\frac{p_{WF}}{\max(\mathbf{p_{out}})} = 1.1 \times \frac{3.3}{0.8} = 4.54\,\text{pu}$$

Subsequent to the reduction of the HVDC voltage, the operation of the unit WT_1 is bounded to its overvoltage capability of 1.1 pu. This is described in Equation (3.17). The voltages of other units are affected as well, but their power production remains unchanged. It can also be observed that the HVDC current increases from 0.66 pu to 0.73 pu. The effect of increased current will be discussed in Section 3.4.5.

3.4.3 Global control strategy with bypass protection

In case of failure of any wind turbine a bypass protection is used to remove the faulted unit from the series connection, so its operation is not interrupted. Bypass methods have already been discussed in Section 2.3.6, either using the diode bridge as the bypass path or using a switch to cut off the faulty wind turbine and short circuit it.

The operation of the global control strategy can ignore the dynamics of the bypass system. This is justified because for other wind turbines in series, the elements that influence their output voltages are the power production of the wind farm, the HVDC voltage and their own power generation. The bypassed faulty unit can be seen as a wind turbine with zero power production and therefore its output voltage equals 0. The wind farm is reduced to a series connection with $(m-k)$ units, where k is the number of bypassed units. In this case, the remaining wind turbines are all exposed to overvoltage if the HVDC voltage is kept at $mU_{out,nom}$. Even if all the rest of wind turbines produce their nominal power, their output voltages clamped to $\frac{m}{m-k}U_{out,nom}$. With this voltage as a base voltage, there is a very little margin left for the voltage variation of wind turbines. It is then proposed to reduce the base HVDC voltage to:

$$u_{HVDC,base} = \frac{m-k}{m}U_{out,nom}. \tag{3.18}$$

The wind farm then operates as a wind farm with $(m-k)$ units. The global control of the onshore converter obeys the strategy proposed in Subsection 3.4.2 with normal control and overvoltage limitation control based on the reduced HVDC voltage.

3.4.4 Communication between the offshore wind farm and the onshore converter

The wind speed variation in the wind farm is unpredictable, and consequently the output voltage variation is also unpredictable. In order to ensure the operation of each wind turbine under its overvoltage capability, it is necessary for the onshore converter to acquire the power production of every wind turbine, so as to calculate the suitable HVDC voltage level.

The information of the wind turbines power production is collected and transmitted to onshore via the fibre optics cable embedded in the HVDC cables, shown in Figure 3.31 [Euro 15]. The fibre optics cable can be used for several purposes [Worz 09]:

1. Data transmission;
2. Measurement of cable strain or vibrations;
3. Fault detection and location;
4. Distributed measurement of temperature;
5. Detection of changes in the cable route, e.g. changes in sediment cover over the cable.

The fibre optics cable transfers data at light speed the glass, whose propagation velocity is extremely fast around 200,000 km/s. Nevertheless, the communication delay or latency is in the order of several dozens of milliseconds. In distributed systems such as protective relay systems, the time delay of communication is usually less than 10 ms. In larger power systems such as in the Bonneville Power Administration system, the latency of fibre optics digital communication has been reported as approximately 38 ms for one way [Wu 04].

The latency is caused by the fact that the electric devices do not have inherent communication capabilities and thus they have to rely on embedded computer systems to serve as communication interfaces. The embedded communication interface is depicted in Figure 3.32.

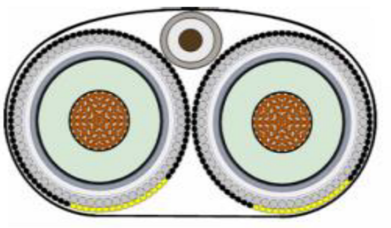

Figure 3.31 – Fibre optics cable embedded between two HVDC cables [Euro 15].

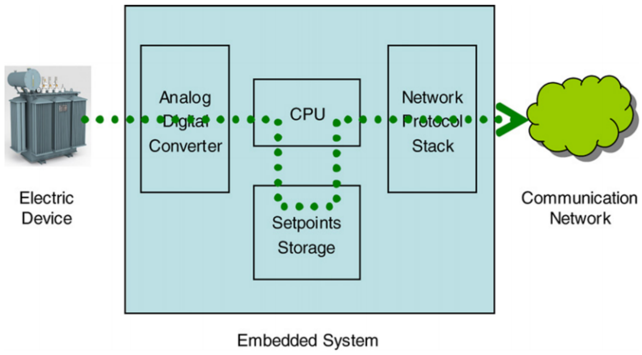

Figure 3.32 – Processing time spent in an intelligent electronic device [Wang 11].

The analogue message generated from the electric devices is first converted to digital representations so that they can be processed by the CPU. The current measurement data is stored in the set-point storage system and formatted by the network protocol stack before being sent to the communication network, such as the fibre. There are several latencies during the whole process, as following [Wang 11]:

1. Data acquisition delay: The measurements are acquired periodically from the electric devices. The delay occurs between two measurements and the time required to convert the analogue signal into digital representation. For example, the measurement of the wind turbines output voltage, and the conversion from their original analogue formats into the digital representations.

2. Packet processing delay: The digital data have to be sent following specific network protocols. To do this, these data are transmitted in the form of packets [Stah 08]. A packet is typically composed of three parts:

   - a header which indicates the packet length, destination address, packet type;
   - a payload where the data are carried;
   - a trailer which informs the receiving device of the end of a packet.

   Each step in the processing induces delays.

3. Packet transmission delay. The packets from different devices are sent to each intermediate node on the path. The packets are received and checked at these relay nodes before being sent to the ultimate receiver. In the SWF, the data from wind turbines are sent one by one to the adjacent wind turbine relay. Assuming that the data is transmitted from $WT_m \rightarrow ... \rightarrow WT_2 \rightarrow WT_1$, each relay node has to await the data before it, check the data exactness, receive the whole data, and then re-composite a new packet. Finally a packet containing the information of the whole wind farm is formed and sent to the onshore converter. The described process is shown in Figure 3.33.

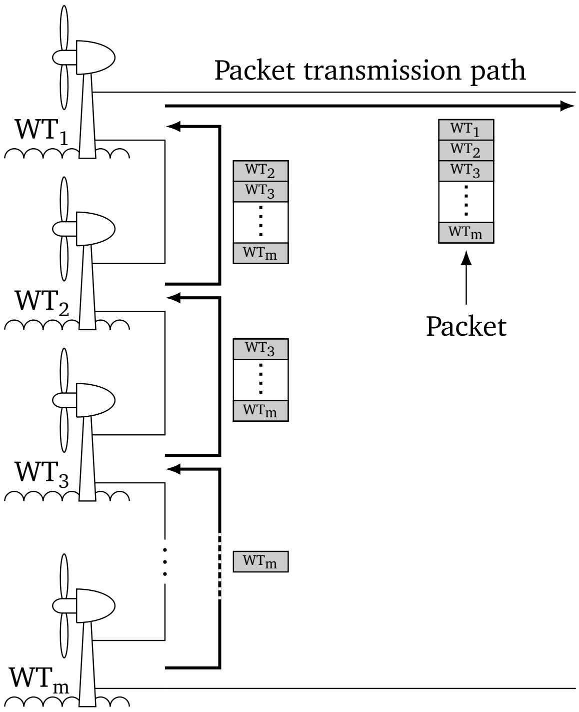

Figure 3.33 – Packet transmission path in the SWF: $WT_m \rightarrow ... \rightarrow WT_2 \rightarrow WT_1 \rightarrow$ the onshore converter.

4. Event responding delay. This is related to the time delay that the actuator takes to decide what response to make according to the events. For example, in the SWF, the computer needs to read the power production of each wind turbine and then calculate the HVDC voltage level that enables all the wind turbines to operate under their overvoltage capability.

3.4.5 Limitations of global control

It is important to note some limitations in the use of the global control strategy:

1. Capacitive cables: The HVDC cables have a capacitive characteristic. It would take some time for the offshore side voltage to be regulated to a safe value. In this situation, some wind turbines would have to operate at a higher voltage than their capability at the instant in which the onshore converter reduces the onshore side HVDC voltage.

2. HVDC voltage reduction limit: In order to prevent the diode bridge from forward biased and thus lose the full control of the MMC, the DC bus voltage u_{HVDC} should always be greater than the peak value of the AC side phase to phase voltage, as

$$u_{HVDC}^{*} > \sqrt{6}V_g \tag{3.19}$$

where V_g is the rms value of the phase-to-neutral grid voltage.

3. Current saturation in other clusters. In this chapter we have proven that in SWF there is no overcurrent possibility caused by the global control. However, in a series parallel offshore wind farm investigated in Section 4.2, the global control could lead to overcurrent in some clusters. If the global control reduces the HVDC voltage when any wind turbine in a specific cluster reaches the overvoltage limitation,while the power production of the other clusters could be higher than this specific cluster. In this case, overcurrent happens.

The above problems of the global control indicate that the local overvoltage limitation controllers have to be installed in the wind turbines for a fast and reliable control of the wind turbine output voltage.

Therefore, the two kinds of overvoltage limitation controls play different roles:

- The local overvoltage limitation control is active during the communication delay and the regulation delay. Furthermore, it serves as a back-up control to limit the output voltages of wind turbines during communication interruptions. Since the local control induces power curtailment, it is not selected as the primary option for voltage limitation.
- The global control serves to limit the wind turbines output voltages without power curtailment by reducing the HVDC voltage. It is selected as the primary option for voltage limitation.

The process of controlling the series wind farm by these two methods is illustrated in Figure 3.34. The local control is activated when the wind turbine output voltage is greater than its overvoltage capability.

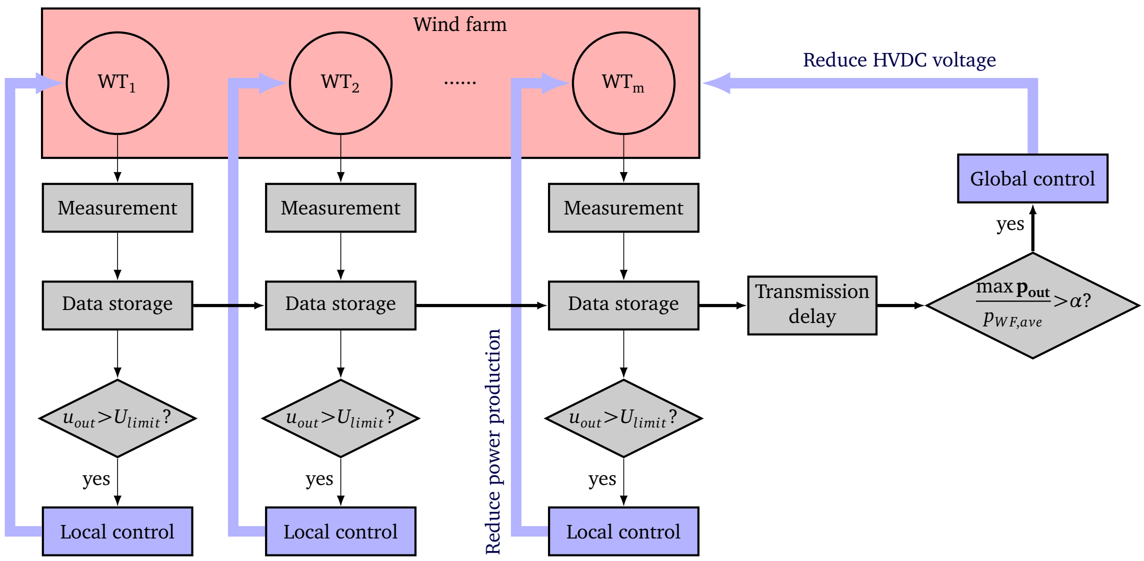

Figure 3.34 – Arrangement of global and local controls of the SWF.

By using the technique described in Section 2.5, the local controller generates a torque compensation to the electrical generator in order to reduce the power generation.

When the local control is activated, the measurement data are stored in the set points storage system and transmitted to the onshore converter by means of packets. The onshore converter receives the data and calculates the corresponding HVDC voltage level for the SWF. When the HVDC voltage is reduced, the local control operates. As noticed, these two control methods function complementarily to enhance the system reliability.

3.4.6 Break-even voltage of the global control strategy

The suggested overvoltage limitation method is established to reduce the HVDC link voltage, which definitely increases the HVDC cable losses. The cable losses should be weighted to take account of the power curtailment induced by the local limitation control. In order to calculate the cable losses, the size of the HVDC cables has first to be determined.

3.4.6.1 Cable sizing & possibility of overcurrent by using global control

In one series connection, since the overvoltage resulting from the wind variation only occurs when not all the wind turbines are producing nominal power, the reduction of the HVDC voltage will not cause overcurrent in the cables. Supposing that the wind turbine nominal voltage and power are both 1 pu. When some wind turbines reach overvoltage limitation, the HVDC voltage should be reduced to $\hat{u}_{HVDC}$ that enables $\max(\hat{\mathbf{u}}_{\mathbf{out}})$ to stay at U_{limit}:

$$\max(\hat{\mathbf{u}}_{\mathbf{out}}) = \frac{\max(\mathbf{p}_{\mathbf{out}})}{p_{WF}}\,\hat{u}_{HVDC}$$

$$\frac{p_{WF}}{\hat{u}_{HVDC}} = \frac{\max(\mathbf{p}_{\mathbf{out}})}{\max(\hat{\mathbf{u}}_{\mathbf{out}})} = \frac{\max(\mathbf{p}_{\mathbf{out}})}{U_{limit}} = \frac{\max(\mathbf{p}_{\mathbf{out}})}{1+\alpha} = \hat{i}_{HVDC}$$

where

- $\hat{\mathbf{u}}_{\mathbf{out}}$ = Wind turbines output voltage array, adjusted according to the overvoltage limitation strategy;
- $\mathbf{p}_{\mathbf{out}}$ = Wind turbines output power production array;
- $\hat{u}_{HVDC}$ = HVDC voltage, adjusted according to the overvoltage limitation strategy;
- $\hat{i}_{HVDC}$ = HVDC current, adjusted according to the overvoltage limitation strategy;
- U_{limit} = Wind turbine overvoltage limitation, U_{limit}=(1+α) $U_{out,nom}$ (kV) = (1+α) (pu);
- α = Overvoltage ratio.

Since $\max(\mathbf{p}_{\mathbf{out}}) \leq 1$, hence:

$$\hat{i}_{HVDC} \leq \frac{1}{1+\alpha} \leq 1$$

Consequently, in the Series Wind Farm (SWF), the global control will not cause overcurrent, thus cables over-rating is not necessary. The cable sizing can refer to the nominal voltage and current level listed in [ABB 06].

3.4.6.2 Break-even voltage

The control of the SWF by both local and global overvoltage limitation control methods has been proposed. The local limitation control restraints the wind turbine output voltage by reducing the power production. The global control reduces HVDC voltage, while increases HVDC current. Although the current will not exceed the nominal level in the SWF in any case, the cable losses are increased in consequence. This entails the determination of the optimal HVDC voltage level $\hat{u}_{HVDC,opt}$, from which the maximum amount of power from offshore can be transmitted to the onshore converter.

- On one hand, considering the wind turbines protected only by local control strategy without global control:(suppose that the wind farm is operated at nominal HVDC voltage $U_{HVDC,nom}$), it causes the maximum wind turbine power curtailment with the minimum cable losses.
- On the other hand, considering the wind turbines protected by the global control, with the local control only activated to protect the wind turbine during the communication delay of the global control: as long as the global control reduces the HVDC voltage to $\hat{u}_{HVDC,gctl}$ according to Equation (3.16), the local control is totally operational. This situation causes the maximum cable losses and the minimum wind turbine power curtailment.

As a result, the optimal voltage level $\hat{u}_{HVDC,opt}$ is a trade-off value, which enables the maximum power received at onshore side. The value of $\hat{u}_{HVDC,opt}$ should remain in the range:

$$\hat{u}_{HVDC,opt} \in [\hat{u}_{HVDC,gctl}, U_{HVDC,nom}]$$

where

$\hat{u}_{HVDC,opt}$ = Optimal HVDC voltage level;
$\hat{u}_{HVDC,gctl}$ = HVDC voltage level adjusted according to the global control strategy;
$U_{HVDC,nom}$ = Nominal HVDC voltage.

In order to find this optimal voltage level, the HVDC voltage is gradually decreased, and then the instant wind farm power production $\hat{p}_{WF}$ is calculated (note that this power production is reduced due to local limitation control) as well as the cables power losses $\hat{p}_{cable}$. At each voltage level, the subtraction of the cables power losses from the wind farm power production gives the amount of power received at onshore $\hat{p}_{received}$:

$$\hat{p}_{received} = \hat{p}_{WF} - \hat{p}_{cable} \tag{3.20}$$

Assuming that at an instant there is no overvoltage limitation control applied, the HVDC voltage level is $\hat{u}_{HVDC}$ ($\leq U_{HVDC,nom}$), while the power production of the m wind turbines in the series wind farm is not reduced:

$$\mathbf{p_{out}} = \begin{pmatrix} p_{out,1} & p_{out,2} & \cdots & p_{out,l} & \cdots & p_{out,m-1} & p_{out,m} \end{pmatrix}^{\mathrm{T}}$$

With these amounts of power generation, there are l wind turbines in which their output voltage increases to the overvoltage limitation. Therefore, the local control has to reduce their power production. It can be assumed that these l units are WT_1, WT_2,..., WT_l. The local controllers of the remaining $(m-l)$ units are not activated, so they produce their initial power. Consequently, the power production of the m units under local control are denoted as:

$$\hat{\mathbf{p}}_{\mathbf{out}} = \begin{pmatrix} \hat{p}_{out,1} & \hat{p}_{out,2} & \cdots & \hat{p}_{out,l} & \cdots & \hat{p}_{out,m-1} & \hat{p}_{out,m} \end{pmatrix}^{\mathrm{T}}$$

where

$$\hat{p}_{out,l+1} = p_{out,l+1}, \quad \ldots, \quad \hat{p}_{out,m-1} = p_{out,m-1}, \quad \hat{p}_{out,m} = p_{out,m}$$

and

$$\hat{p}_{out,1} \leq p_{out,1}, \quad \hat{p}_{out,2} \leq p_{out,2}, \quad \ldots, \quad \hat{p}_{out,l} \leq p_{out,l}$$

Since the local controllers reduce the power production of WT_1, WT_2,..., WT_l for the purpose of maintaining their output voltages at U_{limit}, their power production can be calculated as:

$$\hat{p}_{out,1} = \frac{U_{limit} \sum_{x=1}^{m} \hat{p}_{out,x}}{\hat{u}_{HVDC}} \Longrightarrow \hat{p}_{out,1} = \frac{U_{limit}\left(\hat{p}_{out,2} + \hat{p}_{out,3} + \ldots + \hat{p}_{out,l-1} + \hat{p}_{out,l} + \sum_{x=l+1}^{m} \hat{p}_{out,x}\right)}{\hat{u}_{HVDC} - U_{limit}}$$

$$\hat{p}_{out,2} = \frac{U_{limit} \sum_{x=1}^{m} \hat{p}_{out,x}}{\hat{u}_{HVDC}} \Longrightarrow \hat{p}_{out,2} = \frac{U_{limit}\left(\hat{p}_{out,1} + \hat{p}_{out,3} + \ldots + \hat{p}_{out,l-1} + \hat{p}_{out,l} + \sum_{x=l+1}^{m} \hat{p}_{out,x}\right)}{\hat{u}_{HVDC} - U_{limit}}$$

$$\vdots$$

$$\hat{p}_{out,l} = \frac{U_{limit} \sum_{x=1}^{m} \hat{p}_{out,x}}{\hat{u}_{HVDC}} \Longrightarrow \hat{p}_{out,l} = \frac{U_{limit}\left(\hat{p}_{out,1} + \hat{p}_{out,2} + \hat{p}_{out,3} + \ldots + \hat{p}_{out,l-1} + \sum_{x=l+1}^{m} \hat{p}_{out,x}\right)}{\hat{u}_{HVDC} - U_{limit}}$$

then yields:

$$\begin{gathered}
\hat{p}_{out,1} - \frac{U_{limit}}{\hat{u}_{HVDC} - U_{limit}}\hat{p}_{out,2} - \ldots - \frac{U_{limit}}{\hat{u}_{HVDC} - U_{limit}}\hat{p}_{out,l} = \frac{\sum\limits_{x=l+1}^{m}\hat{p}_{out,x}}{\hat{u}_{HVDC} - U_{limit}} \\
-\frac{U_{limit}}{\hat{u}_{HVDC} - U_{limit}}\hat{p}_{out,1} + \hat{p}_{out,2} - \ldots - \frac{U_{limit}}{\hat{u}_{HVDC} - U_{limit}}\hat{p}_{out,l} = \frac{\sum\limits_{x=l+1}^{m}\hat{p}_{out,x}}{\hat{u}_{HVDC} - U_{limit}} \\
\vdots \\
-\frac{U_{limit}}{\hat{u}_{HVDC} - U_{limit}}\hat{p}_{out,1} - \frac{U_{limit}}{\hat{u}_{HVDC} - U_{limit}}\hat{p}_{out,2} - \ldots + \hat{p}_{out,l} = \frac{\sum\limits_{x=l+1}^{m}\hat{p}_{out,x}}{\hat{u}_{HVDC} - U_{limit}}
\end{gathered}$$

Writing the above equations in the form of matrix, yields:

$$\mathbf{A}\hat{\mathbf{p}}_{\mathbf{out},1\sim l} = \mathbf{B} \tag{3.21}$$

where

$$\begin{aligned}
\mathbf{A} &= \begin{pmatrix} 1 & -a & \cdots & -a \\ -a & 1 & \cdots & -a \\ \vdots & \vdots & \ddots & \vdots \\ -a & -a & \cdots & 1 \end{pmatrix} \text{ with } a = \frac{U_{limit}}{\hat{u}_{HVDC} - U_{limit}} \\
\mathbf{B} &= \begin{pmatrix} b \\ b \\ \vdots \\ b \end{pmatrix} \text{ with } b = \frac{\sum\limits_{x=l+1}^{m}\hat{p}_{out,x}}{\hat{u}_{HVDC} - U_{limit}} \\
\hat{\mathbf{p}}_{\mathbf{out},1\sim l} &= \begin{pmatrix} \hat{p}_{out,1} & \hat{p}_{out,2} & \cdots & \hat{p}_{out,l} \end{pmatrix}^{\mathrm{T}}
\end{aligned} \tag{3.22}$$

Then the reduced power of WT_1, WT_2,..., WT_l can be obtained:

$$\hat{\mathbf{p}}_{\mathbf{out},1\sim l} = \mathbf{A}^{-1}\mathbf{B} \tag{3.23}$$

As long as the power production of each wind turbine is obtained, the entire wind farm power production $\hat{p}_{WF}$ and the increased HVDC current are:

$$\hat{p}_{WF} = \sum_{x=1}^{m}\hat{p}_{out,x} \tag{3.24}$$

$$\hat{i}_{HVDC} = \frac{\hat{p}_{WF}}{\hat{u}_{HVDC}} \tag{3.25}$$

The power losses of the cables are given by

$$\hat{p}_{cable} = n_c \hat{i}^2_{HVDC} R_c = n_c \hat{i}^2_{HVDC} \frac{\rho l_c}{S_c} \tag{3.26}$$

$$\rho = \rho_{20}(1 + K(T - 20)) \tag{3.27}$$

where

n_c = Number of cables;
ρ = Cable conductor resistivity (Ω m);
ρ_{20} = Conductor resistivity at 20 °C, which equals 1.68×10^{-8} Ω m;
K = Temperature coefficient of resistivity, which equals 0.0038 for copper;
T = Working temperature, which is considered at 90 °C;
l_c = Cable conductor length (m);
S_c = Cable conductor section (m^2).

The cable conductor resistivity varies linearly with the temperature.

The subtraction of the power losses in the cables of Equation (3.25) from the power generated in the wind farm of Equation (3.24) is the power received at onshore side.

3.5 Simulation of the global overvoltage limitation control

3.5.1 Case study

To illustrate the above method consisting in finding the optimal HVDC voltage, a wind farm of 20 units of 5 MW is used. The nominal wind turbine output voltage is $U_{out,nom}$=32 kV and the overvoltage ratio α=0.1.

The 20 units generate their instant power production, (in per unit) as:

$$\mathbf{p_{out}} = \big(\underline{1.0} \quad \underline{1.0} \quad \underline{1.0} \quad \underline{1.0} \quad 0.9 \quad 0.9 \quad 0.9 \quad 0.9 \quad 0.85 \quad 0.85$$
$$0.85 \quad 0.85 \quad 0.8 \quad 0.8 \quad 0.8 \quad 0.8 \quad 0.75 \quad 0.75 \quad 0.75 \quad 0.75\big)^{\mathrm{T}}$$

$$p_{WF} = 17.2 P_{out,nom} = 86\,\mathrm{MW}$$

The output voltage of units 1-4, $\mathrm{WT}_{1\text{-}4}$ increases beyond the overvoltage limitation if no control is applied. At nominal HVDC voltage $U_{HVDC,nom}$=$mU_{out,nom}$, the local control reduces the power production of $\mathrm{WT}_{1\text{-}4}$ to maitain their output voltages equal to U_{limit}.

According to Equation 3.23, the reduced power matrix of the SWF, (in per unit), is:

$$\hat{\mathbf{p}}_{\mathbf{out}} = \begin{pmatrix} \underline{0.93} & \underline{0.93} & \underline{0.93} & \underline{0.93} & 0.9 & 0.9 & 0.9 & 0.9 & 0.85 & 0.85 \\ 0.85 & 0.85 & 0.8 & 0.8 & 0.8 & 0.8 & 0.75 & 0.75 & 0.75 & 0.75 \end{pmatrix}^{\mathrm{T}}$$

$$\hat{p}_{WF} = 16.923 P_{out,nom} = 84.615\,\mathrm{MW}$$

The HVDC current is:

$$\hat{i}_{HVDC} = \frac{\hat{p}_{WF}}{U_{HVDC,nom}} = \frac{84.615\,\mathrm{MW}}{640\,\mathrm{kV}} = 132.2\,\mathrm{A}$$

The cable used for the transmission is rated at 100 MW, the cable section S_{cable} is chosen to be 85 mm^2 [ABB 06], and the transmission length is 100 km. Therefore, the Joule losses of the cables are:

$$\hat{p}_{cable} = 2\hat{i}_{HVDC}^{2}\frac{\rho l_c}{S_c} = 0.875\,\mathrm{MW}$$

According to Equation (3.20), the power received at onshore at nominal HVDC voltage is:

$$\hat{p}_{received} = \hat{p}_{WF} - \hat{p}_{cable} = 84.615 - 0.875 = 83.74\,\mathrm{MW}$$

By decreasing the HVDC voltage gradually and calculating the received power at every voltage level, the variation of the received power with the HVDC voltage is plotted in Figure 3.35. As expected, the cable losses increase as the HVDC voltage decreases.

The maximum received power at 605.44 kV equals 85 MW. Note that this voltage equals the $\hat{u}_{HVDC,gctl}$ where the local control is fully operational. This indicates that in this specific case, in the whole range $[\hat{u}_{HVDC,gctl}, U_{HVDC,nom}]$, the reduction of voltage offers higher power generated from the wind farm than the power losses in the cables. Further reduction of the HVDC voltage increases the cable losses while all wind turbines operate at MPPT, and therefore the overall power received at onshore side diminishes.

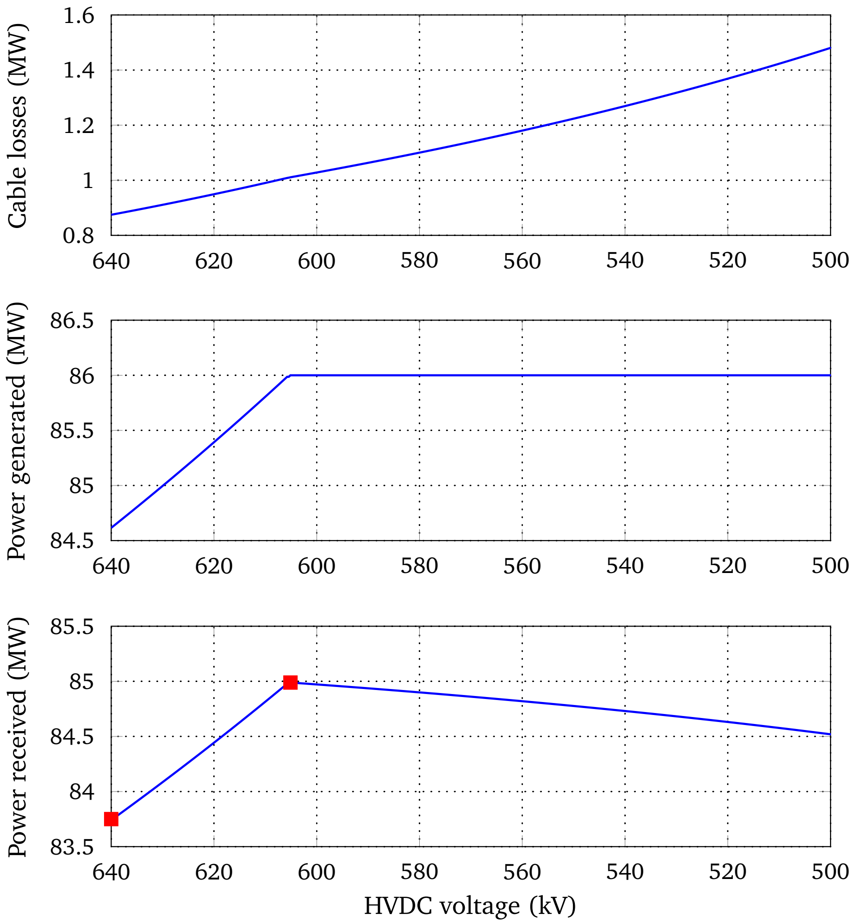

Figure 3.35 – Received power at onshore varies with the HVDC voltage level.

3.5.2 Simulation results

A series connection of 20 wind turbines with the global control strategy has been implemented and evaluated in EMTP-RV [Mahs 07].

For the sake of clarity, the per unit system is used differently for the wind turbine individual and for the HVDC system. For wind turbine, the nominal power and output voltage are 5 MW and 32 kV, and they are considered as 1 pu. The nominal voltage for the MMC is 640 kV and this is taken as 1 pu for the HVDC system. The overvoltage ratio is α=0.1. The HVDC cable used in the simulation is a 100 km WideBand cable model.

The power production variation of the SWF is plotted in Figure 3.36a. The same power variation used in the case study in Subsection 3.5.1 is adopted in this simulation in order to verify the obtained results. During the interval from 1 to 3 s, all the 20 wind turbines have nominal power production at 5 MW. In the next 2 s, the power of the wind turbines decreased as follows: to 0.9 pu for units 5-8 $WT_{5\text{-}8}$, to 0.85 pu for units 9-12 $WT_{9\text{-}12}$, to 0.8 pu for units 13-16 $WT_{13\text{-}16}$ and to 0.75 pu for units 17-20 $WT_{17\text{-}20}$. Units 1-4 $WT_{1\text{-}4}$ produce nominal power.

All units operate under their overvoltage capabilities until 4.6 s, as the power production imbalance increases, and $WT_{1\text{-}4}$ reach their maximal overvoltage capabilities.

In order to show the different behaviour of the local limitation control and the global limitation control, only the local limitation control is activated before 8 s and the global limitation is applied from 8 s to 10 s.

From 4.6 s to 8 s, the local limitation controllers in $WT_{1\text{-}4}$ reduce their power production to 4.65 MW, as seen in Figure 3.36a, equivalent to 0.93 pu as the result obtained in Subsection 3.5.1. Figure 3.36b shows that in this time interval, local limitation controllers regulate the output voltages of $WT_{1\text{-}4}$ at 1.1 pu. The power received at onshore converter is −83.7 MW. The negative sign indicates that the power is transmitted from the HVDC system to the AC grid.

From 8 s, the global limitation control is activated. The HVDC voltage is reduced to the optimal HVDC voltage $\hat{u}_{HVDC,opt}$=605.44 kV as calculated in Subsection 3.5.1. The power production of $WT_{1\text{-}4}$ are restored to their nominal value since the local control is activated owing to the reduction of HVDC voltage. As observed in Figure 3.36e, the received power at onshore steps up to −85 MW.

The results of the simulation follow the analysis in the previous case study. However, the optimal HVDC voltage should be calculated for different power production matrix, which requires power data from the wind farm for real time calculation. Consequently, it should be emphasized again that the communication and calculation of the HVDC voltage level are indispensable.

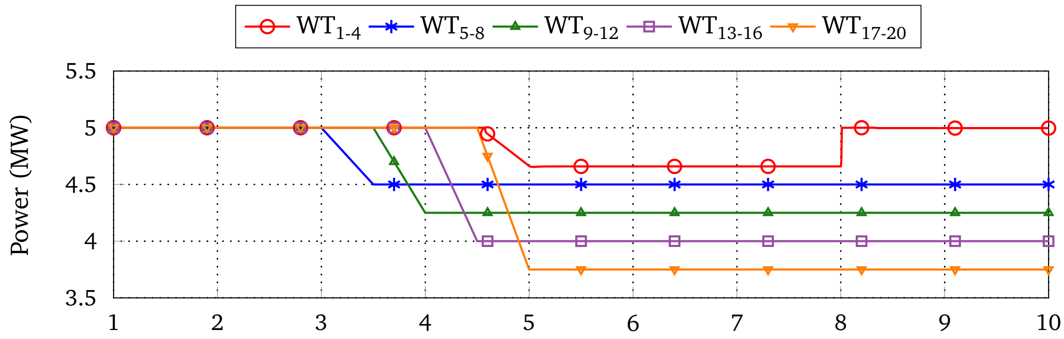

(a) Power production of wind turbines in the series wind farm.

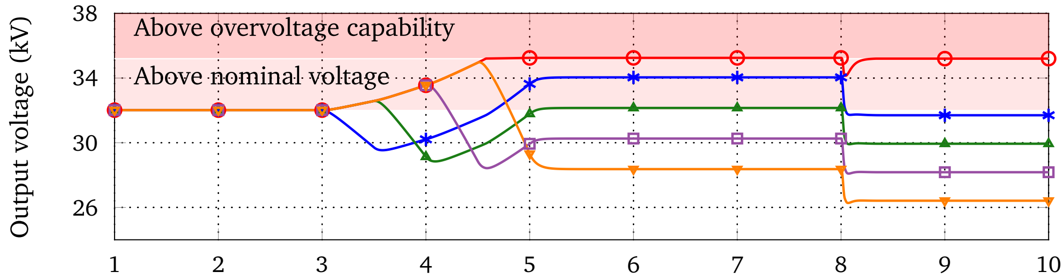

(b) Output voltage of wind turbines.

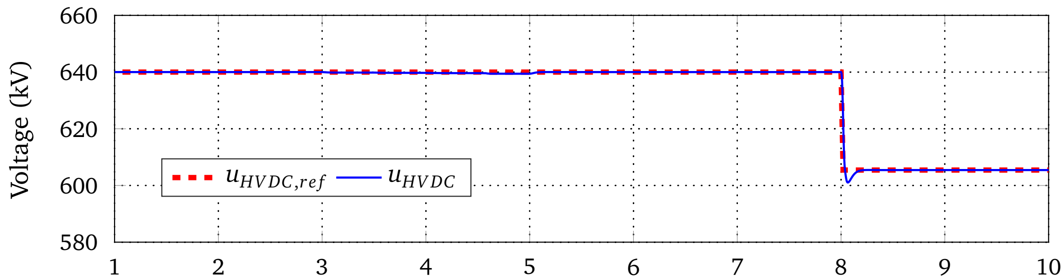

(c) HVDC voltage of the P2P system.

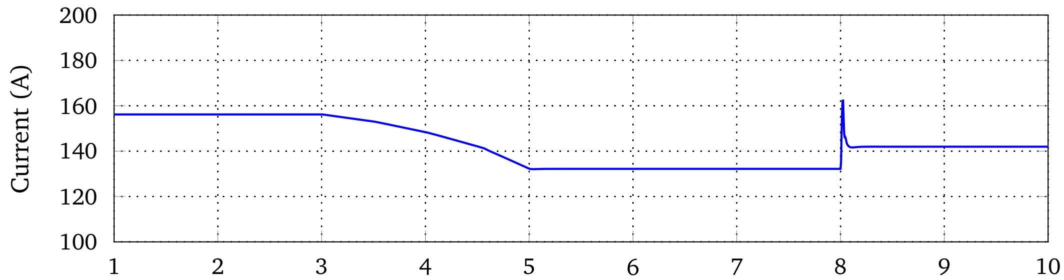

(d) HVDC current of the P2P system.

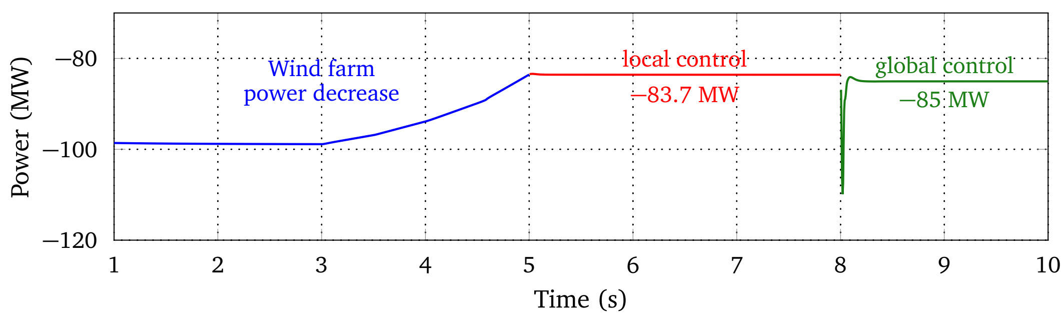

(e) Power received at the onshore MMC end.

Figure 3.36 – The simulation results of the SWF with local and global overvoltage limitation methods.

3.6 Conclusion

In this chapter the HVDC cables models are described and compared to the Universal Line Model (ULM) - Wideband model. It is shown that the RC model, the pi-section model and the coupled pi-section model can only represent the cable characteristics in limited frequency ranges. In this thesis, the Wideband model, taken directly from the EMTP-RV library, is used since the SWF requires a precise cable model at low DC frequency as well as at resonant frequency. The resonant behaviour is due to the fact that the uncontrolled elements, the wind turbine output capacitors, DC smoothing reactors and the HVDC cables, form a resonant circuit in the transmission system.

The onshore MMC model is developed in this chapter and the energy based control is described. After both transmission and integration systems are explained, a global control strategy is proposed, with the purpose of regulating the HVDC transmission voltage in order to reduce the voltage across the wind turbines at the offshore end. The optimal voltage level needs to be calculated depending on the wind farm working conditions. Since the decrease of voltage level results in the increase of current and thus the losses in the cables, an optimal HVDC voltage level associated to the corresponding voltage that leads to maximum power received at onshore end. In addition, the local control strategy is proposed to be complementary to the global control. Finally, the entire control system of a series wind farm is presented.

References

[ABB 06] ABB. *HVDC Light - Cables Submarine and land power cables*. 2006. 120, 124

[Akka 16] S. Akkari. *Control of a multi-terminal HVDC (MTDC) system and study of the interactions between the MTDC and the AC grids*. PhD thesis, Université Paris-Saclay, 2016. XIII, 93, 105

[Anto 09] A. Antonopoulos, L. Angquist, and H.-P. Nee. "On dynamics and voltage control of the modular multilevel converter". In: *Power Electronics and Applications, 2009. EPE'09. 13th European Conference on*, pp. 1–10, IEEE, 2009. 93, 94

[Berg 13] G. Bergna, E. Berne, P. Egrot, P. Lefranc, A. Arzande, J.-C. Vannier, and M. Molinas. "An energy-based controller for HVDC modular multilevel converter in decoupled double synchronous reference frame for voltage oscillation reduction". *IEEE Transactions on Industrial Electronics*, Vol. 60, No. 6, pp. 2360–2371, 2013. 95

[Chau 11] N. R. Chaudhuri, R. Majumder, B. Chaudhuri, and J. Pan. "Stability analysis of VSC MTDC grids connected to multimachine AC systems". *IEEE Transactions on Power Delivery*, Vol. 26, No. 4, pp. 2774–2784, 2011. 104

[Dela 13] P. Delarue, F. Gruson, and X. Guillaud. "Energetic macroscopic representation and inversion based control of a modular multilevel converter". In: *Power Electronics and Applications (EPE), 2013 15th European Conference on*, pp. 1–10, IEEE, 2013. 95

[Euro 15] Europacable. "Introduction to HVDC Subsea Cables". 2015. Available online at `http://www.europacable.com/home/energy-cables/hvdc-cables.html`. XIV, 115, 116

[Frey 16] J. Freytes, L. Papangelis, H. Saad, P. Rault, T. Van Cutsem, and X. Guillaud. "On the modeling of MMC for use in large scale dynamic simulations". In: *Power Systems Computation Conference (PSCC), 2016*, pp. 1–7, IEEE, 2016. 93

[Gnan 11] U. N. Gnanarathna, A. M. Gole, and R. P. Jayasinghe. "Efficient modeling of modular multilevel HVDC converters (MMC) on electromagnetic transient simulation programs". *IEEE Transactions on power delivery*, Vol. 26, No. 1, pp. 316–324, 2011. 92

[Grus 15] F. Gruson, J. Freytes, S. Samimi, P. Delarue, X. Guillaud, F. Colas, and M. Belhaouane. "Impact of control algorithm solutions on Modular Multilevel Converters electrical waveforms and losses". In: *Power Electronics and Applications (EPE'15 ECCE-Europe), 2015 17th European Conference on*, pp. 1–10, IEEE, 2015. XVII, 101

[Li 15] B. Li, R. Yang, D. Xu, G. Wang, W. Wang, and D. Xu. "Analysis of the phase-shifted carrier modulation for modular multilevel converters". *IEEE Transactions on Power Electronics*, Vol. 30, No. 1, pp. 297–310, 2015. 97

[Lund 06] S. Lundberg. *Wind Farm Configuration and Energy Efficiency Studies-Series DC versus AC Layouts*. PhD thesis, Chalmers University of Technology, 2006. 89

[Mahs 07] J. Mahseredjian, S. Dennetière, L. Dubé, B. Khodabakhchian, and L. Gérin-Lajoie. "On a new approach for the simulation of transients in power systems". *Electric power systems research*, Vol. 77, No. 11, pp. 1514–1520, 2007. 90, 126

[Marq 01] R. Marquardt. "Stromrichterschaltungen mit verteilten Energiespeichern". *German Patent DE10103031A1*, Vol. 24, 2001. 90

[Mart 82] J. R. Marti. "Accuarte modelling of frequency-dependent transmission lines in electromagnetic transient simulations". *IEEE Transactions on Power Apparatus and Systems*, No. 1, pp. 147–157, 1982. 104

[Morc 99] A. Morched, B. Gustavsen, and M. Tartibi. "A universal model for accurate calculation of electromagnetic transients on overhead lines and underground cables". *IEEE Transactions on Power Delivery*, Vol. 14, No. 3, pp. 1032–1038, 1999. 104

[Nami 15] A. Nami, J. Liang, F. Dijkhuizen, and G. D. Demetriades. "Modular multilevel converters for HVDC applications: Review on converter cells and functionalities". *IEEE Transactions on Power Electronics*, Vol. 30, No. 1, pp. 18–36, 2015. 90

[Raul 14] P. Rault. *Dynamic Modeling and Control of Multi-Terminal HVDC Grids*. PhD thesis, Ecole Centrale de Lille, Lille, France, 2014. 99, 106

[Rohn 10] S. Rohner, S. Bernet, M. Hiller, and R. Sommer. "Modulation, losses, and semiconductor requirements of modular multilevel converters". *IEEE transactions on Industrial Electronics*, Vol. 57, No. 8, pp. 2633–2642, 2010. 91

[Saad 15] H. A. Saad. *Modélisation et simulation d'une liaison HVDC de type VSC-MMC*. PhD thesis, École Polytechnique de Montréal, 2015. 92

[Saee 10] M. Saeedifard and R. Iravani. "Dynamic performance of a modular multilevel back-to-back HVDC system". *IEEE Transactions on power delivery*, Vol. 25, No. 4, pp. 2903–2912, 2010. 97

[Sami 16a] S. Samimi. *Modélisation et commande des convertisseurs MMC en vue de leur intégration dans le réseau électrique*. PhD thesis, Ecole Centrale de Lille, Lille, France, 2016. 93

[Sami 16b] S. Samimi, F. Gruson, P. Delarue, F. Colas, M. M. Belhaouane, and X. Guillaud. "MMC Stored Energy Participation to the DC Bus Voltage Control in an HVDC Link". *IEEE Transactions on Power Delivery*, Vol. 31, No. 4, pp. 1710–1718, 2016. 95, 99

[Shi 13] G. Shi, Z. Wang, M. Zhu, X. Cai, and L. Yao. "Variable speed control of series-connected DC wind turbines based on generalized dynamic model". In: *Renewable Power Generation Conference (RPG 2013), 2nd IET*, pp. 1–6, IET, 2013. 89

[Stah 08] J. W. Stahlhut, T. J. Browne, G. T. Heydt, and V. Vittal. "Latency viewed as a stochastic process and its impact on wide area power system control signals". *IEEE Transactions on Power Systems*, Vol. 23, No. 1, pp. 84–91, 2008. 116

[Tu 11a] Q. Tu and Z. Xu. "Impact of sampling frequency on harmonic distortion for modular multilevel converter". *IEEE Transactions on Power Delivery*, Vol. 26, No. 1, pp. 298–306, 2011. 98

[Tu 11b] Q. Tu, Z. Xu, and L. Xu. "Reduced switching-frequency modulation and circulating current suppression for modular multilevel converters". *IEEE transactions on power delivery*, Vol. 26, No. 3, pp. 2009–2017, 2011. 94, 97

[Wach 14] R. Wachal, A. Jindal, S. Dennetiere, H. Saad, O. Rui, S. Cole, M. Barnes, L. Zhang, Z. Song, J. Jardini, *et al.* "Guide for the development of models for HVDC converters in a HVDC grid". *Cigré TB604 (WG B4. 57), Paris, Tech. Rep.*, 2014. 105

[Wang 11] W. Wang, Y. Xu, and M. Khanna. "A survey on the communication architectures in smart grid". *Computer Networks*, Vol. 55, No. 15, pp. 3604–3629, 2011. XIV, 116

[Wang 12] W. Wang, M. Barnes, and O. Marjanovic. "Droop control modelling and analysis of multi-terminal HVDC for offshore wind farms". In: *IET Conference Proceedings*, pp. 21–21(1), IET, 2012. 104

[Worz 09] T. Worzyk. *Submarine power cables: design, installation, repair, environmental aspects*. Springer Science & Business Media, 2009. 115

[Wu 04] H. Wu, K. S. Tsakalis, and G. T. Heydt. "Evaluation of time delay effects to wide-area power system stabilizer design". *IEEE Transactions on Power Systems*, Vol. 19, No. 4, pp. 1935–1941, 2004. 115

Chapter 4

Series parallel wind farm in MTDC systems

What matters in life is not what happens to you but what you remember and how you remember it.

Gabriel García Márquez

Contents

4.1 Introduction

Currently, most of the HVDC transmissions have point-to-point schemes, and only a few Multi-Terminal HVDC (MTDC) projects exist worldwide. Two projects exist, using Line Commutated Converter (LCC) based MTDC technology. The first one is the SACOI project used for the exchange of electrical energy between the Italian mainland, Corsica and Sardinia [Bill 89]. The other one is the multi-terminal system connecting Quebec and New England in the North America [Mori 93]. With LCC technology, the reversal of power flow is not easy since it requires complex mechanical switchgear operations to reverse the power flow direction [Rao 15].

In comparison, Voltage Source Converter (VSC)-HVDC can change the direction of power flow without reversing the polarity of the transmission voltage, which makes it more suitable for MTDC than LCC-HVDC. The world's first three-terminal VSC based MTDC system is the Nan'ao project in Guangdong China [Rao 15], followed by the world's first five-terminal MTDC project put into service in 2014 in Zhoushan China [Li 15].

After the design of series connected wind turbines in Chapter 2 and the integration of series offshore wind farm into a point-to-point HVDC transmission system in Chapter 3, this chapter aims at integrating the series offshore wind farm into MTDC systems.

The first part of this chapter is dedicated to extend the structure of a series wind farm with only one cluster into several clusters, named as Series Parallel Wind Farm (SPWF) in [Lund 06]. Parallel connection of several clusters permits a more reliable topology than one single cluster since the fault in one cluster does not affect the operation of wind turbines in other clusters.

The SPWF is controlled with the strategy introduced in a point-to-point HVDC link in Chapter 3. Usually in a point-to-point VSC HVDC link, the converter at one terminal controls the DC voltage, and the one at the other terminal controls the active/reactive power into the AC grid. When it comes to VSC-based MTDC systems, which contain three or more terminals, the function of each converter needs to be distinguished.

MTDC system with different combinations of grid side MMCs, SPWFs and conventional wind farms using MVAC collection system, are discussed in this chapter. For each configuration, the MTDC control methods are selected and the global control strategy is verified with simulations by using EMTP-RV.

4.2 Series Parallel Wind Farm

This section introduces the Series Parallel Wind Farm (SPWF) which is a combination of several parallel connected Series Wind Farm (SWF). The configuration of the SPWF is first discussed and then the design of a 300 MW SPWF is explained.

4.2.1 Scaling of the SPWF

To decide the number of wind turbines to be connected in a series connection to establish the HVDC transmission voltage, there are two main factors to be considered.

On the one hand, as the series system fails when any one component fails, the failure rate for the series system is therefore equal to the sum of the failure rates of its components [Alla 13]. As a result, the fewer the units in one cluster the higher the reliability. Furthermore, with the same HVDC voltage, a lower number of units also leads to a higher voltage level used in the wind turbine, and therefore lower copper losses in the wind turbine electrical system.

On the other hand, the step-up ratio of the DC/DC converter should be designed by taking into account the volume of the transformer. A lower number of units means higher output voltage across each unit. However, with today's commercial available medium-voltage wind turbine conversion technologies, the low voltage side of the transformer can only reach 3.3 to 4 kV [Lise 11]. A very high transformation ratio implies the need for a large transformer in the wind turbine, using a large fraction of the available space, which is not practical for offshore applications.

In Chapter 3, to establish a ±320 kV point-to-point HVDC system, 20 wind turbines of 5 MW power rating and a 32 kV nominal output voltage are connected in series. The power rating of this wind farm equals 100 MW. In order to increase the wind farm power rating, several clusters can be connected in parallel [Lund 06].

4.2.2 Parallel connection of clusters

There are two ways to interconnect clusters in the collection system of the Series Parallel Wind Farm (SPWF). These two methods are illustrated in a m×n SPWF, shown in Figure 4.1. The first one is to connect one cluster to its adjacent cluster as shown in Figure 4.1a. Cables connection of the positive ends of the clusters are from $1^+ \rightarrow 2^+ \rightarrow ... \rightarrow n^+$ then to the hub end h^+, and same for the negative ends $1^- \rightarrow 2^- \rightarrow 3^- \rightarrow ... \rightarrow h^-$. In this case, the sizes of cables are different. Cable between 1^+ and 2^+ transmits the power of one cluster, while the cable between n^+ to the hub h^+ transmits the power of the entire wind farm. Another way for interconnection is shown in Figure 4.1b. All the clusters are connected to the hub directly: $1^+ \rightarrow h^+$, $2^+ \rightarrow h^+$ ... and $n^+ \rightarrow h^+$. In this case the cables have the same size.

These two ways of interconnection correspond to different architectures for the entire wind farm system. The first collection system corresponds to a radial-type or string-type system as shown in Figure 4.2a. The second collection system corresponds to a star-type system shown in Figure 4.2b. The radial system uses less interconnection cables length while the star system is more reliable [Quin 07]. For this reason, in this thesis we adopt the second SPWF layout, the star-type system.

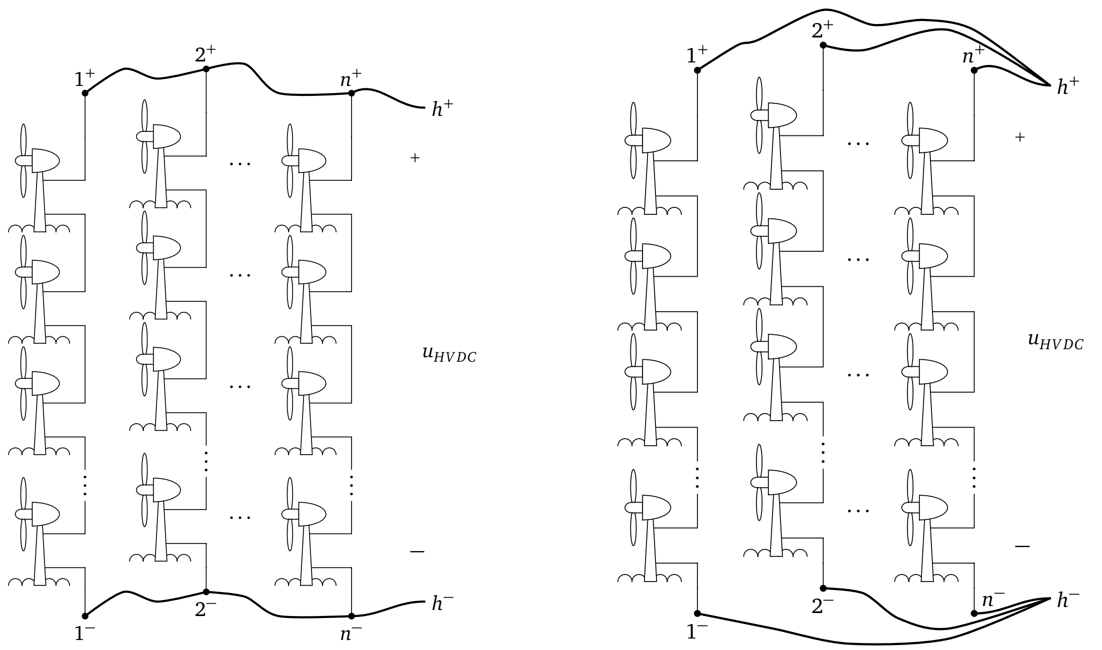

(a) Interconnection of adjacent clusters (b) Interconnection of clusters and the cable hub

Figure 4.1 – Two ways of inter-array connection of SPWF.

(a) Radial system (b) Star system

Figure 4.2 – Layouts of a SPWF-HVDC system using different ways of inter-array connection of wind farm collection system. Rectangle: onshore converter, Circle: a cluster of wind turbines.

A complete type 20×3 SPWF is plotted in Figure 4.3. The notations used for the SPWF are distinguished from the series wind farm by adding an extra index y to the subscript which refers to its cluster.

With a further look at the SPWF type, the three wind turbine clusters are assembled into a simple MTDC system. The three clusters deliver power to the grid side converter then to the AC grid. The onshore converter maintains the HVDC voltage. Assuming that the voltage drops along the DC cables and smoothing reactors can be neglected, all clusters share a common HVDC voltage:

$$u_{HVDC} = \sum_{x=1}^{20} u_{out,x,1} = \sum_{x=1}^{20} u_{out,x,2} = \sum_{x=1}^{20} u_{out,x,3}. \tag{4.1}$$

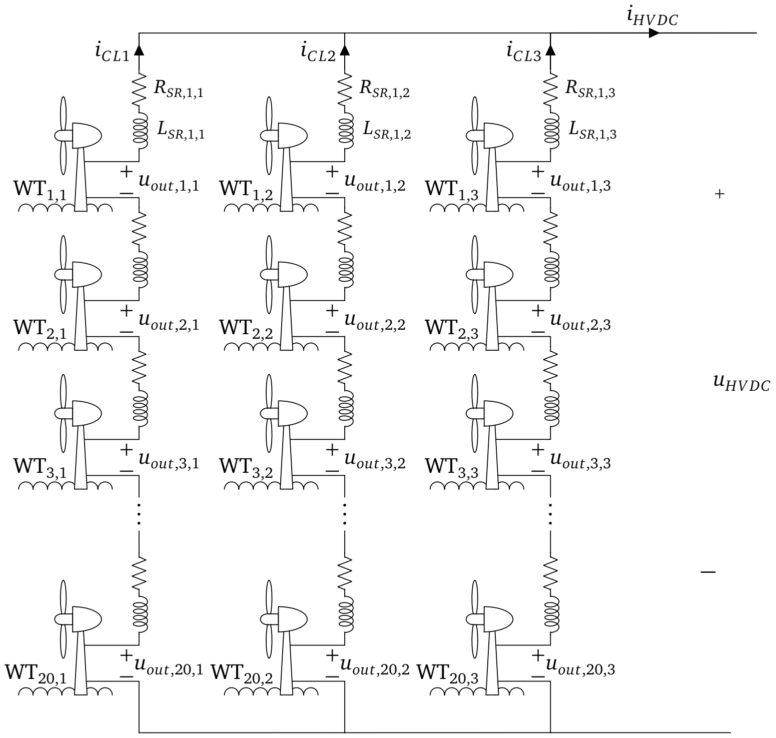

Figure 4.3 – Wind turbine arrangement of the Series Parallel offshore wind farm.

The HVDC current is equal to the sum of three cluster currents:

$$i_{HVDC} = \sum_{y=1}^{3} i_{CL,y} = i_{CL,1} + i_{CL,2} + i_{CL,3} \tag{4.2}$$

4.3 SPWF operating in MTDC systems

After the analysis of the operation of a series wind farm in a point-to-point HVDC system, and extending the wind farm from one cluster to multi-cluster, in this section, the Series Parallel Wind Farm (SPWF) operation in hybrid Multi-Terminal HVDC (MTDC) systems is discussed.

MTDC system is not only more flexible and reliable than point-to-point HVDC from the technical point of view [Jian 98][Gomi 11b][Raul 14], but it is also less expensive and utilises effectively the existing assets [Zhu 10]. For example, a newly-built wind farm can be connected to an existing point-to-point HVDC system for transmitting power to the grid as long as the cumulative power is within the designed ratings of the converter and power cables. As an alternative, an existing offshore wind farm can be used to supply a part of its power to a newly-built offshore oil and gas platform, and the remainder to the grid. In this way, the three-terminal MTDC avoids an extra investment to point-to-point power transmission from onshore grid to the oil and gas platform.

Although various control strategies for MTDC system have been discussed in the literature [Lian 11] [Jovc 09][Raul 14][Naka 99][Hail 08], they basically stem from two control philosophies: endowing the HVDC voltage control on one centralized converter or on a number of converters.

The former one is the idea of the master-slave control method with only one "master" converter responsible for controlling the HVDC voltage. This method was presented for the integration of multiple VSC-based offshore wind farms in [Jovc 09]. The main issue of the master-slave control is that the AC system connected to the master converter is required to provide alone all the balancing power to the MTDC system and the outage of this master converter would bring down the entire system. The second option, which is called the voltage droop control, distributes the DC voltage control over a number of converters. Multiple converters can participate into the DC voltage control by adapting their power according to their droop characteristics. The DC voltage droop control method and its dynamic behaviour are explained in [Raul 14].

Based on the two principles mentioned above, various other control methods are derived in order to take into account abnormal situations, such as outage of one converter. In [Naka 99], a voltage margin control based on master-slave control is used to control a VSC-based MTDC system. A hybrid method with the voltage droop method in addition to the voltage margin control is presented in [Hail 08] for a four-terminal offshore DC system.

4.3.1 SPWF in a MTDC system with master-slave control

A ring type MTDC system illustrated in Figure 4.4 is composed of one onshore converter and two offshore wind farms including one SPWF. This type of MTDC system can only use the master-slave method since only one onshore converter (GSMMC) is available to control the HVDC voltage. The function of the offshore MVAC wind farm converter (OSMMC) as a HVDC voltage regulator is not considered, since in a MTDC system the individual wind farm power rating is relatively small and is not capable of performing regulation of the HVDC voltage [Zhu 10].

One extra power cable ($link_{23}$) is used to connect these two offshore wind farms to form a ring topology. The advantage of the ring topology is that in case of faults on $link_{12}$ or $link_{31}$ the power can be transmitted via this extra power cable. This enables a more reliable operation. Consequently, the cables of $link_{12}$ and $link_{13}$ should be sized at the sum of the power of these two wind farms.

In the following analysis of the MTDC systems, the power flowing into the MTDC cables network is defined as positive, and the power flowing out is defined as negative. For the terminals, transferring AC power into the MTDC system means that they are operating as rectifiers. On the contrary, transferring DC power into the AC grid indicates that they are operating as inverters. Therefore, it can be seen that the presented system in Figure 4.4 is a

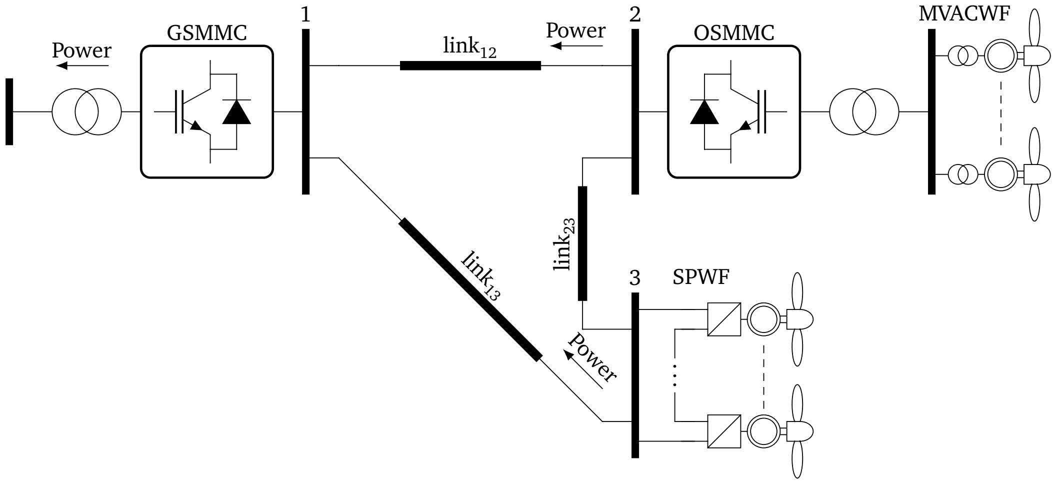

Figure 4.4 – A 3-terminal MTDC system for transferring power from one MVAC wind farm and one SPWF to one onshore grid connected MMC.

double-input-single-output MTDC system.

In this MTDC system which has only one onshore converter, the master-slave control is therefore the only solution for controlling the system. However, the master-slave control can also be applied to systems with multiple onshore converters by using one converter as the HVDC voltage regulator and the others regulating their power. In any case, only one converter is selected as the "Master" for the MTDC system.

4.3.1.1 Characteristics of the MTDC system with master slave control

A voltage source converter can operate in both inverter and rectifier modes. However, in the normal operation of the MTDC system shown in Figure 4.4, the onshore VSC is always in inverter mode, transferring power generated from the offshore side to the onshore grid side, as illustrated in Figure 4.5.

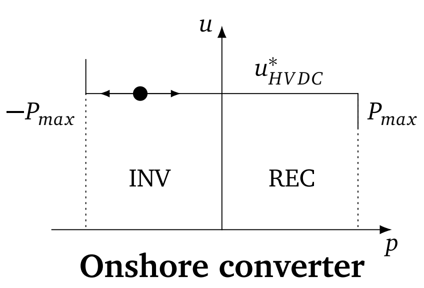

Figure 4.5 – $p-u$ characteristic of a grid side VSC acting as master controller.

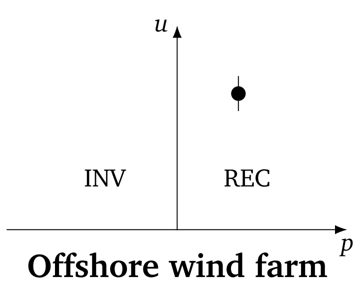

Figure 4.6 – $p-u$ characteristic of an offshore wind farm.

From this figure, the operating point of the VSC only moves left or right if the global control strategy is not applied. In this way, the VSC acts as a slack bus as long as its active power does not reach its limits [Dier 12]. It compensates for the variation of power injected to the MTDC system by moving its operating point along this slack bus. Once its operating point reaches its maximum limit, the HVDC voltage of the MTDC system increases as the amount of the injected power is greater than the power the inverter can absorb. From then, the voltage source inverter is not able to regulate the HVDC voltage to the reference u^*_{HVDC}.

A MVAC offshore wind farm is treated as a wind farm rectifier which is responsible for injecting the generated wind power into the MTDC system [Gomi 11a]. In the literature [Lian 09], the wind farm rectifier is separated into 3 operating modes:

1. *Normal mode*: All generated power from the wind farm is injected into the MTDC system via the offshore VSC. In this case the wind farm can be modelled as a controlled current source.
2. *Voltage droop mode*: During an onshore AC grid fault or the loss of a grid connected inverter, the generated wind power is higher than the amount of power that can be exported to the AC grid, so the HVDC voltage increases. As a result, the wind farm has to reduce its power production by using a droop characteristic.
3. *Current limit mode*: The wind farm rectifier enters into this mode due to the thermal limits of the offshore VSC.

In this thesis, the MVAC wind farm is considered ideally to operate under normal mode, in which the offshore VSC exports all the wind farm power into the MTDC grid. As a result, the $p-u$ characteristic of the MVAC wind farm is illustrated in Figure 4.6 as a black dot denoting its power production. Its voltage is imposed by the onshore converter.

In the same way, the SPWF is also considered as a wind farm rectifier operating in normal mode. Therefore, the SPWF has the same $p-u$ characteristic illustrated in Figure 4.6. However, this rectifier is different from the aforementioned MVAC wind farm rectifier in two aspects: First, the power of MVAC wind farm is injected into the MTDC grid through the offshore VSC, while the SPWF power is exported into the grid through the wind turbine output DC/DC converter directly. Therefore, each wind turbine can be regarded as a controlled current source. Second, the operation of each wind turbine in overvoltage limitation mode should not be neglected.

4.3.1.2 Overview of the control strategy

The overall control strategy of this three-terminal MTDC system is shown in Figure 4.7. The master-slave control endows the onshore MMC as the master controller, which regulates the voltage of the system. The offshore converter is treated as "slave" which injects power to the MTDC system. Moreover, the participation of the SPWF in the MTDC system requires extra controls for the safe operation of the wind farm. For this reason, the global control strategy is adopted, which takes the information of the power production of the wind farm

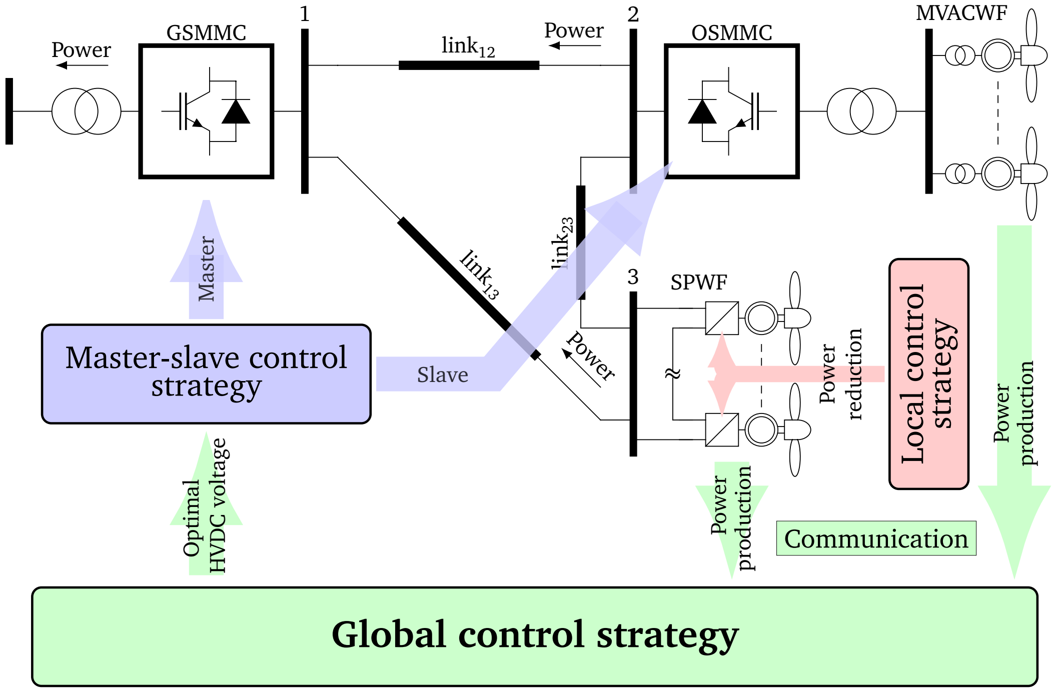

Figure 4.7 – Overview of the control system of the three-terminal MTDC.

and calculates the best HVDC voltage for the whole network. This optimal HVDC voltage is sent to the master-slave control system to set a new operating point. In addition, the local control strategy complements the global control strategy to protect the SPWF.

The overall control strategy must achieve the following targets:

1. Maintain the MTDC transmission voltage.
2. Maintain the MVAC voltage of the conventional wind farm collection grid.
3. Keep the output voltage of each SP wind turbine under its overvoltage limitation level.
4. Maximize the power transmitted to the onshore grid.

Target 1 is accomplished by the onshore converter GSMMC operating at DC voltage mode. Target 2 is met by the offshore converter OSMMC operating at AC voltage mode. The global and the local control strategy are dedicated to accomplish the Targets 3 and 4.

4.3.1.3 Case study and simulation results of a hybrid three-terminal MTDC system

The three-terminal MTDC system shown in Figure 4.4 is sized as follows. The onshore MMC is rated at 650 MW. One 300 MW offshore wind farm (MVACWF) using MVAC collection system and located 80 km away from the shore is already connected to the grid through a point-to-point HVDC. Considering that a newly-built 20×3 SPWF rated at 300 MW is planned to be connected to the grid through the same onshore converter. The wind turbines nominal power and voltage are 5 MW and 32 kV, respectively. The extra power cable interconnecting two offshore wind farms is 60 km long. The converter stations at onshore and offshore are MMC with a nominal HVDC voltage of ± 320 kV. Converters operating points are reported in Table 4.1 and shown in Figure 4.8.

In this case study, the "master" onshore MMC regulates the HVDC voltage with a time constant of 100 ms with the energy based control discussed in Chapter 3. At 2 s, the power of the "slave" MVAC wind farm decreases from nominal 300 MW to 270 MW as shown Figure 4.9a. Moreover, Figure 4.9b shows the maximum wind power that can be extracted by the SP wind turbines.

Assuming that the units in the cluster 2 and 3 are at nominal power production, (5 MW), during all the simulation. The wind speed varies along the units during 3 s to 5 s in the cluster 1. Therefore, the output voltage of $WT_{1\text{-}4,1}$ are pushed beyond their overvoltage limitation 1.1 pu if no overvoltage limitation strategy is applied. In order to see the difference between local control strategy and the global control strategy, in the simulation, the local control is first activated, which restrains the increase of output voltage by means of power curtailment. The global control strategy is activated at 8 s and the results are presented below.

Figure 4.10 shows the simulation results of the three-terminal MTDC system operating in aforementioned conditions and with master-slave control applied.

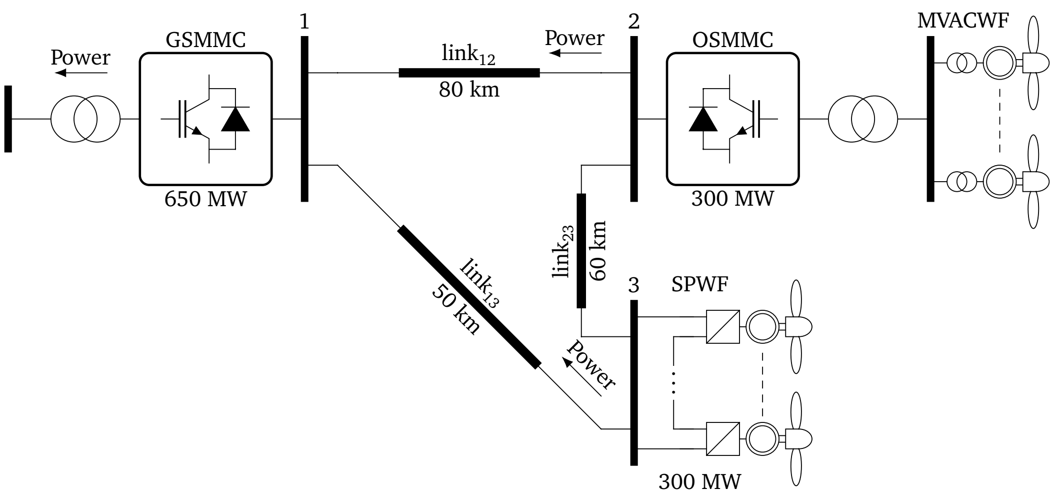

Figure 4.8 – Configuration and ratings of a three-terminal MTDC system.

Table 4.1 – Parameter of converters in the three-terminal MTDC system

Converter	Nominal voltage (kV)	Nominal power (MW)
GSMMC	± 320	650
OSMMC	± 320	300
SPWF	± 320	300

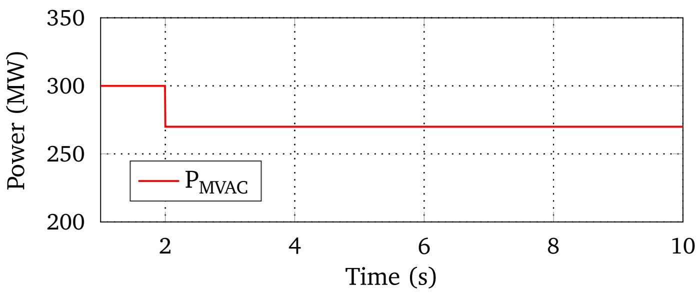

(a) Power of MVAC WF.

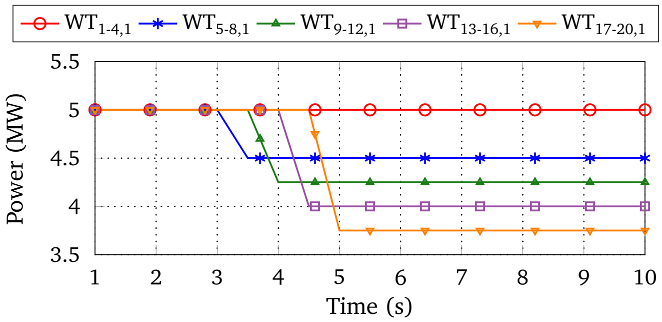

(b) Maximum extractable wind power in Cluster 1 of the SPWF.

Figure 4.9 – Two offshore wind farm power variations.

The system is in steady state from 1 s and both wind farms are operating at nominal power production. The onshore MMC exports all generated power from the wind farms to the onshore AC grid. Due to cable losses, the power received at onshore side is slightly lower than 600 MW as shown in Figure 4.10e. At 2 s, the received power shows a reduction due to the power decrease in the MVAC wind farm. However, The HVDC voltage remains at nominal level because it is stiffly controlled by the GSMMC station, as can be observed in Figure 4.10c. In the interval of 3 s to 5 s, the power varies in the SPWF cluster 1, so as the output voltage of each unit. At around 4.6 s the local overvoltage limitation control activates and restraints units $WT_{1\text{-}4,1}$ under 1.1 pu by reducing their power generation as shown in Figure 4.10a. The received power at onshore end remains at 552.9 MW. For comparison, at 8 s the global overvoltage limitation control is applied by means of sending a lower HVDC voltage reference to the master converter, the onshore MMC. Thanks to this lower voltage level, $WT_{1\text{-}4,1}$ are able to restore their maximum power production and in the same time, their output voltages are kept inside their overvoltage capabilities.

The new HVDC voltage reference is calculated based on the information of real time power production of each wind turbine both in the SPWF and the MVAC wind farm. With such information, the generated power at offshore end as well as the power losses in the cable can be calculated. By comparing the power curtailment with the local control to the cable power losses due to lower HVDC voltage level, an optimal voltage can be obtained. In this case, the HVDC voltage is reduced to 598.4 kV and the total power received at onshore end recovers to 554.3 MW, which is 1.6 MW higher than the operation before the global control is applied.

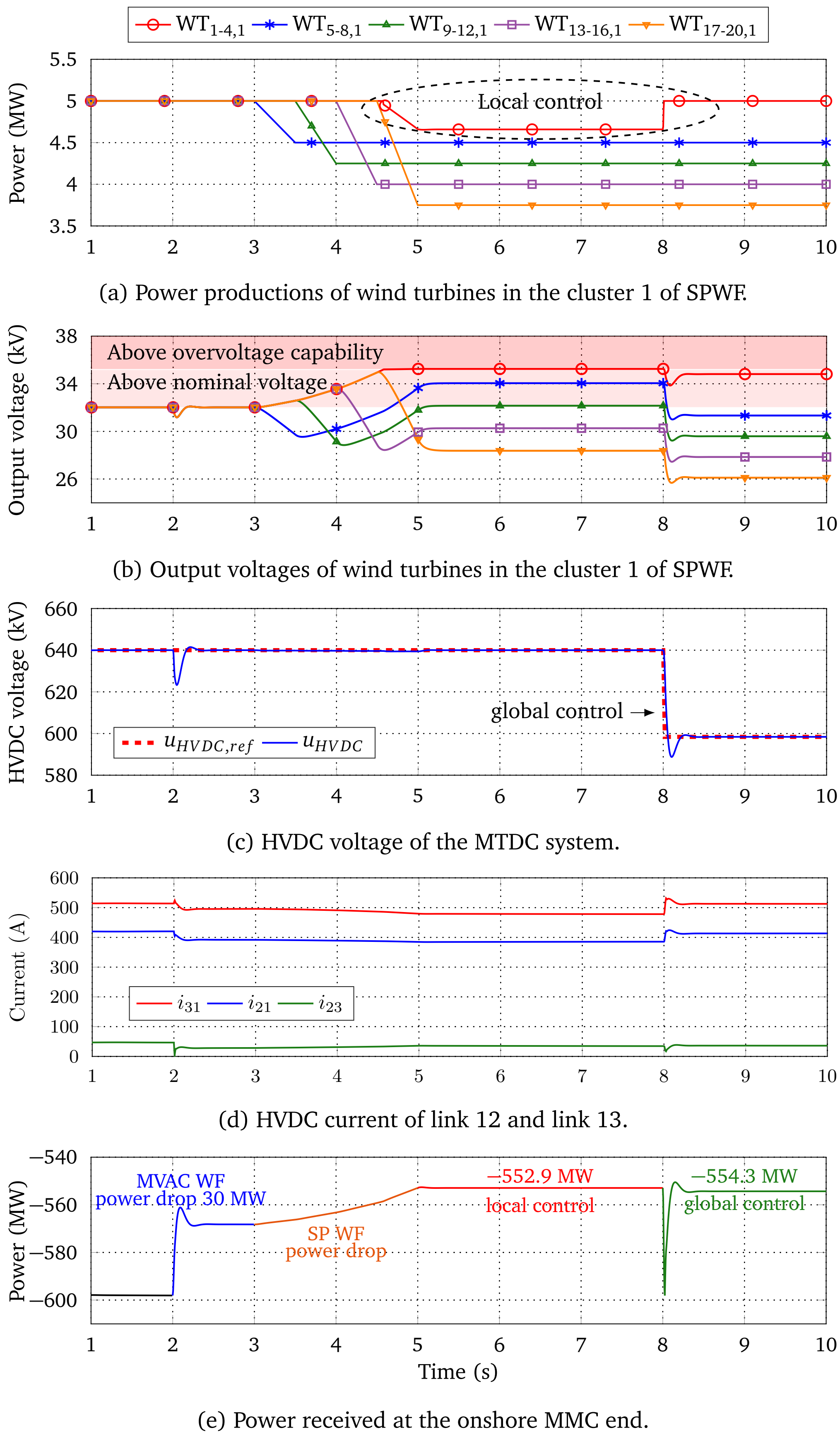

Figure 4.10 – MTDC system responses to the reduction of power of the MVAC wind farm at 2 s, wind turbine power changes during 3 s to 5 s and activation of global control at 8 s.

4.3.1.4 Operating points of the three-terminal MTDC system

Figure 4.11a shows the initial operation points of the three-terminal MTDC system in blue dots. The master converter (GSMMC) controls the HVDC voltage, extracting the power from the MTDC grid and inverting it into AC grid. Offshore wind farms operate in normal rectifier mode and thus, they inject power into the MTDC grid. As a result, their corresponding operating points are on the right side of the frame.

The power of the MVAC wind farm decreases to 270 MW, this loss of production affects only the GSMMC whose power flow decreases from −600 MW to −570 MW, as noted in red squares in the figure. The similar behaviour of the GSMMC can be observed in the next state, the operating point of the GSMMC moves to the right of the previous state to absorb the power loss in the SPWF, as shown in the green diamonds in the figure. In the final state, the global control requires the GSMMC to bring the MTDC voltage system to a lower level, which consequently lowers the operating points of both OSMMC and SPWF as shown in Figure 4.11b.

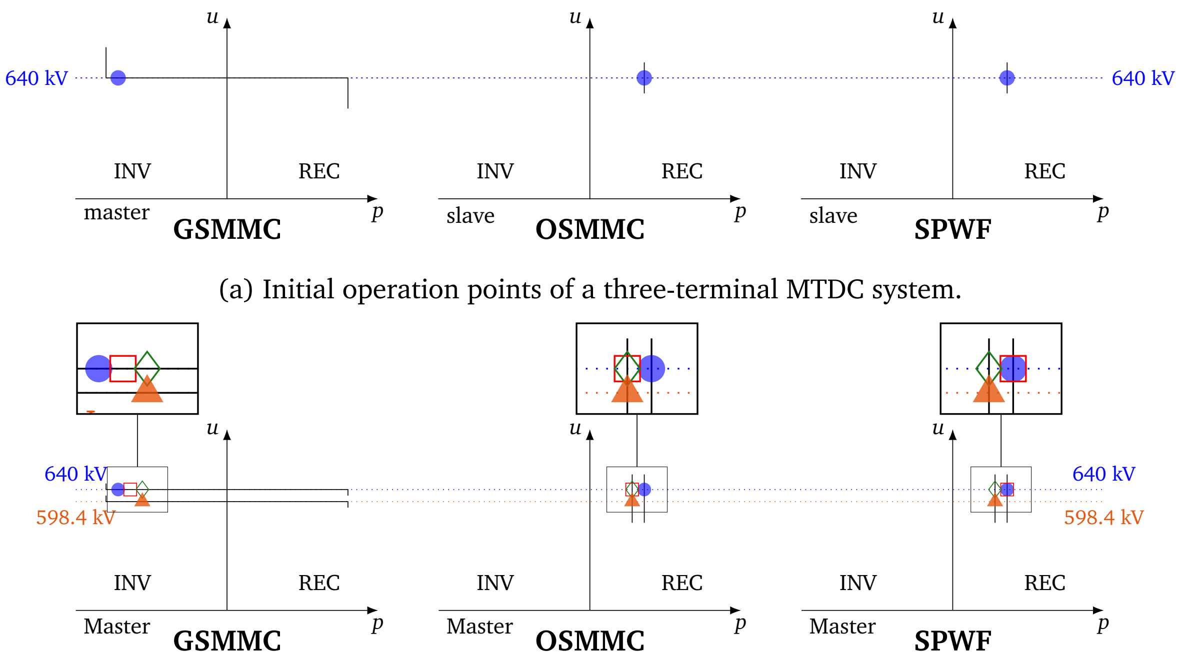

(a) Initial operation points of a three-terminal MTDC system.

(b) Operation points changes: 1) blue circle, initial operating points; 2) red square, following to a power reduction of MVAC wind farm; 3) green diamond, following to wind power reduction in the first cluster of the SPWF; 4) orange triangle, following to the global control.

Figure 4.11 – Operating points of the three-terminal MTDC system.

4.3.2 SPWF in a MTDC system with droop control

The droop control is used when a MTDC system contains more than one converter, and therefore the HVDC voltage regulation can be allocated to several converters instead to only one [Beer 14][Rouz 14][Xu 09][Raul 14]. In this part, the analysis of the SPWF in the MTDC system with droop control is applied to a four-terminal MTDC system shown in Figure 4.12. This system comprises two onshore converters and two offshore wind farms including one SPWF.

4.3.2.1 Characteristics of the MTDC system with droop control

The voltage droop control is inspired by the primary frequency control in AC systems [Guer 11] [Roca 12]. In order to maintain the balance between generation and load and without communication in between, some generation units change their production according to a specific variation in frequency. The characteristic between power and frequency is commonly called droop control. The same idea is taken to establish a power and voltage relationship in the power converters in DC systems [Bark 10]:

$$\Delta p = \frac{1}{k}\Delta u_{HVDC} \tag{4.3}$$

where:

1. k is the voltage droop value and its unit is (V/W). In the inverter-rectifier reference frame described in Figure 4.13, $k < 0$.
2. Δp is the power deviation of the power of the converter p compared to its previous set point p_0, $\Delta p = p - p_0$.
3. Δu_{HVDC} is the voltage deviation of the DC voltage of the system u_{HVDC} compared to its previous set point u_{HVDC0}, $\Delta u_{HVDC} = u_{HVDC} - u_{HVDC0}$. In literature the voltage set point u_{HVDC0} is a constant value which is usually the nominal HVDC voltage of the system. In this thesis, the voltage set point is given by the output of the global control strategy.

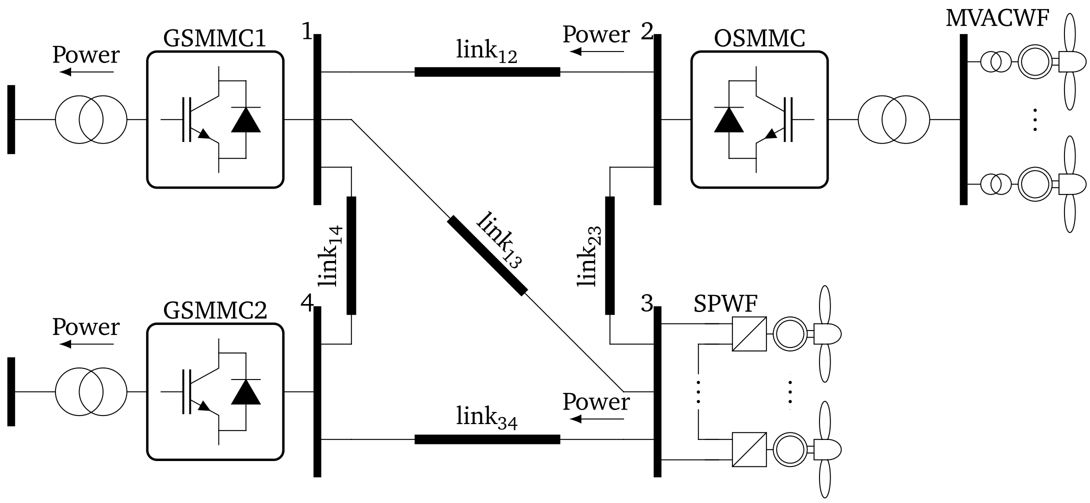

Figure 4.12 – A 4-terminal MTDC system for transferring power from one MVAC wind farm and one SPWF to two onshore grid connected MMCs.

The voltage droop control works as follows: The DC system voltage level changes if the initial power production and consumption balance is modified in response to a sudden system load increase or decrease. This DC voltage variation Δu_{HVDC} is detected by converters equipped with power-voltage droop controllers, which generate proportional deviations of the power references that help to re-balance the total power in the DC grid. The proportion of deviation of the power reference for each station is defined by its droop value k, as shown in Figure 4.13. If the droop value of the first converter is half of the second converter, the deviation of power Δp_1 of the first converter would be twice as much as the second one Δp_2 followed to the same amount of voltage change Δu_{HVDC}.

This method increases the reliability of DC systems with several stations. The deviation of power is shared, reducing the burden of each converter, and very important, the control is simple to be implemented. Figure 4.14 shows the block diagram of the voltage droop controller.

The voltage droop value design is not the focus of this thesis, this parameter is selected to be 0.1. Nevertheless, it is worthy of mentioning that there are some references addressing the design of the voltage droop value. The work in [Raul 14] developed a methodology based on a simplified VSC model taking into account the station DC voltage dynamics. The droop value is sized to achieve a desired response time of the system. The work in [Akka 16] used multi-variable frequency analysis based on the Singular Value Decomposition (SVD) to size the droop value in order to tolerate a maximum DC voltage deviation both in steady and transient states.

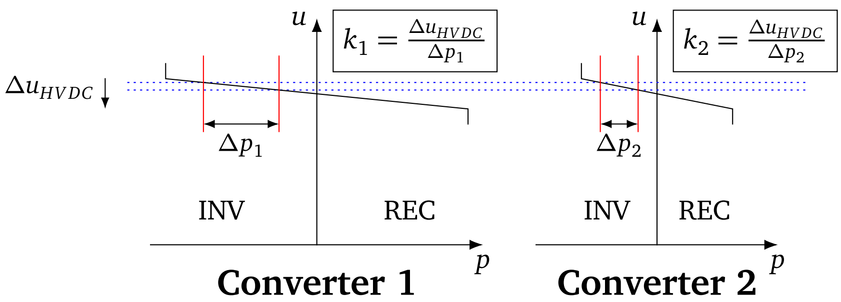

Figure 4.13 – Voltage droop characteristics of two converters, droop value of converter 2 is double of the value of converter 1.

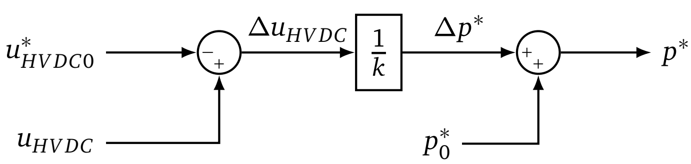

Figure 4.14 – Diagram of the voltage droop controller.

4.3.2.2 Overview of the control strategy

The overall control strategy of this four-terminal MTDC system is shown in Figure 4.15. Technically this MTDC system can also be controlled by using master-slave control method by selecting one of the two onshore VSCs as the master controller to regulate the HVDC voltage, and another VSC operating at active power mode to absorb constant power from the DC grid. However, in this way the variation of the power at the offshore side is only balanced by the master converter. The trigger out of the master converter would mean the loss of the entire MTDC system. In order to enable the two onshore VSCs to participate in the control of the DC grid voltage, the voltage droop control technique is implemented in both of them. As far as the global and local control are concerned, the same methods used in the three-terminal system are here adopted.

The overall control strategy has the same targets as established in the previous three-terminal MTDC system:

1. Maintain the MTDC transmission voltage.
2. Maintain the MVAC voltage of the conventional wind farm collection grid.
3. Keep the output voltage of each SP wind turbine under its overvoltage limitation level.
4. Maximize the power transmitted to the onshore grid.

In this MTDC system, the Target 1 is achieved by the two onshore converters. Target 2 is completed by the offshore converter OSMMC operating at AC voltage mode. The Global control strategy and the local control strategy are dedicated to accomplish Target 3 and Target 4.

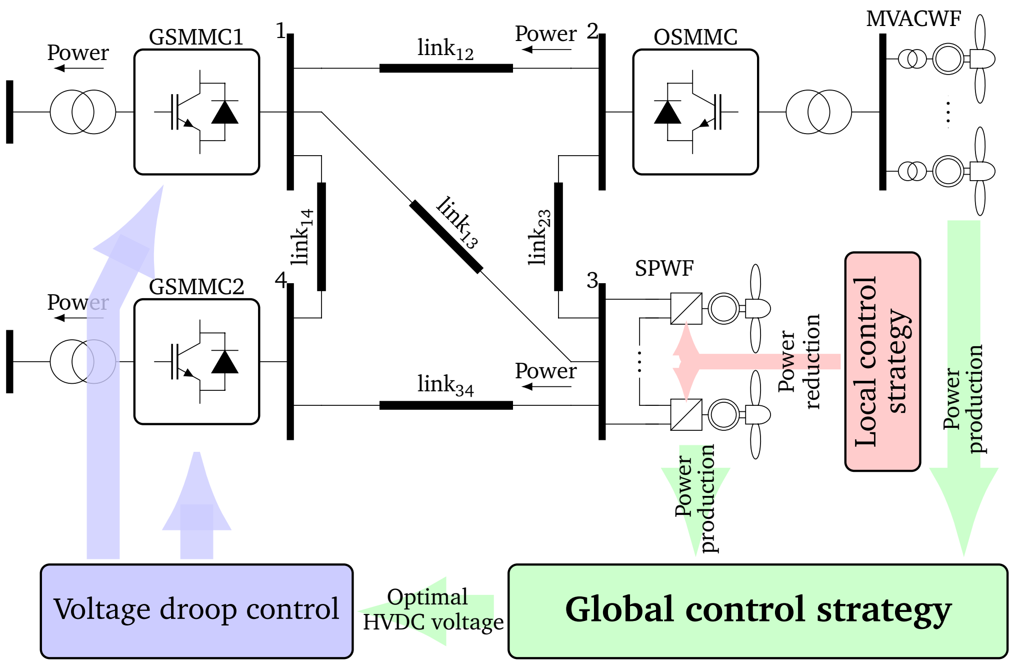

Figure 4.15 – Overview of the control system of the four-terminal MTDC.

4.3.2.3 Case study and simulation results of a hybrid four-terminal MTDC system

This section discusses the second MTDC system shown in Figure 4.16. This is a four-terminal MTDC system comprising two onshore VSCs, one MVAC offshore wind farm and one 20×3 SPWF. The power generated by the MVAC wind farm is injected into the MTDC grid via an offshore VSC. The SPWF directly exports its power to onshore GSMMC1 and GSMMC2 through two HVDC links. There is one extra HVDC link jointing OSMMC and SPWF's hub and another one connecting GSMMC1 and GSMMC 2 to build a more robust DC grid. The power ratings of the four terminals are reported in Table 4.2.

A simulation of the four-terminal MTDC system is carried out. The initial voltage set points for the two onshore MMCs are 640 kV and the initial power set points are −600 MW and −300 MW. Both stations are endorsed with a droop value of 0.05. The simulation scenario is similar to the three-terminal system. At 2 s the power of the MVAC wind farm decreases from 300 MW to 270 MW and the maximum wind power changes according to Figure 4.9b. The global control activates at 8 s and changes the voltage set point of the system to 600 kV.

Figure 4.17 shows the simulation results of the four-terminal MTDC system operating in aforementioned conditions and with voltage droop control applied.

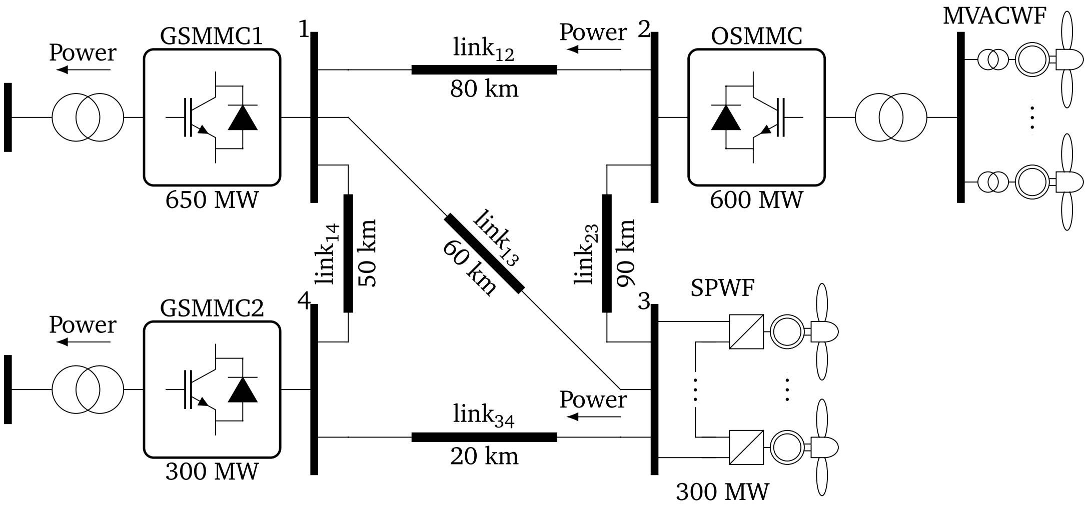

Figure 4.16 – Configuration and ratings of a four-terminal MTDC system.

Table 4.2 – Parameter of converters in the four-terminal MTDC system

Converter	Nominal voltage (kV)	Nominal power (MW)
GSMMC1	± 320	650
GSMMC2	± 320	300
OSMMC	± 320	600
SPWF	± 320	300

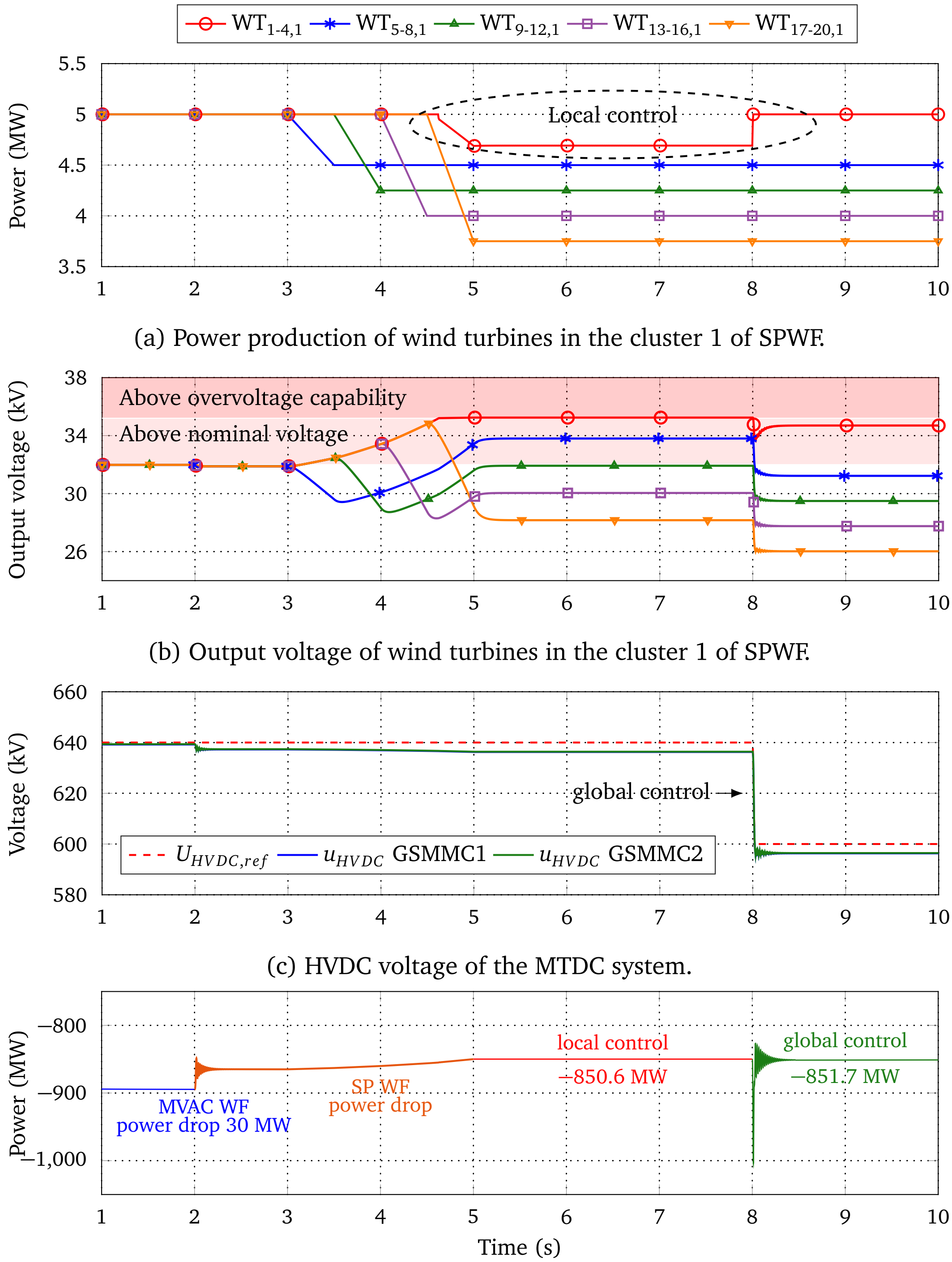

(a) Power production of wind turbines in the cluster 1 of SPWF.

(b) Output voltage of wind turbines in the cluster 1 of SPWF.

(c) HVDC voltage of the MTDC system.

(d) Power received at the onshore MMC end.

Figure 4.17 – MTDC system responses to the reduction of power of the MVAC wind farm at 2 s, wind turbine power changes from 3 to 5 s and the activation of global control at 8 s.

During 1 s to 2 s, the two offshore wind farms operate at nominal power production and the HVDC voltage is 640 kV. Due to cable power losses, the power received at onshore side is slightly lower than 900 MW as shown in Figure 4.17d.

At 2 s, the received power is reduced due to a power decrease in the MVAC wind farm.

Moreover, the HVDC voltage decreases to compensate the power reduction in the MTDC grid by the droop control, as shown in Figure 4.17b. At the interval from 3 to 5 s, the HVDC voltage continues to decrease slightly as the power decreases in the SPWF.

At around 4.6 s, the local overvoltage limitation control activates to restraint the output voltages of units $WT_{1\text{-}4,1}$ under 1.1 pu by reducing their power generation, as seen in Figure 4.10a. The received power at onshore end remains at 850.6 MW. At 8 s, the global limitation control set a new HVDC voltage reference at 600 kV to the droop controller and the received power increases slightly up to 851.7 MW. It can be seen from Figure 4.17d that the new voltage is established below 600 kV. This is caused by the previous voltage deviation of the droop control. The DC voltage will be recovered if the overvoltage is active.

The droop control allows the received power at onshore side of the MTDC system to be shared by two power converters. A zoom-in view in figure 4.18a shows the proportion of power deviation of the two converters with different droop values responding to the offshore power generation decrease at 2 s. It can be seen that the deviation of GSMMC2 is only half of that of GSMMC1 since its droop value is double of the droop value of GSMMC1. Figure 4.18b shows the current variation in the five HVDC links due to the power deviation at 2 s.

4.3.2.4 Operating points of the four-terminal MTDC system

Figure 4.19a shows the initial operation points of the four-terminal MTDC system in blue dots. The MVAC wind farm and SPWF operate at nominal power and they are in power mode to inject their power into the MTDC grid. GSMMC1 and GSMMC2 are endorsed with droop controllers to extract power from the MTDC grid to the AC grid with a proportion subject to their droop value. Neglecting the power losses in the cables, GSMMC1 takes 600 MW from the DC grid and GSMMC2 takes the remained 300 MW.

Following the MVAC wind farm wind power curtailment from 600 MW to 570 MW, the operating points of GSMMC1 and GSMMC2 move to -580 MW and -290 MW respectively. The similar behaviour of both onshore converters can be observed in the next state, their

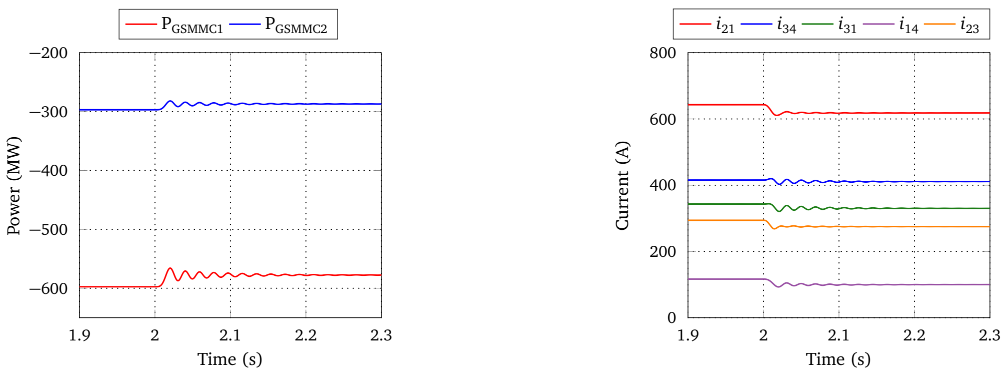

(a) Power deviation of two onshore converters. (b) Currents in the five HVDC links.

Figure 4.18 – Power and current deviation subsequent to power production decrease in the MVAC wind farm at 2 s.

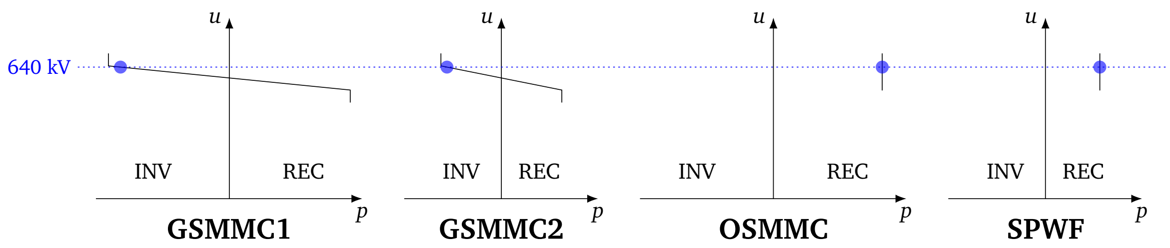

(a) Initial operating points of the four-terminal MTDC grid.

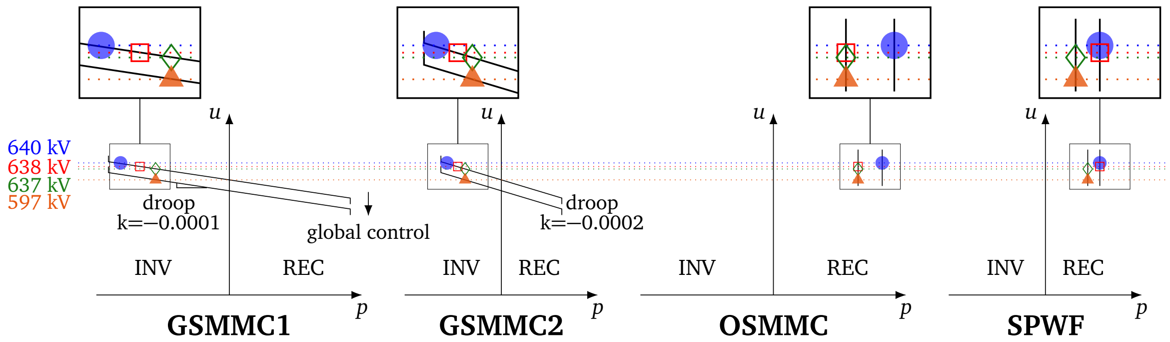

(b) Operation points changes: blue circle, initial operating points; red square, following a power reduction of MVAC wind farm; green diamond, following a wind power variation in the first cluster of the SPWF; orange triangle, following the global control.

Figure 4.19 – Operating point of the four-terminal MTDC grid.

operating points move proportionally to the right of their previous states, which results in 1 kV HVDC voltage drop. At the end, the global control is applied, the entire characteristic curves are degraded with the same droop slopes.

4.4 Conclusion

In this chapter, the Series Wind Farm (SWF) farm is extended to the Series Parallel Wind Farm (SPWF) by connecting several SWFs in parallel. A star-type connection is used since it is more reliable, as the cable fault in one SWF will not influence the power transmission of other SWFs. These SWFs are linked to the same HVDC voltage.

Then, the SPWF operations in MTDC systems are discussed. In the first MTDC system with one onshore converter and two offshore wind farms, the master-slave control method is used. The onshore converter regulates the MTDC transmission voltage. The global control strategy and the local control strategy are dedicated to keep the wind turbines in the SPWF within safe limits as well as maximizing the power transmitted to the onshore grid. The second MTDC system is comprised of two onshore converters and two offshore wind farms, and therefore, the droop control method is adopted to maintain the transmission voltage. Both case studies and simulation results show good performance of the local and global control strategies developed in previous chapters. The global control strategy is applied to help the MTDC system to receive more power than when only the local control is activated.

References

[Akka 16] S. Akkari. *Control of a multi-terminal HVDC (MTDC) system and study of the interactions between the MTDC and the AC grids*. PhD thesis, Université Paris-Saclay, 2016. 148

[Alla 13] R. N. Allan *et al.* *Reliability evaluation of power systems*. Springer Science & Business Media, 2013. 136

[Bark 10] C. Barker and R. Whitehouse. "Autonomous converter control in a multi-terminal HVDC system". 2010. 147

[Beer 14] J. Beerten, S. Cole, and R. Belmans. "Modeling of multi-terminal VSC HVDC systems with distributed DC voltage control". *IEEE Transactions on Power Systems*, Vol. 29, No. 1, pp. 34–42, 2014. 146

[Bill 89] V. C. Billon, J. Taisne, V. Arcidiacono, and F. Mazzoldi. "The Corsican tapping: from design to commissioning tests of the third terminal of the Sardinia-Corsica-Italy HVDC". *IEEE Transactions on Power Delivery*, Vol. 4, No. 1, pp. 794–799, 1989. 135

[Dier 12] C. Dierckxsens, K. Srivastava, M. Reza, S. Cole, J. Beerten, and R. Belmans. "A distributed DC voltage control method for VSC MTDC systems". *Electric Power Systems Research*, Vol. 82, No. 1, pp. 54–58, 2012. 141

[Gomi 11a] O. Gomis-Bellmunt, J. Liang, J. Ekanayake, and N. Jenkins. "Voltage–current characteristics of multiterminal HVDC-VSC for offshore wind farms". *Electric Power Systems Research*, Vol. 81, No. 2, pp. 440–450, 2011. 141

[Gomi 11b] O. Gomis-Bellmunt, J. Liang, J. Ekanayake, R. King, and N. Jenkins. "Topologies of multiterminal HVDC-VSC transmission for large offshore wind farms". *Electric Power Systems Research*, Vol. 81, No. 2, pp. 271–281, 2011. 138

[Guer 11] J. M. Guerrero, J. C. Vasquez, J. Matas, L. G. De Vicuña, and M. Castilla. "Hierarchical control of droop-controlled AC and DC microgrids—A general approach toward standardization". *IEEE Transactions on Industrial Electronics*, Vol. 58, No. 1, pp. 158–172, 2011. 147

[Hail 08] T. M. Haileselassie, M. Molinas, T. Undeland, *et al.* "Multi-terminal VSC-HVDC system for integration of offshore wind farms and green electrification of platforms in the North Sea". In: *Nordic Workshop on Power and Industrial Electronics (NORPIE/2008), June 9-11, 2008, Espoo, Finland*, Helsinki University of Technology, 2008. 139

[Jian 98] H. Jiang and A. Ekstrom. "Multiterminal HVDC systems in urban areas of large cities". *IEEE Transactions on Power Delivery*, Vol. 13, No. 4, pp. 1278–1284, 1998. 138

[Jovc 09] D. Jovcic and N. Strachan. "Offshore wind farm with centralised power conversion and DC interconnection". *IET generation, transmission & distribution*, Vol. 3, No. 6, pp. 586–595, 2009. 139

[Li 15] C. Li, X. Hu, J. Guo, and J. Liang. "The DC grid reliability and cost evaluation with Zhoushan five-terminal HVDC case study". In: *Power Engineering Conference (UPEC), 2015 50th International Universities*, pp. 1–6, IEEE, 2015. 135

[Lian 09] J. Liang, O. Gomis-Bellmunt, J. Ekanayake, and N. Jenkins. "Control of multi-terminal VSC-HVDC transmission for offshore wind power". In: *Power Electronics and Applications, 2009. EPE'09. 13th European Conference on*, pp. 1–10, IEEE, 2009. 141

[Lian 11] J. Liang, T. Jing, O. Gomis-Bellmunt, J. Ekanayake, and N. Jenkins. "Operation and control of multiterminal HVDC transmission for offshore wind farms". *IEEE Transactions on Power Delivery*, Vol. 26, No. 4, pp. 2596–2604, 2011. 139

[Lise 11] M. Liserre, R. Cardenas, M. Molinas, and J. Rodriguez. "Overview of multi-MW wind turbines and wind parks". *IEEE Transactions on Industrial Electronics*, Vol. 58, No. 4, pp. 1081–1095, 2011. 136

[Lund 06] S. Lundberg. *Wind Farm Configuration and Energy Efficiency Studies-Series DC versus AC Layouts*. PhD thesis, Chalmers University of Technology, 2006. 135, 136

[Mori 93] G. Morin, L. Bui, S. Casoria, and J. Reeve. "Modeling of the Hydro-Quebec-New England HVDC system and digital controls with EMTP". *IEEE transactions on power delivery*, Vol. 8, No. 2, pp. 559–566, 1993. 135

[Naka 99] T. Nakajima and S. Irokawa. "A control system for HVDC transmission by voltage sourced converters". In: *Power Engineering Society Summer Meeting, 1999. IEEE*, pp. 1113–1119, IEEE, 1999. 139

[Quin 07] G. Quinonez-Varela, G. Ault, O. Anaya-Lara, and J. McDonald. "Electrical collector system options for large offshore wind farms". *IET Renewable Power Generation*, Vol. 1, No. 2, pp. 107–114, 2007. 136

[Rao 15] H. Rao. "Architecture of Nan'ao multi-terminal VSC-HVDC system and its multi-functional control". *CSEE Journal of Power and Energy Systems*, Vol. 1, No. 1, pp. 9–18, 2015. 135

[Raul 14] P. Rault. *Dynamic Modeling and Control of Multi-Terminal HVDC Grids*. PhD thesis, Ecole Centrale de Lille, Lille, France, 2014. 138, 139, 146, 148

[Roca 12] J. Rocabert, A. Luna, F. Blaabjerg, and P. Rodriguez. "Control of power converters in AC microgrids". *IEEE transactions on power electronics*, Vol. 27, No. 11, pp. 4734–4749, 2012. 147

[Rouz 14] K. Rouzbehi, A. Miranian, A. Luna, and P. Rodriguez. “DC voltage control and power sharing in multiterminal DC grids based on optimal DC power flow and voltage-droop strategy”. *IEEE Journal of Emerging and selected topics in power Electronics*, Vol. 2, No. 4, pp. 1171–1180, 2014. 146

[Xu 09] L. Xu, L. Yao, and M. Bazargan. “DC grid management of a multi-terminal HVDC transmission system for large offshore wind farms”. In: *Sustainable Power Generation and Supply, 2009. SUPERGEN'09. International Conference on*, pp. 1–7, IEEE, 2009. 146

[Zhu 10] J. Zhu and C. Booth. “Future multi-terminal HVDC transmission systems using voltage source converters”. In: *Universities Power Engineering Conference (UPEC), 2010 45th International*, pp. 1–6, IEEE, 2010. 138, 139

Chapter 5

Conclusions and perspectives

They did not know it was impossible so they did it.

Mark Twain

Contents

5.1 Conclusions

Currently installed large offshore wind farms mostly have two types of architectures. The first architecture uses a MVAC collection system and a HVAC transmission system. The second one uses the same collection system, while the power transmission is in HVDC. The former pure AC architecture is less expensive for near-shore projects. However, it is not technically feasible for projects located far from the coast, due to high charging currents in the undersea AC cables. The latter one adopts DC for transmission, and therefore, reactive power loading of the transmission cables is eliminated. The transmission distance is not anymore a barrier for offshore wind farms. In addition, the voltage source type HVDC allows more flexible power control, becoming attractive for far offshore markets. However, current offshore wind farms with VSC-HVDC transmission require bulky and expensive offshore centralized converters and platforms. The elimination of offshore platforms contributes to great cost reduction, and therefore, has been the motivation behind the study described in this thesis. The Series Parallel Wind Farm (SPWF) is, to the best of the author's knowledge, the only wind farm topology without an offshore platform.

The SPWF adopts DC in both collection and transmission systems. Architecturally, the collection system of the SPWF is substantially different from the conventional MVAC-HVDC wind farm. In the conventional collection system, wind turbines are connected in parallel and are operated independently. To the contrary, in the SPWF, wind turbines with MVDC output voltages are connected in series, and thus the wind turbines share the same current. Electrically, the bulky centralized converter used at the offshore substation of the MVAC-HVDC wind farm is replaced with a number of dispersed medium-power-rating DC/DC converters in the wind turbine. In this way, the offshore platform is removed. The output DC/DC converters of wind turbines are series connected, hence the wind farm output voltage is stepped-up to higher power transmission voltage level. Due to these particular characteristics, several challenges of this topology should be identified and tackled before it becomes economical alternative for future high power long distant wind farms. The first objective of this thesis was focused on the identification of the characteristics of the SPWF to proceed with the investigation of suitable control strategies for the safe operation of this topology.

Chapter 1 presents the state of the art of the offshore wind technologies. It describes the structures of offshore wind turbines and the aerodynamics basics of power conversion of the kinetic energy of the wind into electrical energy. Then, a comparison of the three most adopted wind turbines in the offshore market is presented among which the direct drive PMSG with full rating converter is frequently proposed in the literature for future DC wind farms. Afterwards, the configurations for interconnecting all units, so called collection system, are compared. Current collection systems are all based on AC while a number of configurations based on DC can be found in the literature. Same to the collection system, the transmission system can adopt either AC or DC. VSC-based HVDC transmission technologies are considered as the best candidates for long distance and multi-terminal power transmissions. The last part of Chapter 1 compares four most appealing topologies for high power long distant offshore wind farm. It presents as advantages of SPWF over the other three layouts the low cost, low switching losses and low cable losses.

In the next chapter, the system model and control of one cluster of series connected wind turbines, so called Series Wind Farm (SWF), are explained in general. The design of the series connected wind turbines is suggested to be over-sized by taking into consideration the output voltage characteristics of this wind farm. For this reason, Chapter 2 begins with a steady state study of the SWF, and explains the variation of wind turbine output voltages due to imbalanced power production among the series connected units.

The overvoltage is dangerous not only for the individual wind turbine, but also for the entire wind farm. Bearing in mind this fact, the main components of the wind turbine used for series connection are identified. The full bridge DC/DC converter is selected to step-up the generator side voltage to MVDC because the converter can operate in variable transformation ratio, which is necessary for the series connected wind turbines. The whole wind turbine model, normal mode control and bypass protection methods are explained. At the end of the chapter, a local overvoltage limitation method found in the literature is described. This method restraints the increase of the output voltage at the sacrifice of power curtailment. A trade-off between the extra cost of an oversized converter rating, for higher overvoltage capability, and the loss of energy, resulting from the local control strategy, should be identified.

As operation of wind turbines in the SWF are coupled, and the local control owns the drawback of power curtailment, Chapter 3 extends the investigation of the SWF connected to a point-to-point transmission system. The first part of this chapter introduces the MMC-based HVDC technology, and then details the development of the energy based arm average MMC model in EMTP-RV software. The control system of this energy based MMC model includes the DC voltage or active power control, AC voltage or reactive power control, and an extra control loop for the MMC arm stored energy.

The HVDC cable models are investigated in the second part of this chapter. A precise cable model is required because of the presence of uncontrolled variables in the SWF due to the elimination of the offshore centralized converter. The cluster with series connected wind turbines is directly connected to the HVDC cables. The output capacitors of the DC/DC converters of the wind turbines, the smoothing reactors and the HVDC cables form a series RLC-cable resonant circuit. As a result, cable models valid both at very low frequency (DC) and at resonant frequency are required for accurate simulation results of the wind farm behaviour. The Wideband model available in the EMTP-RV library is selected in this chapter.

In the last part of Chapter 3, a global overvoltage limitation control strategy is proposed. It is implemented and simulated in the EMTP-RV. The global control strategy regulates the HVDC voltage to ensure that the voltage across each wind turbine remains under its overvoltage capability. This control strategy is based on data communication between the offshore and onshore terminals. The latency during the data transmission via fibre optics cable is analysed and the local control strategy is proposed as a complementary control to the global control strategy. By combining these two controls, an optimal HVDC voltage can be calculated taking into consideration the cable power losses (due to the global control) and the power curtailment (due to local control). The results are validated by simulation and demonstrated that for a given wind turbine overvoltage capability, the power transmitted to the onshore grid by adopting the global control is higher than only using local control strategy.

Chapter 4 begins with the SPWF by extending the proposed control strategies to the wind farm with several clusters. Since combining a large number of wind turbines in series leads to lower reliability, the proposed solution was to put several clusters in parallel. Parallel connection of several clusters leads to a more reliable topology than one single cluster, because the fault in one cluster does not affect the operation of other clusters and besides increases the power rating of the wind farm. A 300 MW SPWF with 60 wind turbines of 5 MW allocated in 3 clusters is shown and analysed.

Afterwards, the high power rating SPWF is integrated into MTDC systems with different combinations of grid side MMCs, SPWFs and conventional wind farms using MVAC collection system. For each configuration, different MTDC control methods are applied as well as the local and global control strategy whose performance has been evaluated and validated by simulations in EMTP-RV environment. The master-slave control and droop control are explained. The control system of the MTDC systems aims: 1) to maintain the MTDC transmission voltage; 2) to maintain the MVAC voltage of the conventional wind farm collection grid; 3) to limit the output voltage of each series parallel wind turbine based on data of the power production of all the units; 4) to adjust the HVDC voltage to an optimal level, in order to maximize the power transmitted to the onshore grid. Target 1 is achieved by the converters endorsed with either the master-slave control or the droop control. Target 2 is realized by the conventional wind farm offshore substation. Both Targets 3 and 4 are accomplished via the combination of global and local overvoltage limitation strategies. The proposed global control is proven to be feasible for MTDC systems. The simulation results demonstrate that more power can be obtained at the onshore side by reducing the HVDC voltage (global control) than by reducing the power production of wind turbine (local control).

5.2 Suggestions for future research work

This dissertation mainly focuses on the overvoltage limitation control of the SPWF. To further prove the feasibility of this wind farm topology as well as the advantages and drawbacks, the following list of future research, to the author's opinion, is of interest for further investigation:

- The results of a wind farm with only the global control method and only the local control method can be contrasted. A comparison of the power production results in terms of life-time capitalized value might be of interest for feasibility analysis.

- The over-sizing ratio of the series connected wind turbines could be optimised. Calculating the cost for different over-sizing ratio, the power curtailment due to the local control, and the cable losses due to the global control, respectively, would provide the best possible solution for a cost effective selection of the rating of the system components.
- High power medium frequency DC/DC converters can be analysed. In this dissertation the full bridge DC/DC converter is used for an illustrative study, but current technology of DC/DC converter in high power medium frequency domain is not developed enough. The main challenges concern the losses induced by the eddy current in the magnetic core and losses in the windings.
- High potential insulation technology should be carefully studied since it is a key factor in the design and construction of an offshore project. The HVDC transmission voltage is imposed directly on the series wind turbines. Therefore, the wind turbines at both terminals of the cluster, are required to support maximum the half of the transmission voltage.
- The manner in which the communication delay as well as response time of the capacitive cables affect the power devices in the wind turbine can be analysed. This requires the use of a detailed wind turbine model.
- Investigation about whether the resonance during bypass of one unit on one cluster may affect the operation in other clusters, since the smoothing reactor is separately allocated into each wind turbine should be carried out. Again, the detailed wind turbine model should be used for this study. The study about the resonance circuit also involves the optimization of the wind turbine output capacitors. In this thesis, an electrostatic constant of 30-40 ms is used. Further investigation of this value is suggested.
- As the power saved by the global control varies with different wind speed conditions, it is necessary to develop an algorithm to calculate in real-time the optimal HVDC voltage by using the global control method.
- Assess the proposed control strategy with experimental verification.